THÈSE

En vue de l'obtention du

DOCTORAT DE L'UNIVERSITÉ DE TOULOUSE

Délivré par *l'Université Toulouse III - Paul Sabatier*
Discipline ou spécialité : *Géochimie isotopique*

Présentée et soutenue par *Ruoyu Sun*
Le *16/09/2013*

Titre : *Les variations isotopiques du mercure dans le charbon et les produits de combustion du charbon - Une évaluation de la traçabilité des émissions du mercure des centrales au charbon*

Title : *Mercury stable isotope variations in coal and coal combustion products - Evaluating the traceability of coal Hg emissions*

JURY

Jeroen Sonke - CNRS-CR1, OMP-CNRS, Toulouse (Directeur)
Sovan Lek - Professeur UPS, UPS-EDB, Toulouse (Examinateur)
Laurence Maurice - IRD-DR2, OMP-GET, Toulouse (Examinateur)
Jan Wiederhold - Recherche ETH, IBP, Zurich (Rapporteur)
Jiubin Chen - Professeur CAS, SKLEG, Guiyang (Rapporteur)
Xinbin Feng - Professeur CAS, SKLEG, Guiyang (Examinateur)

Ecole doctorale : *Sciences de l'Univers, de l'Environnement et de l'Espace*
Unité de recherche : *Géosciences Environnement Toulouse*
Directeur(s) de Thèse : *Jeroen Sonke*

Abstract

Mercury (Hg) is a toxic, persistent and globally distributed pollutant. Since the industrial revolution, human activities have augmented the global Hg cycle at the Earth's surface by a factor of three. Hg emissions from coal-fired power plants represent at present the largest single anthropogenic source. However, quantitative tracing of the fate of coal Hg emissions from different countries or regions is a challenging issue. The objective of this PhD dissertation was to use Hg stable isotope signatures to address this problem. Firstly, we developed a combustion-trapping protocol to extract, purify and pre-concentrate Hg from solid samples with low Hg levels such as coal and coal combustion products. Purified coal Hg was then measured for its isotope compositions by high-precision (~0.1‰, 2σ) multi-collector inductively coupled plasma mass spectrometry.

In a 1st case study on two coal-bearing sequences in the Huainan Coalfield and the Jining Coalfield (China), we investigate in detail the Hg isotope variation in coal deposited during Permian. We observed a 2‰ variation of the δ^{202}Hg signature and a 0.3‰ variation of the Δ^{199}Hg signature in both continuously deposited coal seams over a period of ~20 million years and within a single coal seam. Correlations between δ^{202}Hg, Δ^{199}Hg, Hg concentration, mineralogy, and other geochemical parameters are visible, but often contradictory and difficult to interpret in terms of Hg sources to coal or biogeochemical transformations of Hg in coal. In a 2nd case study we develop an international coal Hg isotope library, based on 108 new coal samples and 50 published coals that cover major coal-producing basins in Africa, China, Europe, India, Indonesia, former USSR and the USA. We observe a 4.7‰ range for the δ^{202}Hg signature (−3.9 to 0.8‰) and a 1.0‰ range in the Δ^{199}Hg signature (−0.6 to 0.4‰). In total, 14 ($p<0.05$) and 17 ($p<0.10$) of the 28 pairwise comparisons between eight global regions are statistically distinguishable on the basis of δ^{202}Hg, Δ^{199}Hg or both. Finally, in a 3rd case study we address the question whether Hg emissions from coal-fired power plants preserve the Hg isotope signatures of feed coals. We compare the Hg isotope compositions of feed coal, bottom ash, fly ash and gypsum by-products in six utility boilers of two large Chinese coal-fired power plants. We find that fly ash and gypsum Hg capture by-products are systematically enriched in the lighter isotopes. A Hg isotope mass balance suggests that stack flue gas emissions are enriched in heavy isotopes by at most 0.3‰ for δ^{202}Hg while Δ^{199}Hg signatures remain unchanged. Coal fired power plants, therefore, do not dramatically change coal Hg isotope signatures.

In summary we find that coals from different global coal basins are often isotopically distinguishable at the p=0.05 or 0.10 level, and that combustion and capture processes in coal-fired power plants do

not substantially change feed coal Hg isotope signatures. We consider these combined results to be sufficiently promising to recommend detailed atmospheric Hg isotope tracer studies of coal plant Hg emissions. However, we anticipate that the different gaseous and particulate forms of Hg in coal flue gas emissions may carry more contrasting Hg isotope signatures than we estimated for bulk emissions. Therefore, caution should be taken in near-field and far-field coal Hg emission tracing, and additional studies on the Hg isotope signatures of coal plant Hg emissions are necessary.

Résumé

Le mercure (Hg) est un élément toxique et récalcitrant dans notre environnement. Depuis la révolution industrielle, les activités humains ont augmenté la quantité du Hg qui cycle à la surface de la Terre d'un facteur trois. Les émissions du Hg des centrales au charbon représentent à elles-seules la moitié de tous les émissions anthropiques du Hg. Désormais, le traçage quantitatif de ces émissions des différentes régions du globe n'est pas simple. L'objectif de cette thèse a été d'explorer les signatures isotopiques du Hg comme traceur potentiel des émissions du Hg des centrales au charbon. Dans un premier temps un protocole d'extraction, purification et de pré-concentration du Hg par voie de combustion et re-piégeage acide a été développé. Une fois purifie, le Hg a été analyse par spectrométrie de masse à haute précision (~0.1‰, 2σ).

Dans une 1^{ier} étude de cas, deux séquences géologiques de charbon du Carbonifère et Permien ont été examinées dans les bassins de charbon de Huainan et Jining en Chine. Une variation de 2‰ de la signature δ^{202}Hg, et une variation de 0.3‰ de la signature Δ^{199}Hg a été observé au sein d'une séquence de charbon encompassant 20 millions d'années, mais egalement au sein d'une seule couche de charbon. Ces variations isotopiques sont parfois corrélées entre eux, ou avec les teneurs en Hg ou encore avec des paramètres minéralogiques et/ou géochimiques. Cependant il a été difficile d'interpréter les tendences isotopiques de façon inéquivoque. Dans une 2^{ieme} étude de cas, une compilation isotopique du Hg dans les charbons a été établie par l'analyse de 108 nouveaux échantillons de charbon, augmenté par les 50 valeurs déjà publiés. La compilation inclut des charbon provenant de l'Afrique, Europe, Inde, Indonesie, l'ancien USSR et les USA. Une variation isotopique de 4.7‰ de la signature δ^{202}Hg, et une variation de 1.0‰ de la signature Δ^{199}Hg est observeé dans l'ensemble des charbon. 14 ($p<0.05$) and 17 ($p<0.10$) des 28 comparaisons possibles entre les huit principales régions producteur du charbon du monde sont statistiquement différenciable selon leurs δ^{202}Hg, Δ^{199}Hg ou les deux. Enfin, dans une 3^{ieme} étude de cas, nous nous intéressons à la question si les émissions du Hg à la cheminée d'un centrale au charbon préservent la signature isotopique du charbon combusté. Afin d'y répondre les charbons, cendres résiduels, cendres volants, et gypse de six chaudrons industriels de deux grand centrales de charbon chinoise ont été étudiés. Nous observons que les produits secondaires des centrales, i.e. cendres et gypse, sont systématiquement enrichis en isotopes légers par rapport au charbon combusté. Par conséquence, un bilan de masse isotopique suggère que les émissions du Hg par la cheminée doivent être légèrement enrichis en isotopes lourds, jusqu'à 0.3‰ (δ^{202}Hg). En parallèle, les signatures Δ^{199}Hg restent

inchangées et on estime qu'en fin de compte que les centrales au charbon ne modifient pas dramatiquement les signatures isotopiques caractéristiques des charbons combustés.

En résumé, nous observons que les charbons provenant du globe entier sont isotopiquement discernable à un niveau de p de <0.05 ou <0.1. Les processus de combustion et de captage du Hg dans les centrales au charbon ne modifient que minimalement les signatures isotopiques du Hg. Nous considérons ces deux résultats suffisamment prometteur à fin de recommander des études plus élaborées au sujet du traçage des émissions du Hg des centrales au charbon dans l'environnement. Il sera important d'étudier les signatures isotopiques des formes gazeuses et particulaires du Hg dans les panaches des centrales au charbon, afin de vérifier leur variation et évolution. La difficulté de tracer les sources du Hg réside dans la modification de ses signatures isotopiques par les transformations biogéochimiques omniprésentes dans l'atmosphère.

Acknowledgments

The priority of my acknowledgements is to give my foremost appreciation to my supervisor Jeroen Sonke for the priorities that he always gives to me. Without his advice, I would not have completed this dissertation within the scheduled deadline. Throughout this dissertation, it contains his thousands of corrections, thoughtful exploration and constructive suggestions. I will be always indebted to his guidance and inspiration during the entire PhD study besides his further support for my future research. Equal appreciation is given to other members of our Mercury Research Group at the OMP-GET laboratory (Laurence Maurice, David Point, Lars-Eric Heimbürger, Cecile Dufour, Nicolas Marusczak, Xuewu Fu, Jeremy Masbou, Maxime Enrico, Laure Laffont). The team collaboration for method development and the passionate viewpoints discussed during our Club MIF form an important part of this dissertation.

Most of my coal samples in this dissertation come from USTC Coal Laboratory led by Prof. Guijian Liu, my former MSc supervisor. It is his generous share of samples that has made my research move on. I am very grateful for his long-term support. I am also very grateful for other coal samples donated by Harvey Belkin (USGS), Debasish Shome (India) and Oleg Pokrovsky (OMP-GET). I would not have completed my experiments without the helps from the excellent engineers and scientists in the Service de Chimie (Carole Causserand, Stéphane Audry), Service Salle Blanche (Jonathan Prunier, Manuel Henry), Service ICPMS (Jérôme Chmeleff) and Service XRD (Damien Guillaume) of OMP-GET, and in LCABIE of Pau University (David Amouroux and Sylvain Berail). Their efforts are highly appreciated.

I thank the Chinese Scholarship Council for providing me three years of PhD scholarship, and financial support of research grants ANR-09-JCJC-0035-01 from the French Agence Nationale de Recherche and ERC-2010-StG_20091028 from the European Research Council for this dissertation.

Des remerciements spéciaux vont à mes collègues de bureau qui me font sentir que mon français n'est pas aussi bon que je le pensais. Finally, I would like to thank my family. You are always my emotional connection.

Table of Contents

Abstract I
Résumé III
Acknowledgments V
Table of Contents ..... A
List of abbreviations ..... E
Chapter 1. Introduction 2
Chapitre 1. Introduction 5
References 8
Chapter 2. Mercury (Hg) emission from coal combustion and its role in the global biogeochemical Hg cycle 10
2.1. Hg and its toxicology/epidemiology 10
2.1.1. Hg and its physicochemical properties 10
2.1.2. Hg toxicology/epidemiology 10
2.2. Hg geochemistry in coal and Hg emissions from coal combustion 11
2.2.1. Coal formation and coalification 11
2.2.2. Coal as an energy base 12
2.2.3. Hg geochemistry in coal 14
2.2.4. Hg partitioning during coal combustion 15
2.2.5. Atmospheric Hg emissions from coal combustion 16
2.3. Global Hg emissions and biogeochemical cycling 17
References 21
Chapter 3. Theory of Hg isotope fractionation 27
3.1. General concepts 27
3.1.1. Isotope effect 27
3.1.2. Isotope fractionation factor 28
3.1.3. Delta value (δ) and conversion 28
3.2. Literature review on Hg isotopes fractionation 29
3.3. Hg isotopes fractionation mechanisms 30
3.3.1. Mass dependent fractionation (MDF) 30
3.3.2. Mass independent fractionation (MIF) 31

References 35

Chapter 4. Sample descriptions and Hg isotope measurements 40

4.1. Sample descriptions 40

4.1.1. Samples from continuous coal-bearing sequences 40

4.1.2. World coal samples 43

4.1.3. Coal and coal combustion products 45

4.2. Hg stable isotope measurements 48

4.2.1. Instrumental mass bias 50

4.2.2. Matrix effect 55

References 57

Chapter 5. A double-stage tube furnace – acid trapping protocol for the pre-concentration of mercury from solid samples for isotopic analysis (*Analytical and Bioanalytical Chemistry, in press*) 60

Chapter 6. Hg stable isotope variations in coal-bearing sequences and its implication for Hg sources and geochemistry in coal (article in preparation) 71

6.1. Introduction 73

6.2. Study area 74

6.2.1. Coal-forming environment 75

6.2.2. Coal-bearing sequences 75

6.3. Samples and analyses 76

6.3.1. Sample collection 76

6.3.2. Analyses 79

6.4. Results 81

6.4.1. Hg concentrations 81

6.4.2 Hg isotope compositions 83

6.5. Discussion 86

6.5.1. ZJ coals 86

6.5.2. DZ coals 87

6.5.3. Hg isotope compositions in natural cokes 89

6.6. Implications 89

References 90

Chapter 7. Hg stable isotope compositions of selected world coals (article in preparation for *Environmental Science and Technology*) 96
7.1. Introduction 98
7.2. Samples and analysis 99
7.2.1. Samples collection and processing 99
7.2.2. Hg and Hg isotope determinations 100
7.2.3. Blank, recovery and uncertainty 100
7.3. Results and discussions 101
7.3.1. Mercury isotope compositions 101
7.3.2. Biogeochemical factors influencing Hg isotope compositions in coals 112
7.3.3. Industrial processes influencing Hg isotope compositions of coal Hg emissions 119
7.3.4. Coal import-export flow control on a regional/national coal Hg isotope emission inventory 120
7.4. Implications 121
References 122
Chapter 8. Mercury stable isotope fractionation in six utility boilers of two large coal-fired power plants (published article in *Chemical Geology*) 127
Appendix A: supplementary data for Chapter 8 137
Chapter 9. Conclusions and perspectives 149
9.1. Conclusions 149
9.2 Perspectives 150
9.2.1. Species-specific Hg isotope compositions of coal Hg emissions 151
9.2.2. Post-emission Hg isotope fractionation in coal flue gases 151
9.2.3. Geological controls on Hg isotope fractionation in coal deposits 152
9.2.4. Reconstructing the historical evolution of anthropogenic Hg isotope emission signatures 152
Chapitre 9. Conclusions et perspectives 153
9.1. Conclusions 153
9.2 Perspectives 155
9.2.1. Les signatures isotopiques de formes spécifiques des émissions du Hg 155
9.2.2. Post-emission Hg isotope fractionation in coal flue gases 155
9.2.3. L'origine des variations isotopiques du Hg d'un bassin de charbon. 156

9.2.4. L'evolution historique des emissions isotopiques du Hg 156

References 157

List of Figures 158

List of Tables 161

Appendix A: supplementary data for Chapter 7 162

Appendix B: supplementary data for Chapter 7 173

Figure B3. World coal import-export flow (short Million tons/yr) 174

Figure B4. A preliminary Hg isotope evolution model of world coals from 1815-2010 175

List of abbreviations

AFS	Atomic-fluorescence spectrometry
APCD	Air pollution control device
CFUB	Coal-fired utility boiler
CV	Cold vapor
DMA	Direct mercury analyzer
ESP	Electrostatic precipitator
FGD	Flue-gas desulfurization
GEM	Gaseous elemental Hg(0)
GOM	Gaseous oxidized Hg(II)
Hg	Mercury
MC-ICPMS	Multi-collector inductively coupled plasma mass spectrometry
MDF	Mass dependent fractionation
MIF	Mass independent fractionation
PBM	Particulate-bound Hg(II)
TSP	Total suspended particle

Chapter 1

Introduction

Chapter 1. Introduction

Mercury (Hg) is a persistent toxic element. Following Hg emission into the atmosphere from natural and anthropogenic sources, atmospheric circulation can distribute Hg globally. Depending on its chemical form and on atmospheric oxidants, the atmospheric lifetime of Hg ranges from several days to more than one year. For millennia, and especially since the industrial revolution, human activities such as gold mining, coal combustion and non-ferrous metallurgy have augmented the amount of Hg in the Earth's land-ocean-atmosphere system by a factor of three. Currently, anthropogenic Hg emissions (~2000 tons/year) far surpass those derived from natural processes (~500 tons/year) such as volcanic eruptions and soil degassing.

Mercury is a chalcophile element, and its concentration in coal is determined by many factors such as coal rank, coal provenance, depositional environment of coal deposits and geological activities during and after coal deposition. Sulfide minerals and organic matter are the main Hg carriers in coal. In general, Hg is present at trace levels of 10-1000 ng/g in coal. However, the large volumes of coal used in industrial processes have made coal the dominant Hg emission source. Hg emission from stationary coal combustion, primarily coal-fired power plants, is the largest single source, accounting at present for approximately half of all anthropogenic Hg emissions (~700-900 tons/year) (Pacyna et al., 2010; Pirrone et al., 2010).

Quantitative assessment of the impact of coal Hg emission on local, regional and global ecosystems is of substantial interest to environmental scientists and decision-makers. Moreover, with the implementation of the first global, legally-binding UNEP treaty aimed at reducing anthropogenic Hg emissions, the identification and traceability of coal Hg emissions from different countries or regions is critically important. Hg stable isotope signatures are promising tracers of Hg sources and biogeochemical transformations of Hg. Different Hg sources are characterized by distinct Hg isotope compositions that can be resolved within the analytical uncertainty of modern mass spectrometers. Biogeochemical processes have been shown to fractionate the seven stable Hg isotopes as a function of mass, nuclear volume or nuclear magnetic moment. Most natural samples, including the coals considered here, show Hg isotope variations that are controlled by mass dependent fractionation (MDF, denoted by δ^{202}Hg) and mass independent fractionation related to the magnetic isotope effect (MIF, denoted by Δ^{199}Hg and Δ^{201}Hg). The objective of this PhD dissertation was to evaluate the usefulness of Hg stable isotope signatures to 1) understand the origin of Hg in coal, and 2) trace coal-fired power plant emissions from different global regions.

A 3‰ variation in δ^{202}Hg and a 1‰ variation in Δ^{199}Hg and Δ^{201}Hg have been reported in worldwide coal deposits (Biswas et al., 2008; Lefticariu et al., 2011; Sherman et al., 2012; Sun et al., 2013). In addition, coals from different coal deposits are distinguishable by δ^{202}Hg and Δ^{199}Hg. This suggests that atmospheric Hg emissions from coal combustion in different regions can be distinguished. However, coal combustion processes, Hg inter-species transformations and Hg removal by air pollution control devices in coal-fired power plants potentially generate coal Hg emissions that are significantly different from coal in Hg isotope signatures. Therefore, for successful Hg emission tracing, we need to know at least the following information:

1) Hg isotope signatures of major coal deposits and the ability to distinguish them from each other;

2) The degree to which the Hg isotope compositions are shifted between the emitted bulk flue gases and feed coal;

3) The isotope signatures of gaseous and particulate Hg forms in bulk flue gases at the coal plant smoke stack. This has important implications for near-field and far-field environmental Hg tracing as different Hg species have varying atmospheric reactivities and life-times.

This PhD dissertation is divided into eight chapters to address the above outlined points. Chapters 2 and 3 respectively give a brief review on Hg emissions and cycling, and on Hg isotope fractionation theory. Sampling protocols and Hg isotope measurement techniques are summarized in Chapter 4. Chapters 5-8 contain the main scientific findings, organized in four scientific papers of which two were published. Chapter 5 details a new analytical protocol for extracting Hg from solid samples of low-level Hg. The solid samples were combusted in a tube furnace and trapped into acid solution before measurement by multi-collector inductively coupled plasma mass spectrometry. In Chapter 6 we examine in detail the Hg isotope variations of the Huainan and Jining coal basins in China. We find that natural processes caused a ~2‰ variation of δ^{202}Hg and 0.35‰ of Δ^{199}Hg among coal seams deposited at the same location over a period of 20 Ma. Yet, the same variation is found back within a single coal seam. Correlations between δ^{202}Hg, Δ^{199}Hg, Hg concentration, mineralogy, and other geochemical parameters are visible, but often contradictory and difficult to interpret. In Chapter 7, we develop a coal Hg isotope library by reporting the isotope compositions of 108 new coal samples from major coal-producing basins in Africa, China, Europe, India, Indonesia, former USSR and the USA, adding to the thusfar ~50 published coal samples. A 4.7‰ range in δ^{202}Hg (−3.9 to 0.8‰) and a 1‰ range in Δ^{199}Hg (−0.6 to 0.4‰) are observed. 14 ($p<0.05$) to 17 ($p<0.1$) of the 28 pairwise comparisons between eight global regions are statistically distinguishable on the basis of

δ^{202}Hg, Δ^{199}Hg or both. These findings justify the potential application of Hg isotope signatures to coal Hg emission tracing. Chapter 8 addresses the question whether Hg emissions from coal-fired power plants preserve the Hg isotope signatures of feed coals. To do so, we examined the Hg isotope compositions of feed coals, bottom ash, fly ash and gypsum at six utility boilers of two modern Chinese power plants. Results suggest that stack Hg emissions are only slightly enriched by up to 0.3‰ (δ^{202}Hg) in the heavier Hg isotopes relative to feed coal. Moreover, we are able to develop a generalized Hg isotope fractionation model that relates stack emission δ^{202}Hg to feed coal δ^{202}Hg and Hg removal efficiencies of electrostatic precipitator and wet flue-gas desulfurization emission control technologies.

We conclude in Chapter 9 by summarizing our main findings as follows. The Hg isotope compositions of coal are sufficiently different to distinguish Chinese coals from African, European, Indian and Mongolian coals at $p<0.05$, and from Indonesian, former USSR, and the USA coals at $p<0.10$. Overall, half of all global coal deposits are isotopically distinguishable ($p<0.05$). We evaluated whether coal combustion in coal-fired power plants changes Hg isotope signatures from feed coal to stack emissions, and find that the changes are minor (δ^{202}Hg, <0.3‰) to negligible (Δ^{199}Hg). We consider these combined results to be sufficiently promising to recommend detailed atmospheric Hg isotope tracer studies of coal plant Hg emissions. Nevertheless, as we note in Chapter 9, the different gaseous and particulate forms of Hg emitted from coal plants may carry contrasting Hg isotope signatures. Published work on Hg deposition near a coal plant also points at rapid post-emission changes in Hg isotope signatures (Sherman et al., 2012). More work is needed to address both of these uncertainties. An in-depth exploration of Hg isotope variations in individual coal mines and across a single coal seam point at a complex interplay between multiple factors, including the coal depositional environment, conditions of coalification and post-depositional Hg dynamics. No conclusive relationship between Hg isotope signatures and these factors could be made.

Chapitre 1. Introduction

Le mercure (Hg) est un élément toxique et persistent dans notre environnement. Suite aux émissions naturels et anthropiques du Hg, les courant atmosphériques le distribuent a travers du globe. Selon la forme chimique du Hg et la présence des oxydants, le temps de résidence du Hg dans l'atmosphère varie de quelques jours a plus d'un an. Pendant des millénaires, et en particulier depuis la révolution industrielle, les activités humains tels que l'orpaillage, la combustion du charbon ou les activités métallurgiques ont augmente les teneurs en Hg à la surface de notre planète par un facteur trois. Aujourd'hui, les émissions anthropiques du Hg (~2000 tonnes/an) dépassent largement les émissions naturels (~500 tonnes/an) tels que les éruptions volcaniques et le dégazage des sols.

Le Hg, élément chalcophile, est présent dans le charbon ou son concentration est détermine par le type et l'origine du charbon, l'environnement de déposition du charbon, et les conditions géologiques pendant et après la formation du charbon. Les minéraux soufrés et la matière organique sont les phases porteuses du Hg dans le charbon. Typiquement, les teneurs du Hg dans le charbon sont de l'ordre de 10-1000 ng/g. L les grandes quantités du charbon utilisé par les industries ont propulsé ce secteur comme émetteur du Hg numéro un. En particulier, l'émission du Hg par les centrales au charbon est la première source du Hg vers l'atmosphère et représente à elle seule la moitié des émissions anthropiques du Hg (~700-900 tonnes/an) (Pacyna et al., 2010; Pirrone et al., 2010).

L'évaluation quantitative de l'impact des émissions du Hg par les centrales au charbon sur l'environnement local, régional et globale est devenue une priorité pour les scientifiques et les décideurs en politique d'environnement. La mise en action de la première traité internationale, élaboré sous les auspices de l'UNEP en 2013, sur la réduction des émissions anthropiques du Hg demande des outils adaptés à l'identification et le traçage des différents émissions du Hg provenant des régions du monde. Depuis 2001, la recherche scientifique a montré que les signatures isotopiques du Hg sont des traceurs promettants des sources du Hg et des transformations biogéochimiques du Hg. Différentes sources naturels et anthropiques du Hg ont souvent des signatures isotopiques qui sont suffisamment différents pour être résolues par la spectrométrie de masse moderne. Des processus biogéochimiques ont été montrés de séparer les sept isotopes stable du Hg en fonction de leur masse, volume nucléaire, ou leur moment magnétique nucléaire lors des transformations partièlles. La majorité des échantillons naturels, les charbons étudiés ici inclus, montrent des fractionnements isotopiques soit dépendents de la masse (MDF, représenté par δ^{202}Hg), ou

indépendants de la masse des isotopes (MIF, représenté par Δ^{199}Hg and Δ^{201}Hg). Les objectives principales de ces travaux de thèse ont été d'évaluer l'applicabilité des signatures isotopiques du Hg à 1) comprendre l'origine du Hg dans les charbons, et 2) tracer les émissions du Hg des centrales au charbon de différentes régions du monde.

Deux études précédentes ont montrés des variations isotopiques de 3‰ du δ^{202}Hg et de 1‰ du Δ^{199}Hg et Δ^{201}Hg dans des charbons d'origines différentes (Biswas et al., 2008; Lefticariu et al., 2011; Sherman et al., 2012; Sun et al., 2013). Ces résultats suggérèrent que les émissions du Hg des centrales au charbon de différentes régions du monde sont potentiellement traçable. Cependant la combustion du charbon comprend des transformations des formes physicochimiques du Hg et une dépollution partièlle des gaz de combustion qui peuvent dans son ensemble modifier les signatures isotopiques du charbon. Afin d'évaluer la traçabilité des émissions du Hg des centrales au charbon, il est désormais nécessaire de comprendre les aspects suivants :

1) Les signatures isotopiques du Hg dans les charbons alimentant les centrales au charbon.

2) L'amplitude du fractionnement isotopique eventuelle entre le charbon et les emissions du charbon à la cheminee d'une centrale au charbon.

3) Les signatures isotopiques des formes gazeuses et particulaires du Hg émis par les centrales au charbon. Ceci a un impact sur le traçage de ces émissions vers l'environnement locale (formes particulaires) et globale (formes gazeuses), car les différentes formes du Hg ont des demi-vies atmosphériques très contrastés.

Cette thèse a été organisé en huit Chapitres afin de traiter les objectifs établies ci-dessus. Chapitres 2 et 3 dressent l'état de l'art sur les émissions et cycle biogéochimique du Hg, et sur la théorie du fractionnement isotopique du Hg respectivement. Chapitre 4 résume les protocoles de mesure des rapports isotopiques par spectrométrie de masse. Les Chapitres 5-8 résument les principaux résultats scientifiques organises sous quatre publications scientifiques de rang A (dont 2 publies). Chapitre 5 détaille un nouveau protocole d'extraction du Hg par méthode de combustion et piégeage acide, adapté aux charbons et d'autres échantillons solides de faible teneurs en Hg. Le Chaptire 6 explore les variations isotopiques du mercure au sein d'une seule mine de charbon, et au sein d'une seule couche de charbon dans le bassin d'Huainan et d'Jining en Chine. Nous observons une variation de ~2‰ en δ^{202}Hg et de 0.35‰ en Δ^{199}Hg tout au long des couches de charbon déposés pendant 20 millions d'années. Des corrélations entre δ^{202}Hg, Δ^{199}Hg, concentrations en Hg, minéralogie, et

autres paramètres géochimiques sont observés, mais parfois contradictoires et difficile à interpréter. Le Chapitre 7 présente une libraire de signatures isotopiques du Hg dans les charbons basé sur ~50 données publies auparavant, et 108 nouvelles mésures de nombreuses basins de charbon mondiales, incluant, l'Afrique, la Chine, l'Europe, l'Inde, l'Indonésie, la Mongolie, l'ancient USSR et les Etats-Unis. Nous observons une variation isotopique de 4.7‰ en δ^{202}Hg (−3.9 a 0.8‰) et de 1‰ en Δ^{199}Hg (−0.6 a 0.4‰). 14 ($p<0.05$) à 28 ($p<0.1$) des 28 comparaisons possibles entre les huit principales régions producteur du charbon du monde sont statistiquement différenciable selon leurs δ^{202}Hg, Δ^{199}Hg ou les deux. Cette observation justifie pleinement l'application potentiel de tracer les émissions du Hg provenant des centrales au charbon du monde. Le Chapitre 8 examine la question si les émissions du Hg des centrales au charbon préservent les signatures isotopiques des charbons combustés. Nous avons étudiés les compositions isotopiques du Hg dans les charbons, les cendres résiduels, les cendres volants et le gypse de six chaudrons de deux grands centrales de charbon Chinoises. Les résultats montrent que les émissions du Hg par la cheminée sont enrichis au maximum de 0.3‰ en δ^{202}Hg par rapport au Hg dans le charbon combusté. Nous avons également pu établir un modèle du fractionnement isotopique du Hg dans les centrales de charbon, lequel estime le δ^{202}Hg des émissions en fonction du δ^{202}Hg du charbon et les techniques de lavage de gaz comme la précipitation électrostatique et le désulfurisation.

Le Chapitre 9 conclue la thèse en résumant les avancées et perspectives principales. Nous proposons que les signatures isotopiques du Hg dans les charbon du globe sont suffisamment différents qu'on peut distinguer par exemple le charbon Chinois des charbons Africains, Européens, Indiens et Mongoliens (avec une intervalle de confiance de 95%), et des charbons Indonésiens, Américains et Russes (avec une intervalle de confiance de 90%). Plus de la moitié de tous les charbons du globe, organises par régions, sont différenciable par leurs signature isotopiques du Hg. Notre évaluation du fractionnement isotopique du Hg dans les centrales de charbons mêmes montre que cet artefact est mineur (δ^{202}Hg, <0.3‰) à négligeable (Δ^{199}Hg). Nous considérons que l'ensemble de ces deux résultats est assez prometteur pour recommander des études plus approfondis sur le traçage des émissions du Hg des centrales au charbon à l'échelle de notre planète. Désormais, comme nous le soulignons dans le Chapitre 8, les différentes formes gazeuses et particulaires du Hg sortant des cheminées peuvent avoir des signatures isotopiques très contrastes. Une étude publiée récemment contraste les signatures isotopiques des dépôts du Hg par précipitation humide dans l'environnement locale d'un centrale à charbon avec les signatures du charbon combusté, et trouve qu'elles ne ressemblent pas. Des études supplémentaires sur les formes du Hg sortant de la cheminée et sur les transformations atmosphériques du Hg doivent être fait afin de comprendre ces observations. Notre

exploration des variations isotopiques du Hg au sein d'une seule mine et couche de charbon montre des interactions complexes entre l'environnement de déposition de charbon, la charbonification même, et les processus géologiques post-dépositionels. Des relations claires entre ces facteurs et les signatures isotopiques des charbons nous échappent pour l'instant.

References

Biswas, A., Blum, J.D., Bergquist, B.A., Keeler, G.J., Xie, Z., 2008. Natural Mercury Isotope Variation in Coal Deposits and Organic Soils. Environmental Science & Technology 42, 8303-8309.

Lefticariu, L., Blum, J.D., Gleason, J.D., 2011. Mercury Isotopic Evidence for Multiple Mercury Sources in Coal from the Illinois Basin. Environmental Science & Technology 45, 1724-1729.

Pirrone, N., Cinnirella, S., Feng, X., Finkelman, R.B., Friedli, H.R., Leaner, J., Mason, R., Mukherjee, A.B., Stracher, G.B., Streets, D.G., Telmer, K., 2010. Global mercury emissions to the atmosphere from anthropogenic and natural sources. Atmospheric Chemistry and Physics 10, 5951-5964.

Pacyna, E.G., Pacyna, J.M., Sundseth, K., Munthe, J., Kindbom, K., Wilson, S., Steenhuisen, F., Maxson, P., 2010. Global emission of mercury to the atmosphere from anthropogenic sources in 2005 and projections to 2020. Atmospheric Environment 44, 2487-2499.

Sherman, L.S., Blum, J.D., Keeler, G.J., Demers, J.D., Dvonch, J.T., 2012. Investigation of Local Mercury Deposition from a Coal-Fired Power Plant Using Mercury Isotopes. Environmental Science & Technology

Sun, R., Heimbürger, L.-E., Sonke, J.E., Liu, G., Amouroux, D., Berail, S., 2013. Mercury stable isotope fractionation in six utility boilers of two large coal-fired power plants. Chemical Geology 336, 103-111.

Chapter 2

Mercury (Hg) emission from coal combustion and its role in the global biogeochemical Hg cycle

Chapter 2. Mercury (Hg) emission from coal combustion and its role in the global biogeochemical Hg cycle

2.1. Hg and its toxicology/epidemiology

2.1.1. Hg and its physicochemical properties

Mercury (Hg) is a naturally occurring d-block element with atomic number 80 and approximate atomic weight 200.59. It is the only metal that is in liquid state at standard temperature and pressure. Elemental Hg has a unique electronic configuration of [Xe] $4f^{14}$ $5d^{10}$ $6s^2$, in which electrons occupy all the available 1s, 2s, 2p, 3s, 3p, 3d, 4s, 4p, 4d, 4f, 5s, 5p, 5d and 6s subshells. The presence of the filled 4f shell poorly screens the nuclear charge and thus enhances the attractive force between 6s shell electrons and the nucleus. Hg has three redox states in nature: 0, I and II. Different Hg forms can be transformed between each other. For example, Hg(0) can be oxidized into Hg(II) by atmospheric oxidants such as OH, halogen radicals and ozone. Aqueous forms of Hg(II) can be reduced into Hg(0) by specific ligands of organic matter, photochemistry and biotic reactions (Holmes et al., 2010; Selin, 2009; Zhang, 2006). Hg of zero valence state is in form of Hg(0) vapor or liquid metal, whereas Hg(I) and Hg(II) are in form of inorganic and organic complexes. Due to the filled electronic structure, gaseous Hg(0) is rather stable under natural condition and has an atmospheric lifetime ranging from several months to >1 year (Selin et al., 2008). The high volatility and mobility of atmospheric Hg(0) make it a globally transported pollutant (Mason et al., 1994). Hg(I) usually forms simple compounds by metal-metal bonds, such as Hg_2(II), and has a high tendency to be further oxidized to Hg(II). Hg(II) is the most common oxidation state in nature and forms stable derivatives with the anions of chalcogens and halogens, such as HgS, HgSe, $HgCl_2$ and HgI_2. Hg in most naturally occurring minerals (e.g. cinnabar, metacinnabar, HgS) is also in the form of Hg(II). In addition, Hg(II) forms organo-mercury complexes, in formulas of HgR_2 or HgRX (R= aryl or alkyl; X=halide or acetate), observed in various environmental compartments. Monomethylmercury (CH_3Hg, abbreviated as MMHg), produced from inorganic Hg(II) by biotic and/or abiotic processes, is a potent neurotoxin (Hsu-Kim et al., 2013).

2.1.2. Hg toxicology/epidemiology

Modern research interest in Hg toxicology and epidemiology dates back to the 1950s MMHg poisoning incident in Minamata Bay, Japan (Harada, 1995; McAlpine and Araki, 1958). The general

human population is commonly exposed to low or moderate doses of MMHg through consumption of fish (Sunderland, 2007). MMHg exposure can cause a variety of adverse effects on human health such as sensory disturbances, ataxia, dysarthria, constriction of the visual field, auditory disturbances and tremor as seen in Minamata disease (Harada, 1995). Moreover, MMHg can affect the neurological development of infants even when pregnant women are subjected to low-level MMHg exposure (Davidson et al., 2004).

A reference dose for fetal MMHg neurotoxicity (defined as the estimate of daily MMHg exposure to a human population that is likely without appreciable risk of deleterious effects during a lifetime) has been reviewed and established by the National Research Council of the US National Academy of Sciences (NRC/NAS, 2000). The reference dose level for women of childbearing age and infants by the United States Environmental Protection Agency (US EPA) is 5.8 μg/l Hg in cord blood, which is translated to 0.1 μg Hg per kg bodyweight per day (μg/kg bw/day) or 1.4 μg/g Hg in human hair. Twenty percent of women in the United States surpass the US EPA guidelines. Public health institutions in developed countries commonly provide fish consumption advisories for citizens. The World Health Organization recommends a provisional tolerable MMHg intake of 3.3 μg/kg bw/week for adults, which corresponds to approximately 7 μg/g Hg in human hair.

However, fish consumption has a variety of health benefits when dietary MMHg is present at low levels because of the nutrient components in fish (e.g. n-3 polyunsaturated fatty acids) (Daniels et al., 2004). Therefore, it is important to balance the trade-offs between health benefits from fish consumption and potential MeHg exposure risks (Egeland and Middaugh, 1997). Nevertheless, limiting anthropogenic Hg emissions to our environment can only have beneficial effects on human (child neurodevelopment) and wildlife health.

2.2. Hg geochemistry in coal and Hg emissions from coal combustion

2.2.1. Coal formation and coalification

Coal is a combustible, sedimentary and organic rock formed from prehistoric vegetation remains that accumulated in swamps and peat bogs. The build-up of sediments (silt, sand, mud) and multi-phases of tectonic movements buried these decayed vegetations at great depth where they were subjected to high temperature/pressure and subsequently evolved from peat to coal. According to the organic maturity of coal, it can be divided into two broad ranks: low-rank coal (i.e. brown coal including lignite and sub-bituminous coal) and high-rank coal (i.e. hard coal including bituminous coal and

anthracite) (Figure 1). Low-rank coal could be transformed to high-rank coal at appropriate geological conditions. As compared to high-rank coal, low-rank coal is characterized by higher moisture and lower calorific values. Low-rank coal is used for power generation and industrial manufacturing. Bituminous coal is widely used in the metallurgical industry (coking coal) and in electricity generation (thermal coal). Anthracite, which represents only 1% of all coal reserves, mainly serves as domestic fuel.

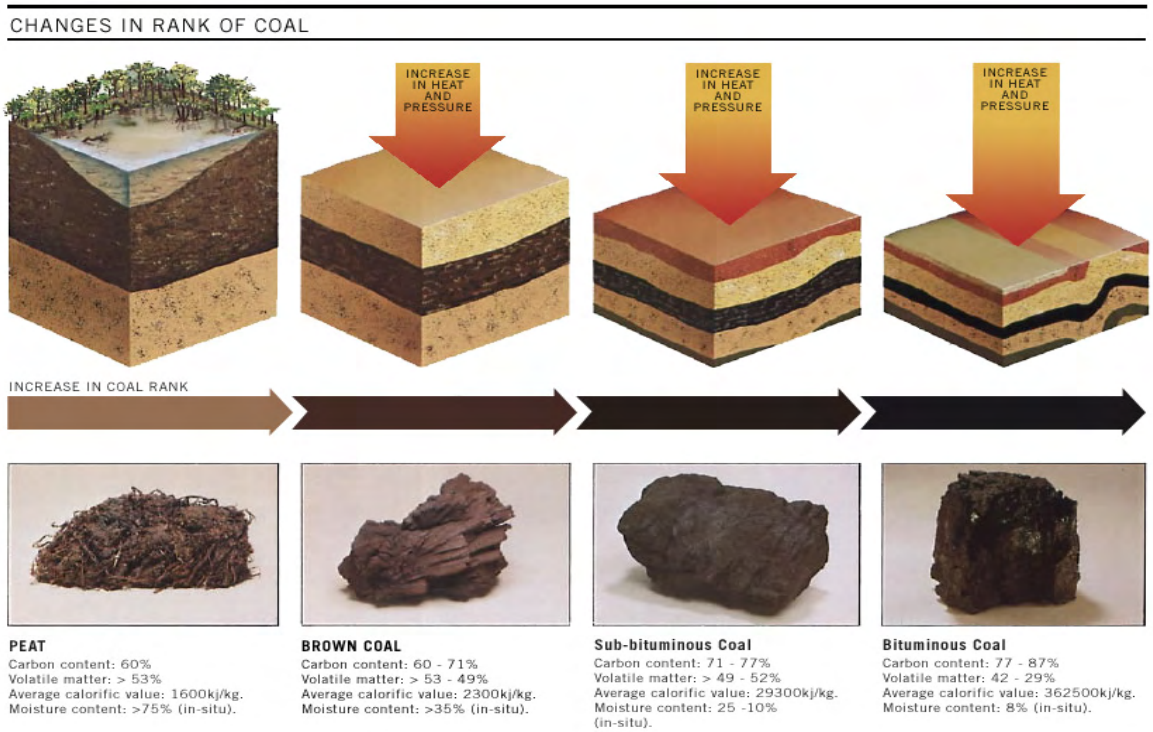

Figure 1 Classification and evolution of coal (Source: ACARP)

2.2.2. Coal as an energy base

The estimated coal reserve that can be recovered in the world is ~86100 Mt (Million tons), which can last for more than 100 years, the longest lifetime among all fossil fuels, if coal production continues at present rate. The USA (28%), Russia (18%), China (13%), Australia (9%) and India (7%) are the 5 countries that hold ~75% of the world coal reserves (Table 1). As compared to 2010, the world coal production grew by 6.1% in 2011, reaching to 3955 Mtoq (oil equivalent). Meanwhile, coal consumption grew by 5.4%, reaching ~3724 Mtoq, the fastest growing energy among fossil fuels. Coal (3724 Mtoq) accounts for approximately 30% of world energy consumption (12275 Mtoq) in which 87% is contributed by fossil fuels (~10689 Mtoq) (BP, 2012). The proportion of coal in fossil fuel consumption is as high as 75% for China and South Africa, 60% in India, which are well above

Table 1. Summary of world coal reserve, production, consumption, export and import in 2011

Reserve (Mt)						Production (Mt oil equivalent)			
Counties	**Hard coal[a]**	**Brown coal[b]**	**Total**	**Share of Total**	**R/P ratio[c]**		**2011**	**growth rate[d]**	**share**
USA	108501	128794	237295	27.6%	239	**China**	1956.0	8.8%	49.5%
Russia	49088	107922	157010	18.2%	471	**USA**	556.8	0.9%	14.1%
China	62200	52300	114500	13.3%	33	**Australia**	230.8	-2.2%	5.8%
Australia	37100	39300	76400	8.9%	184	**India**	222.4	2.3%	5.6%
India	56100	4500	60600	7.0%	103	**Indonesia**	199.8	18.1%	5.1%
Germany	99	40600	40699	4.7%	216	**Russia**	157.3	4.1%	4.0%
Ukraine	15351	18522	33873	3.9%	390	**South Africa**	143.8	0.3%	3.6%
Kazakhstan	21500	12100	33600	3.90%	290	**Kazakhstan**	58.8	4.5%	1.5%
South Africa	30156		30156	3.5%	118	**Poland**	56.6	2.0%	1.43%
Colombia	6366	380	6746	0.78%	79	**Colombia**	55.8	15.4%	1.41%
Total 10 countries	**386461**	**404418**	**790879**	**92%**	**212**	**Total 10 countries**	**3638**	**5.4%**	**92%**
Total World	**404762**	**456176**	**860938**	**100%**	**112**	**Total World**	**3956**	**6.1%**	**100%**
Consumption (Mt oil equivalent)				**Export (Mt)**			**Import (Mt)**		
	2011	**Growth rate[d]**	**Share**		**2011**	**Share**		**2011**	**Share**
China	1839.4	9.7%	49.4%	**Indonesia**	309	29.7%	**China**	177	17.7%
USA	501.9	-4.6%	13.5%	**Australia**	285	27.4%	**Japan**	175	17.5%
India	295.6	9.2%	7.9%	**Russia**	99	9.5%	**South Korea**	129	12.9%
Japan	117.7	-4.8%	3.2%	**USA**	85	8.2%	**India**	101	10.1%
South Africa	92.9	1.7%	2.5%	**Colombia**	76	7.3%	**Taiwan**	66	6.6%
Russia	90.9	0.8%	2.4%	**South Africa**	70	6.7%	**Germany**	41	4.1%
South Korea	79.4	4.6%	2.13%	**Kazakhstan**	34	3.3%	**UK**	32	3.2%
Germany	77.6	1.2%	2.1%	**Canada**	24	2.3%	**Turkey**	24	2.4%
Poland	59.8	6.0%	1.6%	**Vietnam**	23	2.2%	**Italy**	23	2.3%
Australia	49.8	13.6%	1.3%	**Mongolia**	22	2.1%	**Malaysia**	21	2.1%
Total 10 countries	**3205**	**3.7%**	**86%**	**Total 10 countries**	1027	98.7%	**Total 10 countries**	**798**	**79%**
Total World	**3247**	**5.4%**	**100%**		1041	100%		**1002**	**100%**

Note: 1 t oil equivalent equals approximately 1.5 tons hard coal or 3 tons lignite; coal reserve, production, consumption data are cited from BP (2012) and export and import data are cited from IEA (2012). [a]bituminous coal and anthracite; [b]lignite and sub-bituminous coal; [c] length of time (years) that the remaining coal reserves would last if production were to continue at 2011 rate; [d] change of production or consumption in 2011 over 2010

the world average value of 35%. Most of the growth in coal production and consumption was contributed by non-OECD (Organization for Economic Co-operation and Development) countries. China, alone, overwhelmingly contributed to ~50% of world coal production and consumption in 2011. Besides, China is also the largest coal importer. Although Indonesia only accounts for 0.6% of world coal reserves, its coal production had the highest growth rate of 18.1% and reached a 5.1%

share (~200 Mtoq) of world coal production (Table 1). While it only accounts for 1.2% (44 Mtoq) of world coal consumption, most of its coal production is exported to the Asia-Pacific region (primarily to Japan and Taiwan and lesser amounts to South Korea, the Philippines and China) (Belkin et al., 2009). Indonesia has become the largest exporter of thermal (steam) coal and the second largest combined thermal and metallurgical (coking) coal exporter in the world market. As Japan and South Korean have very small coal reserves and production shares (<0.05%), most of their coal consumption relies on imports. Coal plays an important role in worldwide energy production, 55% of the produced coal is used in electricity plants (IEA, 2012). More than 40% of electricity in the world is powered by coal. China, USA, India, South Africa and Australia use coal to generate 79%, 45%, 68%, 93% and 78% of their respective national electricity needs.

2.2.3. Hg geochemistry in coal

Coal is mainly composed of C, H, O, N, S that are derived primarily from vegetation. Abundant inorganic elements can be carried into coal through overlying sediments, river inputs and geological activities. The elements in coal can be generally grouped by their abundances (Swaine, 1990). Elements with abundances ≥0.1% such as C, H, O, N, S, Si, Al, Fe, Ca, K, Na, Mg and Ti are defined as major elements, whereas the remaining elements with abundances <0.1% are trace elements.

Hg is a chalcophile element and is present at trace levels in coal. The concentration of Hg in coal is determined by many factors such as coal rank and provenance, depositional environment, and geological activities (e.g. igneous intrusion and groundwater infiltration) during and after coal deposition (Dai et al., 2012). Since the second half of the 20th century, coal geochemists have continued to investigate Hg geochemistry (e.g. concentrations, distributions, modes of occurrences and provenances) in worldwide coals (Bouška, 1981; Swaine, 1990; Swaine and Goodarzi, 1995; Valković, 1983). These studies conclude that Hg in coal mainly combines with S-containing functional groups of organic matter and sulfides. Generally, Hg in coal varies from 10 to 1000 ng/g, although extremely high coal Hg, up to several tens of μg/g, were found in geologically active areas (Dai et al., 2012; Dai et al., 2006b; Yudovich and Ketris, 2005). The newly updated average Hg abundance in world coals is 100 ng/g regardless of coal rank (Ketris and Yudovich, 2009), which is lower than Chinese (163 ng/g) (Dai et al., 2012) and US coals (170 ng/g) (Finkelman, 1993). Hg is classified as high coalphile element (i.e. how efficiently coal acted as a geochemical sink for elements, during all of its geologic history), with a coal affinity index (dividing the average

elemental abundance in coal on ash basis by that in sedimentary rocks) of more than 10 (Ketris and Yudovich, 2009). The higher the coal affinity index of a given element, the higher is the contribution of its authigenic fraction (organic matter or micro-minerals), and the lower is the contribution of its clastogenic fraction (macro-minerals in alumino- and silicatic-forms). Therefore, authigenic minerals (primary sulfides such as pyrite) and organic matter are the main Hg carriers in coal, and their contributions to whole coal Hg vary according to the coal-forming environment. In some coals extremely enriched in Hg, Hg can occur as cinnabar (HgS) and metallic Hg (Piedad-Sánchez et al., 2004; Yudovich and Ketris, 2005). Other minerals such as marcasite (Hower et al., 2008), Au minerals (Seredin, 2004; Seredin and Finkelman, 2008), Pb, Zn and Se minerals (galena, sphalerite, clausthalite) (Dai et al., 2006b; Hower and Robertson, 2003), getchellite (Dai et al., 2006a), calcite and chlorite (Zhang et al., 2004) are also detected in coal with varying Hg levels.

Low-temperature fluids such as deep-circulating meteoric waters are enriched in many kinds of transition metals (notably chalcophile elements As, Hg, Zn and Pb), and can penetrate coal seams along surrounding faults. As a rule of thumb, late-stage pyrite (or secondary pyrite, in cleat-, vein-, fracture-infilling and massive bedding forms, with Hg concentrations up to 100 μg/g) derived from mineralization of epigenetic low-temperature fluids is found to be the main Hg phase in high Hg coals (Diehl et al., 2004; Kolker, 2012). In contrast, pyrite in the from of framboidal aggregates, which are hollow nuclei and vesicles that formed during coal diagenesis, are commonly much less enriched in Hg, generally less than 1 μg/g. Hg in pyrite exists in the form of solid solutions (Finkelman, 1994). Hg containing pyrite distributed throughout the coal matrix is commonly rejected during pulverizing processes before coal combustion in power plants. In doing so, sulfur along with Hg in coal will be significantly reduced. In addition, coal beneficiation at coal clean plants before coal delivery to power plants also serves to reduce Hg in coal.

2.2.4. Hg partitioning during coal combustion

The behavior of elements during coal combustion in a coal-fired utility boiler (CFUB, i.e. boiler at a coal fired electricity plant) can be generally classified into three categories: non-volatile, semi-volatile and volatile (Meij, 1994). Like Cl and F, Hg is classified as a volatile element. A large portion of Hg in CFUB exists as gaseous Hg(0) and is not readily concentrated in ash fractions (Hassett and Eylands, 1999). For the CFUBs installed with electrostatic precipitator (ESP) and wet flue-gas desulfurization (WFGD) systems, the Hg emission can be significantly reduced (Hower et al., 2010; Lee et al., 2006). Taking a >20 years case study in the Netherlands as an example, Hg is

partitioned as follows: <1% in the bottom ash, 49% in the fly ash collected in the ESP, 17% in the FGD gypsum, 9% in the sludge of the wastewater treatment plant, <1% in the effluent of the wastewater treatment plant, <1% in fly dust (leaving the stack), and 25% as gaseous Hg in the flue gases and emitted into the air (Meij and te Winkel, 2006; Meij et al., 2002). Thus, the total removal efficiency of CFUB with ESP+WFGD is ca. 75%. In addition, for CFUB with additional selective catalytic reduction (SCR for NO*x* reduction), the total Hg removal efficiency can reach up to 90%.

The Hg partitioning in different coal combustion residuals is primarily determined by the Hg speciation in flue gas. Hg speciation in itself largely depends on feed coal ranks (in terms of elements such as Cl and S that dominate the conversion of Hg(0) to Hg(II)), combustion systems conditions (in terms of unburned carbon in fly ash) and operating condition of ESP and WFGD (in terms of temperature, the compositions of limestone slurry etc.) (Gale et al., 2008; Niksa et al., 2001; Zhang et al., 2012). In coal combustion flue gas, Hg exists in three operational forms: gaseous elemental Hg(0) (GEM), gaseous oxidized Hg(II) (GOM), and particulate-bound Hg(II) (PBM). The main physicochemical processes acting during the combustion assembly can be divided into four stages: 1) thermal reduction of matrix Hg(II) in feed coal and vaporization of generated GEM in the boiler at 1200-1500 °C; 2) partial oxidation of GEM below 600 °C into GOM and PBM compounds, of which PBM is quantitatively removed with fly ash in the ESPs; 3) partial dissolution of residual GOM compounds into the limestone slurry and subsequent incorporation into WFGD products (mainly gypsum) and 4) the emission of remaining gaseous Hg (primarily GEM and GOM) contained in flue gas into the atmosphere.

2.2.5. Atmospheric Hg emissions from coal combustion

The combustion of fossil fuels (primarily coal) in stationary combustion facilities such as utility, industrial and residential boilers is the single largest anthropogenic Hg emission source globally. According to estimations of Pacyna and co-workers, coal atmospheric Hg emissions account for 60% of total anthropogenic Hg in 1990 (1295 out of 2140 t) (Pacyna and Pacyna, 1996), 77% in 1995 (1475 out of 1910 t) (Pacyna and Pacyna, 2002) , and then 65% in 2000 (1422 out of 2190 t) (Pacyna et al., 2006) and 45% in 2005 (880 out of 1930 t) (Pacyna et al., 2010). The decreased trend of Hg emissions from fossil fuels relates to the expansion of air pollution control devices (ESP, FGD) which largely countered increasing Hg emissions due to the increasing coal consumption. As compared to other anthropogenic Hg sources, the Hg emission inventory from stationary fuel combustion is the most accurate with the lowest uncertainty of ±25%. Globally, China, India and the

USA have the largest Hg emission inventories from stationary fuel combustion besides other anthropogenic sources (Pacyna et al., 2010). On average, the major chemical forms of Hg species in coal combustion emissions are GEM (50%), followed by GOM (40%) and then PBM (10%). As coal Hg emissions dominate global Hg emissions, the same speciation is estimated for global anthropogenic Hg emissions (53%, 47% and 10%, respectively, for GEM, GOM and PBM, Pacyna et al., 2010).

Nowadays, nearly half of the Hg emissions from anthropogenic sources in China (600-800 t/yr) derive from coal combustion (Pacyna et al., 2010; Pirrone et al., 2010; Streets et al., 2005; Wu et al., 2006). Hg emissions from coal combustion were stable at 200-210 t during 1995-2001, but increased to 257 t in 2003 and 334 t in 2005, with an annual average growth rate of 5.1 % per year during a decade (1995-2005) (Wang et al., 2000; Wu et al., 2006). Correspondingly, coal consumption for coal-fired power plants was 446 Mt in 1995 (31% of total coal consumption of 1460 Mt) and doubled to 1050 Mt in 2005 (40% of total coal consumption of 2650 Mt), with an annual average growth rate of ~9%. Among various coal combustion facilities, Hg emissions from coal-fired power plants had the largest annual growth rate of 7% that increased from 63 Mt in 1995 to 125 Mt in 2005 (Streets et al., 2009). The recent 2008 estimation of power plant Hg emissions, using a chlorine-based probabilistic model, was 102.5 t (P50) within a confidence interval of 71.7 (P10) -183 t (P90) (Zhang et al., 2012). Different scenarios have been proposed for estimating the future power plant Hg emissions which will largely depend on the amount of fuel (mainly coal) consumption and the implementation and effectiveness of air pollution control devices.

2.3. Global Hg emissions and biogeochemical cycling

Hg emissions include contributions from natural and anthropogenic sources. Geological Hg emissions derived from volcanic and hydrothermal activity and Hg-enriched crusts are the primary natural sources, estimated to be between 90 and 700 t/yr (Bagnato et al., 2011; Nriagu and Becker, 2003; Pyle and Mather, 2003; Varekamp and Buseck, 1986). For millennia, especially after the industrial revolution (1850 AD), human activities such as mining and fossil fuel combustion greatly augmented Hg emissions to the atmosphere. At present, anthropogenic Hg emissions far surpass natural Hg emissions. Earlier estimations of present-day primary anthropogenic Hg emissions vary between 1900 and 4000 t/yr (Lamborg et al., 2002; Mason et al., 1994; Mason and Sheu, 2002; Pacyna et al., 2010; Pirrone et al., 2010; Sunderland and Mason, 2007). Recent estimation of anthropogenic Hg emissions converge to 1930-2320 t/yr (Pacyna et al., 2010; Pirrone et al., 2010;

Streets et al., 2011). Besides Hg emissions from coal combustion, other dominant sources include artisanal small-scale gold mining, non-ferrous metals manufacturing, cement production, waste disposal and caustic soda production (Figure 2A). Geographically, anthropogenic Hg emissions in Europe and North America decreased significantly since the 1990s, accounting for <25% of total anthropogenic Hg emissions, whereas anthropogenic Hg emissions in Asia have increased substantially to 50-70% (Figure 2B), particularly in China and India.

Following atmospheric deposition of primary natural and anthropogenic Hg to land and ocean surfaces, a portion of Hg termed secondary natural and anthropogenic Hg or 'legacy Hg', can be re-emitted back into the atmosphere (Figure 3). Secondary Hg sources derive from re-emission of newly and historically deposited Hg on vegetation, land and water surfaces. A well-known Canadian enriched Hg isotope field experiment (METAALICUS) (Hintelmann et al., 2002) has shown that the newly deposited atmospheric Hg (II) to terrestrial surfaces is more available for Hg re-emission (termed as prompt recycling) on a timescale of days to months than the historical Hg stored in soil and vegetation on a timescale of centuries to millennia. It is estimated that prompt cycling Hg accounts for 5-60% of atmospherically deposited Hg. Selin et al. (2008) estimated a value of 600 t/yr for prompt recycling Hg. Hg incorporated into soils can be reduced to Hg(0) vapor by a series of abiotic and biotic processes and re-emitted into the atmosphere. Evapotranspiration and volatilization are the main processes to mobilize Hg in soil water and solid soil pools, which emit comparable Hg fluxes of ~550 t/yr. Large re-emissions of Hg, with a flux of ~5000 t/yr, occur from the oceans through Hg(0) evasion (Selin et al., 2008). By incorporating 4000 years of historic Hg emissions, a recent model study suggests that the contribution of re-emitted legacy Hg is much larger than thus far appreciated (Amos et al., 2013). The estimated legacy Hg contribution to modern atmospheric Hg deposition is as large as 60%, and the accumulated legacy Hg in the surface ocean contributed by North American and European (31%) outweighs Asian contributions (18%).

Atmospheric Hg deposition to land and surface oceans will eventually be buried in deep ocean sediments at a time-scale of centuries to millennia. By parameterizing Hg inventory and Hg transfer rates, various global 3-D land-ocean-atmosphere Hg models have been developed to simulate the biogeochemical cycling of Hg (Figure 3) (Seigneur et al., 2001; Selin, 2009; Selin et al., 2008; Streets et al., 2011). These models fit well to the general observations on the distribution of Hg species on the earth, and are able to predict the response of atmosphere-ocean-terrestrial systems to future Hg emission fluctuations.

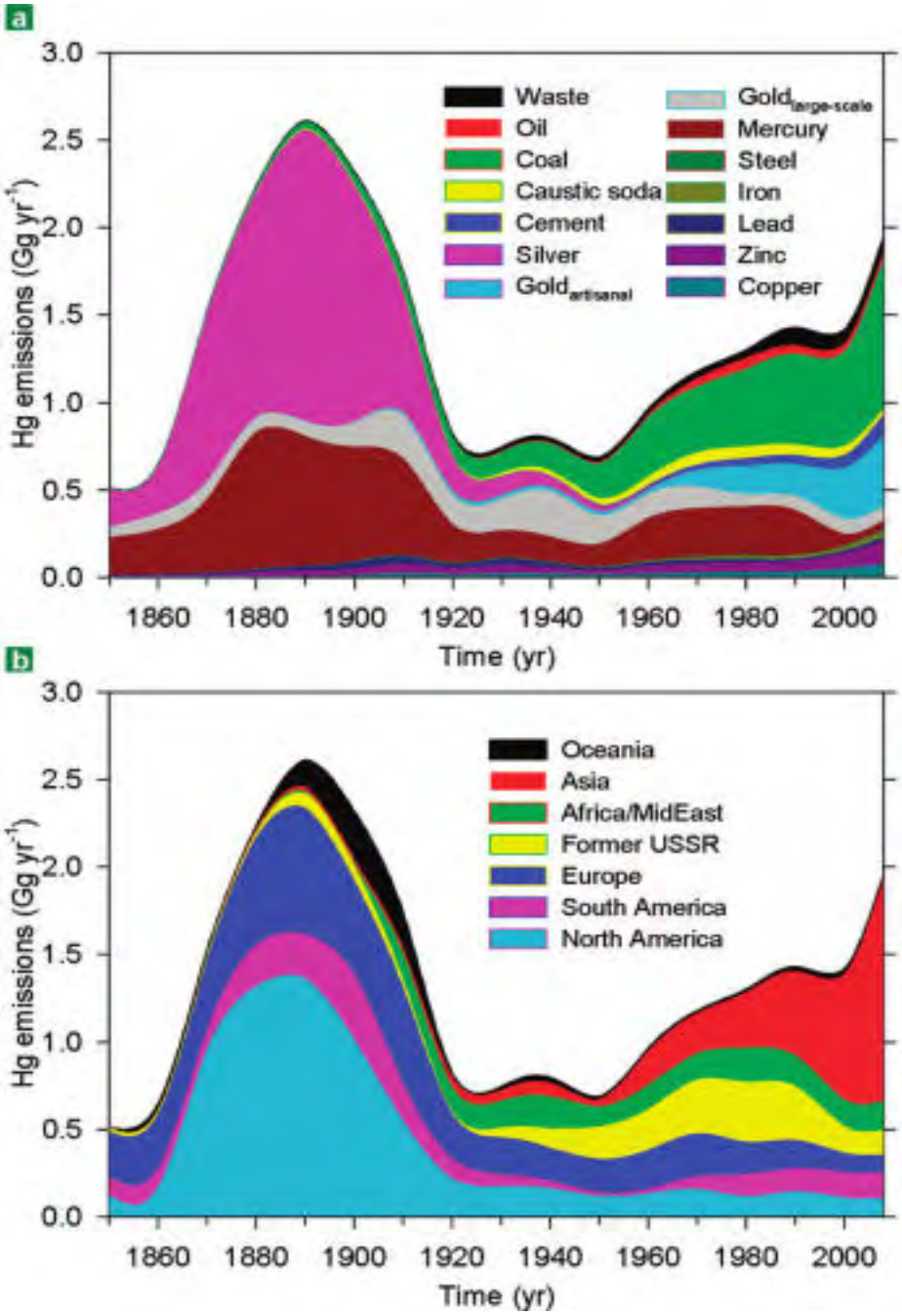

Figure 2 Trends in Hg emissions by (a) source types and (b) world regions (Source: Streets et al., 2011)

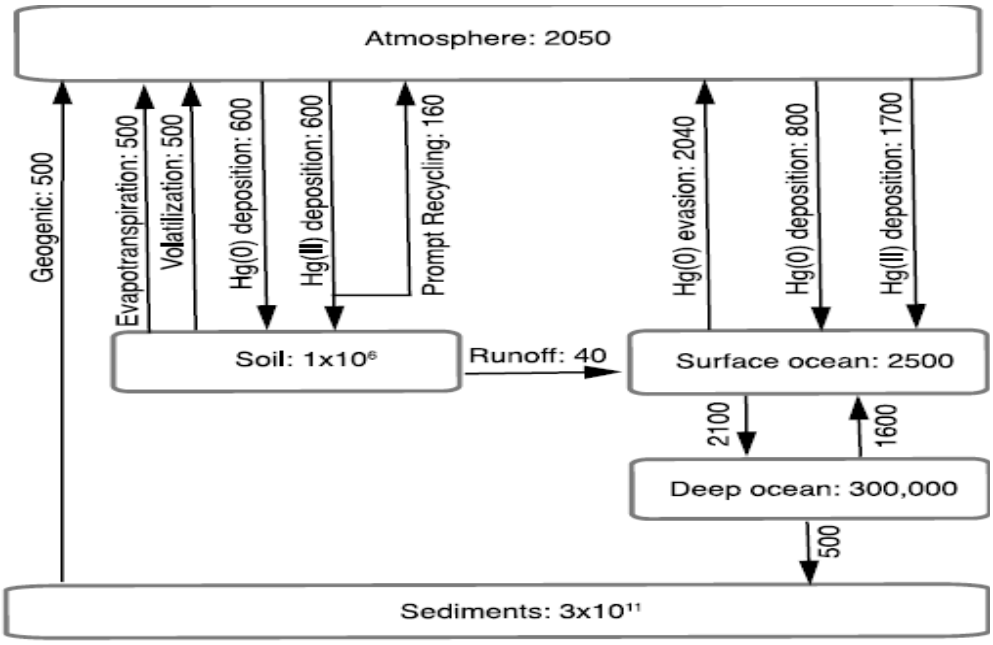

(A)

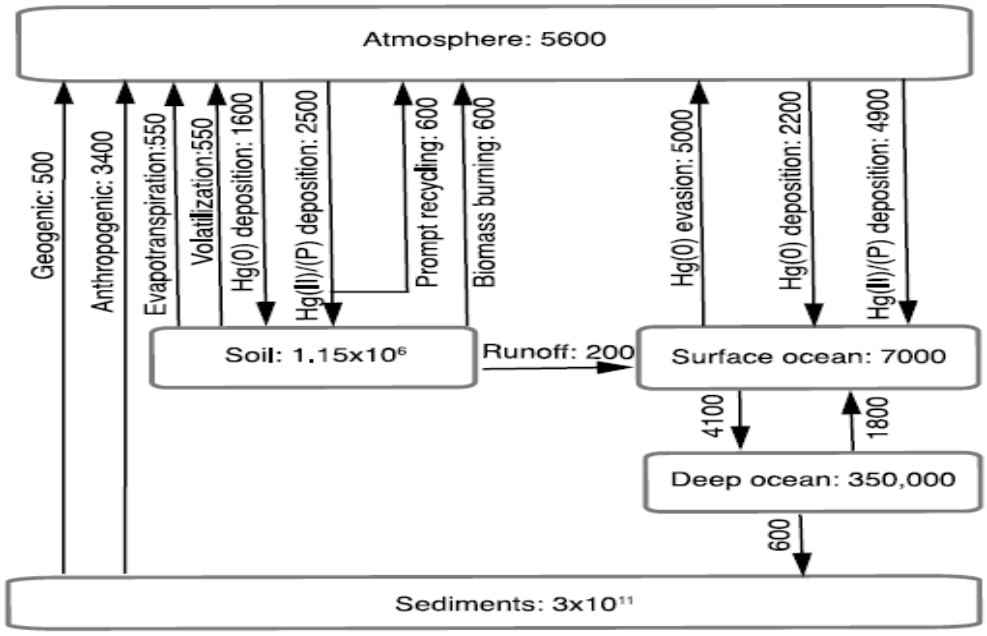

(B)

Figure 3 Global pre-industrial (a) and present-day biogeochemical cycle of mercury in GEOS-Chem. Inventories are in Mg, and rates are in Mg/yr (Source: Selin et al., 2008)

References

ACARP, Underground Coal Australian Coal Association Research Program. accessed by http://www.acarp.com.au/index.aspx.

Amos, H.M., Jacob, D.J., Streets, D.G., Sunderland, E.M., 2013. Legacy impacts of all-time anthropogenic emissions on the global mercury cycle. Global Biogeochem. Cycles 27, 410-421.

Bagnato, E., Aiuppa, A., Parello, F., Allard, P., Shinohara, H., Liuzzo, M., Giudice, G., 2011. New clues on the contribution of Earth's volcanism to the global mercury cycle. Bulletin of Volcanology 73, 497-510.

Belkin, H.E., Tewalt, S.J., Hower, J.C., Stucker, J.D., O'Keefe, J.M.K., 2009. Geochemistry and petrology of selected coal samples from Sumatra, Kalimantan, Sulawesi, and Papua, Indonesia. International Journal of Coal Geology 77, 260-268.

Bouška, V., 1981. Geochemistry of coal. Elsevier Scientific Pub. Co.

BP, 2012. BP (Petroleum British) Statistical Review of World Energy (2011).

Dai, S., Ren, D., Chou, C.-L., Finkelman, R.B., Seredin, V.V., Zhou, Y., 2012. Geochemistry of trace elements in Chinese coals: A review of abundances, genetic types, impacts on human health, and industrial utilization. International Journal of Coal Geology 94, 3-21.

Dai, S., Ren, D., Chou, C.-L., Li, S., Jiang, Y., 2006a. Mineralogy and geochemistry of the No. 6 Coal (Pennsylvanian) in the Junger Coalfield, Ordos Basin, China. International Journal of Coal Geology 66, 253-270.

Dai, S., Zeng, R., Sun, Y., 2006b. Enrichment of arsenic, antimony, mercury, and thallium in a Late Permian anthracite from Xingren, Guizhou, Southwest China. International Journal of Coal Geology 66, 217-226.

Daniels, J., Longnecker, M., Rowland, A., Golding, J., 2004. Fish intake during pregnancy and early cognitive development of offspring. Epidemiology 15, 394-402.

Davidson, P.W., Myers, G.J., Weiss, B., 2004. Mercury Exposure and Child Development Outcomes. Pediatrics 113, 1023-1029.

Diehl, S.F., Goldhaber, M.B., Hatch, J.R., 2004. Modes of occurrence of mercury and other trace elements in coals from the warrior field, Black Warrior Basin, Northwestern Alabama. International Journal of Coal Geology 59, 193-208.

Egeland, G.M., Middaugh, J.P., 1997. Balancing Fish Consumption Benefits with Mercury Exposure. Science 278, 1904-1905.

Finkelman, R.B., 1993. Trace and minor elements in coal in: M.H. Engel, S.M. (Ed.), Org. Geochem. Plenum, New York, pp. 593-607.

Finkelman, R.B., 1994. Modes of occurrence of potentially hazardous elements in coal: levels of confidence. Fuel Processing Technology 39, 21-34.

Gale, T.K., Lani, B.W., Offen, G.R., 2008. Mechanisms governing the fate of mercury in coal-fired power systems. Fuel Processing Technology 89, 139-151.

Harada, M., 1995. Minamata Disease: Methylmercury Poisoning in Japan Caused by Environmental Pollution. Critical Reviews of Toxicology 25, 1-24.

Hassett, D.J., Eylands, K.E., 1999. Mercury capture on coal combustion fly ash. Fuel 78, 243-248.

Hintelmann, H., Harris, R., Heyes, A., Hurley, J.P., Kelly, C.A., Krabbenhoft, D.P., Lindberg, S., Rudd, J.W.M., Scott, K.J., St.Louis, V.L., 2002. Reactivity and Mobility of New and Old Mercury Deposition in a Boreal Forest Ecosystem during the First Year of the METAALICUS Study. Environmental Science & Technology 36, 5034-5040.

Holmes, C.D., Jacob, D.J., Corbitt, E.S., Mao, J., Yang, X., Talbot, R., Slemr, F., 2010. Global atmospheric model for mercury including oxidation by bromine atoms. Atmos. Chem. Phys 10, 12037-12057.

Hower, J.C., Campbell, J.L., Teesdale, W.J., Nejedly, Z., Robertson, J.D., 2008. Scanning proton microprobe analysis of mercury and other trace elements in Fe-sulfides from a Kentucky coal. International Journal of Coal Geology 75, 88-92.

Hower, J.C., Robertson, J.D., 2003. Clausthalite in coal. International Journal of Coal Geology 53, 219-225.

Hower, J.C., Senior, C.L., Suuberg, E.M., Hurt, R.H., Wilcox, J.L., Olson, E.S., 2010. Mercury capture by native fly ash carbons in coal-fired power plants. Progress Energy Combustion Science 36, 510-529.

Hsu-Kim, H., Kucharzyk, K.H., Zhang, T., Deshusses, M.A., 2013. Mechanisms Regulating Mercury Bioavailability for Methylating Microorganisms in the Aquatic Environment: A Critical Review. Environmental Science & Technology 47, 2441-2456.

IEA, 2012. Key World Energy Statistics 2012.

Ketris, M.P., Yudovich, Y.E., 2009. Estimations of Clarkes for Carbonaceous biolithes: World averages for trace element contents in black shales and coals. International Journal of Coal Geology 78, 135-148.

Kolker, A., 2012. Minor element distribution in iron disulfides in coal: A geochemical review. International Journal of Coal Geology 94, 32-43.

Lamborg, C.H., Fitzgerald, W.F., Damman, A.W.H., Benoit, J.M., Balcom, P.H., Engstrom, D.R., 2002. Modern and historic atmospheric mercury fluxes in both hemispheres: Global and regional mercury cycling implications. Global Biogeochemical Cycles 16, 1104.

Lee, S.J., Seo, Y.-C., Jang, H.-N., Park, K.-S., Baek, J.-I., An, H.-S., Song, K.-C., 2006. Speciation and mass distribution of mercury in a bituminous coal-fired power plant. Atmospheric Environment 40, 2215-2224.

Mason, R.P., Fitzgerald, W.F., Morel, F.M.M., 1994. The biogeochemical cycling of elemental mercury: Anthropogenic influences. Geochimica et Cosmochimica Acta 58, 3191-3198.

Mason, R.P., Sheu, G.R., 2002. Role of the ocean in the global mercury cycle. Global Biogeochemical Cycles 16, 1093.

McAlpine, D., Araki, S., 1958. Minamata disease an unusual neurological disorder caused by contaminated fish. The Lancet 272, 629-631.

Meij, R., 1994. Trace element behavior in coal-fired power plants. Fuel Processing Technology 39, 199-217.

Meij, R., te Winkel, H., 2006. Mercury emissions from coal-fired power stations: The current state of the art in the Netherlands. Science of Total Environment 368, 393-396.

Meij, R., Vredenbregt, L.H.J., Winkel, H.T., 2002. The fate and behavior of mercury in coal-fired power plants. Journal of Air & Waste Management Association 52, 185.

Niksa, S., Helble, J.J., Fujiwara, N., 2001. Kinetic Modeling of Homogeneous Mercury Oxidation: The Importance of NO and H2O in Predicting Oxidation in Coal-Derived Systems. Environmental Science & Technology 35, 3701-3706.

NRC/NAS, 2000. Toxicological Effects of Methylmercury. National Research Council/National Academy of Sciences. Washington, DC.

Nriagu, J., Becker, C., 2003. Volcanic emissions of mercury to the atmosphere: global and regional inventories. Science of Total Environment 304, 3-12.

Pacyna, E.G., Pacyna, J.M., 2002. Global Emission of Mercury from Anthropogenic Sources in 1995. Water, Air, & Soil Pollution 137, 149-165.

Pacyna, E.G., Pacyna, J.M., Steenhuisen, F., Wilson, S., 2006. Global anthropogenic mercury emission inventory for 2000. Atmospheric Environment 40, 4048-4063.

Pacyna, E.G., Pacyna, J.M., Sundseth, K., Munthe, J., Kindbom, K., Wilson, S., Steenhuisen, F., Maxson, P., 2010. Global emission of mercury to the atmosphere from anthropogenic sources in 2005 and projections to 2020. Atmospheric Environment 44, 2487-2499.

Pacyna, J.M., Pacyna, E.P., 1996. Global emissions of mercury to the atmosphere. Emissions from anthropogenic sources, A Report for the Arctic Monitoring and Assessment Programme (AMAP), Oslo, Norway.

Piedad-Sánchez, N., Izart, A., Martínez, L., Suárez-Ruiz, I., Elie, M., Menetrier, C., 2004. Paleothermicity in the Central Asturian Coal Basin, North Spain. International Journal of Coal Geology 58, 205-229.

Pirrone, N., Cinnirella, S., Feng, X., Finkelman, R.B., Friedli, H.R., Leaner, J., Mason, R., Mukherjee, A.B., Stracher, G.B., Streets, D.G., Telmer, K., 2010. Global mercury emissions to the atmosphere from anthropogenic and natural sources. Atmospheric Chemistry and Physics 10, 5951-5964.

Pyle, D.M., Mather, T.A., 2003. The importance of volcanic emissions for the global atmospheric mercury cycle. Atmospheric Environment 37, 5115-5124.

Seigneur, C., Karamchandani, P., Lohman, K., Vijayaraghavan, K., Shia, R.-L., 2001. Multiscale modeling of the atmospheric fate and transport of mercury. Journal of Geophysical Research 106, 27795-27809.

Selin, N.E., 2009. Global Biogeochemical Cycling of Mercury: A Review. Annual Review of Environment and Resources 34, 43-63.

Selin, N.E., Jacob, D.J., Yantosca, R.M., Strode, S., Jaeglé, L., Sunderland, E.M., 2008. Global 3-D land-ocean-atmosphere model for mercury: Present-day versus preindustrial cycles and anthropogenic enrichment factors for deposition. Global Biogeochemical Cycles 22, GB2011.

Seredin, V.V., 2004. The Au-PGE mineralization at the Pavlovsk brown coal deposit, Primorye. Geology of Ore Deposits 46, 36-63.

Seredin, V.V., Finkelman, R.B., 2008. Metalliferous coals: A review of the main genetic and geochemical types. International Journal of Coal Geology 76, 253-289.

Streets, D.G., Devane, M.K., Lu, Z., Bond, T.C., Sunderland, E.M., Jacob, D.J., 2011. All-Time Releases of Mercury to the Atmosphere from Human Activities. Environmental Science & Technology 45, 10485-10491.

Streets, D.G., Hao, J., Wang, S., Wu, Y., 2009. Mercury emissions from coal combustion in China, in: Mason, R., Pirrone, N. (Eds.), Mercury Fate and Transport in the Global Atmosphere. Springer US, pp. 51-65.

Streets, D.G., Hao, J., Wu, Y., Jiang, J., Chan, M., Tian, H., Feng, X., 2005. Anthropogenic mercury emissions in China. Atmospheric Environment 39, 7789-7806.

Sunderland, E.M., 2007. Mercury Exposure from Domestic and Imported Estuarine and Marine Fish in the U.S. Seafood Market. Environmental Health Perspectives 115, 235-242.

Sunderland, E.M., Mason, R.P., 2007. Human impacts on open ocean mercury concentrations. Global Biogeochemical Cycles 21, GB4022.

Swaine, D.J., 1990. Trace elements in coal. Butterworth.

Swaine, D.J., Goodarzi, F., 1995. Environmental Aspects of Trace Elements in Coal. Kluwer Academic Publishers, Dordrecht.

Valković, V., 1983. Trace elements in coal. CRC Press.

Varekamp, J.C., Buseck, P.R., 1986. Global mercury flux from volcanic and geothermal sources. Applid Geochemistry 1, 65-73.

Wang, Q., Shen, W., Ma, Z., 2000. Estimation of Mercury Emission from Coal Combustion in China. Environmental Science & Technology 34, 2711-2713.

Wu, Y., Wang, S., Streets, D.G., Hao, J., Chan, M., Jiang, J., 2006. Trends in Anthropogenic Mercury Emissions in China from 1995 to 2003. Environmental Science & Technology 40, 5312-5318.

Yudovich, Y.E., Ketris, M.P., 2005. Mercury in coal: a review: Part 1. Geochemistry. International Journal of Coal Geology 62, 107-134.

Zhang, H., 2006. Photochemical Redox Reactions of Mercury, in: Atwood, D. (Ed.), Recent Developments in Mercury Science. Springer Berlin / Heidelberg, pp. 37-79.

Zhang, J., Ren, D., Zhu, Y., Chou, C.-L., Zeng, R., Zheng, B., 2004. Mineral matter and potentially hazardous trace elements in coals from Qianxi Fault Depression Area in southwestern Guizhou, China. International Journal of Coal Geology 57, 49-61.

Zhang, L., Wang, S., Meng, Y., Hao, J., 2012. Influence of Mercury and Chlorine Content of Coal on Mercury Emissions from Coal-Fired Power Plants in China. Environmental Science & Technology 46, 6385-6392.

Chapter 3

Theory of Hg isotope fractionation

Chapter 3. Theory of Hg isotope fractionation

Seven stable Hg isotopes (^{196}Hg, ^{198}Hg, ^{199}Hg, ^{200}Hg, ^{201}Hg, ^{202}Hg and ^{204}Hg) occur in nature with a 4 % relative mass difference (Table 2). Their relative abundances are approximately 0.15%, 9.97%, 16.9%, 23.1%, 13.2%, 29.9% and 6.87%, respectively (Cohen et al., 2008; Nier, 1950). In addition to the 4% mass variation of Hg isotopes, the active oxidation–reduction chemistry, tendency to form covalent bonds, existence of volatile Hg^0 and co-occurrence of inorganic and organic species of Hg induce small but significant Hg isotope fractionation in many physicochemical and biological reactions (Bergquist and Blum, 2009; Blum and Bergquist, 2007). As such, recent developments in Hg stable isotope biogeochemistry offer a new dimension to study Hg sources, transport, transformation and deposition in environmental and geological applications (Bergquist and Blum, 2009; Blum 2012; Kritee et al., 2013; Sonke, 2011; Sonke and Blum, 2013; Yin et al., 2010).

Table 2. Characteristics of stable Hg isotopes

Isotope	Atomic mass (m_a/u)	Natural abundance (atom %)	Nuclear spin (I)	Magnetic moment (μ/μ_N)
^{196}Hg	195.965833 (3)	0.15 (1)	0+	0
^{198}Hg	197.9667690 (4)	9.97 (20)	0+	0
^{199}Hg	198.9682799 (4)	16.87 (22)	½-	+0.5058855(9)
^{200}Hg	199.9683260 (4)	23.10 (19)	0+	0
^{201}Hg	200.9703023 (6)	13.18 (9)	$^3/_2$-	-0.5602257(14)
^{202}Hg	201.9706430 (6)	29.86 (26)	0+	0
^{204}Hg	203.9734939 (5)	6.87 (15)	0+	0

All data are cited from compilation of IUPAC Green Book (Cohen et al., 2008). Note: number in parentheses denotes uncertainty applicable to the last digit

3.1. General concepts

3.1.1. Isotope effect

Differences in chemical and physical properties of a substance arising from variations in atomic mass of an element are called isotope effects (Hoefs, 2009). The small variation in physicochemical properties can affect chemical reaction rate, diffusion rate etc. This variation can be calculated by statistical mechanics methods and experimentally determined by measuring changes in isotope ratios (Criss, 1999).

3.1.2. Isotope fractionation factor

The isotope fractionation factor is defined as the ratio of the abundances of two isotopes in substance A divided by the corresponding ratio in substance B. For Hg isotopes, the fractionation factor is expressed as:

$$^{xxx/198}\alpha_{A\text{-}B} = \frac{R^{xxx/198}Hg_A}{R^{xxx/198}Hg_B} = \frac{(^{xxx}Hg/^{198}Hg)_A}{(^{xxx}Hg/^{198}Hg)_B} \quad [1]$$

where XXX is a Hg isotope mass other than the reference isotope ^{198}Hg.

3.1.3. Delta value (δ) and conversion

The measured isotope ratios of samples are commonly anchored to a common reference standard (e.g. NIST SRM 3133 for Hg isotopes) to facilitate data inter-comparison. Relative isotope ratio differences from the NIST 3133 standard on the per mil (‰) scale are defined by the delta (δ) notation as follows (Blum and Bergquist, 2007):

$$\delta^{XXX}Hg\ (‰) = \left(\frac{R^{xxx/198}Hg_{Sample}}{R^{xxx/198}Hg_{NIST\ 3133}} - 1\right) \times 1000 = \left(\frac{\left(^{XXX}Hg/^{198}Hg\right)_{Sample}}{\left(^{XXX}Hg/^{198}Hg\right)_{NIST\ 3133}} - 1\right) \times 1000 \quad [2]$$

For two substances, A and B, whose δ values are expressed as:

$$\delta^{xxx}Hg_A = \left(\frac{R^{xxx/198}Hg_A}{R^{xxx/198}Hg_{standard}} - 1\right) \times 10^3 \quad [3]$$

$$\delta^{xxx}Hg_B = \left(\frac{RHg_B^{xxx/198}}{RHg_{standard}^{xxx/198}} - 1\right) \times 10^3 \quad [4]$$

Their δ values and fractionation factor α between A and B can be related by:

$$\alpha^{xxx/198}Hg_{A\text{-}B} = \frac{R^{xxx/198}Hg_A}{R^{xxx/198}Hg_B} = \frac{10^{-3}\delta^{xxx}Hg_A + 1}{10^{-3}\delta^{xxx}Hg_A + 1} \quad [5]$$

which can be approximated, for small δ values (<10‰), to another form by taking the logarithm on both sides:

$$\ln\alpha^{xxx/198}Hg_{A-B} \doteq 10^{-3} \times (\delta^{xxx}Hg_A - \delta^{xxx}Hg_B) \quad [6]$$

As most of fractionation factors α approach unity, another useful simplification can be obtained:

$$\ln\alpha^{xxx/198}Hg_{A-B} \doteq \alpha^{xxx/198}Hg_{A-B} - 1 \quad [7]$$

Although not recommended by IPUAC (Coplen, 2011), in some publications, the epsilon notation (Ɛ) is used to represent fractionation factors on the ‰ scale:

$$\varepsilon^{xxx/198}Hg_{A-B} = 1000 \times (\alpha^{xxx/198}Hg_{A-B} - 1) \quad [8]$$

The following equations are used to convert δ value using ^{202}Hg as reference isotope into δ value using ^{198}Hg as reference isotope:

$$\delta^{xxx/202}Hg \doteq \delta^{xxx/198}Hg - \delta^{202/198}Hg \quad [9]$$

$$\Delta^{xxx/202}Hg \doteq \Delta^{xxx/198}Hg \quad [10]$$

The capital Delta notation (Δ) for MIF is explained in Section 3.3.2

3.2. Literature review on Hg isotopes fractionation

Mercury isotope fractionation was observed in laboratory-controlled experiments as early as one century ago. By evaporating liquid Hg onto a cooled surface positioned at low pressure conditions, Bronsted and von Hevesy (1920) precisely measured the density of residual and condensed Hg relative to original liquid Hg using a pycnometry (density) method with <1 ppm uncertainty. In the first set of experiments with ~14% Hg evasion, they found a density depletion by a factor of 0.999980 in the condensed vapor phase. In the second experiment with ~75% Hg evasion, a density depletion of 0.999990 (density in residual liquid was 1.000031) was observed. This indicates that lighter Hg isotopes with a higher evaporation rate escape faster than heavier ones and the degree to which evaporation fractionates Hg isotopes could be quantified. Shortly afterwards, more detail evaporation and condensation experiments were performed (Brönsted and von Hevesy, 1921; Mulliken and Harkins, 1922), in which one order of magnitude larger density fractionation was observed. Although several studies tried to measure Hg isotope compositions of natural systems in the following eight decades (Haeffner, 1953; Jackson, 2001; Koval et al., 1977; Kuznetsov and Obolenskii, 1980; Obolenskii and Doilnitsyn, 1976), their data are either questionable or subjected to

large uncertainty until the fist Hg isotopes study of Murchison and Allende meteorites by MC-ICPMS (Lauretta et al., 2001).

Recent advances in high-precision inductively coupled plasma mass spectrometry (MC-ICPMS) and associated techniques have allowed high-precision determination of Hg stable isotope ratios in natural samples (Blum and Bergquist, 2007; Chen et al., 2012; Lauretta et al., 2001). Photochemical and microbial reduction of Hg(II) (Bergquist and Blum, 2007; Kritee et al., 2007, 2008; Zheng et al., 2009), demethlyation of methylmercury (Bergquist and Blum, 2007; Kritee et al., 2009), methylation of Hg(II) (Jiménez-Moreno et al., 2013), evaporation of liquid Hg(0) (Estrade et al., 2009; Ghosh et al., 2013), and volatilization of aqueous Hg(0) vapor (Zheng et al., 2007) could induce significant and measurable Hg isotope fractionation. Both mass-dependent Hg isotope fractionation (MDF, indicated by δ^{202}Hg) and mass-independent Hg isotope fractionation (MIF, odd ^{199}Hg and ^{201}Hg isotopes mostly, indicated by Δ^{199}Hg) vary more than a range of 10‰ in geological and environmental samples. A synthesis of these observations can be found in recently published reviews (Bergquist and Blum, 2009; Sonke, 2011; Sonke and Blum, 2013; Kritee et al., 2013; Yin et al., 2010)

3.3. Hg isotopes fractionation mechanisms

The physicochemical reactions involving Hg not only depend on isotopic mass, but also on nuclear spin (magnetic moment) and nuclear structure (radius, volume) (Buchachenko, 2001, 2013; Schauble, 2007). The resulting isotope fractionation effects are termed respectively as mass dependent fractionation (MDF), magnetic isotope effect (MIE) and nuclear volume effect (NVE; also called nuclear field shift effect, NFS). In addition, the isotope fractionation of Hg also possibly depends on isotope abundances (Chen et al., 2012; Mead et al., 2013), via the isotope self-shielding effect as observed for C and O in solar nebula (Clayton, 2002; Lyons and Young, 2005).

3.3.1. Mass dependent fractionation (MDF)

MDF is the most common isotope fractionation mechanism for Hg and the majority of elements in the periodic system. MDF is a result of quantum mechanical effects (zero-point vibrational energy differences of different isotopes), which is governed by the chemical energy of starting and transition states of reactant molecules. The theoretical basis for MDF resulting from equilibrium and kinetic processes was established by Bigeleisen and Urey more than half a century ago (Bigeleisen, 1949;

Bigeleisen and Mayer, 1947; Urey, 1947). MDF factors for different Hg isotope ratios can be described by:

$$\alpha^{xxx/198}Hg_{A-B} = (\alpha^{202/198}Hg_{A-B})^{\beta} \quad [11]$$

Where the exponent β varies depending upon the process. For equilibrium isotope exchange:

$$\beta = \frac{\left(\frac{1}{m^{xxx}Hg} - \frac{1}{m^{198}Hg}\right)}{\left(\frac{1}{m^{202}Hg} - \frac{1}{m^{198}Hg}\right)} \quad [12]$$

For kinetic fractionation:

$$\beta = \frac{\ln\frac{m^{xxx}Hg}{m^{198}Hg}}{\ln\frac{m^{202}Hg}{m^{198}Hg}} \quad [13]$$

Eq. 11 can be rewritten in δ' form:

$$\delta'^{xxx/198}Hg = \beta \times \delta'^{202/198}Hg \quad [14]$$

where δ' and δ are related by:

$$\delta'^{xxx/198}Hg = \ln\left(\frac{R^{xxx/198}Hg_{sample}}{R^{xxx/198}Hg_{NIST3133}}\right) \times 1000 \doteq \left(\frac{R^{xxx/198}Hg_{sample}}{R^{xxx/198}Hg_{NIST3133}} - 1\right) \times 1000 = \delta^{xxx/198}Hg \quad [15]$$

Eq. 14 allows the construction of three-isotope plots with a reference MDF line (Figure 4). This curve is very important to identify the underlying MDF or MIF fractionation mechanism (Sonke, 2011; Young et al., 2002). For MDF, the data set will be plotted against the reference MDF line with slopes varying as a function of δ^{xxx}Hg. Significant departures (>0.1 ‰) from a reference MDF line imply a potential MIF.

3.3.2. Mass independent fractionation (MIF)

In addition to MDF, Hg isotopes are affected by MIF in specific reactions, e.g. photochemical reduction, evaporation of liquid Hg (Bergquist and Blum, 2007; Estrade et al., 2009; Zheng and Hintelmann, 2009). MIF values are indicated by capital delta (Δ) notation in per mil, which is the difference between the measured values of δ^{199}Hg, δ^{200}Hg, δ^{201}Hg and those predicted from δ^{202}Hg using the kinetic MDF law (Blum and Bergquist, 2007):

$$\Delta^{xxx}\mathbf{Hg} = \delta'^{xxx}\mathbf{Hg} - \beta_{xxx} \times \delta'^{202}\mathbf{Hg} \quad [16]$$

where the mass-dependence scaling factor β_{xxx} is 0.252 for ^{199}Hg, 0.502 for ^{200}Hg and 0.752 for ^{201}Hg (Table 3).

Two potential mechanisms have been postulated to explain MIF of Hg isotopes: MIE and NVE. MIE is a purely kinetic process and is caused by nuclear-spin coupling in radical-pair reactions (Buchachenko, 2001; Zheng and Hintelmann, 2010a). As only odd Hg isotopes ^{199}Hg and ^{201}Hg possess nuclear spin and associated magnetic moment (Table 2), MIE fractionate odd from the even Hg isotopes. MIE is mainly observed in photochemical reduction of Hg species, which could enrich reactant odd isotopes, i.e. (+)MIE, or even isotopes, i.e. (-)MIE, depending on the initial spin multiplicity of the paramagnetic intermediates during spin-selective reactions (Zheng and Hintelmann, 2010a). Photoreduction experiments showed that Hg(II) bound to O-ligands resulted in (+)MIE and bound to S-ligands resultrd in (-)MIE. Both (+)MIE and (-)MIE show that the ratios of Δ^{199}Hg/Δ^{201}Hg are in the range of 1.00-1.36 (Bergquist and Blum, 2007; Zheng and Hintelmann, 2009, 2010a) (Figure 5).

Table 3 'β' scaling factors for isotope ratios relative to ^{202}Hg/^{198}Hg

	$S_{E\text{-}MDF}$*	$S_{K\text{-}MDF}$**	S_{NVE}***		
			S_{NVE1}	$S_{NVE\ 2}$	$S_{NVE\ 3}$
$^{196/198}$Hg	-0.5151	-0.5074	-0.4660		-0.42
$^{199/198}$Hg	0.2539	0.2520	0.1076	0.0804	0.0525
$^{200/198}$Hg	0.5049	0.5024	0.4966	0.4712	0.4732
$^{201/198}$Hg	0.7539	0.7520	0.7003	0.6838	0.6312
$^{202/198}$Hg	1	1	1	1	1
$^{204/198}$Hg	1.4855	1.4928	1.6543	1.4994	1.5277

* scaling factor of equilibrium MDF, **scaling factor of kinetic MDF, ***scaling factor of NVE. Scaling factors for NVE are based on $<r^2>$ from different sources: S_{NVE1} from (Angeli, 2004); S_{NVE2} from (Hahn et al., 1979); S_{NVE3} from (Landolt-Boernstein)

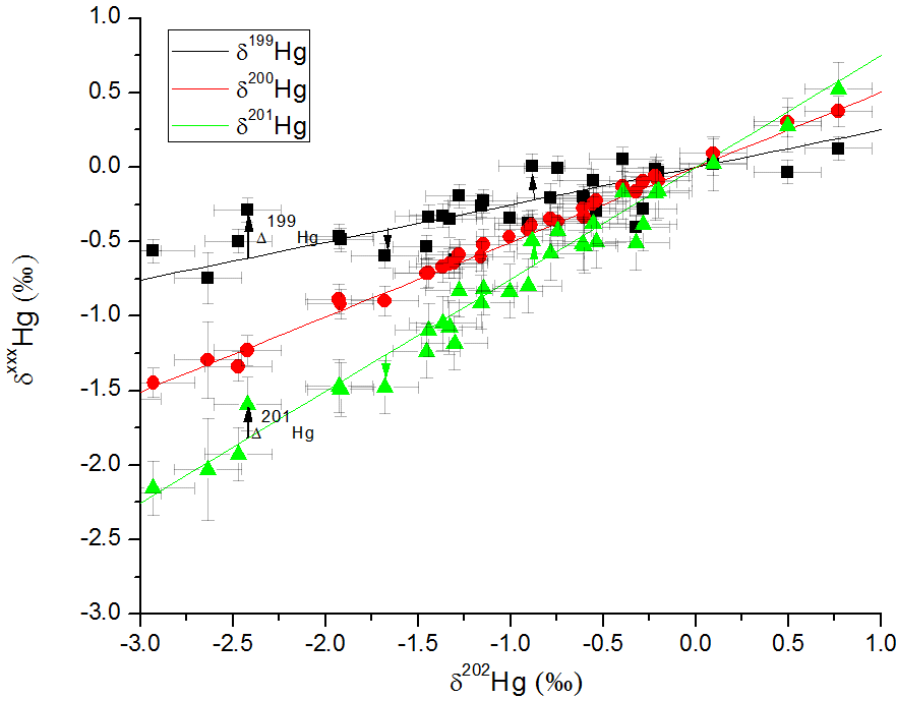

Figure 4 Three isotope plots of studied Chinese coals showing only MDF for the even isotope ^{200}Hg, and both MDF and MIF (Δ^{199}Hg and Δ^{201}Hg) for the odd isotopes ^{199}Hg and ^{201}Hg

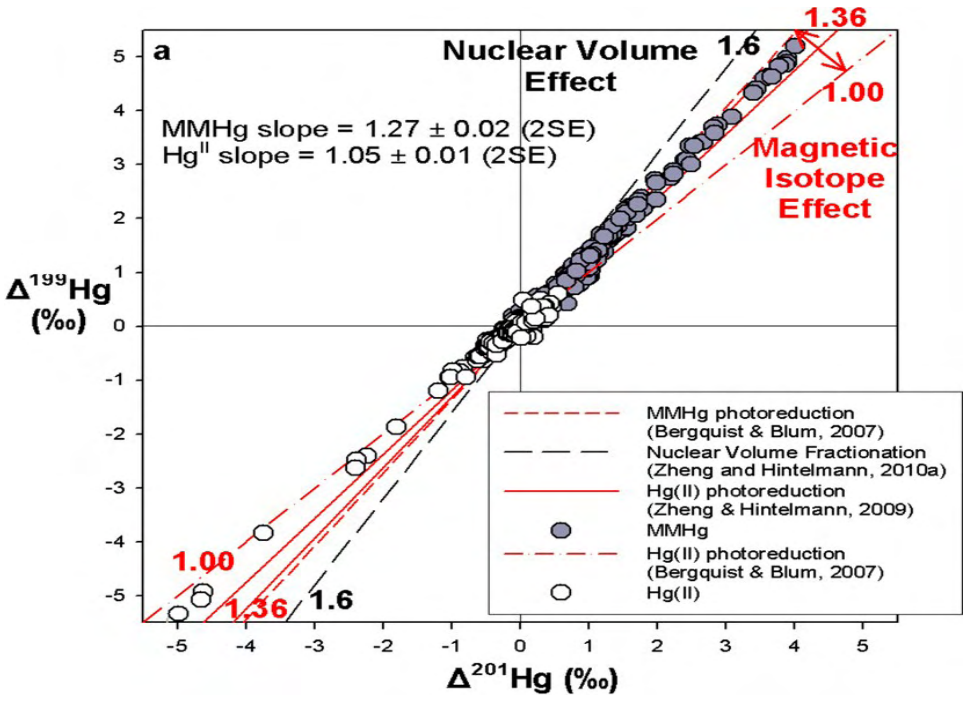

Figure 5 Summary of Δ^{199}Hg and Δ^{201}Hg data (n =722) for biological samples containing predominantly MMHg (dark grey circles), and for geochemical samples containing predominantly inorganic Hg(II) (open circles). Experimentally observed $\Delta^{199/201}$Hg slopes for aquatic Hg(II) (1.0-1.3) (Bergquist and Blum, 2007; Zheng and Hintelmann, 2009) and MMHg photodegradation (Bergquist and Blum, 2007), and the experimental slope for NVE fractionation (Zheng and Hintelmann, 2009). (Source: Sonke, 2011)

NVE was firstly proposed by Bigeleisen (1996a,b) to explain isotope variations of elements with high atomic number, such as U. As equilibrium Hg MDF is expected to be relatively small, NVE has been suggested to explain large Hg isotope variation in natural samples (Schauble, 2007). NVE arises from the overlap between electronic and nuclear wave functions, and its magnitude is a measure of the depletion of 6s orbital electron density (King, 1984). The isotope variation driven by NVE is proportional to the variation of mean-squared nuclear charge radii $<r^2>$, whereby nuclear radii are not in linear relationship with isotope mass, especially for odd isotopes. Therefore, isotope fractionation by NVE will not scale in proportion to the mass difference of the isotopes of interest. The relationship (scaling factors) between fractionation factors of two paired isotope ratios is expressed as (Schauble, 2007):

$$\frac{10^3 \ln a^{xxx/198}Hg}{10^3 \ln a^{202/198}Hg} = \frac{<r^{xxx}Hg^2> - <r^{198}Hg^2>}{<r^{202}Hg^2> - <r^{198}Hg^2>} \quad [17]$$

Table 3 lists the scaling factors for different isotope ratios fractionated by NVE. Although NVE has the same isotope fractionation signs as MDF, they can be distinguished by different scaling factors, especially for odd isotopes ^{199}Hg and ^{201}Hg. NVE has been theoretically estimated (Schauble, 2007) (Figure 6) and observed during liquid Hg evaporation (Estrade et al., 2009; Ghosh et al., 2008) and abiotic (non-photochemical) reduction of Hg (Zheng and Hintelmann, 2009, 2010b), and equilibrium exchange of dissolved Hg(II) species and thiol-bound Hg(II) (Wiederhold et al., 2010). Theoretically predicted ratios of Δ^{199}Hg/ Δ^{201}Hg using different nuclear radii (Angeli, 2004; Hahn et al., 1979; Landolt-Boernstein, 2004; Nadjakov et al., 1994; Ulm et al., 1987) vary from 1.65 to 2.79 (Sonke, 2011). Experimental NVE Δ^{199}Hg/ Δ^{201}Hg ratios appear to be approximately 1.6 ± 0.1 (Ghosh et al., 2013; Zheng and Hintelmann, 2009). Δ^{199}Hg/Δ^{201}Hg ratio can therefore potentially distinguish between MIE and NVE mass independent fractionation effect. In addition to common MDF and MIF of odd Hg isotopes, MIF of even isotopes (Δ^{200}Hg), more than 1‰ range, was observed in precipitation Hg(II) (rain, snow) in North America (Chen et al., 2012; Gratz et al., 2010; Sherman et al., 2012). MIF of ^{200}Hg is suggested to be related to the photo-initiated oxidation of Hg (0) vapor on aerosol or solid surfaces in the tropopause (Chen et al., 2012). However, it is still unknown whether this process only causes MIF of ^{200}Hg. The isotope analysis of trapped Hg in the glass wall of compact fluorescent lamps showed that unusual MIF occurred across multiple even mass and odd mass isotopes (Mead et al., 2013). The fractionated patterns of Hg isotopes in compact fluorescent lamps were thought to be partially caused by photochemical the self-shielding effect, an isotope fractionation mechanism that fractionates isotopes according to their abundances.

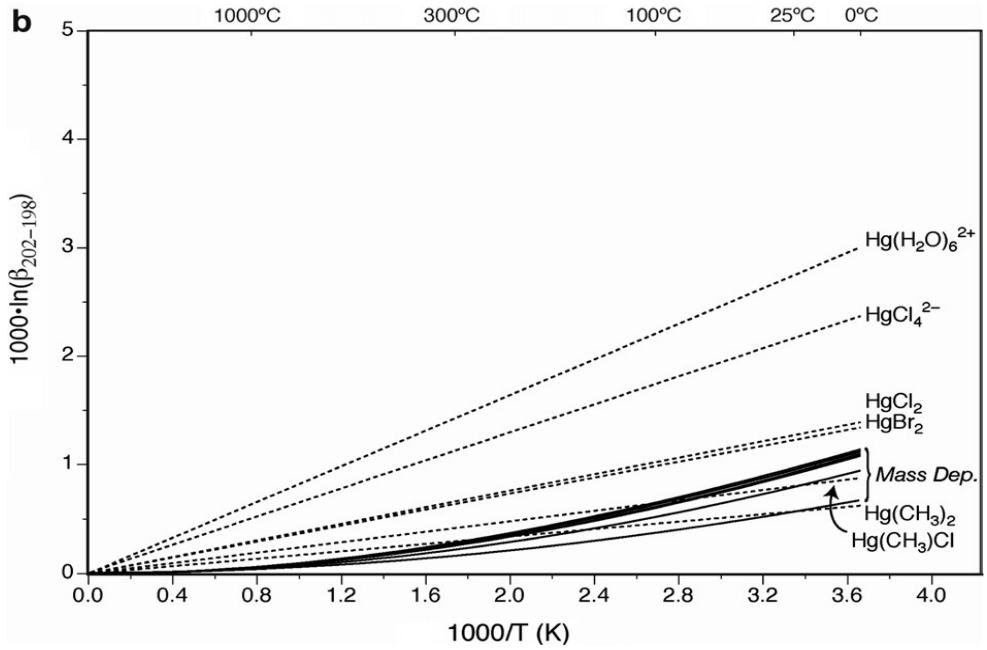

Figure 6 Fractionation factor (1000*ln $\beta^{202\text{-}198}$Hg) for Hg-bearing molecules relative to Hg(0) vapor. The solid line denotes MDF and dotted line denotes NVE (Source: Schauble, 2007)

References

Angeli, I., 2004. A consistent set of nuclear rms charge radii: properties of the radius surface R(N,Z). At. Data Nucl. Data Tables 87, 185-206.

Bergquist, B.A., Blum, J.D., 2007. Mass-Dependent and -Independent Fractionation of Hg Isotopes by Photoreduction in Aquatic Systems. Science 318, 417-420.

Bergquist, B.A., Blum, J.D., 2009. The Odds and Evens of Mercury Isotopes: Applications of Mass-Dependent and Mass-Independent Isotope Fractionation. Elements 5, 353-357.

Bigeleisen, J., 1949. The Relative Reaction Velocities of Isotopic Molecules. The Journal of Chemical Physics 17, 675-678.

Bigeleisen, J., 1996a. Nuclear Size and Shape Effects in Chemical Reactions. Isotope Chemistry of the Heavy Elements. J. Am. Chem. Soc. 118, 3676-3680.

Bigeleisen, J., 1996b. Temperature dependence of the isotope chemistry of the heavy elements. Proceedings of the National Academy of Sciences of the United States of America 93, 9393-9396.

Bigeleisen, J., Mayer, M.G., 1947. Calculation of Equilibrium Constants for Isotopic Exchange Reactions. The Journal of Chemical Physics 15, 261-267.

Blum, J., Bergquist, B., 2007. Reporting of variations in the natural isotopic composition of mercury. Anal. Bioanal. Chem. 388, 353-359.

Blum, J., 2012. Applications of stable mercury isotopes to biogeochemistry. In Baskaran, M. (Ed), Handbook of Environmental Isotope Geochemistry. Springer Berlin Heidelberg, pp 229-245.

Brönsted, J.N., von Hevesy, G., 1920. The separation of the isotopes of mercury. Nature 106, 144.

Brönsted, J.N., von Hevesy, G., 1921. Uber die trennung der isotopen des quecksilbers. Z. Phys. Chem. 99, 189-206.

Buchachenko, A.L., 2001. Magnetic Isotope Effect: Nuclear Spin Control of Chemical Reactions. The Journal of Physical Chemistry A 105, 9995-10011.

Buchachenko, A.L., 2013. Mass-Independent Isotope Effects. The Journal of Physical Chemistry B 117, 2231-2238.

Chen, J., Hintelmann, H., Feng, X., Dimock, B., 2012. Unusual fractionation of both odd and even mercury isotopes in precipitation from Peterborough, ON, Canada. Geochimica et Cosmochimica Acta 90, 33-46.

Clayton, R.N., 2002. Solar System: Self-shielding in the solar nebula. Nature 415, 860-861.

Cohen, E.R., Cvitas, T., Frey, J.G., Holmström, B., Kuchitsu, K., Marquardt, R., Mills, I., Pavese, F., Quack, M., J. Stohner, Strauss, H.L., Takami, M., Thor, A.J., 2008. Quantities, Units and Symbols in Physical Chemistry, IUPAC Green Book, 3rd Edition, 2nd Printing. IUPAC & RSC Publishing, Cambridge.

Coplen,T.B., 2011. Guidelines and recommended terms for expression of stable-isotope-ratio and gas-ratio measurement results. Rapid Communications in Mass Spectrometry 25, 2538-2560.

Criss, R.E., 1999. Principles of stable isotope distribution. Oxford University Press.

Estrade, N., Carignan, J., Sonke, J.E., Donard, O.F.X., 2009. Mercury isotope fractionation during liquid-vapor evaporation experiments. Geochimica et Cosmochimica Acta 73, 2693-2711.

Ghosh, S., Schauble, E.A., Lacrampe Couloume, G., Blum, J.D., Bergquist, B.A., 2013. Estimation of nuclear volume dependent fractionation of mercury isotopes in equilibrium liquid–vapor evaporation experiments. Chem. Geol. 336, 5-12.

Ghosh, S., Xu, Y., Humayun, M., Odom, L., 2008. Mass-independent fractionation of mercury isotopes in the environment. Geochem. Geophys. Geosyst. 9, Q03004.

Gratz, L.E., Keeler, G.J., Blum, J.D., Sherman, L.S., 2010. Isotopic Composition and Fractionation of Mercury in Great Lakes Precipitation and Ambient Air. Environmental Science & Technology 44, 7764-7770.

Haeffner, E., 1953. A Method of Changing the Isotope Abundance in Mercury. Nature 172, 775-776.

Hahn, A.A., Miller, J.P., Powers, R.J., Zehnder, A., Rushton, A.M., Welsh, R.E., Kunselman, A.R., Roberson, P., Walter, H.K., 1979. An experimental study of muonic X-ray transitions in mercury isotopes. Nucl. Phys. A 314, 361-386.

Hoefs, J., 2009. Stable Isotope Geochemistry (6th Edition). Springer-Verlag, Berlin Heidelberg.

Jackson, T.A., 2001. Variations in the isotope composition of mercury in a freshwater sediment sequence and food web. Can. J. Fish. Aquat. Sci. 58, 185-196.

Jiménez-Moreno, M., Perrot, V., Epov, V., Monperrus, M., Amouroux, D., 2013. Chemical kinetic isotope fractionation of mercury during abiotic methylation of Hg(II) by methylcobalamin in aqueous chloride media 336, 26-36.

King, W.H., 1984. Isotope shifts in atomic spectra. Plenum Press, New York.

Koval, N.A., Zakharchenko, V.V., Savin, O.R., Vinogradov, V.I., Shkurdoda, V.A., Simonovskii, V.I., 1977. Problem of natural fractionation of mercury isotopes. Doklady Akademii Nauk SSSR 235, 936-938.

Kritee, K., Blum, J.D., Johnson, M.W., Bergquist, B.A., Barkay, T., 2007. Mercury stable isotope fractionation during reduction of Hg(II) to Hg(0) by mercury resistant microorganisms. Environmental Science & Technology 4, 1889-1895.

Kritee, K., Blum, J.D., Barkay, T., 2008. Mercury stable isotope fractionation during reduction of Hg(II) by different microbial pathways. Environmental Science & Technology 42, 9171-9177.

Kritee, K., Barkay, T., Blum, J.D., 2009. Mass dependent stable isotope fractionation of mercury during mer mediated microbial degradation of monomethylmercury. Geochimica et Cosmochimica Acta 73 (5), 1285-1296.

Kritee, K., Blum, J.D., Barkay, T., Barkay, T., 2013. Microbial stable isotope fractionation of mercury: A synthesis of present understanding and future directions 336, 13-25.

Kuznetsov, V.V., Obolenskii, A.A., 1980. Possible mechanism of the natural fractionation of mercury isotopes. Doklady Akademii Nauk SSSR 252, 459-460.

Landolt-Boernstein, 2004. Numerical Data and Functional Relationships in Science and Technology. Group I: Elementary Particles, Nuclei and Atoms, Volume 20. Nuclear Charge Radii. Springer, Heidelberg.

Lauretta, D.S., Klaue, B., Blum, J.D., Buseck, P.R., 2001. Mercury abundances and isotopic compositions in the Murchison (CM) and Allende (CV) carbonaceous chondrites. Geochimica et Cosmochimica Acta 65, 2807-2818.

Lyons, J.R., Young, E.D., 2005. CO self-shielding as the origin of oxygen isotope anomalies in the early solar nebula. Nature 435, 317-320.

Mead, C., Lyons, J.R., Johnson, T.M., Anbar, A.D., 2013. Unique Hg Stable Isotope Signatures of Compact Fluorescent Lamp-Sourced Hg. Environmental Science & Technology 47, 2542-2547.

Mulliken, R.S., Harkins, W.D., 1922. The separation of isotopes. Theory of resolution of isotopic mixtures by diffusion and similar processes. Experimental separation of mercury by evaporation in a vacuum. J. Am. Chem. Soc. 44, 37-65.

Nadjakov, E.G., Marinova, K.P., Gangrsky, Y.P., 1994. Systematics of Nuclear Charge Radii. At. Data Nucl. Data Tables 56, 133-157.

Nier, A.O., 1950. A Redetermination of the Relative Abundances of the Isotopes of Neon, Krypton, Rubidium, Xenon, and Mercury. Physical Review 79, 450.

Obolenskii, A.A., Doilnitsyn, E.F., 1976. Natural fractionation of mercury isotopes. Akademiya Nauk SSSR Doklady 230, 701-704.

Schauble, E.A., 2007. Role of nuclear volume in driving equilibrium stable isotope fractionation of mercury, thallium, and other very heavy elements. Geochimica et Cosmochimica Acta 71, 2170-2189.

Sherman, L.S., Blum, J.D., Keeler, G.J., Demers, J.D., Dvonch, J.T., 2012. Investigation of Local Mercury Deposition from a Coal-Fired Power Plant Using Mercury Isotopes. Environmental Science & Technology

Sonke, J.E., 2011. A global model of mass independent mercury stable isotope fractionation. Geochimica et Cosmochimica Acta 75, 4577-4590.

Sonke, J.E., Blum, J.D., 2013. Advances in mercury stable isotope biogeochemistry. Chem. Geol. 336, 1-4.

Ulm, G., Bhattacherjee, S.K., Dabkiewicz, P., Huber, G., Kluge, H.J., Kühl, T., Lochmann, H., Otten, E.W., Wendt, K., Ahmad, S.A., Klempt, W., Neugart, R., 1987. Isotope shift of182Hg and an update of nuclear moments and charge radii in the isotope range181Hg-206Hg Zeitschrift für Physik A: Atomic Nuclei 325, 247-259.

Urey, H.C., 1947. The thermodynamic properties of isotopic substances. Journal of the Chemical Society (Resumed), 562-581.

Wiederhold, J.G., Cramer, C.J., Daniel, K., Infante, I., Bourdon, B., Kretzschmar, R., 2010. Equilibrium Mercury Isotope Fractionation between Dissolved Hg(II) Species and Thiol-Bound Hg. Environmental Science & Technology 44, 4191-4197.

Yin, R., Feng, X., Shi, W., 2010. Application of the stable-isotope system to the study of sources and fate of Hg in the environment: A review. Applied Geochemistry 25: 1467-1477.

Young, E.D., Galy, A., Nagahara, H., 2002. Kinetic and equilibrium mass-dependent isotope fractionation laws in nature and their geochemical and cosmochemical significance. Geochimica et Cosmochimica Acta 66, 1095-1104.

Zheng, W., Foucher. D, Hintelmann, H., 2007. Mercury isotope fractionation during volatilization of Hg(0) from solution into the gas phase. Journal of Analytical Atomic Spectrometry 22: 1097-1104.

Zheng, W., Hintelmann, H., 2009. Mercury isotope fractionation during photoreduction in natural water is controlled by its Hg/DOC ratio. Geochimica et Cosmochimica Acta 73, 6704-6715.

Zheng, W., Hintelmann, H., 2010a. Isotope Fractionation of Mercury during Its Photochemical Reduction by Low-Molecular-Weight Organic Compounds. The Journal of Physical Chemistry A 114, 4246-4253.

Zheng, W., Hintelmann, H., 2010b. Nuclear Field Shift Effect in Isotope Fractionation of Mercury during Abiotic Reduction in the Absence of Light. The Journal of Physical Chemistry A 114, 4238-4245.

Chapter 4

Sample descriptions and Hg isotope measurements

Chapter 4. Sample descriptions and Hg isotope measurements

4.1. Sample descriptions

In line with the objectives of this thesis, the collected samples are generally divided into three categories: coal from continuous coal-bearing sequences (Anhui, China); mined coal from worldwide coal deposits and; coal and coal combustion products (bottom ash, fly ash, gypsum) from typical Chinese power plants.

4.1.1. Samples from continuous coal-bearing sequences

In order to investigate the temporal variations of Hg isotope signatures with the evolution of coal deposits, coal samples from different coal seams in a complete coal-bearing sequence were sampled in the Huainan Coalfield, Anhui Province, China. Coal associated sandstone and mudstone were sampled to trace the detrital Hg source isotope composition in coal. We also sampled natural cokes metamorphosed by elevated heat and pressure derived from magmatic intrusions, with the aim to characterize the influence of geological processes on the fractionation of Hg isotopes in coal.

4.1.1.1. Study area and geological settings

The Permian coal-bearing sequences in the Zhuji Coal Mine (Huainan Coalfield, Anhui Province) and Daizhuang Coal Mine (Jining Coalfield, Shandong Province) were selected for this study (Figure 7). Both coal mines produce low sulfur bituminous coals that are widely used in power plants of East China.

The data from 88 boreholes drilled during the exploration period showed that there are 28 coal seams in the Permian strata, and 9 coal seams in the Carboniferous strata (Figure 8) (Sun et al., 2010a). The Taiyuan Formation (with a thickness ranging from 112.1 to 114.2 m; 113 m on average) in the upper part of the Carboniferous strata comprises 7–9 thin, unworkable coal seams. The Permian strata comprise the Shanxi Formation (with a thickness ranging from 52.6 to 82.3 m; 67.5 m on average), the Lower Shihezi Formation (with a thickness ranging from 480.6 to 554.7 m; 517.7 m on average), the Upper Shihezi Formation (with a thickness ranging from 116.7 to 162.1 m; 145.6 m on average) and the Shiqianfeng Formation (with a thickness ranging from 210.3 to 256.2 m; 233.6 m on average). The average total thickness of the Permian coal-bearing sequences is about 964.4 m. Coal seams of 17-1, 16-2 13-1, 11 (split into 11-2, 11-1) in the Upper Shihezi Formation, 8, 7-2, 6, 5 (split into 5-2, 5-1), 4 (split into 4-2, 4-1) in the Lower Shihezi Formaton and 3 in the Shanxi Formation

are economically minable. The total minable thickness is about 21.6 m. The major coal seams of the Jining Coalfield occur in the Upper Carboniferous Taiyuan Formation (mean thickness of 165.6 m in range of 148.2-193.4 m, comprising coal seams Nos. 18 to 4) and the Lower Permian Shanxi Formation (mean thickness of 75.6 m in range of 59.9-114.7 m, comprising coal seams Nos. 3 to 2) (Figure 8). Coal seams Nos. 17, 16, 15-2, 6, 3-2, 3-1 are economically minable. The total minable thickness is about 8.4 m.

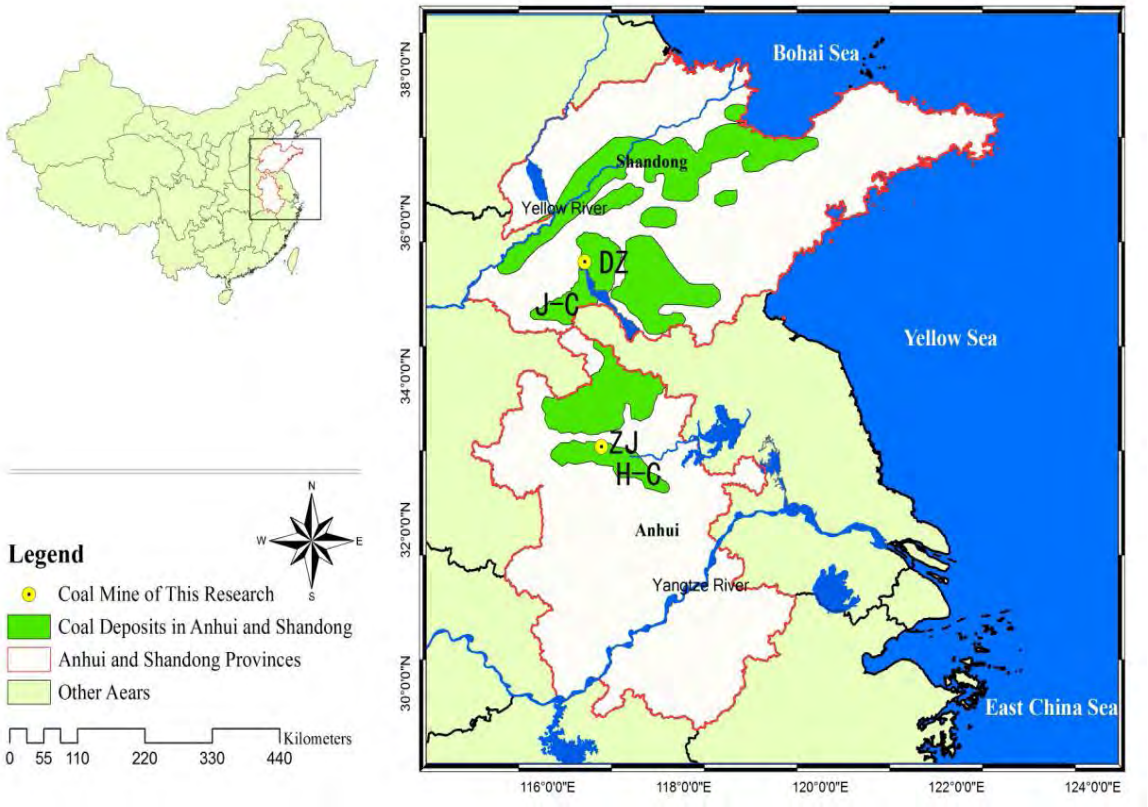

Figure 7 Geographical map showing the locations of studied coal mines. DZ: Daizhuang Coal Mine; ZJ: Zhuji Coal Mine; J-C: Jining Coalfield; H-C: Huainan Coalfied

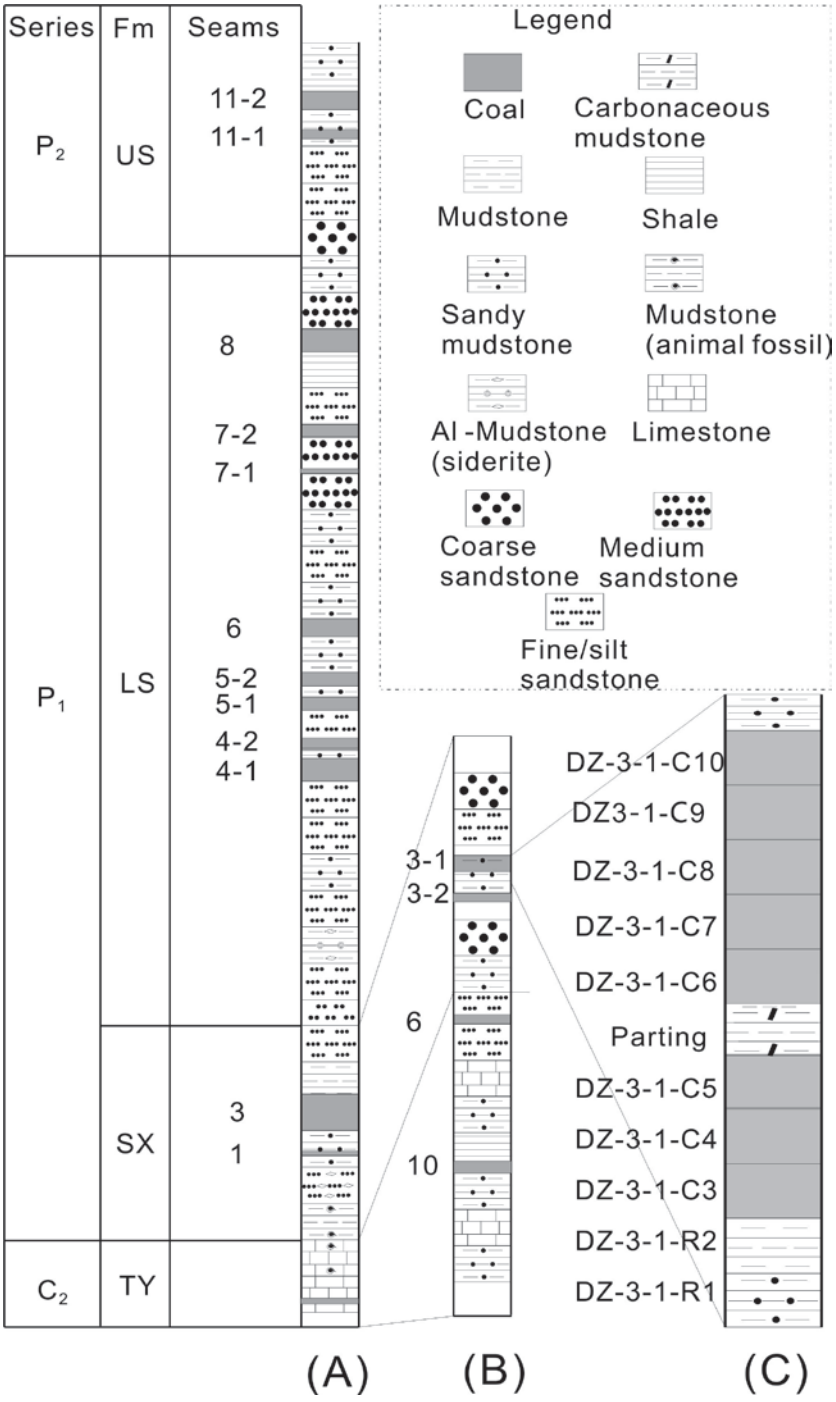

Figure 8 Generalized stratigraphic column and lithological characteristics of coal-bearing sequences in Zhuji Coal Mine of Huainan Coalfield (A) and Daizhuang Coal Mine of Jining Coalfield (B) showing sampled benches in No. 3-1 coal seam (C). C_2: Upper Carboniferous; P_1: Lower Permian; P_2: Upper Permian; Fm: Formation; TY: Taiyuan Formation; SX: Shanxi Formation; LS: Lower Shihezi Formation; US: Upper Shihezi Formation. Note that the coal seams are numbered in ascending order in Zhuji Coal Mine, and in descending order in Daizhuang Coal Mine along coal seams upward

4.1.1.2. Igneous activity

Both Zhuji and Daizhuang coal mines were influenced by intense tectonic movements during the Late Jurassic to Early Cretaceous (Querol et al., 1999; Yang et al., 2012). This large-scale event (the Yanshan Movement in China) was characterized by intense lithospheric extension and widespread volcano-magmatic activity. Large areas of high volatile bituminous coal seams (mainly Nos. 3 and 4 coal seams in the lower strata) in Zhuji Coal Mine were upgraded to high-rank bituminous coal and anthracite while others were transformed to natural coke due to igneous intrusions. The size of intrusive bodies in Zhuji Coal Mine decreases significantly upward along coal-bearing sequences. The igneous influence on Daizhuang coal was limited to lower coal-bearing sequences, and no obvious intrusive bodies were observed surrounding the studied No. 3-1 coal seam.

4.1.1.3. Sampling protocol

Bench coal samples and natural coke samples were taken from Nos. 1, 3, 4-1, 4-2, 5-1, 5-2, 6, 7-2, 8, 11-1 and 11-2 coal seams in borehole cores of Zhuji coal mine (Figure 8 and Figure 9). As compared to the coal samples, the natural coke samples are significantly lower in bulk density. In addition, natural cokes are fragmental in structure with abundant fractures. Generally, three samples (each of ~200 g) were collected from each coal seam, namely upper, middle and lower benches, in line with their relative locations in individual coal seams. Bench coal samples, siltstone and mudstone were sampled from No. 3-1 coal seam in Daizhuang coal mine. Bench coal samples of uniform sizes (20 cm thickness × 5 cm depth) were cut upward from a 2 m fresh working face. All samples were immediately sealed in plastic bags to prevent contamination and weathering.

4.1.2. World coal samples

Coal samples were chosen from the world main coal-forming basins in primary coal production/consumption regions including South Africa, China, the USA, India, Indonesia, former USSR (Russia, Kazakhstan, Ukraine), Mongolia and some European counties (mainly Romania) (Figure 10). Coal samples from China and the USA are from the University of Science and Technology in China, and were homogenized before delivery. Indonesian (large-granular coal), Mongolian (large-granular coal) and Romanian (pulverized coal) coal samples are from the USGS WoCQI project (Tewalt et al., 2010). Bulk Indian coal samples are from the Dept. of Geology collection, Jadavpur University, India. Pulverized coal samples from South African power plants shared from a Hg speciation project (Lusilao-Makiese et al., 2012), coal from Former USSR came

(A)

(B)

Figure 9 Digital photographs of field drilling (A) and sampled coal and associated rocks (B)

from the Moscow State University collection, and from other regions were supplied by C. Liousse (Laboratoire d'Aerologie, Toulouse, France). Bulk and large-granular coal samples were pulverized in a motorized agate grinder (Fritsch pulverizer 2) to <250 μm mesh particles before analysis. The agate mortar was cleaned with high purity ethanol and then Milli-Q water, and dried by compressed

air before processing each sample. In between samples, ~15 g Hg-clean quartz sand was processed in the same way as coal samples to monitor and minimize the possible cross-contamination.

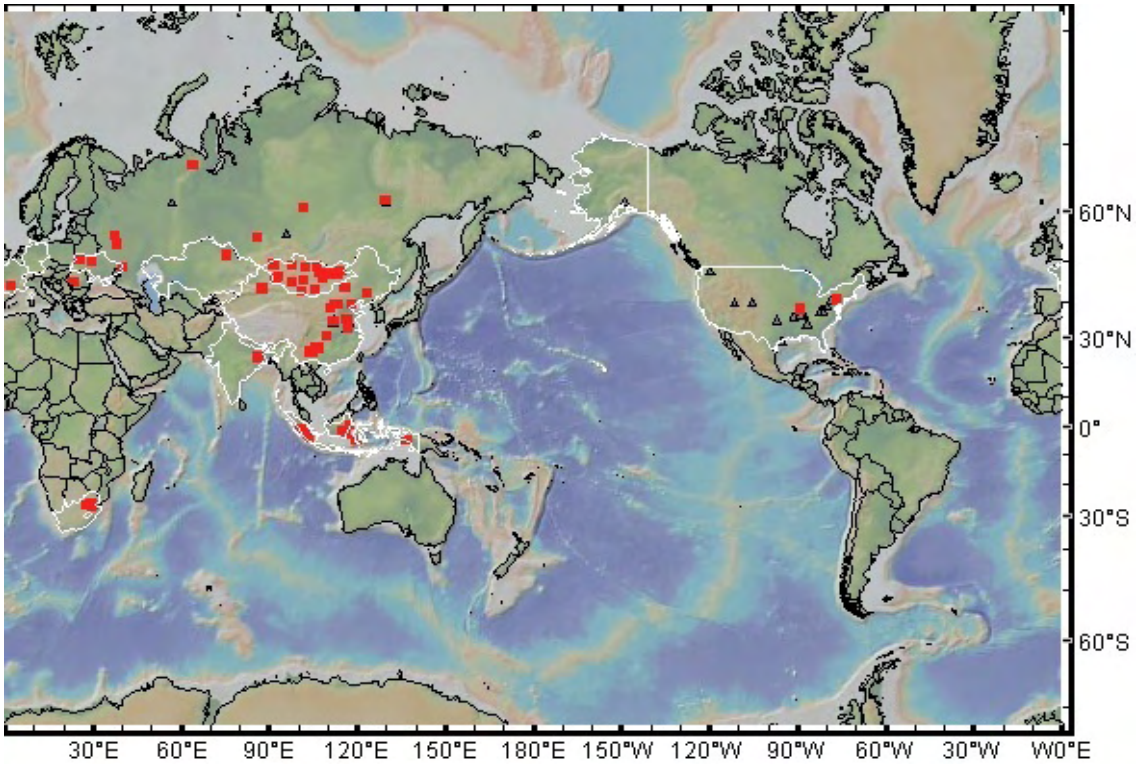

Figure 10 The geographical locations of world coal samples

4.1.3. Coal and coal combustion products

4.1.3.1. Site Description

Huainan City is located in north Anhui Province, China. It is known as "Thermal Power Three Gorges", and is the energy base of Eastern China. The estimated total coal reserves of the Huainan coalfield are approximately 44,000 Mt and have recently transformed Huainan City from a coal supplier to an electricity producer (Sun et al., 2010a). At present there are three main power plants (others are under construction) with a total capacity of nearly 10,000 MW and an electric power output of > 80 billion KWh/yr. The increasing coal production (~100 Mt in the year 2010) in several dozens of coal mines and large coal consumption (~27 Mt in the year 2010) in Huainan coal-fired power plants have generated environmental challenges such as air pollution control and the disposal of coal combustion by-products. Emission data showed that SO_2 and dust emission in Huainan city were 119 Mt and 33 Mt respectively in the year 2005, corresponding to an increase of 28% and 12% relative to the year 2000 (NAE&NAC, 2008). Moreover, the generated amount of coal waste (fly ash

and bottom ash) and desulfurization by-product gypsum have been estimated at 11.6 Mt and 0.4 Mt respectively in the year 2010 (NAE&NAC, 2008).

4.1.3.2. Sample collection and preparation

Huainan-1 (HPP-1) and Huainan-2 (HPP-2) power plants (Figure 11) had a similar installed capacity of 2400 MW in the year 2007. Solid samples consisting of feed coal (bulk and pulverized), fly ash, bottom ash and gypsum were collected from three boilers (H1-1, H1-2 and H1-3, all subcritical units) at Huainan HPP-1 and three boilers (H2-1 and H2-2 of subcritical, and H2-3 of supercritical units) at HPP-2, representing different combustion technologies and air pollution control devices (APCD) (Figure 12). All tested units were typical Chinese pulverized coal utility boilers. The supercritical boiler is operated at higher steam temperature and pressure conditions resulting in 10% higher thermal efficiency than the subcritical boilers. All six utility boilers were equipped with ESP for capturing particulate matter with a removal efficiency of >99%. Half of the utility boilers had wet FGD to sequester SO_2 in flue gas, and the SO_2 removal efficiency was always >90%. No NOx control devices were in place at the plants during the period. Combustion temperatures are in the range of 1200-1500 °C in the combustion zone of the boiler and decrease downstream to about 100-200 °C at the ESPs, to 40–100 °C at the WFGD, and to >80 °C (re-heating) at the stack (Figure 12).

(A)

(B)

(C)

Figure 11 Location of Huainan City (A) showing Huainan-1 (B) and Huain-2 Power Plants (C)

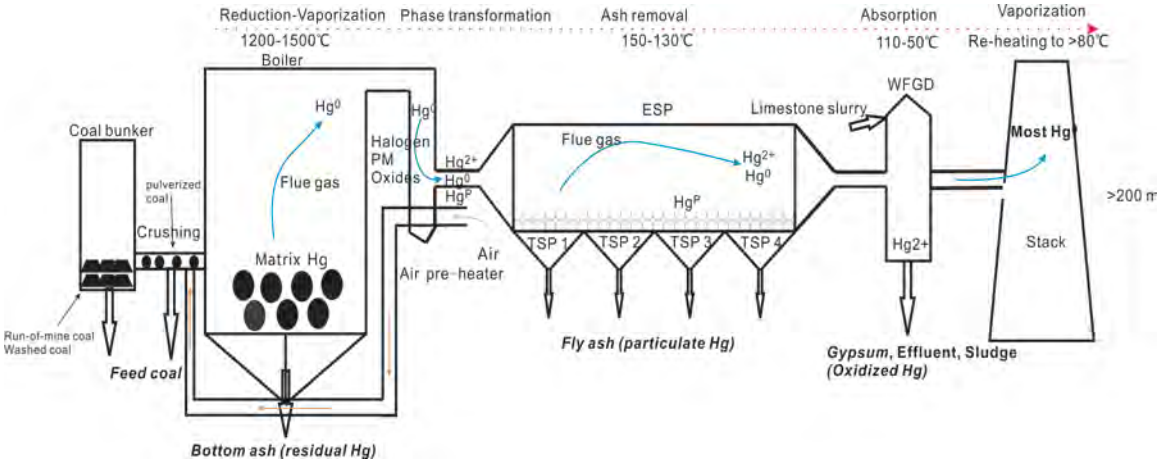

Figure 12 Configuration diagram of Huainan pulverized coal utility boiler at HPP-1 and HPP-2 showing the input and output materials, and temperature gradient. Note the different deployment of ESPs for these two power plants: in HPP-1, there are four hoppers (TSP 1-4) for each ESP, whereas in HPP-2, there are only two hoppers (hoppers A and B) for each ESP. Only boilers H1-3, H2-2 and H2-3 are equipped with WFGD. Abbreviation: TSP-Total particulate matter; ESP: electrostatic precipitator; WFGD: wet flue-gas desulfurization

Feed coals of HPP-1 and HPP-2 were mainly provided by coal mines from the Huainan Coalfield. The main coal suppliers for HPP-1 and for HPP-2 were the Xinji and Panji Coal Mines, respectively (>90%). The feed coal for both plants was characterized by low sulfur contents (on average < 0.5 wt.%), medium calorific value (on average of 19 – 23 MJ/Kg) and high ash yields (on average of 26 – 41 wt.%) (Sun et al., 2010b; Tang et al., 2012). The bulk feed coal was collected at the coal bunker and the pulverized feed coal was sampled from pneumatic conveying ducts connected to the CFUBs. Bottom ash evacuated below the boilers, fly ash removed by ESPs and gypsum produced by the WFGD reaction of limestone slurry with SO_2 were sampled during the active combustion process. Sample collection was conducted over a limited time period of 2 h for each boiler. Each time 3-4 subsamples were taken at 30 min intervals and pooled. In addition, bottom ash, fly ash and gypsum were obtained 15 min after sampling the pulverized coal in order to assure representativeness of all samples. About 1 kg of various composite samples were collected and stored in sealed polyethylene bags.

4.2. Hg stable isotope measurements

Hg stable isotope ratios were determined by CV-MC-ICPMS with Hg(0) vapor introduction into the plasma (Figure 13). Faraday Cups of MC-ICPMS were configured to simultaneously collect the signals of the ^{198}Hg, ^{199}Hg, ^{200}Hg, ^{201}Hg and ^{202}Hg isotopes. The least abundant ^{196}Hg and ^{204}Hg are

commonly excluded because of larger measurement uncertainty arising from their lower natural abundance, potential interference from other molecules and ions (known as isobar effect) and limitations of the MC-ICPMS cup configuration.

For over a decade MC-ICPMS and associated techniques (e.g. sample preparation, purification and introduction) have become the standard in high-precision measurement of Hg stable isotope ratios. In order to facilitate comparison between laboratories and to evaluate uncertainty of reported Hg isotope values, Blum and Bergquist (2007) proposed a general analysis protocol, consistent nomenclatures and data-reporting conventions for the Hg isotope community. The biggest challenge of high-precision Hg isotope measurement is the correction of instrumental mass bias and matrix effects both on mass bias and on cold vapor generation which could shift significantly the isotope ratios of analytes from their real values.

(A)

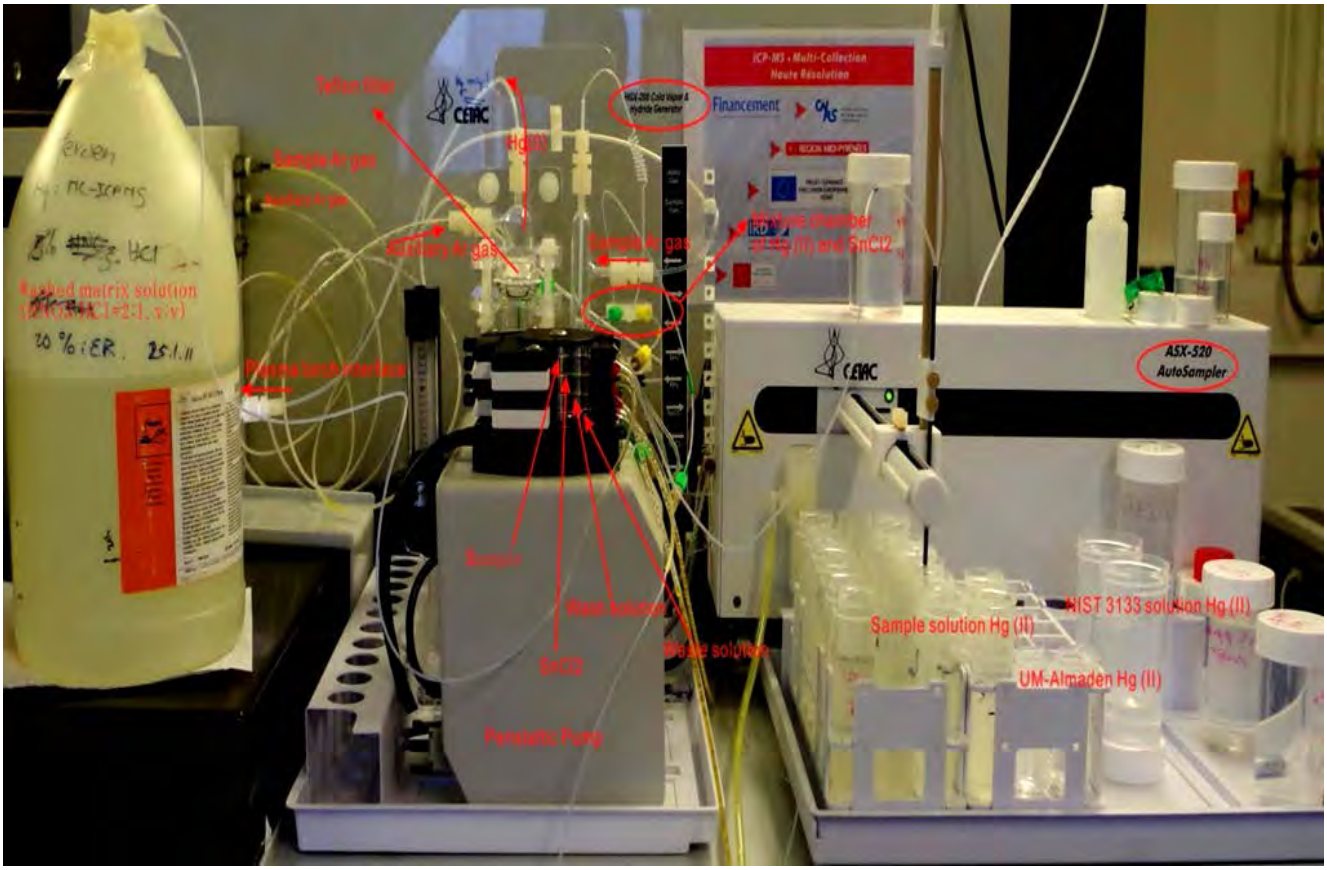

(B)

Figure 13 Overview of MC-ICPMS (Thermo-Finnigan Neptune at the Midi-Pyrenees Observatory, Toulouse, France) (A) and introduction system for Hg isotope measurement (B).

4.2.1. Instrumental mass bias

Instrumental mass bias is an isotope fractionation process by which the isotopes of elements of interest are transmitted through a MS with efficiencies depending on mass of the isotopes (Albarède and Beard, 2004; Maréchal et al., 1999). Instrumental isotope fractionation during atomization and ionization of analyte isotopes in the plasma and transport of the ion beam through the MS interface and flight tube changes the measured isotope ratios from their true values. The measured Hg isotope ratios therefore have to be corrected. According to practices for other isotopic systems, several methods can be utilized to correct the measured Hg isotope ratios (Blum and Bergquist, 2007):

1) Isotope double-spiking: two different enriched Hg isotopes are spiked to the sample;

2) Internal correction (or external standardization): admixture of dry aerosols containing thallium with Hg vapor and;

3) Sample-standard bracketing (SSB): bracketing the sample with NIST 3133 during the measurement session.

Most of the corrections for Hg isotope ratios are based on methods 2) and/or 3) (Blum and Bergquist, 2007). Recently, the isotope double-spiking method has been used, which gave an even smaller uncertainty for isotope ratios (Bartov et al., 2012; Mead and Johnson, 2010).

4.2.1.1. Internal standard correction

The mass-dependent transmission of isotopes in MS can be depicted by a general phenomenological theory by assuming that transmission is a function of mass. Three mass-dependent fractionation laws have been proposed for internal correction: linear, power and exponential (Albarède and Beard, 2004; Maréchal et al., 1999). Because a linear correction is inconsistent between the ratio of two isotope ratios, the latter two laws are usually applied for mass bias correction, which are two particular cases of the generalized power law (Albarède and Beard, 2004; Maréchal et al., 1999). Following Albarede and Beard (2004), assuming that the transmission T(^{i}M) of isotope beams at mass ^{i}M is a function of the mass difference ($\Delta M^{n}= {}^{i}M^{n}- {}^{r1}M^{n}$, n is an arbitrary number) between $^{i}M^{n}$ and a reference mass $^{r1}M^{n}$:

$$\ln T(^{i}M)=\ln T(^{r_1}M)+\frac{\partial \ln T(^{r_1}M)}{\partial\left(M^{n}\right)}(^{i}M^{n}-{}^{r_1}M^{n})+O(^{i}M^{n}-{}^{r_1}M^{n})^{2} \quad [18]$$

where O stands for the terms of order and:

$$\ln T(^{i(r_1)}M)=\ln \frac{^{i(r_1)}n}{^{i(r_1)}N} \quad [19]$$

which represents the number of isotope ions (n) received by collectors relative to the number of isotope atoms (N) introduced into the MS. To the first order, the mass bias can be approximated as:

$$\ln T(^{i}M)-\ln T(^{r_1}M)=\ln \frac{T(^{i}M)}{T(^{r_1}M)}=\ln \frac{\frac{^{i}n}{^{i}N}}{\frac{^{r_1}n}{^{r_1}N}}=\ln \frac{\frac{^{i}n}{^{r_1}n}}{\frac{^{i}N}{^{r_1}N}}=\ln \frac{^{i/ri}R_m}{^{i/ri}R_T}\doteq u(^{i}M^{n}-{}^{r_1}M^{n}) \quad [20]$$

$^{i/r1}R_m$ and $^{i/r1}R_T$ are the measured and true isotope ratios, respectively, and the parameter u stands for the derivative at M = ^{r1}M, and is a mass-independent coefficient. When n=1, Eq. 20 corresponds to power fractionation law:

$$\frac{^{i/ri}\mathbf{R_m}}{^{i/ri}\mathbf{R_T}} = \mathbf{e}^{\mathbf{u}(^{i}\mathbf{M}-^{r_1}\mathbf{M})} = \mathbf{g}^{(^{i}\mathbf{M}-^{r_1}\mathbf{M})} \quad [21]$$

Eq. 18 can be rewritten as:

$$\ln \mathbf{T}(^{i}\mathbf{M}) = \ln \mathcal{T}(^{r_1}\mathbf{M}) + \frac{\partial \ln \mathcal{T}(^{r_1}\mathbf{M})}{\partial \exp(\mathbf{n}\ln \mathbf{M})}\left[\exp\left(\mathbf{n}\ln^{i}\mathbf{M}\right) - \exp\left(\mathbf{n}\ln^{r_1}\mathbf{M}\right)\right] + \mathbf{O}(^{i}\mathbf{M}^{n} -^{r_1}\mathbf{M}^{n})^2 \quad [22]$$

When n→0, Eq. 22 is approximated as:

$$\ln \mathbf{T}(^{i}\mathbf{M}) = \ln \mathbf{T}(^{r_1}\mathbf{M}) + \frac{\partial \ln \mathcal{T}(^{r_1}\mathbf{M})}{\partial \ln \mathbf{M}}\left(\ln^{i}\mathbf{M} - \ln^{r_1}\mathbf{M}\right) = \ln \mathbf{T}(^{r_1}\mathbf{M}) + \mathbf{u}^{r_1}\mathbf{M}\left(\ln^{i}\mathbf{M} - \ln^{r_1}\mathbf{M}\right) \quad [23]$$

By arranging Eq. 23, we can obtain:

$$\ln \frac{^{i/ri}\mathbf{R_m}}{^{i/ri}\mathbf{R_T}} = ^{r_1}\mathbf{M}\mathbf{u}\ln \frac{^{i}\mathbf{M}}{^{r_1}\mathbf{M}} = \mathbf{f}\ln \frac{^{i}\mathbf{M}}{^{r_1}\mathbf{M}} \quad [24]$$

which can be rewritten as:

$$\frac{^{i/ri}\mathbf{R_m}}{^{i/ri}\mathbf{R_T}} = \left(\frac{^{i}\mathbf{M}}{^{r_1}\mathbf{M}}\right)^{\mathbf{f}} \quad [25]$$

where f =u^{r1}M is the mass fractionation coefficient. To the first order, the mass fractionation per amu is:

$$\frac{\frac{^{i/ri}\mathbf{R_m}}{^{i/ri}\mathbf{R_T}} - \mathbf{1}}{(^{i}\mathbf{M} -^{r_1}\mathbf{M})} \doteq \frac{\ln \frac{^{i/ri}\mathbf{R_m}}{^{i/ri}\mathbf{R_T}}}{(^{i}\mathbf{M} -^{r_1}\mathbf{M})} = \ln \mathbf{e}^{\mathbf{u}} = \ln \mathbf{g} = \mathbf{u} \quad [26]$$

for the power fractionation law and is

$$\frac{\frac{^{i/ri}R_m}{^{i/ri}R_T}-1}{^{i}M-^{r_1}M} \doteq \frac{\ln\frac{^{i/ri}R_m}{^{i/ri}R_T}}{^{i}M-^{r_1}M} = \frac{\frac{\ln\frac{^{i/ri}R_m}{^{i/ri}R_T}}{\frac{^{i}M-^{r_1}M}{^{r_1}M}}}{^{i}M-^{r_1}M} \doteq \frac{\ln\frac{^{i/ri}R_m}{^{i/ri}R_T}}{\ln(1+\frac{^{i}M-^{r_1}M}{^{r_1}M})} = \frac{\ln\frac{^{i/ri}R_m}{^{i/ri}R_T}}{\ln(\frac{^{i}M}{^{r_1}M})} = \frac{f}{^{r_1}M} = u \quad [27]$$

for the exponential fraction law.

We can derive a second set of isotope ratio $^{j/r2}R$, similar to Eqs. 21 and 25, using power and exponential law, respectively:

$$\frac{^{j/r_2}R_m}{^{j/r_2}R_T} = e^{u(^{j}M-^{r2}M)} \quad [28]$$

$$\frac{^{j/r_2}R_m}{^{j/r_2}R_T} = (\frac{^{j}M}{^{r_2}M})^{f} \quad [29]$$

For the power fractionation law, taking logarithm on both sides of Eqs. 21 and 28, and dividing Eq. 22 by Eq. 29 gives the slope $S^{i/ri}_{j/r2}$ of the $\ln^{i/r1}R_m$ vs. $\ln^{j/r2}R_m$ array:

$$\frac{\ln^{i/r_1}R_m-\ln^{i/r_1}R_T}{\ln^{j/r_2}R_m-\ln^{j/r_2}R_T} = \frac{\lg^{i/r_1}g}{\lg^{j/r_2}g}\frac{^{i}M-^{r_1}M}{^{j}M-^{r_2}M} = S^{i/r_1}_{j/r_2} \quad [30]$$

Similarly, for exponential fractionation law, the slope $S^{i/ri}_{j/r2}$ is

$$\frac{\ln^{i/r_1}R_m-\ln^{i/r_1}R_T}{\ln^{j/r_2}R_m-\ln^{j/r_2}R_T} = \frac{^{i/r_1}f}{^{j/r_2}f}\frac{\ln^{i}M-\ln^{r_1}M}{\ln^{j}M-\ln^{r_2}M} = S^{i/r_1}_{j/r_2} \quad [31]$$

During Hg isotope measurement, a dry Tl aerosol (NIST SRM 997; $^{205}Tl/^{203}Tl = 2.38714$) generated by a desolvating nebulizer (e.g., Aridus II from Cetac in this work) is mixed with the sample Hg vapor in a gas-liquid separator, and then they are simultaneously introduced into the plasma (Blum and Bergquist, 2007). In this case, we can substitute the isotopes in Eqs. 30 and 31 using Hg and Tl isotopes:

$$\frac{\ln R^{xxx/198}Hg_m-\ln R^{xxx/198}Hg_T}{\ln R^{205/203}Tl_m-\ln R^{205/203}Tl_T} = \frac{\ln g^{^{xxx/198}Hg}}{\ln g^{^{205/203}Tl}}\frac{M^{xxx}Hg-M^{198}Hg}{M^{205}Tl-M^{203}Tl} = S^{xxx/198}_{205/203} \quad [32]$$

$$\frac{\ln R^{xxx/198}Hg_m - \ln R^{xxx/198}Hg_T}{\ln R^{205/203}Tl_m - \ln R^{205/203}Tl_T} = \frac{f^{xxx/198\,Hg}}{f^{205/203\,Tl}} \frac{\ln M^{xxx}Hg - \ln M^{198}Hg}{\ln M^{205}Tl - \ln M^{203}Tl} = S^{xxx/198}_{205/203} \quad [33]$$

For MC-ICPMS, the fractionation factors, either g or f vary smoothly, even though both are dependent of the respective element. Thus, $\ln g^{xxx/198Hg}/\ln g^{205/203}Tl$ or $f^{xxx/198}Hg/ f^{205/203}Tl$ is expected to be constant, and $\ln R^{xxx/198}Hg_m$ vs. $\ln R^{205/203}Tl_m$ still follows a linear array. The exponential law is found to be optimal to account for the fractionation of non-traditional isotopes including Hg on MC-ICP-MS (Albarède and Beard, 2004; Blum and Bergquist, 2007). Eq. 33 can be rewritten as a linear equation:

$$\ln R^{xxx/198}Hg_m = S^{xxx/198}_{205/203} \ln R^{205/203}Tl_m + \ln R^{xxx/198}Hg_T - S^{xxx/198}_{205/203} \ln R^{205/203}Tl_T \quad [34]$$

in which the slope is:

$$S^{xxx/198}_{205/203} = \frac{f^{xxx/198\,Hg}}{f^{205/203\,Tl}} \frac{\ln M^{xxx}Hg - \ln M^{198}Hg}{\ln M^{205}Tl - \ln M^{203}Tl} \quad [35]$$

and intercept y_0 is:

$$y_0 = \ln R^{xxx/198}Hg_T - \frac{f^{xxx/198\,Hg}}{f^{205/203\,Tl}} \frac{\ln M^{xxx}Hg - \ln M^{198}Hg}{\ln M^{205}Tl - \ln M^{203}Tl} \ln R^{205/203}Tl_T \quad [36]$$

For the case when $g^{xxx/198Hg}=g^{205/203}Tl$ or $f^{xxx/198}Hg= f^{205/203}Tl$, i.e. fractionation factor is independent of the element, then slope and intercept would be fixed, and the slope could be estimated a priori (Table 4). Figure 14 shows a one-day analytical session for Hg isotope ratios on a Nu Plasma MC-ICPMS. By plotting $\ln R^{xxx/198}Hg_M$ vs. $\ln R^{205/203}Tl_M$, we can obtain a linear relationship with a slope of 2.03±0.16 (2σ) for $^{202/198}$Hg, which is indistinguishable from theoretical estimate (2.0 for power law and 2.04 for exponential law) assuming the same fractionation factor from Hg and Tl isotopes.

Table 4 Slopes of linear array of $\ln R^{xxx/198}Hg_m$ vs. $\ln R^{205/203}Tl_m$ assuming fractionation factors are identical for Hg and Tl

	$^{196/198}$Hg	$^{199/198}$Hg	$^{200/198}$Hg	$^{201/198}$Hg	$^{202/198}$Hg	$^{204/198}$Hg
Power	-0.999428	0.500235	0.999738	1.500206	1.999856	3.000241
Exponential	-1.034983	0.514109	1.024891	1.534103	2.039958	3.045278

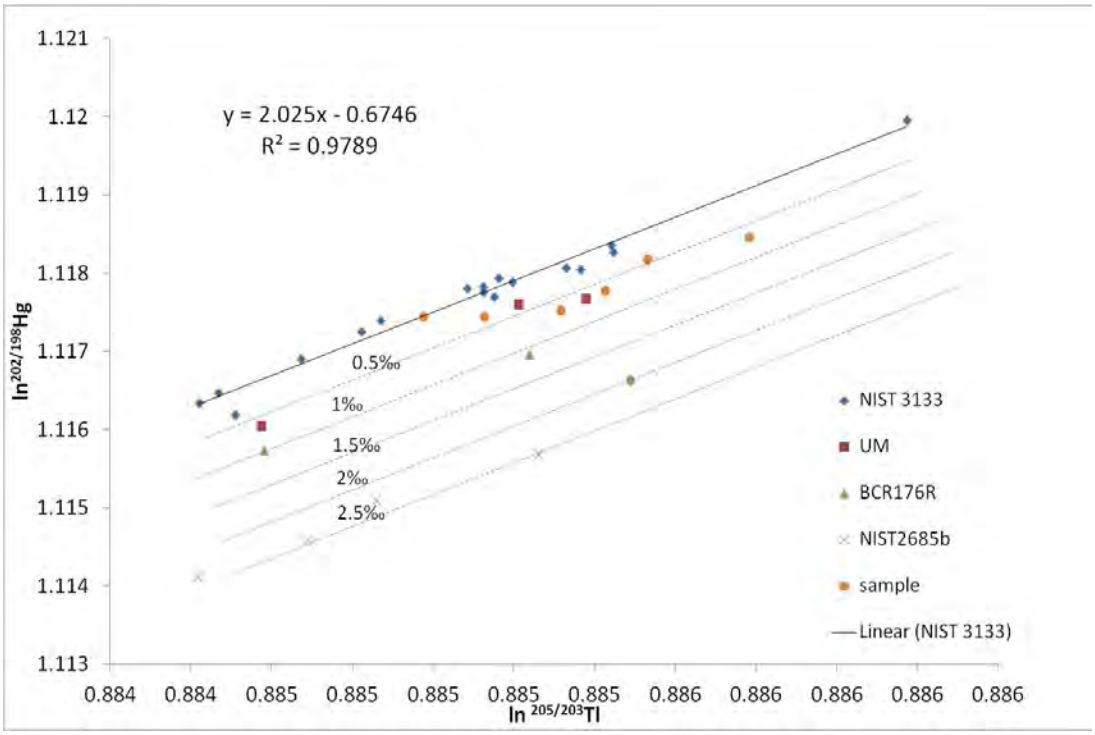

Figure 14 Plot of $\ln^{202/198}$Hg vs. $\ln^{205/203}$Tl of NIST 3133 Hg standard, secondary standard (UM-Almaden, BCR176R, NIST2685b) and samples (coal, coal combustion residuals) in a one-day analytical session on Nu plasma, Pau University, France. All the solutions were measured at ~1 ng/g. The dashed lines represent the $\delta^{202/198}$Hg values of samples and secondary standards relative to NIST 3133 Hg standard.

4.2.1.2. Sample-standard bracketing

In this method, the mass bias of an unknown sample is linearly interpolated between those of two NIST 3133 standards measured before and after the sample (Blum and Bergquist, 2007). This method is more precise when mass fractionation changes smoothly between standards and sample. The sample and standard should be purified and analyzed under similar conditions to exclude matrix effects which could shift the Hg mass bias fractionation factor irregularly (Albarède and Beard, 2004). Detailed formula deviations can be found in the experimental section of Chapter 5.

4.2.2. Matrix effect

Sample matrix can shift Hg isotope ratios through spectral (isobaric effect) and non-spectral interferences.

4.2.2.1. Isobaric effect

An isobar effect is caused by spectral overlapping of different species with unresolved mass differences. For Hg isotope measurement, the potential interferences can be classified into elemental isobar effects (e.g. ^{196}Pt on ^{196}Hg; ^{198}Pt on ^{198}Hg; ^{204}Pb on ^{204}Hg) and molecular isobar effect (e.g. ^{118}Sn^{40}Ar^{40}Ar on ^{198}Hg and HgH^+ interferences). Considering that Hg is introduced in a gas form after reduction by $SnCl_2$ and separated by a gas-liquid separator, potentially interfering species should be and are in practice negligible. In addition, the Tl aerosol is desolvated before mixing with the Hg vapor, which eliminates the molecular HgH^+ isobar effect (Belshaw et al., 2000; Roe et al., 2003). During our measurement, the potential for ^{118}Sn^{40}Ar^{40}Ar isobar formation is monitored on a daily basis by checking ^{118}Sn blank levels, which are always <1mV.

4.2.2.2. Non-spectral interferences

One of the most important non-spectral matrix interferences is the space charge effect behind the skimmer cone where positive ions in the ion beam repulse each other (Praphairaksit and Houk, 2000). Non-spectral matrix interferences can decrease the sensitivity of isotope signals and suppress or enhance instrumental mass bias. This commonly occurs when the matrix element concentration is significantly higher than the analyte of interest. In the case of Hg isotope analyses by cold vapor generation this effect is negligible because Hg is introduced as a vapor in the MC-ICPMS and no other elements are reduced into volatile form by $SnCl_2$. However cold vapor generation is sensitive to matrix effects in itself, as a sample matrix may influence the reduction efficiency of $SnCl_2$. A good example is the addition of dissolved organic matter (DOM) into a UM-Almaden Hg solution, which has been shown to shift the δ^{202}Hg values of UM-Almaden from -0.5‰ at 1 mg/L DOM to -0.18‰ at 15 mg/L DOM (Chen et al., 2010). The mechanism at work here is the presence of strong Hg-DOM complexes at functional thiol (sulfur) groups that inhibit complete reduction of sample Hg(II) to Hg(0) vapor. Matrix constituents also tend to stick to tubing and glass reactor surfaces, thereby complicating signal stabilization and wash-out times for CV-MC-ICPMS and inducing small amounts of imprecision into the final Hg isotope analyses. Thus, purification of Hg from its original sample matrix is ideal before Hg isotope measurement. For aqueous Hg solution, a chromatographic method was used to exclude matrix effects (Chen et al., 2010; Malinovsky et al., 2008). Combustion-trapping procedures are widely used in Hg purification of solid samples (Figure 15) (Biswas et al., 2008; Sun et al., 2013). Finally, a close match (within 10%) of the acid matrix component and Hg concentration between NIST 3133 bracketing standard and analyzed samples is essential to limit non-spectral matrix interferences (Blum and Bergquist, 2007; Sonke et al., 2008).

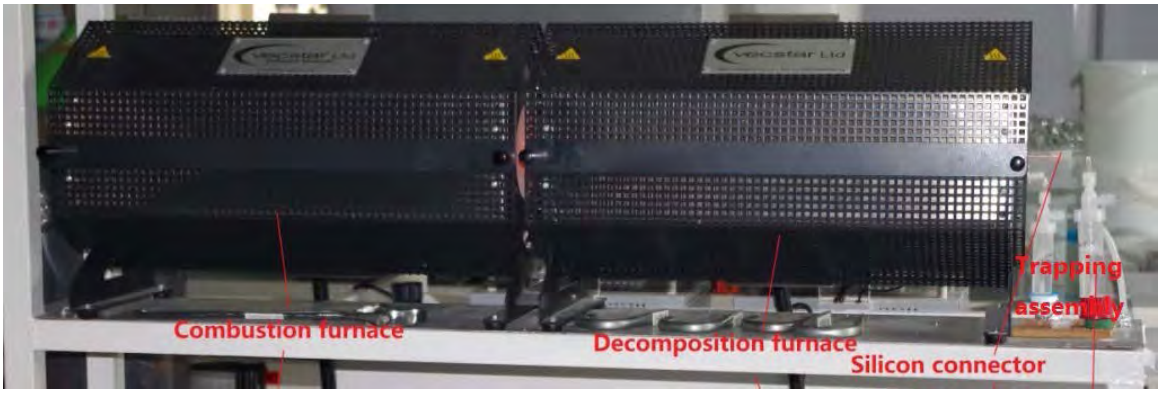

Figure 15 Overview of combustion-trapping system for Hg purification (for more detail, refer to Chapter 5)

References

Albarède, F., Beard, B., 2004. Analytical Methods for Non-Traditional Isotopes, in: Clark M. Johnson, Beard, B.L., Albarède, F. (Eds.), Geochemistry of non-traditional stable isotopes. Reviews in Mineralogy and Geochemistry, pp. 113-152.

Bartov, G., Deonarine, A., Johnson, T.M., Ruhl, L., Vengosh, A., Hsu-Kim, H., 2012. Environmental Impacts of the Tennessee Valley Authority Kingston Coal Ash Spill. 1. Source Apportionment Using Mercury Stable Isotopes. Environmental Science & Technology 47, 2092-2099.

Belshaw, N.S., Zhu, X.K., Guo, Y., O'Nions, R.K., 2000. High precision measurement of iron isotopes by plasma source mass spectrometry. International Journal of Mass spectrometry 197, 191-195.

Biswas, A., Blum, J.D., Bergquist, B.A., Keeler, G.J., Xie, Z., 2008. Natural Mercury Isotope Variation in Coal Deposits and Organic Soils. Environmental Science & Technology 42, 8303-8309.

Blum, J., Bergquist, B., 2007. Reporting of variations in the natural isotopic composition of mercury. Analytical and Bioanalytic Chemistry 388, 353-359.

Chen, J., Hintelmann, H., Dimock, B., 2010. Chromatographic pre-concentration of Hg from dilute aqueous solutions for isotopic measurement by MC-ICP-MS. Journal of Analytical Atomic Spectrometry 25, 1402-1409.

Lusilao-Makiese, J., Tessier, E., Amouroux, D., Tutu, H., Chimuka, L., Cukrowska, E.M., 2012. Speciation of mercury in South African coals. Toxicological & Environmental Chemistry 94, 1688-1706.

Malinovsky, D., Sturgeon, R.E., Yang, L., 2008. Anion-Exchange Chromatographic Separation of Hg for Isotope Ratio Measurements by Multicollector ICPMS. Analytic Chemistry 80, 2548-2555.

Maréchal, C.N., Télouk, P., Albarède, F., 1999. Precise analysis of copper and zinc isotopic compositions by plasma-source mass spectrometry. Chemical Geology 156, 251-273.

Mead, C., Johnson, T.M., 2010. Hg stable isotope analysis by the double-spike method. Analytical and Bioanalytic Chemistry 397, 1529-1538.

NAE&NAC, 2008. Energy Futures and Urban Air Pollution Challenges for China and the United States. National Academy of Engineering and National Research Council, Washington, DC.

Praphairaksit, N., Houk, R.S., 2000. Reduction of Space Charge Effects in Inductively Coupled Plasma Mass Spectrometry Using a Supplemental Electron Source inside the Skimmer: Ion Transmission and Mass Spectral Characteristics. Analytic Chemistry 72, 2356-2361.

Querol, X., Alastuey, A., Lopez-Soler, A., Plana, F., Zeng, R., Zhao, J., Zhuang, X., 1999. Geological controls on the quality of coals from the West Shandong mining district, Eastern China. International Journal of Coal Geology 42, 63-88.

Roe, J.E., Anbar, A.D., Barling, J., 2003. Nonbiological fractionation of Fe isotopes: evidence of an equilibrium isotope effect. Chemical Geology 195, 69-85.

Sonke, J.E., Zambardi, T., Toutain, J.-P., 2008. Indirect gold trap-MC-ICP-MS coupling for Hg stable isotope analysis using a syringe injection interface. Journal of Analytical Atomic Spectrometry 23, 569-573.

Sun, R., Heimbürger, L.-E., Sonke, J.E., Liu, G., Amouroux, D., Berail, S., 2013. Mercury stable isotope fractionation in six utility boilers of two large coal-fired power plants. Chemical Geology 336, 103-111.

Sun, R., Liu, G., Zheng, L., Chou, C.-L., 2010a. Characteristics of coal quality and their relationship with coal-forming environment: A case study from the Zhuji exploration area, Huainan coalfield, Anhui, China. Energy 35, 423-435.

Sun, R., Liu, G., Zheng, L., Chou, C.-L., 2010b. Geochemistry of trace elements in coals from the Zhuji Mine, Huainan Coalfield, Anhui, China. International Journal of Coal Geology 81, 81-96.

Tang, Q., Liu, G., Yan, Z., Sun, R., 2012. Distribution and fate of environmentally sensitive elements (arsenic, mercury, stibium and selenium) in coal-fired power plants at Huainan, Anhui, China. Fuel 95, 334-339.

Tewalt, S.J., Belkin, H.E., SanFilipo, J.R., Merrill, M.D., Palmer, C.A., Warwick, P.D., Karlsen, A.W., Finkelman, R.B., Park, A.J., comp., 2010. Chemical analyses in the World Coal Quality Inventory, version 1, U.S. Geological Survey p. 4.

Yang, M., Liu, G., Sun, R., Chou, C.-L., Zheng, L., 2012. Characterization of intrusive rocks and REE geochemistry of coals from the Zhuji Coal Mine, Huainan Coalfield, Anhui, China. International Journal of Coal Geology 94, 283-295.

Chapter 5

A double-stage tube furnace – acid trapping protocol for the pre-concentration of mercury from solid samples for isotopic analysis

Chapter 5. A double-stage tube furnace – acid trapping protocol for the pre-concentration of mercury from solid samples for isotopic analysis (*Analytical and Bioanalytical Chemistry, in press*)

Résumé

Ce Chapitre résume le protocole d'extraction, purification and pré-concentration du Hg pour l'analyse isotopique. La méthode a été développé pour des échantillons solides divers tel que le charbon, des roches, cendres, tourbes et schistes noirs ayant des teneurs en Hg de <5 ng/g à 10 µg/g. Suivant des optimisations du mélange acide (HNO_3/HCl), flux et type de gaz vecteur, et rampe de température, nous recommandons l'utilisation de 40% (v/v) $2HNO_3$/1HCl dans le piège acide, 25 ml/min O_2 en gaz vecteur et un programme dynamique de rampe de température (15 °C/min for 25-150 °C and 600-900 °C; 2.5 °C/min for 150-600 °C) pour le 1^{ier} four de combustion. Le 2^{ieme} four, le pyrolyseur, est maintenu à 1000 °C durant tous les extractions du Hg. Nous avons testé et effectué 340 extractions de Hg durant 20 mois, montrant une efficacité d'extraction de 89% (médiane) pour les différents types d'échantillons. L'extraction des matériaux de référence montre une absence de biais isotopique pour des rendements entre 81-102%. Ce protocole a l'avantage d'être rapide (3.5h), d'éviter le transfert de la matrice vers le piège acide, et permets une analyse directe des compositions isotopiques par spectrométrie de masse après dilution à 20% (v/v) acide. Cependant, nous avons remarqué des transferts rares de l'iode de la matrice du charbon vers le piège acide, posant des problèmes de réduction du Hg dans le générateur à vapeur froide du spectromètre de masse.

Anal Bioanal Chem (2013) 405:6771–6781
DOI 10.1007/s00216-013-7152-2

RESEARCH PAPER

A double-stage tube furnace—acid-trapping protocol for the pre-concentration of mercury from solid samples for isotopic analysis

Ruoyu Sun · Maxime Enrico · Lars-Eric Heimbürger · Clint Scott · Jeroen E. Sonke

Received: 3 May 2013 / Revised: 12 June 2013 / Accepted: 17 June 2013 / Published online: 14 July 2013

Abstract High-precision mercury (Hg) stable isotopic analysis requires relatively large amounts of Hg (>10 ng). Consequently, the extraction of Hg from natural samples with low Hg concentrations (<1–20 ng/g) by wet chemistry is challenging. Combustion–trapping techniques have been shown to be an appropriate alternative [1]. Here, we detail a modified off-line Hg pre-concentration protocol that is based on combustion and trapping. Hg in solid samples is thermally reduced and volatilized in a pure O_2 stream using a temperature-programmed combustion furnace. A second furnace, kept at 1,000 °C, decomposes combustion products into H_2O, CO_2, SO_2, etc. The O_2 carrier gas, including combustion products and elemental Hg, is then purged into a 40 % (*v*/*v*) acid-trapping solution. The method was optimized by assessing the variations of Hg pre-concentration efficiency and Hg isotopic compositions as a function of acid ratio, gas flow rate, and temperature ramp rate for two certified reference materials of bituminous coals. Acid ratios of $2HNO_3$/1HCl (*v*/*v*), 25 mL/min O_2 flow rate, and a dynamic temperature ramp rate (15 °C/min for 25–150 and 600–900 °C; 2.5 °C/min for 150–600 °C) were found to give optimal results. Hg step-release experiments indicated that significant Hg isotopic fractionation occurred during sample combustion. However, no systematic dependence of Hg isotopic compositions on Hg recovery (81–102 %) was observed. The tested 340 samples including coal, coal-associated rocks, fly ash, bottom ash, peat, and black shale sediments with Hg concentrations varying from <5 ng/g to 10 μg/g showed that most Hg recoveries were within the acceptable range of 80–120 %. This protocol has the advantages of a short sample processing time (~3.5 h) and limited transfer of residual sample matrix into the Hg trapping solution. This in turn limits matrix interferences on the Hg reduction efficiency of the cold vapor generator used for Hg isotopic analysis.

Keywords Mercury isotopes · Inductively coupled plasma mass spectrometry · Combustion · Coal · Peat · Black shale

R. Sun (✉) · M. Enrico · L.-E. Heimbürger · J. E. Sonke
Observatoire Midi-Pyrénées, Laboratoire Géosciences Environnement Toulouse, CNRS/IRD/Université de Toulouse, 14, avenue Édouard Belin, 31400 Toulouse, France
e-mail: roysun1986@gmail.com

M. Enrico
Laboratoire Ecologie Fonctionnelle et Environnement, INP/ENSAT/Université de Toulouse, Avenue de l'Agrobiopole, 31326 Castanet-Tolosan, France

C. Scott
Department of Earth and Planetary Sciences, McGill University, 3450 University Street, Montreal, QC H3A 0E8, Canada

C. Scott
US Geological Survey, 12201 Sunrise Valley Dr, Reston 20191, VA, USA

Introduction

For over a decade, multi-collector inductively coupled plasma mass spectrometry (MC-ICPMS) and associated techniques (e.g., sample preparation, purification, and introduction) have become the standard in high-precision measurement of mercury (Hg) stable isotopic ratios [2–5]. Approximately 10‰ variation in both mass-dependent Hg isotopic fractionation (MDF, expressed as δ^{202}Hg) and mass-independent fractionation (MIF, expressed here as Δ^{199}Hg) has been observed in different environmental compartments and upon controlled experiments [6–8]. Hg MDF and MIF have been shown to be useful tracers for a variety of natural and anthropogenic Hg sources and Hg transformations [9–11]. For high-precision

(~0.1‰ 2σ on δ^{202}Hg) Hg isotopic ratio measurement, MC-ICPMS requires stable and continuous introduction of elemental Hg(0) vapor into the plasma ionization source. This is typically achieved by coupling a cold vapor (CV) generator in which sample solution Hg(II) is reduced into Hg(0) vapor by stannous chloride ($SnCl_2$). CV generator in turn requires appropriate sample preparation to quantitatively transform original sample matrix Hg into soluble ionic Hg(II).

Wet acid digestion using hot plates, microwave, or high T/P equipment is a classic protocol to extract trace metals from powdered solid samples and has been extensively applied to Hg for subsequent Hg isotopic determination [5, 12–14]. Wet chemistry has the advantages of being rapid and widely available but also has disadvantages. For some geo-environmental samples in which Hg resides in acid-resistant, insoluble refractory matrix components, acids may not effectively extract Hg from samples [15, 16]. In parallel, acid digestion solubilizes a large fraction of the matrix which may inhibit the Hg reduction rate in the CV generator and affect CV generator washout characteristics. Inefficient CV generation or insufficient washout biases Hg isotopic measurements. Finally, in a range of natural materials (e.g., igneous and metamorphic rocks, soils, peat, sediments, industrial waste or products, or biological matrices) Hg is present at trace levels (<1–20 ng/g). Therefore, the order of 0.5–10 g sample is needed to obtain sufficient Hg (>10 ng) for high-precision isotopic ratio analysis. This would require large volumes of acid to solubilize Hg and additional processing steps (e.g., transfer, centrifugation, filtration, evaporation, or dilution). Consequently, the soluble matrix to Hg ratio is even higher, blanks are higher, final solution Hg concentrations are near or below CV-MC-ICPMS detection limit, and overall risk of isotopic measurement bias is higher.

A combustion (or pyrolysis) and trapping method, which thermally reduces matrix Hg(II) in solid samples to Hg(0) vapor followed by purging and pre-concentration into a liquid trap, has been shown to be a viable alternative protocol for Hg purification and pre-concentration [1, 17, 18]. The combustion step uses two in-series tube furnaces. Samples, introduced in ceramic boats and covered with sodium carbonate and alumina, are slowly heated from room temperature to 1,000 °C in the first furnace. The second furnace is constantly held at 1,000 °C and acts as a decomposition furnace for large volatile (organic) compounds. In the original method, different gases (Ar, O_2, air) can be introduced into both furnaces. At the outlet of the second furnace, the carrier gas containing Hg(0) vapor and decomposed products (CO_2, CO, H_2O, SO_2, etc.) are purged into a liquid trap made up of 1 wt% $KMnO_4$ in 1.8 M H_2SO4 [1]. This method typically assures full recovery of sample Hg and has been applied to a range of geo-environmental samples with Hg concentrations spanning from several nanogram per gram to several hundreds microgram per gram [1, 17, 19, 20]. It has also been shown that for Hg recoveries down to 50 %, no significant Hg isotopic fractionation takes place [21].

Here, we test and characterize in detail a similar but simplified combustion and trapping method, with major modifications of temperature ramping rate, sample loading approach, carrier gas type, and trapping solution type. Our combustion–trapping assembly was optimized and its performance was evaluated by testing-certified reference materials (CRMs) of bituminous coal (NIST SRM 1632d and NIST SRM 2685b) and geo-environmental samples (coal, coal-associated rocks, bottom ash, fly ash, black shale, and peat) with Hg levels varying form <5 ng/g to 10 μg/g. Hg recoveries of samples were assessed and the effect of Hg recovery on reproducibility of Hg isotopic ratios was investigated.

Experimental section

Reagents and materials

Milli-Q water (18.2 MΩ) was used for all dilutions. Commercial concentrated HCl (Analab NORMAPUR) and HNO_3 (Analab NORMAPUR) were purified through a subboiling system to produce double-distilled 10 M HCl and 15 M HNO_3. ACS reagent-grade $SnCl_2$ (>98 % purity) was dissolved into hot concentrated HCl to prepare $SnCl_2$ solution and diluted to 3 % (*w*/*v*) for MC-ICPMS and 20 % (*w*/*v*) for cold vapor atomic fluorescence spectrometry (CV-AFS) analysis. NIST SRM 3133 Hg standard (10 μg/g) was diluted and used to calibrate CV-AFS Hg concentration measurements and bracket samples during Hg isotopic determination by MC-ICPMS. The solid CRMs are two bituminous coals (NIST SRM 1632d and NIST SRM 2685b) distributed by the National Institute of Standards and Technology.

Analytical protocol

The following protocol is proposed for high-efficiency Hg pre-concentration from solid sample for Hg isotopic determination. Solid samples were firstly determined on a direct mercury analyzer (DMA, Milestone DMA-80) for Hg concentrations in order to determine the samples mass introducing into combustion furnace. Following combustion–trapping processes, a CV-AFS (Brooks Rand Model III) was used to determine Hg concentrations in trapping solutions. By comparing introduced solid sample Hg mass (sample mass × Hg concentration determined by DMA) and measured Hg mass (trapping solution mass × Hg concentration determined by AFS), the recovery of Hg pre-concentration from solid samples was calculated. For samples with acceptable Hg recoveries, generally within the 80–120 % range, subsequent Hg isotopic determination was performed. This range

reflects the long-term uncertainty of Hg concentration measurement in solid samples by DMA (±10 %, 2 RSD) and in trapping solutions by AFS (±10 %, 2 RSD).

Hg concentration in solid samples

The DMA-80 instrument was calibrated monthly with bituminous coal NIST 2685b and NIST 1632d at low Hg range of 0 20 ng (n>10, R^2>0.999) and high Hg range of 20 150 ng (n>8, R^2>0.998). Two blank sample boats and two boats with coal CRMs were run in between ten samples. The periodically analyzed NIST 2685b and NIST 1632d showed excellent agreement with their certified values within ±10 % (2 RSD, n>50). Relative differences of Hg concentrations for 90 % of replicated samples were within 10 %, indicating sufficient stability of the instrument and homogeneity of the samples.

Hg pre-concentration by combustion trapping assembly

Figure 1 describes the double-stage combustion trapping assembly. Two tube furnaces (Vecstar Ltd., UK) with a common quartz tube (24 mm OD, 22 mm ID, 1.2 m length) were used in series as combustion furnace (from ambient temperature ~25 to 900 °C) and decomposition furnace (held at 1,000 °C), respectively. A sand-coated gold trap (Brooks Rand) was used to produce Hg-purified O_2 (or air in a small subset of samples). The O_2 was fed into the combustion furnace at a constant flow rate using a small quartz tube inserted into a silicone stopper (Versilic® Peroxide-Cured, resistant to 250 °C). Powdered sample was weighed into a 20-cm length sample quartz tube (20 mm OD and 18 mm ID, pre-cleaned at 550 °C) and capped with quartz wool (pre-cleaned at 550 °C) at both ends to avoid particle release during combustion of samples. The sample quartz tube is then inserted into the combustion furnace central quartz tube.

The trapping device consists of a 60-ml Savillex PFA impinger (1/4 in. OD tube top and side ports, 33 mm closure) and an elbow-shaped custom-made fritted glass tube (porosity # 40 100 μm). Thick-walled silicone tubing (10 mm OD, 4 mm ID, replaced for each sample) is used to connect the O_2 cleaning gold trap to the furnace tube inlet, and the impinger elbow to the furnace tube outlet. Aluminum foil is wrapped around the furnace tube impinger connection to avoid condensation of water and other volatile compounds. O_2 carrier gas and sample combustion products are evacuated from the impinger outlet to a fume hood. The 60-ml Savillex PFA impinger vial is adapted to hold the trapping solution, yet requires a transfer step to a secondary vial for storage and analysis. Therefore, we replaced the PFA trapping vial with a homologous 33-mm, 50-ml (68 ml total volume) polypropylene vial (PP, Environmental Express, Ref. #SC475) and eliminated the transfer step. The PFA/PP impinger was filled with 30 ml 40 % (*v*/*v*, 2HNO_3/1HCl) acid-trapping solution. After a combustion trapping procedure, the PP trapping vial was unscrewed from the PFA impinger closure. The acid residue on the impinger closure and inside the fritted glass tube was rinsed back into the PP trapping vial with 30 ml Milli-Q water. The final diluted trapping solution (60 ml, 20 % acid, *v*/*v*) was stored at 4 °C prior to subsequent Hg concentration and Hg isotopic determinations. CV-MC-ICPMS measurements are made directly on the 20 % acid solutions in the PP vials that can be fitted into the autosampler. Acid blanks, procedural blanks, standards, and replicates were periodically processed with the samples.

For solid samples with low Hg concentrations in 1 10 ng/g range, we scaled down the impinger design by using narrow 15-ml PP centrifuge tubes (Gosselin X500) that fit directly into the 60-ml PFA/PP trapping assembly (tube in tube). A trapping solution volume of 10 ml 40 % (*v*/*v*) 2HNO_3/1HCl was used and afterwards diluted during the rinsing step to 20 ml 20 % (*v*/*v*) acid solution for Hg isotopic analysis.

Hg concentrations in trapping solutions

Either CV-AFS or CV-MC-ICPMS (Thermo-Finnigan Neptune with CETAC HGX-200) was used to analyze Hg concentrations in 20 % acid-trapping solutions to evaluate Hg pre-concentration recovery and match Hg concentrations of standards during sample standard bracketing. Argon gas for CV-

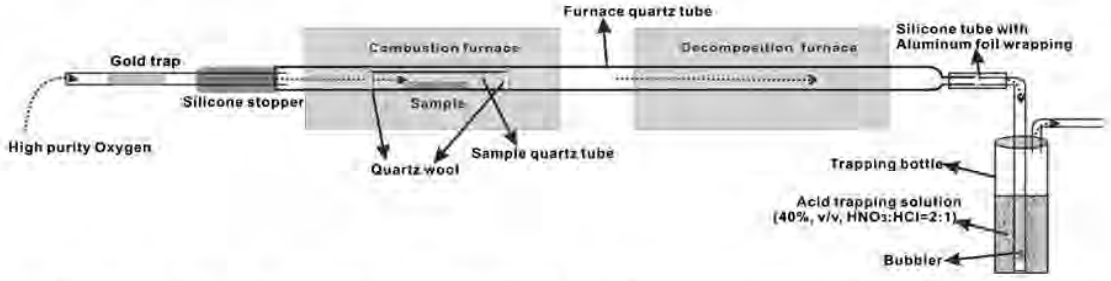

Fig. 1 Schematic diagram of the combustion–trapping assembly. The gas flow direction is indicated by the *dashed arrow*. Thick-walled (3 mm) silicone tubing is used for connecting the outlet of furnace quartz tube to the impinger

AFS was cleaned in-line using a gold trap. $SnCl_2$ (20 %, *w/v*) solution was purged overnight with Ar to eliminate traces of Hg. CV-AFS was calibrated using 0.1 ng/g NIST 3133 Hg working standard solution in range of 10–100 pg Hg (n=6, R^2=0.999), and checked against ORSM-5 river water Hg standard (0.026 ng/g). Hg concentrations in small portions of sample trapping solutions were determined by CV-MC-ICPMS by referring to the ^{202}Hg signal intensities of the trapping solutions relative to that of a 1-ng/g NIST 3133 Hg standard solution. The final uncertainty of Hg concentration determination in trapping solutions was estimated to be within 10 % (2 RSD) for both methods.

Hg isotopic analysis

Hg isotopic ratios in trapping solutions were determined by CV-MC-ICPMS at the Midi-Pyrenees Observatory, Toulouse, France. NIST 3133 Hg standard and in-house UM-Almaden standard were matched to the Hg concentration and 20 % acid (*v/v*, 2HNO_3/1HCl) matrix of the sample solutions within 10 %. An on-line cold vapor generator (CETAC HGX-200) was used to reduce Hg(II) in the trapping solutions into Hg(0) vapor by $SnCl_2$ solution (3 %, *w/v*, in 1 M HCl). The Faraday cups were positioned to simultaneously collect five Hg isotopes: ^{202}Hg (H1), ^{201}Hg (C), ^{200}Hg (L1), ^{199}Hg (L2), and ^{198}Hg (L3). The instrumental baseline was measured by de-focusing before each sample and standard. Acquisition time for Hg isotopic measurements was 12 min (12 blocks, 7 cycles, 8 s integration time). In between samples, the 8-min washout time was sufficient to ensure that the blank levels were <1 % of the preceding sample or bracketed standard signals. For optimum washout, we recommend regular (typically weekly) cleaning of the HGX-200 gas–liquid separator in 50 % HNO_3 (*v/v*, 12 h at 120 °C) and replacement of the 1.0 μm Teflon filter. The sample introduction flow rate of the peristaltic pump was optimized by verifying the linearity of sample flow rate (0.25, 0.50, 0.75, and 1.0 ml/min) versus ^{202}Hg signal intensity. Incomplete Hg(II) reduction was progressively observed at 0.75 and 1.0 ml/min, and therefore the sample flow rate was set at 0.5 ml/min to avoid analytical artifacts. This typically gave an instrumental sensitivity of 1 V on ^{202}Hg for 2 ng/g Hg solutions (Table 1).

Instrumental mass bias of MC-ICPMS was corrected by the standard–sample bracketing method (SSB). The Hg isotopic ratios corrected by SSB have been shown to give comparable accuracy and precision as mass bias correction using a thallium internal standard [22, 23]. Hg isotopic ratios of UM-Almaden and NIST 1632d corrected by SSB in this study are also in excellent agreement with our previous values corrected by thallium [16]. In the SSB method, the mass bias of an unknown sample (f^{smp}) is linearly interpolated between those of two NIST 3133 standards that measured before (f^{std1}) and after (f^{std2}) sample:

$$f^{smp} = \frac{f^{std1} + f^{std2}}{2} \quad (1)$$

Instrumental mass fractionation in MC-ICPMS is optimally accounted for by an exponential law. Following Albarede and Beard [24], we can express the measured ($^{xxx/198}R_m$) and true ($^{xxx/198}R_T$) isotopic ratios of Hg as follows:

$$\frac{^{xxx/198}R_m}{^{xxx/198}R_T} = \left(\frac{^{xxx}M}{^{198}M}\right)^{f} \quad (2)$$

in which M is the isotopic mass and XXX is Hg isotopic mass number between 199 and 202. Expressing Eq. 2 for a sample and two NIST 3133 standards, and then dividing the equation of standard by sample, we obtain:

$$\frac{^{xxx/198}R_T^{sam}}{^{xxx/198}R_T^{std1}} = \frac{^{xxx/198}R_m^{smp}}{^{xxx/198}R_m^{std1}} \left(\frac{^{xxx}M}{^{198}M}\right)^{f^{std1} - f^{smp}} \quad (3)$$

$$\frac{^{xxx/198}R_T^{sam}}{^{xxx/198}R_T^{std1}} = \frac{^{xxx/198}R_m^{smp}}{^{xxx/198}R_m^{std1}} \left(\frac{^{xxx}M}{^{198}M}\right)^{f^{std2} - f^{smp}} \quad (4)$$

Table 1 Analytical settings of CV-MC-ICPMS (Thermo-Finnigan Neptune)

RF power	1,200 W	Data acquisition	12 min (12 blocks, 7 cycles, 8 s integration time)
Mass bias correction	Standard–sample bracketing	Washout time	8 min
Sample gas rate	0.65 l/min Ar	Cups configuration	^{202}Hg (H1), ^{201}Hg (C), ^{200}Hg (L1), ^{199}Hg (L2), and ^{198}Hg (L3)
Auxiliary gas rate	0.70 l/min Ar	Sample uptake	0.5 ml/min by peristaltic pump
Additional gas rate	0.35 l/min Ar	Sensitivity (^{202}Hg)	0.5 V per ng/g Hg solution
Cold vapor generator	CETAC HGX-200 using 3 % (*w/v*) Sncl2 in 10 % (*v/v*) bi-distilled HCl		

Table 2 Summary of Hg pre-concentration recovery and isotopic composition of CRMs trapping solutions

CRMs	Sample ID	HCl/HNO$_3$ (v/v)	T ramp rate (°C/min)	Gas flow rate (ml/min)	Expected Hg[a] (ng/g)	Recovery (%)	No.[b]	δ^{202}Hg (‰)	2σ (‰)	Δ^{199}Hg (‰)	2σ (‰)	Δ^{201}Hg (‰)	2σ (‰)
NIST 1632d	1632d-C-1	1:1	2.5	25 (O_2)	1.40	85	2	−1.68	0.22	−0.04	0.03	−0.10	0.02
	1632d-C-2	1:2			1.46	91	2	−2.03	0.12	−0.02	0.07	−0.11	0.04
	1632d-C-3	1:3			1.39	85	2	−1.95	0.04	0.04	0.09	0.07	0.24
	1632d-C-4	2:1			1.46	75	2	−2.31	0.02	0.03	0.03	−0.12	0.00
	1632d-C-5	3:1			1.42	83	2	−1.94	0.06	−0.02	0.01	−0.07	0.06
	1632d-1	1:2			1.19	87	1	−1.76		−0.07		−0.04	
	1632d-2				1.17	83	1	−1.78		−0.06		0.05	
	1632d-3				1.00	95	1	−1.89		−0.04		−0.07	
	1632d-4				1.00	102	1	−1.94		−0.01		−0.04	
	1632d-5		Dynamic[c]		2.24	97	2	−1.69	0.04	0.00	0.01	0.02	0.13
	1632d-6		Dynamic[c]		2.73	85	2	−1.71		−0.05	0.16	−0.04	0.13
	A-1632d-1[d]		2.5	25 (air)	1.17	75	1	−1.63		−0.16		−0.14	
	A-1632d-2		2.5	25 (air)	1.16	86	1	−1.77		−0.03		0.03	
NIST 2685b	2685b-1		1.5	25 (O_2)	1.21	93	1	−2.83		0.00		0.00	
	2685b-2		2	25 (O_2)	1.14	94	1	−2.67		0.01		0.00	
	2685b-3		2	25 (O_2)	1.60	81	1	−2.67		0.01		0.00	
	2685b-4		2.5	25 (O_2)	1.15	99	1	−2.91		0.01		0.00	
	2685b-5			25 (O_2)	1.10	100	1	−2.66		0.01		0.01	
	2685b-6			25 (O_2)	1.60	85	1	−2.66		−0.06		0.05	
	2685b-7			15 (O_2)	1.14	89							
	2685b-8			15 (O_2)	1.23	82							
	A-2685b-1			25 (air)	1.96	96	1	−2.75		0.00		−0.05	
	2685b-9		Dynamic[c]	25 (O_2)	0.50	99	1	−2.82		0.01		−0.06	

[a] Expected Hg concentration in 20 % (v/v) acid-trapping solution

[b] Number of Hg isotopic measurement for one sample trapping solution

[c] A 3.5-h scheme (15 °C/min at 25–150 and 600–900 °C; 2.5 °C/min at 150–600 °C)

[d] MIF values outliers

Table 3 Hg volatilization fractions and isotopic compositions in different step trapping solutions and bulk samples during Hg step-release experiment for lignite (WL-lignite) and bituminous (NIST 1632d)

T (°C)	Sample ID	Hg mass (ng)	Fraction (%)	No.[a]	δ^{202}Hg (‰)	2σ (‰)	Δ^{199}Hg (‰)	2σ (‰)	Δ^{201}Hg (‰)	2σ (‰)
25–150	WL-S-1	0.53	0.19							
150–275	WL-S-2	27.2	10	1	−3.02		0.44		0.28	
275–400	WL-S-3	172	63	1	−3.35		0.31		0.23	
400–550	WL-S-4	62	23	1	−2.90		0.18		0.07	
550–700	WL-S-5	7.3	3							
700–900	WL-S-6	3.1	1.1							
Sum[b]		272	100		−3.08		0.28		0.19	
	WL-Lignite			3	−3.07	0.12	0.21	0.05	0.13	0.10
25–150	1632d-S-1	1.30	0.72							
150–275	1632d-S-2	1.36	0.75							
275–400	1632d-S-3	24.2	13.3	1	−2.39	0.16	0.06	0.07	0.13	0.03
400–550	1632d-S-4	126	70	1	−1.56	0.10	−0.03	0.01	0.01	0.12
550–700	1632d-S-5	25.8	14.2	1	−1.10	0.03	−0.01	0.01	0.11	0.24
700–900	1632d-S-6	2.5	1.4							
Sum[b]		181	100		−1.56		−0.01		0.04	
	NIST 1632d[c]				−1.82	0.22	−0.03	0.05	−0.03	0.10

[a] Number of Hg isotopic measurement for one sample trapping solution

[b] Hg isotopic values are the average of three-step trapping solutions weighted by their corresponding Hg fractions

[c] Long-term average values

largest proportion of 17 %. The recoveries that were slightly lower or higher than the acceptable range were possibly affected by the inherent heterogeneity of solid samples. We typically reanalyze recovery outliers for Hg concentration on the DMA-80 before re-combusting them.

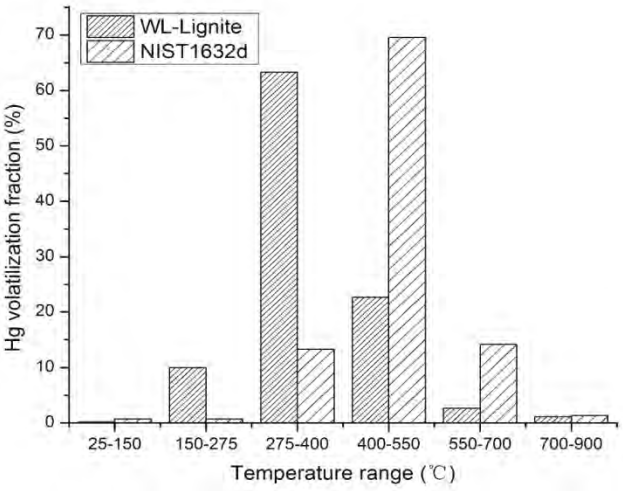

Fig. 4 Hg volatilization fractions trapped by step trapping solutions over different temperature ranges. The sum of all Hg fractions is normalized to 100 %. WL-lignite is a lignite sample from China and NIST 1632d is a bituminous CRM from the USA

Hg release rate and isotopic fractionation during combustion processes

The Hg step-release experiment indicates that the Hg release rate is coal rank-specific. Hg in lignite was volatilized earlier than Hg in bituminous coal, with 10 versus <1 % at 150–300 °C (Fig. 4). Above 550 °C, only 4 % of Hg was still retained in lignite, whereas up to 16 % in bituminous coal. The most effective Hg release ranges for lignite and bituminous coal are 275–400 and 400–550 °C, respectively, over which >60 % Hg was volatilized. The variable Hg release rates in different coal ranks are possibly a reflection of different Hg-bound forms in coal. According to other Hg release experiments of coal pyrolysis, organic-bound Hg was released first followed by sulfide- (mainly pyrite-) bound Hg and then silicate-bound Hg [27, 29]. Lefticariu et al. [20] showed that different coal fractions may carry different Hg isotope signatures. In Illinois coals, the epigenetic pyrite fractions have circum-zero δ^{202}Hg and Δ^{199}Hg values, which are respectively 0.9–1.3 and 0.04–0.15‰ higher than their corresponding organic-enrich fractions, demonstrating a significant Hg isotopic distinction between organic- and inorganic-bound Hg in coal. In our two sets of Hg step-release experiments, both δ^{202}Hg and Δ^{199}Hg showed significant differences between selected step fractions and bulk coal (Fig. 5). The step fractions of lignite were fractionated between −0.28 and 0.18‰ (δ^{202}Hg) relative to bulk lignite,

while the step fractions of bituminous coal were fractionated between 0.57 and 0.72‰ (δ^{202}Hg) relative to bulk bituminous coal (Fig. 5). There is no difference in Δ^{199}Hg values between step fractions and bulk bituminous coal within the analytic uncertainty. However, Δ^{199}Hg is shifted by 0.23‰ for one-step fraction of lignite (150 275 °C) relative to bulk lignite (Fig. 5).

The observed Hg isotopic variation among three-step fractions may be explained by species-specific isotopic variation in coal and/or isotopic fractionation during combustion processes. As the combustion does not induce MIF [16], the observed Δ^{199}Hg variation for different step fractions should reflect the progressive combustion of different Hg-bound fractions in coal. There is a decrease in Δ^{199}Hg values (from 0.44 to 0.18±0.08‰, 2 SD) for lignite step fractions with the increase of temperature as compared to the constant values for bituminous coal step fractions. The NIST 1632d bituminous coal is a washed coal with reduced ash level (~7 wt%) and is expected to have a more homogeneous organic-dominated Hg speciation. WL-lignite is a raw coal sample without artificial processing. In contrast to the small, unsystematic δ^{202}Hg variation in lignite step fractions, δ^{202}Hg values in bituminous coal step fractions increased significantly with increasing temperature. This suggests a Rayleigh-type Hg isotopic MDF for bituminous coal during combustion processes. Although we only had three observations for bituminous coal Hg step-release experiment and the fractionation factor was potentially variable, we still could fit a fractionation factor for δ^{202}Hg ($^{202/198}\alpha$=0.99976±0.00002, 1 SE) between volatilized Hg and residual Hg. This value approximates the theoretically estimated fractionation factor of 0.99976 between various Hg compounds and Hg vapor at 300 °C [30]. We cannot exclude however that NIST 1632d has a heterogeneous δ^{202}Hg distribution and homogeneous Δ^{199}Hg distribution across its different released Hg fractions.

The effect of Hg pre-concentration recovery on isotopic composition

The Hg step-release experiment showed that different temperatures release Hg with variable isotope signatures. Therefore, the isotopic compositions of samples for which Hg was not quantitatively trapped possibly deviated from their true values. Variations of both δ^{202}Hg and Δ^{199}Hg for NIST 1632d and 2685b as a function of Hg recovery are shown in Fig. 6. Within the Hg recovery range of 83 102 % for NIST 1632d and 81 100 % for NIST 2685b, both δ^{202}Hg and Δ^{199}Hg showed no systematic variation. For NIST 1632d, δ^{202}Hg varied from −2.03±0.12 to 1.69±0.11 (2 SD) with an average value of −1.82±0.22 (2 SD, n=8) and Δ^{199}Hg varied from −0.07±0.08 to 0.00±0.08 (2 SD) with an average value of −0.03±0.05 (2 SD, n=8). These values are in accordance with its predecessor NIST 1632c (−1.86±0.13 for δ^{202}Hg and −0.03±0.10 for Δ^{199}Hg, 2 SD) within measurement uncertainty [20, 25]. For NIST 2685b, δ^{202}Hg varied from −2.91±0.11 to −2.66±0.11 (2 SD) with an average value of 2.75±0.18 (2 SD, n=8) and Δ^{199}Hg varied from −0.06±0.08 to 0.01±0.08 (2 SD) with an average value of 0.00±0.05 (2 SD, n=8). Given that sample combustion residues and impinger exhaust gases did not contain any Hg, we speculate that the average 92 % Hg recovery reflects minor loss of Hg at the connection of furnace tube and impinger at a temperature that is high enough to avoid Hg isotopic fractionation.

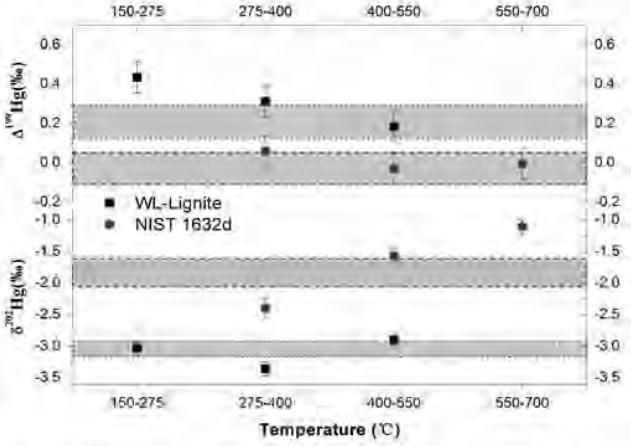

Fig. 5 δ^{202}Hg and Δ^{199}Hg values of three-step trapping solutions under different temperature ranges. The *shaded regions* are δ^{202}Hg and Δ^{199}Hg values for bulk coals (*dotted line border* for WL-lignite; *dashed line border* for NIST 1632d). WL-lignite is a lignite sample from China and NIST 1632d is a bituminous CRM from the USA

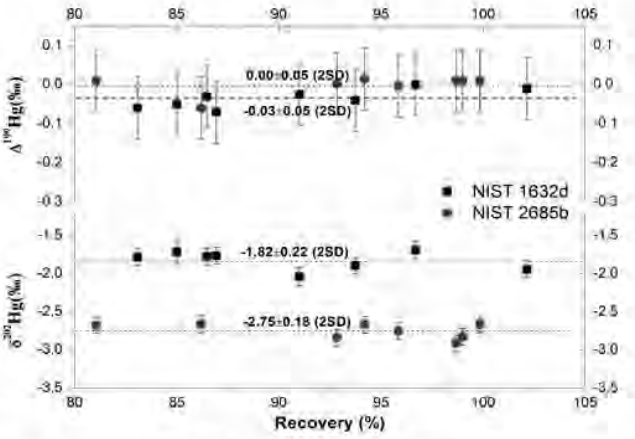

Fig. 6 Variations of δ^{202}Hg and Δ^{199}Hg for NIST 1632d and 2685b as a function of Hg recovery. The average δ^{202}Hg and Δ^{199}Hg values are indicated by the *dashed lines* (NIST 1632d) and *dotted lines* (NIST 2685b). The isotopic compositions of NIST 1632d trapped by acids other than 2HN O_3/1HCl are not included

Problems and suggestions

Early combustion experiments were attempted using two separate quartz tubes for each furnace, using a ball connection. This resulted in low Hg recovery due to gas leaks. Use of a single quartz tube and silicone connections is recommended. Other tube furnace types, other than the 2,000-W Vecstar used in this work, have been used by our group. Lab space and energy can be saved by using smaller furnaces such as the 1,300-W Barnstead and 400-W Carbolite furnaces.

Iodine interference

The combustion–trapping method limits carry-over of sample matrix components to the trapping solution. However, we found that some volatile elements, such as iodine, are partially transferred to the trapping solution and strongly perturbed CV-AFS and CV-MC-ICPMS analysis. Two sapropel samples (90–100 ng/g Hg) and three coal samples (500–650 ng/g Hg) treated with diiodomethane (CH_2I_2) in an attempt to separate the mineral and organic fractions gave systematic <50 and <30 % recoveries, respectively. The extremely low recoveries for these samples are suspected to be caused by iodide interference during Hg determination. High iodide concentrations in the sample solutions are known to decrease the reduction efficiency of Hg(II) by $SnCl_2$ [31]. Marine sapropels may enrich iodine up to 150 μg/g, whereas coal commonly has iodine concentrations in the range of 0.5–15 μg/g as most of its original iodine was lost during diagenesis and metamorphic processes [32–34]. An attempt to analyze the iodine-rich trapping solution of the CH_2I_2-treated coal fraction for its Hg isotopic composition resulted in complete failure of the HGX-200 CV generator. CV-MC-ICPMS signal stabilization increased from the typical 2 to 10 min, while washout (<1 %) increased from the typical 5 to 20 min. Hg isotopic measurements were highly biased. We suspect that iodine precipitates or adsorbs to the HGX-200 glass reactor and provides a cation exchange site that strongly fractionates Hg isotopes. Overnight cleaning of the HGX-200 glass reactor in 50 % HNO_3 (*v*/*v*) at 120 °C and changing the 1.0 μm Teflon filter restored the HGX-200 to optimal running conditions.

Sample loading mass

The mass of samples loaded into the sample quartz tubes depends on Hg concentrations in samples and varied from 0.1 g for coal to 10 g for bottom ash. Because of abundant volatile matters in coal, the loading mass of coal samples should be strictly controlled. According to our experience, >4 g of coal sample exceeds the oxidation ability of the decomposition furnace and resulted in black deposits on the combustion–trapping assembly. Mixing of coal samples with sodium carbonate and alumina could be useful to inhibit the vigorous release of coal particles through formation of sinter [1] when high mass of coal samples or other organic material needs to be combusted.

Conclusions

In this contribution, we detailed a modified combustion–trapping protocol to purify and pre-concentrate Hg for isotopic analysis from various kinds of solid samples with Hg levels varying from <5 ng/g to 10 μg/g. Key aspects of the method are an optimized sample combustion time, use of an oxidizing trapping solution that can be directly analyzed by CV-MC-ICPMS, and a sufficient Hg trapping efficiency to avoid Hg isotopic fractionation artifacts. We recommend to use a 40 % (*v*/*v*) $2HNO_3$/1HCl acid-trapping solution, 25 ml/min O_2 flow rate as carry gas, and dynamic temperature programming (15 °C/min for 25–150 and 600–900 °C; 2.5 °C/min for 150–600 °C) as ramp scheme for the first combustion furnace. After dilution to 20 % (*v*/*v*) acid, the trapping solution can be analyzed directly by CV-MC-ICPMS. The 340 samples combusted over ~20 months demonstrate that this method can achieve a median 89 % recovery for most of samples. Within the Hg recovery range of 81–102 %, no significant Hg isotopic fractionation was observed for CRMs. Special attention should be paid to iodine-rich samples, which possibly interfere with Hg isotopic determination.

Acknowledgments This work is supported by research grants ANR-09-JCJC-0035-01 from the French Agence Nationale de Recherche and ERC-2010-StG_20091028 from the European Research Council to JES. RS acknowledges his PhD scholarship from the Chinese Scholarship Council. We thank Damien Guillaume for providing lab space to host the tube furnace lines at the GET laboratory.

References

1. Biswas A, Blum JD, Bergquist BA, Keeler GJ, Xie Z (2008) Natural mercury isotope variation in coal deposits and organic soils. Environ Sci Technol 42:8303–8309
2. Epov VN, Rodriguez-Gonzalez P, Sonke JE, Tessier E, Amouroux D, Bourgoin LM, Donard OFX (2008) Simultaneous determination of species-specific isotopic composition of Hg by gas chromatography coupled to multicollector ICPMS. Anal Chem 80:3530–3538
3. Lauretta DS, Klaue B, Blum JD, Buseck PR (2001) Mercury abundances and isotopic compositions in the Murchison (CM) and Allende (CV) carbonaceous chondrites. Geochim Cosmochim Acta 65:2807–2818
4. Blum J, Bergquist B (2007) Reporting of variations in the natural isotopic composition of mercury. Anal Bioanal Chem 388:353–359
5. Foucher D, Hintelmann H (2006) High-precision measurement of mercury isotope ratios in sediments using cold-vapor generation multi-collector inductively coupled plasma mass spectrometry. Anal Bioanal Chem 384:1470–1478

6. Blum J (2011) Applications of stable mercury isotopes to biogeochemistry. In: Baskaran M (ed) Handbook of environmental isotope geochemistry. Advances in isotope geochemistry. Springer, Berlin, pp 229–245
7. Bergquist BA, Blum JD (2009) The odds and evens of mercury isotopes: applications of mass-dependent and mass-independent isotope fractionation. Elements 5:353–357
8. Sonke JE (2011) A global model of mass independent mercury stable isotope fractionation. Geochim Cosmochim Acta 75:4577–4590
9. Point D, Sonke JE, Day RD, Roseneau DG, Hobson KA, Vander Pol SS, Moors AJ, Pugh RS, Donard OFX, Becker PR (2011) Methylmercury photodegradation influenced by sea-ice cover in Arctic marine ecosystems. Nat Geo 4:188–194
10. Sherman LS, Blum JD, Johnson KP, Keeler GJ, Barres JA, Douglas TA (2010) Mass-independent fractionation of mercury isotopes in Arctic snow driven by sunlight. Nat Geo 3:173–177
11. Sonke JE, Blum JD (2013) Advances in mercury stable isotope biogeochemistry. Chem Geol 336:1–4
12. Estrade N, Carignan J, Sonke JE, Donard OFX (2010) Measuring Hg Isotopes in bio-geo-environmental reference materials. Geostand Geoanal Res 34:79–93
13. Sonke JE, Schäfer J, Chmeleff J, Audry S, Blanc G, Dupré B (2010) Sedimentary mercury stable isotope records of atmospheric and riverine pollution from two major European heavy metal refineries. Chem Geol 279:90–100
14. Feng X, Foucher D, Hintelmann H, Yan H, He T, Qiu G (2010) Tracing mercury contamination sources in sediments using mercury isotope compositions. Environ Sci Technol 44:3363–3368
15. Liang L, Horvat M, Li H, Pang P (2003) Determination of mercury in minerals by combustion/trap/atomic fluorescence spectrometry. J Anal At Spectrom 18:1383–1385
16. Sun R, Heimbürger L-E, Sonke JE, Liu G, Amouroux D, Berail S (2013) Mercury stable isotope fractionation in six utility boilers of two large coal-fired power plants. Chem Geol 336:103–111
17. Smith CN, Kesler SE, Klaue B, Blum JD (2005) Mercury isotope fractionation in fossil hydrothermal systems. Geology 33:825–828
18. EPA-7471B (2007) Mercury in solid or semisolid waste (manual cold-vapor technique). United States Environmental Protection Agency
19. Smith CN, Kesler SE, Blum JD, Rytuba JJ (2008) Isotope geochemistry of mercury in source rocks, mineral deposits and spring deposits of the California Coast Ranges, USA. Earth Planet Sci Lett 269:399–407
20. Lefticariu L, Blum JD, Gleason JD (2011) Mercury isotopic evidence for multiple mercury sources in coal from the Illinois Basin. Environ Sci Technol 45:1724–1729
21. Sherman LS, Blum JD, Nordstrom DK, McCleskey RB, Barkay T, Vetriani C (2009) Mercury isotopic composition of hydrothermal systems in the Yellowstone Plateau volcanic field and Guaymas Basin sea-floor rift. Earth Planet Sci Lett 279:86–96
22. Stetson S, Gray J, Wanty R, Macalady D (2009) Isotopic variability of mercury in ore, mine-waste calcine, and leachates of mine-waste calcine from areas mined for mercury. Environ Sci Technol 43:7331–7336
23. Mead C, Lyons J, Johnson T, Anbar A (2013) Unique Hg stable isotope signatures of compact fluorescent lamp-sourced Hg. Environ Sci Technol 47:2542–2547
24. Albarède F, Beard BL (2004) Analytical methods for non-traditional isotopes. In: Johnson CM, Beard BL, Albarède F (eds) Geochemistry of non-traditional stable isotopes. Reviews in mineralogy & geochemistry 55. Mineralogical Society of America, Washington, DC, pp 113–152
25. Sherman LS, Blum JD, Keeler GJ, Demers JD, Dvonch JT (2012) Investigation of local mercury deposition from a coal-fired power plant using mercury isotopes. Environ Sci Technol 46:382–390
26. Fletcher T, Ma J, Rigby J, Brown A, Webb B (1997) Soot in coal combustion systems. Prog Energ Combust 23:283–301
27. Luo G, Yao H, Xu M, Gupta R, Xu Z (2011) Identifying modes of occurrence of mercury in coal by temperature programmed pyrolysis. P Combust Inst 33:2763–2769
28. Strezov V, Evans TJ, Ziolkowski A, Nelson PF (2009) Mode of occurrence and thermal stability of mercury in coal. Energ Fuel 24:53–57
29. Guo S, Yang J, Liu Z (2012) Characterization of Hg in coals by temperature-programmed decomposition–atomic fluorescence spectroscopy and acid-leaching techniques. Energ Fuel 26:3388–3392
30. Schauble EA (2007) Role of nuclear volume in driving equilibrium stable isotope fractionation of mercury, thallium, and other very heavy elements. Geochim Cosmochim Acta 71:2170–2189
31. EPA-1631E (2002) Mercury in water by oxidation, purge and trap, and cold vapor atomic fluorescence spectrometry. United States Environmental Protection Agency, EPA-821-R-02-019
32. Swaine DJ (1990) Trace elements in coal. Butterworths, London
33. Wu D, Deng H, Zheng B, Wang W, Tang X, Xiao H (2008) Iodine in Chinese coals and its geochemistry during coalification. Appl Geochem 23:2082–2090
34. Martinez-Ruiz F, Kastner M, Paytan A, Ortega-Huertas M, Bernasconi SM (2000) Geochemical evidence for enhanced productivity during S1 sapropel deposition in the eastern Mediterranean. Paleoceanography 15:200–209

Chapter 6

Hg stable isotope variations in coal-bearing sequences and its implication for Hg sources and geochemistry in coal

Chapter 6. Hg stable isotope variations in coal-bearing sequences and its implication for Hg sources and geochemistry in coal (article in preparation)

Résumé

Ce Chapitre fait l'objet d'une étude de cas sur le fractionnement isotopique du Hg au sein d'une séquence de charbons déposé au même endroit géographique. Le but était d'explorer les signatures isotopiques du Hg comme traceurs des sources ou processus du Hg dans le charbon. Nous observons une variation ~2‰ en δ^{202}Hg (−1.62 to 0.44±0.12‰, 2SD, n=18) et de 0.35‰ en Δ^{199}Hg (−0.12 to 0.22±0.08‰, 2SD, n=18) au sein des couches de charbons déposées pendant 20 Ma (Mine de Zhuji, basin de Huainan, province d'Anhui, Chine). Une même variation est observée au sein d'une seule couche de charbon (mine de Daizhuang, basin de Jining, province de Shandong, Chine). Une corrélation entre le δ^{202}Hg et 1/Hg a Zhuji suggère une mélange binaire entre deux sources de Hg, témoignant d'un décalage dans la source dominante du Hg dans le bassin de Huainan. Dans la couche de charbon de Daizhuang aucune relation claire ne parait entre δ^{202}Hg vs. 1/Hg. Enfin, des cokes naturels, une forme métamorphosé du charbon au contact avec des intrusions magmatiques, montre un fort fractionnement isotopique dépendent de la masse, avec δ^{202}Hg élevé (0.70 to 0.91±0.12‰, 2SD, n=2) ou plus bas (−4.00 to −3.47±0.12‰, 2SD, n=3).

Hg stable isotope variations in coal-bearing sequences and its implication for Hg sources and geochemistry in coal

Sun Ruoyu[1]*, Sonke E. Jeroen[1], Liu Guijian[2]

[1]Observatoire Midi-Pyrénées, Laboratoire Géosciences Environnement Toulouse, CNRS/IRD/Université de Toulouse, France

[2]CAS Key Laboratory of Crust-Mantle Materials and Environment, School of Earth and Space Sciences, University of Science and Technology of China, Hefei, Anhui 230026, China

Abstract

The sources and geochemical processes that control mercury (Hg) occurrences in coal deposits are a topic of debate. Hg stable isotope signatures are a useful tool to trace Hg provenances and transformation mechanisms. Here, we explore the variations in Hg isotope compositions in coal benches of a single coal seam (Daizhuang Coal Mine, Jining Coalfield, Shandong Province), and coals seams of a 20 Ma spanning coal-bearing sequence (Zhuji Coal Mine, Huainan Coalfield, Anhui Province) to assess the potential of using Hg isotope ratios as the geochemical tracer in coal deposits. Coal benches of the Daizhuang No. 3-1 coal seam varied from −2.34 to −0.25±0.12‰ in δ^{202}Hg (2SD, n=8), with no significant mass independent Hg isotope fractionation (MIF) in most samples (−0.04 to 0.12±0.08‰ for Δ^{199}Hg, 2SD, n=8). In contrast, Zhuji coal seams were enriched in the heavier Hg isotopes (−1.62 to 0.44±0.12‰ for δ^{202}Hg, 2SD, n=18), with significant MIF in the younger No's 7-11 coal seams (from 0.06 to 0.22±0.08‰ for Δ^{199}Hg, 2SD, n=7). Increasing trends were seen for both Hg concentrations and δ^{202}Hg going from older to younger Zhuji coal seams. The significant (r^2=0.77, p=0.002) correlation of δ^{202}Hg vs. 1/Hg suggests that Hg in Zhuji coal possibly reflects the mixing of two end-members with distinct δ^{202}Hg. Natural cokes, a metamorphosed form of coal, have either distinctly higher (0.7 to 0.91±0.12‰, 2SD, n=2) or lower δ^{202}Hg (−4.00 to −3.47±0.12‰, 2SD, n=3) than coal samples, demonstrating that significant Hg isotope fractionation occurred when coals were subjected to the perturbation of magmatic intrusions.

*Corresponding author: Ruoyu Sun, E-mail: roysun1986@gmail.com

6.1. Introduction

Mercury (Hg) is a naturally occurring toxic element. As a geological sink for atmospheric, aquatic, sedimentary and hydrothermal Hg inputs, coal is commonly several folds enriched in Hg as compared to sedimentary host rocks (Dai et al., 2012a; Ketris and Yudovich, 2009) In some geological-active areas such as Southwest China and Eastern Russia, Hg can be locally enriched by several orders of magnitude through coal matrix sequestration of Hg-bearing hydrothermal fluids (Yudovich and Ketris, 2005). The utilization of coal for heat and electricity generation and for industrial production of raw materials has emitted large amounts of historically fixed Hg to the atmosphere (Pacyna et al., 2010) At present, coal combustion contributes to approximate half of anthropogenic Hg emissions into the atmosphere, with an annual emission flux of 700-900 tons (Pacyna et al., 2010; Pirrone et al., 2010; Streets et al., 2011).

Extensive studies have been conducted on Hg abundances, affinities and geological provenances in coal and its associated rocks (i.e. coal roof, parting and floor) (e.g. Hower et al., 2005b; Quick et al., 2003; Toole-O'Neil et al., 1999; Yudovich and Ketris, 2005; Zheng et al., 2007a, and references therein). Hg in coal varies significantly, up to several orders of magnitude, among different countries, coal basins, coal mines and even benches within individual coal seams. Although Hg affinities for coal also vary largely, the reduced-sulfur groups in plant-derived organic matter and inorganic sulfide minerals (primarily pyrite) are commonly identified as the main Hg carriers in coal (Diehl et al., 2004b; Hower et al., 2008; Yudovich and Ketris, 2005). The controlling factors that influence Hg accumulation and migration in coal-forming swamps are still a matter of debate, and quantitative tracing of primary Hg sources in coal seams is subject to large uncertainty (Toole-O'Neil et al., 1999; Yudovich and Ketris, 2005). Therefore, an appropriate and robust tracer is needed to help constrain the geochemical controls on Hg occurrences in coal.

Recent advances in multiple collectors inductively coupled plasma mass spectrometry (MC-ICPMS) and associated techniques (e.g. sample preparation, purification and introduction) have allowed high-precision determination of Hg stable isotope ratios in natural samples with Hg concentrations down to ultra-trace levels (Blum and Bergquist, 2007; Chen et al., 2010; Lauretta et al., 2001). Both mass-dependent Hg isotope fractionation (MDF, indicated by δ^{202}Hg) and mass-independent Hg isotope fractionation (MIF, odd ^{199}Hg and ^{201}Hg isotopes mostly, indicated by Δ^{199}Hg) vary within a range of 10‰ in geological and environmental samples (Bergquist and Blum, 2009; Sonke, 2011, Yin et al., 2010). In addition, observations on atmospheric precipitations (snow and rain) also show up to 1‰

variation of MIF of even Hg isotopes (indicated by Δ^{200}Hg) (Chen et al., 2012; Gratz et al., 2010; Sherman et al., 2011). Measurable Hg MDF is caused by most biogeochemical processes that affect Hg, such as reduction (biotic and abiotic), oxidation, adsorption, condensation, evaporation, volatilization, methylation and demethylation (Bergquist and Blum, 2007; Estrade et al., 2009; Kritee et al., 2007; Zheng et al., 2007b; Zheng and Hintelmann, 2010). Previous work has shown that significant Hg isotope variation, as large as 3.5‰ for δ^{202}Hg and 1‰ for Δ^{199}Hg, occurs in coal deposits worldwide (Biswas et al., 2008; Lefticariu et al., 2011; Sherman et al., 2011; Sun et al., 2013a). By using the combination of δ^{202}Hg and Δ^{199}Hg signatures, it has been demonstrated that coals from different countries, coal deposits and coal seams are broadly distinguishable (Biswas et al., 2008; Lefticariu et al., 2011). In addition, the main Hg carriers, i.e. hydrothermal pyrite and organic matter, may possess characteristic and distinguishable Hg isotope signatures (Lefticariu et al., 2011). These observations highlight the potential of Hg isotope signatures to trace Hg sources and occurrences in coal, and to understand the geochemical processes controlling Hg migration and accumulation in coal basins.

Here, we systematically collected low-sulfur (<1 wt.%) coal samples, natural cokes, and coal associated rocks from 12 Permian coal seams in two well-documented coal-bearing strata of Huainan Coalfield and Jining Coalfield, North China (Figure 7). Our study focuses on: 1) Hg isotope characterization of coals deposited in different coalfields and coal-forming periods; 2) identification of Hg provenances and geochemical processes occurring during and after coal deposition and; 3) the impact of high-temperature magmatic intrusion events on Hg isotope fractionation in coal.

6.2. Study area

The Huainan Coalfield and Jining Coalfield, located respectively in northern Anhui and western Shandong provinces, are ones of the most active coal-producing districts in China (Figure 7). Abundant Permo-Carboniferous bituminous coal with middle-high volatile matters (35-40 wt.%, dry ash-free basis) and calorific values (20-30 kJ/kg, dry basis) occur underground in both coalfields (Liu et al., 2005; Sun et al., 2010a, b). The Zhuji Coal Mine (ZJ, covering an area of 45 Km^2 with a coal reserve of 947 Mt) and Daizhuang Coal Mine (DZ, covering an area of 66 Km^2 with a coal reserve 370 Mt) in these two coalfields were selected in the present study. The sampled coals generally have <1 wt.% total sulfur contents (average values is ~0.5% for No's. 1 to 11-2 coal seams of ZJ and ~0.7% for No. 3-1 coal seam of DZ, Figure 8), classifying them as low-sulfur coal. Coal macerals are dominated by vitrinite (>50%) followed by inertinite (<30%) and liptinite (<10%). In

ZJ, abundant intrusive rocks in the forms of dikes and sills were observed at Shanxi Formation coals and decrease upward. The Rb/Sr isotope age for these intrusion bodies is ~110 Ma during the Late Cretaceous Period (Yang et al., 2012). The radiated heat during intrusion and crystallization processes of magma upgraded the surrounding coal to natural coke.

6.2.1. Coal-forming environment

In the Middle Carboniferous, the North China Platform subsided and formed the largest down-warped coal basin, North China Coal Basin (NCCB), with an area of 1,200,000 km^2, representing ~60% of Chinese coal reserves (Dai et al., 2012b; Han et al., 1996; Han and Yang, 1980). The continuous uplift of northern Yinshan Oldland and subsidence of the NCCB during the Later Carboniferous (corresponding to the Taiyuan Formation, Figure 8) resulted in enhanced clastic sediment input to the NCCB. Thick coal seams developed along deltaic-littoral plains at the northern NCCB, while medium-thickness coal seams developed along complex sedimentary settings such as deltaic plains, lagoons and barrier islands at the centre NCCB (including Jining Coalfield, Figure 7). Only thin and unworkable coal seams developed within abundant limestone deposited in a shallow epicontinental sea at the southern NCCB (including Huainan Coalfield, Figure 7) (Han and Yang, 1980; Wu et al., 1995). Following the last large-scale southeastern seawater transgression at the onset of the Permian, seawater completely retreated out of the NCCB at the Early Permian (corresponding to middle-upper sections of Shanxi Formation, Figure 8) and the coal accumulating belt began to shift southwards. Thick coal seams along the deltaic plain developed in the southern and center NCCB. Afterwards, minable coal seams were only deposited at the southern NCCB in LowerShihezi and Upper Shihezi formations (Figure 8). The studied coal seams in Huainan and Jining coalfields were both deposited along transitional deltaic plains after seawater regression (Han, 1990; Querol et al., 1999; Sun et al., 2010a). These coal seams were formed in oxidizing terrestrial environments and contained significantly lower sulfur, boron, strontium and calcium contents, but higher inertinite components than Taiyuan Formation coals formed in marine-influenced reducing environments (Han, 1990; Liu et al., 2004; Querol et al., 1999).

6.2.2. Coal-bearing sequences

Upwards along the coal-bearing sequence, the coal seams are numbered in an ascending order from No's. 1 to 25 in ZJ, Huainan Coalfield, and in a descending order from No's. 18 to 1 in DZ, Jining Coalfield (Figure 8). Laterally, one seam may have 0-3 sub-seams due to splitting and pinch-out

effects. The Carboniferous coal seams in Huainan Coalfield are thin and unworkable. The Permian strata in ZJ comprise coal seams No's. 1-3 in the Shanxi Formation (mean thickness of 67.5 m in range of 52.6-82.3 m), No's. 4-9 in the Lower Shihezi Formaton (mean thickness of 517.7 m in range of 480.6-554.7 m) and No's. 10-25 in the Upper Shihezi Formation (mean thickness of 145.6 m in range of 116.7-162.1 m). Coal seams of No's. 17-1, 16-2, 13-1, 11 (splitting into 11-2 and 11-1), 8, 7-2, 6, 5 (splitting into 5-2 and 5-1), 4 (splitting into 4-2 and 4-1) and 3 are economically minable. The total minable thickness is about 21.6 m. The major coal seams of the Jining Coalfield occurred in the Upper Carboniferous Taiyuan Formation (mean thickness of 165.6 m in range of 148.2-193.4 m, comprising coal seams No's. 18 to 4) and the Lower Permian Shanxi Formation (mean thickness of 75.6 m in range of 59.9-114.7 m, comprising coal seams No's. 3 to 2). Coal seams No's. 17, 16, 15-2, 6, 3-2, 3-1 are economically minable. The total minable thickness is about 8.4 m. A detailed description of stratigraphic and lithological characteristics of coal-bearing sequences in both coal mines can be found elsewhere (Liu et al., 2005; Sun et al., 2010a, b).

6.3. Samples and analyses

6.3.1. Sample collection

Two sampling strategies were used for sample collection. In the first one, 43 bench coal samples and 5 natural coke samples were taken from No's. 1, 3, 4-1, 4-2, 5-1, 5-2, 6, 7-2, 8, 11-1 and 11-2 coal seams in borehole cores of ZJ (Table 5, Table 6 and Figure 8). Most of the samples were collected from coal seams in borehole #12-8 (the distribution of boreholes can be found in Figure 2 of Sun et al., 2010b).

Table 5 Ash yield, sulfur and iron content, Hg concentration and $\delta^{13}C$ values of coal and coke samples in the Zhuji Coal Mine, Huainan Coalfield

Coal seam	Sample ID	Sample lithology	Ash yield (%)	S (%)	Fe (%)	Hg (ng/g)	$\delta^{13}C$	2σ
11-2	ZJ-12-8-11-2U	Coal	15.5	0.36	1.72	59	-24.2	
	ZJ-12-8-11-2M	Coal	38.9	0.57	1.95	168	-24.5	
	ZJ-12-8-11-2D	Coal	17.2	0.29	1.94	57	-24.3	
	ZJ-7-8-11-2U	Coal	14.3	0.37	0.59	71	-24.4	
	ZJ-7-8-11-2M	Coal	33.3	0.63	2.01	357		
	ZJ-7-8-11-2D	Coal	13.2	0.31	1.15	51		
11-1	ZJ-7-8-11-1U	Coal	25.4	0.69	2.23	144	-24.4	0.07
	ZJ-7-8-11-1M	Coal	26.5	0.53	2.92	93		
	ZJ-7-8-11-1D	Coal	22.9	0.59	0.85	228		
8	ZJ-12-8-8U	Coal	18.7	0.61	1.55	169	-23.1	
	ZJ-12-8-8M	Coal	19.1	0.23	1.54	55	-24.2	
	ZJ-12-8-8D	Coal	19.6	0.3	2.18	47	-24.0	1.1
7-2	ZJ-12-8-7-2U	Coal	21.7	0.26	2.23	38	-24.0	
	ZJ-12-8-7-2M	Coal	21.9	0.29	1.29	25	-26.0	0.2
	ZJ-12-8-7-2D	Coal	18.5	0.24	1.83	42	-24.2	

	ZJ-20-4-7-2U	Coal	24.3	0.19	1.95	149	-23.8	
	ZJ-20-4-7-2M	Coal	14.0	0.27	0.90	48		
	ZJ-20-4-7-2D	Coal	16.5	0.26	10.01	63		
	ZJ-12-6-7-2-U-J	Natural coke	18.0			52		
6	ZJ-12-6-6U	Coal	15.3	0.32	6.93	43	-24.6	
	ZJ-12-6-6M	Coal	22.3	0.3	3.30	75		
	ZJ-12-6-6D	Coal	27.4	0.25	6.62	36		
	ZJ-12-8-6U	Coal	21.2	0.41	1.68	150	-24.8	
	ZJ-12-8-6M	Coal	27.6	0.82	4.25	125	-23.7	
	ZJ-12-8-6D	Coal	24.6	0.43	2.89	52	-24.0	
5-2	ZJ-12-8-5-2U	Coal	17.1	0.55	2.88	54	-24.2	
	ZJ-12-8-5-2M	Coal	21.5	0.37	2.06	51	-24.2	
	ZJ-12-8-5-2D	Coal	16.7	0.5	1.48	27	-24.5	
5-1	ZJ-12-8-5-1U	Coal	26.7	0.9	4.17	163	-23.6	
	ZJ-12-8-5-1M	Coal	21.1	0.37	1.92	44	-26.1	
	ZJ-12-8-5-1D	Coal	21.6	0.54	2.87	52	-26.0	
4-2	ZJ-12-8-4-2U	Coal	28.8	0.1	4.49	22	-24.2	
	ZJ-12-8-4-2M	Coal	19.0	0.2	1.48	55	-24.1	
	ZJ-12-8-4-2D	Coal	13.9	0.56	0.41	23	-24.9	
	ZJ-14-5-4-2-D-J	Natural coke	10.8	0.43	0.86	23		
4-1	ZJ-12-8-4-1U	Coal	15.0	0.45	1.15	36	-24.4	
	ZJ-12-8-4-1M	Coal	18.8	0.41	2.05	31	-24.5	
	ZJ-12-8-4-1D	Coal	21.2	0.37	1.99	37	-23.9	
3	ZJ-12-6-3U	Coal	26.6	0.64	3.89	98		
	ZJ-12-6-3M	Coal	17.8	0.31	3.14	21		
	ZJ-12-6-3D	Coal	11.1	0.29	1.91	17	-24.6	
	ZJ-E4-3U	Coal		0.29	0.45	39		
	ZJ-8+1-3U-J	Natural coke	54.8	0.11	1.99	75		
	ZJ-8-5-3U-J	Natural coke	17.5	0.27	0.32	445		
	ZJ-8-5-3D-J	Natural coke	37.5	0.27	0.69	103		
1	ZJ-9+1-1U	Coal	47.3	0.32	2	95		
	ZJ-9+1-1M	Coal	74.7	0.14	5.69	104		
	ZJ-9+1-1D	Coal	65.6	0.32	4.56	113		

Note: sample ID indicates the name of the coal mine followed by borehole number, coal seam number and relative location of bench (and sample lithology). ZJ: Zhuji Coal Mine; U, M and D: the upper, middle and lower benches of each coal seam; J: natural coke; n_1: sample replicates for Hg concentration determination; n_2-replicate analyses of the sample for $\delta^{13}C$

Additional samples from other boreholes were sampled to complement the unavailable coal seams in borehole #12-8 due to undesirable coal-forming environments, and to increase the representativeness of coal seams. Generally, three samples (each of ~200 g) were collected from each coal seam, namely upper, middle and lower benches, in line with their relative locations in individual coal seams. As compared to the coal samples, the natural coke samples are significantly lower in bulk density. In addition, natural cokes are fragmental in structure with abundant fracture development. Intrusive dikes of granite porphyry and gabbro can be found in contact with cokes or as interlayer between coal associated rocks. In the second sampling, 8 bench coal samples (DZ-3-1-C3 to DZ-3-1-C10), 1 siltstone (DZ-3-1-R1) and 1 mudstone (DZ-3-1-R2) that underlie coal benches were sampled from No. 3-1 coal seam in DZ (Table 7 and Figure 8). An interlayer of mudstone and carbonaceous mudstone parting (~20 cm) occurred between coal benches DZ-3-1-C5 and DZ-3-1-C6. Bench coalsamples of uniform sizes (20 cm thickness × 5 cm depth) were cut upward from a 2 m fresh working face. All samples were immediately sealed in plastic bags to prevent contamination and

weathering. Upon transport to the laboratory, bulk samples were air-dried, crushed and sieved to <120 μm particles for subsequent analyses.

Table 6 Hg isotope compositions of coal and coke samples in Zhuji Coal Mine, Huainan Coalfield

Sample ID	Hg (ng/g)	δ^{199}Hg (‰)	2σ (‰)	δ^{200}Hg (‰)	2σ (‰)	δ^{201}Hg (‰)	2σ (‰)	δ^{202}Hg (‰)	2σ (‰)	Δ^{199}Hg (‰)	2σ (‰)	Δ^{200}Hg (‰)	2σ (‰)	Δ^{201}Hg (‰)	2σ (‰)
ZJ-12-8-11-2	95	0.19		0.27		0.39		**0.44**	0.31	**0.08**		0.05		0.06	
ZJ-7-8-11-2	160	-0.06		-0.20		-0.31		**-0.49**		**0.06**		0.05		0.06	
ZJ-7-8-11-1U	144	-0.01	0.09	-0.14	0.09	-0.10	0.12	**-0.31**	0.15	**0.07**	0.05	0.02	0.02	0.14	0.01
ZJ-7-8-11-1M	93	-0.08		-0.38		-0.54		**-0.93**		**0.16**		0.09		0.16	
ZJ-12-8-8	90	0.04		-0.06		-0.01		**-0.19**		**0.09**		0.03		0.13	
ZJ-12-8-7-2	35	0.04	0.02	-0.02	0.03	-0.08	0.06	**-0.21**	0.08	**0.09**	0.04	0.08	0.01	0.07	0.00
ZJ-20-4-7-2	87	0.06	0.03	-0.25	0.03	-0.27	0.01	**-0.66**	0.01	**0.22**	0.03	0.08	0.04	0.23	0.02
ZJ-12-6-6	51	-0.06	0.03	-0.06	0.02	-0.09	0.01	**-0.19**	0.04	**-0.01**	0.04	0.04	0.04	0.05	0.04
ZJ-12-8-6	109	-0.20		-0.33		-0.52		**-0.71**		**-0.03**		0.02		0.02	
ZJ-12-8-5-2	44	-0.18	0.04	-0.40	0.04	-0.63	0.09	**-0.91**	0.15	**0.05**	0.00	0.06	0.03	0.06	0.02
ZJ-12-8-5-1	86	-0.07	0.04	-0.13	0.02	-0.23	0.05	**-0.30**	0.03	**0.00**	0.03	0.02	0.01	0.00	0.07
ZJ-12-8-4-2	33	0.06	0.09	0.10	0.05	0.19	0.13	**0.15**	0.04	**0.02**	0.08	0.03	0.03	0.08	0.11
ZJ-12-8-4-1	35	-0.27	0.03	-0.59	0.00	-0.85	0.01	**-1.27**	0.01	**0.05**	0.02	0.05	0.01	0.10	0.02
ZJ-12-6-3	45	-0.21		-0.36		-0.61		**-0.78**		**-0.02**		0.02		-0.02	
ZJ-E4-3U	39	-0.28	0.07	-0.33	0.05	-0.69	0.12	**-0.63**	0.03	**-0.12**	0.07	-0.01	0.04	-0.21	0.09
ZJ-9+1-1U	95	-0.29	0.11	-0.85	0.06	-1.25	0.21	**-1.62**	0.10	**0.11**	0.08	-0.04	0.01	-0.03	0.14
ZJ-9+1-1M	104	-0.12	0.02	-0.35	0.06	-0.57	0.01	**-0.68**	0.06	**0.05**	0.00	-0.01	0.03	-0.06	0.06
ZJ-9+1-1D	113	-0.21	0.05	-0.36	0.00	-0.68	0.02	**-0.75**	0.01	**-0.02**	0.04	0.01	0.01	-0.12	0.01
ZJ-8-5-3U-J	445	0.17	0.04	0.39	0.07	0.49	0.19	**0.91**	0.05	**-0.06**	0.02	-0.07	0.04	-0.20	0.15
ZJ-8-5-3D-J	103	-0.90	0.07	-2.03	0.08	-3.09	0.12	**-4.00**	0.07	**0.11**	0.05	-0.02	0.04	-0.09	0.07
ZJ-8+1-3U-J	75	-0.72	0.10	-1.74	0.12	-2.53	0.21	**-3.47**	0.10	**0.15**	0.08	0.00	0.07	0.08	0.13
ZJ-14-5-4-2-D-J	23	-0.80	0.04	-1.99	0.01	-2.87	0.12	**-3.93**	0.06	**0.19**	0.02	-0.01	0.02	0.09	0.07
ZJ-12-6-7-2-U-J	52	0.17	0.03	0.35	0.08	0.52	0.15	**0.70**	0.05	**-0.01**	0.02	0.00	0.05	0.00	0.11

Table 7 Hg concentrations and isotope compositions of coal and rock samples in Daizhuang Coal Mine, Jining Coalfield

Sample ID	Hg (ng/g)	Sample Lithology	δ^{199}Hg (‰)	2σ (‰)	δ^{200}Hg (‰)	2σ (‰)	δ^{201}Hg (‰)	2σ (‰)	δ^{202}Hg (‰)	2σ (‰)	Δ^{199}Hg (‰)	2σ (‰)	Δ^{200}Hg (‰)	2σ (‰)	Δ^{201}Hg (‰)	2σ (‰)
DZ-3-1-R1	39	Sandstone	-0.19	0.04	-0.34	0.03	-0.51	0.02	**-0.70**	0.03	**-0.01**	0.04	0.01	0.01	0.02	0.04
DZ-3-1-R2	205	Mudstone	-0.24	0.03	-0.37	0.07	-0.58	0.03	**-0.79**	0.05	**-0.04**	0.04	0.02	0.10	0.01	0.01
DZ-3-1-C3	104	Coal	-0.48	0.01	-1.16	0.02	-1.62	0.04	**-2.34**	0.05	**0.11**	0.02	0.02	0.05	0.14	0.01
DZ-3-1-C4	139	Coal	-0.34	0.05	-0.85	0.01	-1.29	0.02	**-1.82**	0.03	**0.12**	0.06	0.07	0.02	0.09	0.01
DZ-3-1-C5	754	Coal	-0.22	0.02	-0.45	0.03	-0.77	0.01	**-1.05**	0.03	**0.05**	0.02	0.08	0.05	0.03	0.03
DZ-3-1-C6	86	Coal	-0.02	0.02	-0.01	0.06	-0.11	0.05	**-0.12**	0.08	**0.01**	0.00	0.05	0.02	-0.02	0.02
DZ-3-1-C7	114	Coal	-0.10	0.08	-0.16	0.14	-0.38	0.11	**-0.50**	0.10	**0.02**	0.05	0.09	0.08	0.00	0.03
DZ-3-1-C8	85	Coal	-0.01	0.08	-0.07	0.00	-0.16	0.03	**-0.25**	0.00	**0.05**	0.08	0.05	0.00	0.03	0.03
DZ-3-1-C9	578	Coal	-0.35	0.01	-0.78	0.02	-1.13	0.04	**-1.65**	0.01	**0.07**	0.02	0.05	0.02	0.11	0.04
DZ-3-1-C10	522	Coal	-0.31	0.04	-0.67	0.03	-1.03	0.07	**-1.43**	0.12	**0.05**	0.07	0.05	0.09	0.05	0.02
DZ-3-1-C5-F	630	Coal float fraction	-0.32	0.04	-0.69	0.02	-1.03	0.07	**-1.45**	0.05	**0.04**	0.03	0.03	0.00	0.06	0.04
DZ-3-1-C9-F	500	Coal float fraction	-0.47	0.01	-0.85	0.04	-1.31	0.03	**-1.69**	0.04	**-0.04**	0.00	0.00	0.01	-0.03	0.02
DZ-3-1-C10-F	500	Coal float fraction	-0.40	0.01	-0.69	0.02	-1.10	0.00	**-1.43**	0.01	**-0.04**	0.01	0.03	0.02	-0.02	0.00

Note: referring to Figure 8 (c) for sample locations

6.3.2. Analyses

6.3.2.1. Mineralogical analysis and float-sink experiments

Mineralogical analysis of the raw coal samples and rocks was performed on a Inel CPS120 X-ray powder diffractometer (XRD) with a Co-Kα radiation, 40 kV Voltage and 25 mA current. The XRD pattern was recorded over a 2θ interval of 2-120°, with a step size of 0.03. Two samples with the highest Hg concentrations in coal benches in DZ (DZ-3-1-C5, DZ-3-1-C9, Table 7) were found to contain pyritic phases. In order to test whether pyrite and organic matter of coal have different Hg isotope compositions, float-sink experiments were conducted on both coal benches and on a third high Hg coal bench DZ-3-1-C10. About 0.5 g of each coal sample was well mixed with reagent-grade diiodomethane (CH_2I_2) solvent with a density of 3.3 g/ml and densimetrically separated 24 hours before collecting the float and sink fractions onto two separate filter papers. The float and sink fractions were then air-dried in a fume hood.

6.3.2.2. Hg concentrations

A direct combustion mercury analyzer (Milestone DMA-80) consisting of a decomposition furnace, catalyst tube, amalgamator and atomic absorption spectrometer was used to analyze Hg concentrations in solid samples. Hg concentrations of periodically analyzed bituminous coal standards NIST 2685b and NIST 1632d had mean Hg values of 156±10 ng/g (2SD, n = 34) and 90±10 ng/g (2SD, n = 20), respectively, in excellent agreement with certified values. Relative standard deviations of Hg concentrations for replicated samples were within 10% 2RSD.

6.3.2.3. Hg isotope determination

Hg in solid samples was pre-concentrated into acidic aqueous solution, according to the combustion-trapping method described in Sun et al. (2013a). Briefly, Hg in solid samples was thermally volatilized in a pure oxygen stream using a temperature-programmed combustion furnace (25-900 °C). A second furnace, kept at 1000 °C, decomposes combustion products before collecting Hg into a 30 ml 40% (v/v) acid-filled impinger ($2HNO_3$/1HCl, double distilled). Hg in float fractions of float-sink experiments was pre-concentrated by a modified combustion-trapping method that uses a DMA-80 catalyst tube in the second furnace (kept at 680 °C) to absorb iodine from the diiodomethane treatment. We didn't concentrate sufficient Hg from the sink minerals for Hg isotope analysis. Procedural blanks and bituminous coal standards NIST 1632d and NIST 2685b were periodically processed with the solid samples. Some coal benches in the same coal seam of ZJ were

combined for pre-concentrating sufficient Hg for isotope analysis. All the trapping solutions were analyzed for Hg concentrations by cold vapor atomic fluorescence spectrometry (CV-AFS, Brooks Rand Model III) before Hg isotope analysis to evaluate Hg pre-concentration recovery and match Hg concentrations of standards for sample-standard bracketing on CV-MC-ICPMS. The trapping solutions of samples and standards were adjusted to a Hg concentration of 1-2 ng/g in 20% (v/v 2HNO3/1HCl) acidic solutions. Recoveries for all the samples and procedural standards were in the range of 80-120% and procedural blanks had negligible Hg concentrations (<0.03 ng/g) relative to samples and procedural standards.

A CV-MC-ICPMS (Cetac HGX-200 coupled to a Thermo-Finnigan Neptune) at the Observatoire Midi-Pyrenees (France) was used to determine Hg isotope ratios in sample trapping solutions. The detailed analytic protocol can be found in Sun et al. (2013a). Hg isotope composition is expressed in delta notation referenced to the bracketed NIST 3133 Hg standard (Blum and Bergquist, 2007):

$$\delta^{XXX}\mathrm{Hg}\,(‰) = \left(\left(^{XXX}\mathrm{Hg}/^{198}\mathrm{Hg}\right)_{\mathrm{Sample}} \Big/ \left(^{XXX}\mathrm{Hg}/^{198}\mathrm{Hg}\right)_{\mathrm{NIST\ 3133}} - 1\right) \times 1000$$

Where *XXX* is Hg isotope mass between 199 and 202, $(^{XXX}\mathrm{Hg}/^{198}\mathrm{Hg})_{\mathrm{sample}}$ is the measured isotope ratio of the sample, and $(^{XXX}\mathrm{Hg}/^{198}\mathrm{Hg})_{\mathrm{NIST\ 3133}}$ is the average isotope ratio of the bracketing Hg standard solutions measured before and after each sample. In the following, only δ^{202}Hg values are discussed to represent MDF. MIF values are indicated by capital delta (Δ) notation in permil, which is the difference between the measured values of δ^{199}Hg, δ^{200}Hg, δ^{201}Hg and those predicted from δ^{202}Hg using the kinetic MDF law (Blum and Bergquist, 2007) :

$$\Delta^{xxx}\mathrm{Hg} = \delta^{xxx}\mathrm{Hg} - \beta_{xxx} \times \delta^{202}\mathrm{Hg}$$

Where the mass-dependence scaling factor β_{xxx} is 0.252 for ^{199}Hg, 0.502 for ^{200}Hg and 0.752 for ^{201}Hg.

The long-term external uncertainty of the method was determined by repeated analyses of the in-house UM-Almaden standard, which yielded an average δ^{202}Hg value of −0.53±0.12‰ (2SD, n=33) for δ^{202}Hg and −0.02±0.05‰ (2SD, n=33) for Δ^{199}Hg, in agreement with published values (Blum and Bergquist, 2007). The measured δ^{202}Hg and Δ^{199}Hg of four independent combustions of procedural bituminous coal standard NIST 1632d were −1.74 ± 0.12‰ (2SD, n=4) and −0.08 ± 0.08‰ (2SD, n=4), respectively, which were similar to our previous reported values (Sun et al.,

2013b) and its predecessor NIST 1632c as analyzed by others (Lefticariu et al., 2011; Sherman et al., 2011). The largest of either the 2SD (i.e. δ^{202}Hg uncertainty=0.12‰, Δ^{199}Hg uncertainty=0.08‰) of the isotope compositions for the procedural standards NIST 1632d and UM-Almaden or the 2SD on sample replicates (n=2) was taken as the analytical uncertainty of sample isotope compositions.

6.3.2.4. Other analyses

The carbon isotope compositions in coals were determined by a MAT-251 gas source mass spectrometer with dual inlet system at the State Key Laboratory of Loess and Quaternary Geology, CAS (Xian, China). The coal samples were treated to remove carbonates by 2M HCl and then were combusted in a sealed quartz tube in the presence of silver foil and cupric oxide to produce CO_2 for carbon isotope analyses. Carbon isotope ratios are expressed in delta notation (δ^{13}C) in permil deviation relative to the PDB standard (Table 5). The uncertainty of δ^{13}C values is <0.2‰ (2SD). Ash yield, total sulfur and iron contents of samples (Table 5) were determined using methods described in Sun et al., (2010b), with 2SD uncertainties <10%.

6.4. Results

6.4.1. Hg concentrations

Total Hg concentrations in ZJ coals range from 17 to 357 ng/g with an average value of 79± 66 ng/g (1SD, n=43) (Table 5), which is comparable to averaged world coals of 100 ng/g Hg (Ketris and Yudovich, 2009) but is only half of the average Hg content of Chinese coals of 163 ng/g Hg (Dai et al., 2012a). Broadly, there is an increasing trend in Hg concentrations in minable coal seams from No's. 3 to 11-2 in ZJ (Figure 16). The No. 3-1 coals of Shanxi Formation in DZ have an average Hg concentration of 298±256 ng/g (1SD, n=8, in a range of 85-754 ng/g), which is approximately 4 times that of ZJ coals (Table 7). However, excluding the three highest Hg containing coal benches (i.e. DZ-3-1-C5, DZ-3-1-C9 and DZ-3-1-C10), Hg concentrations in the remaining benches are rather homogeneous (85-139 ng/g). Coal benches DZ-3-1-C5 and DZ-3-1-C9 are the only samples that were identified with pyrite phases. Therefore, the significant enrichment of Hg in these three benches likely suggests pyrite to be the host phase (Diehl et al., 2004b; Hower et al., 2005a; Yudovich and Ketris, 2005). Only one coke sample (ZJ-8-5-3U-J, Table 5) was found to have significant Hg enrichment (445 ng/g) as compared to coal.

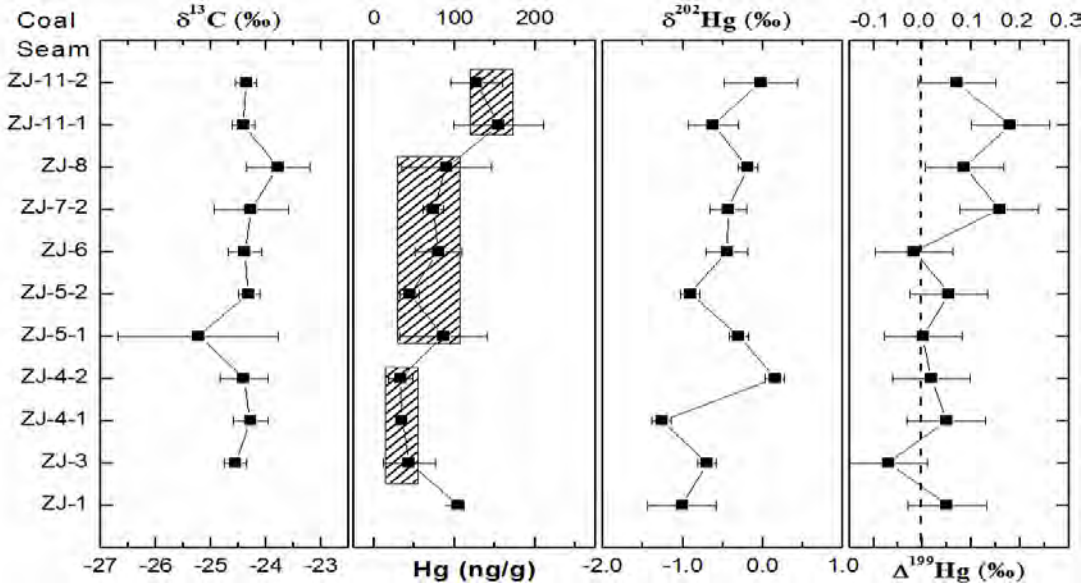

(A)

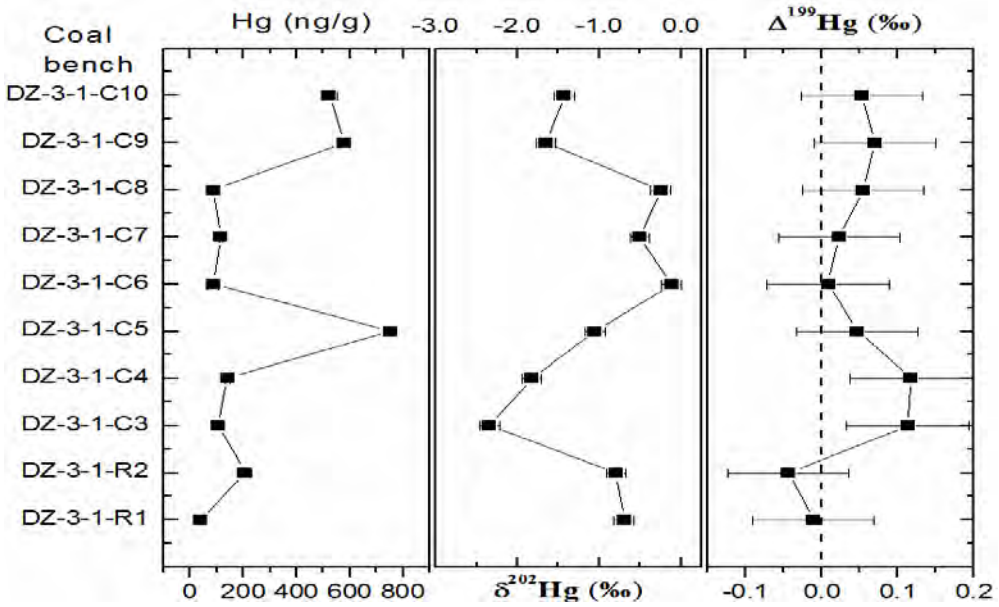

(B)

Figure 16 Inter-seam variation of $\delta^{13}C$, Hg concentration, $\delta^{202}Hg$ and $\Delta^{199}Hg$ values in the Zhuji Coal Mine (A) and intra-seam variation of Hg concentration, $\delta^{202}Hg$ and $\Delta^{199}Hg$ values in No. 3-1 coal seam of Daizhuang Coal Mine (B). The shaded areas for Hg concentrations of Zhuji coals depict the overall increasing trend; the vertical dashed line shows the zero value for $\Delta^{199}Hg$; for individual Zhuji coal seams with multiple samples, 1SD uncertainty of multiple samples is used if this value is larger than 2SD analytical uncertianty; the error bars in Hg concentrations of Daizhuang samples are covered by symbols.

Coal beneficiation experiments show no difference in S content for ZJ between raw coal and its cleaned equivalent (AICE, 2007). As organic associated S is not amenable to removal by cleaning procedures, most sulfur in ZJ coals is therefore probably present in organic forms. A significantly positive correlation is observed for Hg vs. S (R^2=0.30, n=43, p<0.05) in ZJ coals. However, no correlations are observed for Hg vs. Fe or S vs. Fe. This suggests that Hg in ZJ coals mainly associates with reduced S groups (e.g. thiols) in organic macerals rather than Fe-sulfide minerals like pyrite (Diehl et al., 2004a; Skyllberg et al., 2006). Sequential leaching experiments conducted on low sulfur coals from Huaibei Coalfield (bordering Huainan Coalfield) also suggested a dominant organically-bound Hg form (Zheng et al., 2008). In contrast, XRD mineral analysis in DZ suggests that pyritic Hg is a dominant Hg occurrence at least for the high Hg coal benches. This is coherent with a ~10% reduction in S content that was observed for DZ No. 3 coal seam after the raw coal underwent cleaning procedures (SICE, 2010).

6.4.2 Hg isotope compositions

An approximate 2.8‰ range in δ^{202}Hg (−2.34 to 0.44‰) and 0.35‰ range in Δ^{199}Hg (−0.12 to 0.22‰) is observed in the investigated coal deposits (Table 6 and Figure 17). The δ^{202}Hg and Δ^{199}Hg values in ZJ and DZ coals overlap those of selected world coals (−2.98 to 0.45‰ for δ^{202}Hg and −0.63 to 0.34‰ for Δ^{199}Hg, including China, USA and Russia-Kazakhstan) (Biswas, 2008; Sherman et al., 2012; Sun et al., 2013a) (Figure 18). Our data on ZJ coals δ^{202}Hg (−1.62 to 0.44±0.12‰, 2SD) and Δ^{199}Hg (−0.12 to 0.22±0.08‰, 2SD) expands the ranges previously reported for Huainan coals (−0.89 to −0.18‰ for δ^{202}Hg and −0.03 to 0.10‰ for Δ^{199}Hg) (Figure 18) (Biswas et al., 2008; Sun et al., 2013a). A fluctuating but upwards increasing trend of δ^{202}Hg values in coal seams along the coal-bearing sequence in ZJ is observed (Figure 16A).

Statistically, Shanxi Formation coals (i.e. No's. 1 and 3 coal seams) in ZJ (mean δ^{202}Hg = −0.89±0.37, 1SD, n=5) cannot be distinguished from coevally deposited No. 3-1 coal seam of DZ (man δ^{202}Hg =−1.15±0.75‰, 1SD, n=8) (t-test, p=0.23) based on δ^{202}Hg values. However, on a whole coal mine basis, coals from ZJ (mean δ^{202}Hg=−0.56±0.47, 1SD, n=18) can be distinguished from DZ (t-test, p=0.04). Up to ~5‰ variation in δ^{202}Hg values (from −4.00 to 0.91±0.12 ‰, 2SD, n=5) is seen for natural coke samples, and these values are significantly separated from those of coal samples (Figure 17). The δ^{202}Hg values of both rock benches (0.70 and 0.79±0.12‰, 2SD) are within the range for typical sedimentary rocks (mean δ^{202}Hg of −0.6‰ with a range of −0.9 to

−0.2‰, n=15) (Smith et al., 2008), possibly representing the isotope compositions of primary weathering

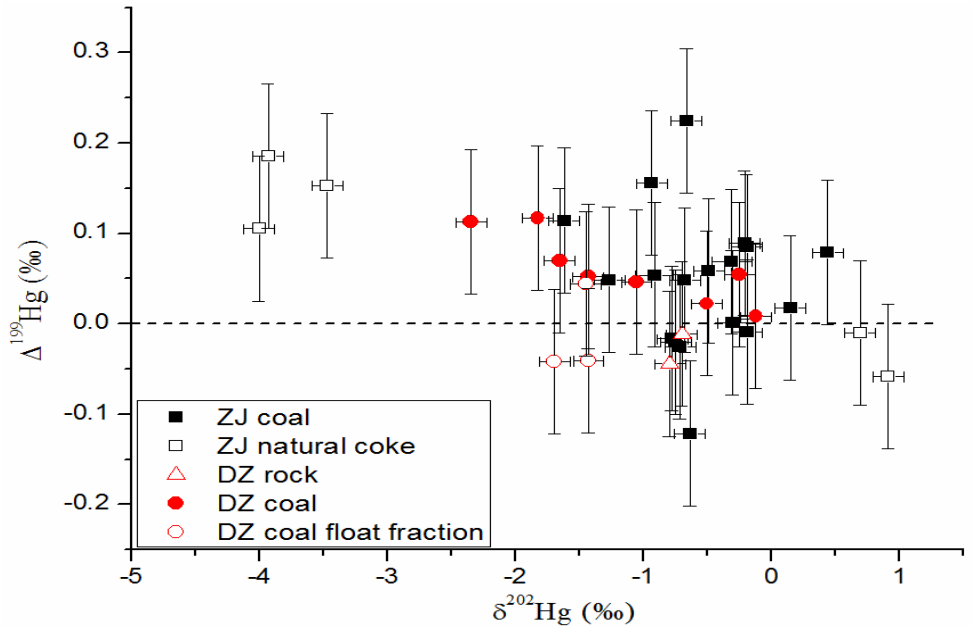

Figure 17 δ^{202}Hg vs. Δ^{199}Hg diagram for coal and natural coke samples in the Zhuji Coal Mine, and for coal, coal floatfraction and rock samples in Daizhuang Coal Mine. The horizontal dashed line shows zero value for Δ^{199}Hg

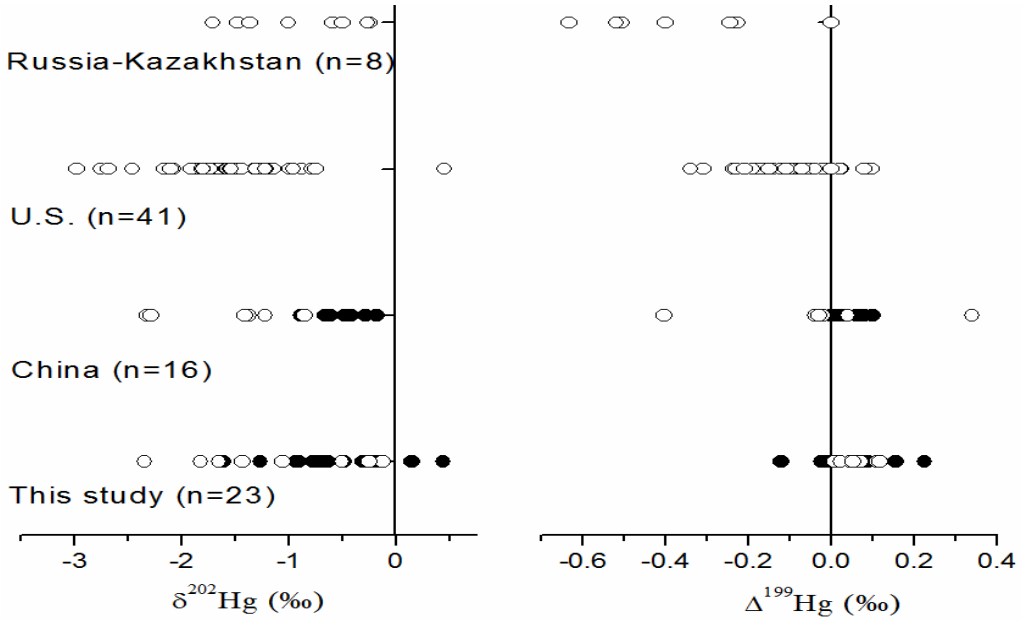

Figure 18 Comparison of δ^{202}Hg and Δ^{199}Hg values between studied coals and coals form other areas. Russia-Kazakhstan coal data are from Biswas et al, (2008); the USA coal data are from Biswas et al. (2008), Lefticariu et al. (2011) and Sherman et al. (2012); Chinnese coal data are from Biswas et al. (2008) and Sun, et al. (2013b). The filled black circles in categories of China and "This study" indicate Huainan coals.

products of source rocks. Only organic float fraction DZ-3-1-C5-F (δ^{202}Hg=−1.45±0.12, 2SD) shows significant depletion in the heavier Hg isotopes relative to the corresponding raw coal (δ^{202}Hg=−1.05±0.12, 2SD) (Table 7), which implies that the separated heavy mineral fraction is enriched in the heavier Hg isotopes relative to coal. A similar observation was made on hand-picked pyrite minerals from the Illinois coal basin, USA (Lefticariu et al., 2011).

Most of the ZJ and DZ samples show insignificant MIF (Δ^{199}Hg and Δ^{201}Hg) (Figure 16). Significant MIF is observed only in coals from upper coal-bearing sequences of ZJ (i.e. No's. 7-2 to 11-2 coal seams) with Δ^{199}Hg values up to 0.22‰ (Figure 16A). Only the two lowest coal benches (DZ-3-1-C3 and DZ-3-1-C4) in DZ show small but significant MIF (Δ^{199}Hg = 0.11 and 0.12±0.08‰, 2SD). Similar to crustal and mantle derived Hg reported elsewhere (Sherman et al., 2009; Smith et al., 2008; Smith et al., 2005; Zambardi et al., 2009), no significant MIF values were observed in the underlying rock benches. All Δ^{201}Hg and Δ^{199}Hg data define a Δ^{199}Hg/ Δ^{201}Hg slope of 0.87±0.23 (2SE) (Figure 19), which is not significantly different from the slope observed during photo-reduction of dissolved organic matter-bound inorganic Hg (II) in aqueous environments (Bergquist and Blum, 2007; Zheng and Hintelmann, 2009).

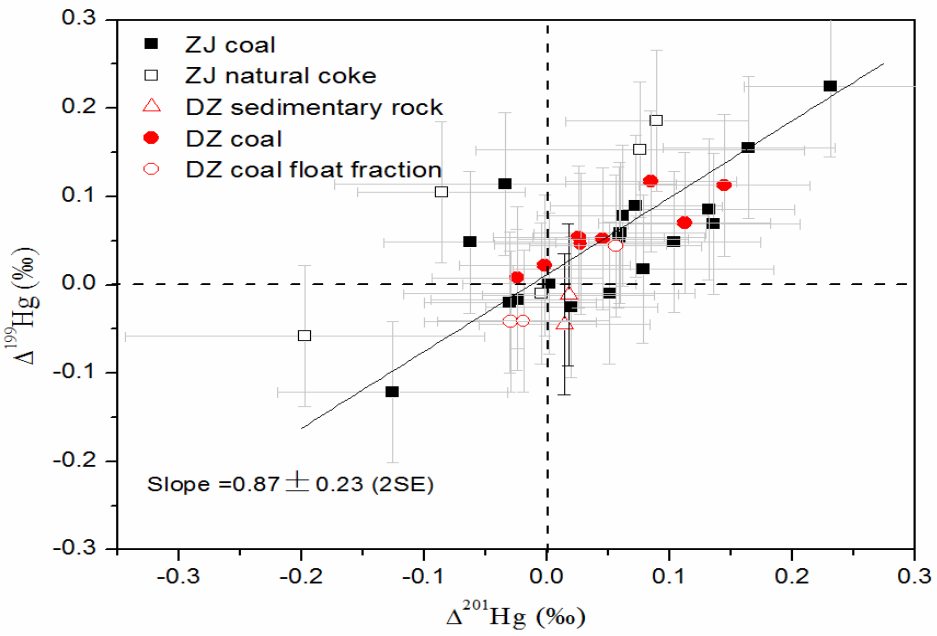

Figure 19 Δ^{199}Hg vs. Δ^{201}Hg values in coal and natural coke samples in Zhuji Coal Mine, and in coal, coal float fraction and rock samples in Daizhuang Coal Mine. Error bar represents measurement uncertainty of samples. The slope and intercept of samples regression line are calculated by the York regression method (York, 1968) that takes into account uncertainties in both Δ^{199}Hg and Δ^{201}Hg. The vertical and horizontal dashed lines show the zero values for Δ^{199}Hg and Δ^{201}Hg.

6.5. Discussion

Hg isotope compositions in coal are a combined result of different Hg sources and biogeochemical processes that occurred during and after coal deposition (Biswas et al., 2008; Lefticariu et al., 2011). Coal-forming plants, sediments sources, depositional environments, coalification degrees, and hydrothermal alteration control the concentration and distribution of Hg in coal (Dai et al., 2012a; Ren et al., 1999). Therefore, these factors also likely determine the Hg isotope compositions of coal.

6.5.1. ZJ coals

A 3‰ variation in $\delta^{13}C$ values, from −26.1 to −23.1‰, is observed in ZJ coals with no systematic trend along coal-bearing sequences (Table 5 and Figure 16A). Most of the $\delta^{13}C$ values in coals (25 out of 29) vary between −25 and −23.5‰. The small variation in $\delta^{13}C$ values indicates a limited fluctuation of coal-forming plant species (primary C3 plants such as *Cordaitopsida, Lepidode-ndron, Pteridosperm, Ginkgopsida and Filicinae* between 250-300 Ma), a contemporaneous climate, and a similar degree of coalification (Bechtel et al., 2002; Holdgate et al., 2009). No correlation is observed between Hg concentrations and $\delta^{13}C$ values for ZJ coals, which indicates that the coal Hg levels were not primarily controlled by plant species. Terrestrial plants, which were brought by floods or lived within the coal-forming basin, were the major materials to form coal deposits. It is difficult to estimate Hg concentration and Hg isotope compositions of ancient plants living during the Late Paleozoic Period (~300 Ma). Terrestrial plants mainly sequester atmospheric Hg through dry/wet Hg deposition (Graydon et al., 2009; Yudovich and Ketris, 2005). Hg isotope compositions of plants were probably inherited by coals during coal formation.

No obvious relationship exists between Hg concentrations and $\delta^{202}Hg$ values in all ZJ coal samples. However, when the coal samples from an individual coal seam are averaged, a significant negative correlation is observed for $\delta^{202}Hg$ vs. 1/Hg ($R^2 = 0.77$, n = 9, p=0.002, excluding coal seams No's. 1 and 4-2) (see explanation in legend of Figure 20). Considering the differences in depositional environments and source rocks for ZJ coal deposit, spanning ~20 Ma, this correlation is quite remarkable. This correlation can potentially be explained by mixing of two Hg end-members, i.e. a Hg depleted end-member with lower $\delta^{202}Hg$ (<−1.3‰) and a Hg enriched end-member with higher $\delta^{202}Hg$ exceeding zero. Along coal seams from Shanxi Formation (No's. 1-3) to Lower Shihezi Formation (No's. 4 to 8) in ZJ, the depositional environments evolved from a subaqueous deltaic plain environment to a lower deltaic plain environment (Sun et al., 2010a, b). The coal seam No. 11

in the Upper Shihezi Formation of ZJ was developed in a transitional environment between an abandoned lower deltaic plain with well-developed channels and an upper deltaic plain. The difference in coal depositional environment indicates possible variations of Hg inputs from rivers, atmospheric deposition and rock weathering to the coal swamps. In parallel, the pH, Eh and redox environment of the swamp water column also varied (Dai et al., 2012a). Together, these factors determine the Hg isotope compositions in coal. The epiclastic fragments of source rocks are the main contributors of mineral elements, which could be introduced into the coal basin by rivers, flooding events and airborne dust deposition. Immobile Al and coal ash content show an increasing trend along coal seams No. 3 to 11-2, whereas other Al-normalized major elements (Na/Al, Mg/Al, K/Al, Fe/Al, Mn/Al) show decreasing trends (Sun et al., 2010b). This suggests that the chemical compositions of source rocks were altered during long-term denudation and coal seams deposited during the late-stage received more intensively weathered minerals. Yinshan Oldland made up of Archean and Proterozoic metamorphic rocks and middle Proterozoic-Ordovician sedimentary rocks was the primary sediment source to NCCB (Dai et al., 2012a). The only Hg isotope compositions in crustal rocks were reported for the California Coast Range, USA (Smith et al., 2008). Only metamorphic rocks were identified with positive δ^{202}Hg up to 1.6‰. As compared to δ^{202}Hg of sedimentary rocks (mean = −0.63‰, from −1 to −0.2 ‰), metamorphic rocks are on average enriched in heavy isotopes (mean=−0.41‰, from −1.7 to 1.6‰). The increasing trend of δ^{202}Hg towards upper coal seams probably reflects the shift of source rocks from sedimentary rocks to metamorphic rocks.

6.5.2. DZ coals

Three distinct groups can be identified in DZ No. 3-1 coal seam: the lower benches DZ-3-1-C3 and DZ-3-1-C4 of normal Hg concentrations (104-139 ng/g) and lowest δ^{202}Hg values (−2.34 to −1.82±0.12‰, 2SD), the upper benches DZ-3-1-C6, DZ-3-1-C7 and DZ-3-1-C8 of normal Hg concentrations (85-114 ng/g) and highest δ^{202}Hg values (−0.50 to −0.12±0.12‰, 2SD), and the parting-, roof-contacted benches DZ-3-1-C5, DZ-3-1-C9 and DZ-3-1-C10 of highest Hg enrichment (522-754 ng/g) and intermediate δ^{202}Hg values (−1.65 to −1.05±0.12‰, 2SD) (Table 7). No clear relationship is seen in the plot of δ^{202}Hg vs. 1/Hg (Figure 20). However, a significantly negative correlation of δ^{202}Hg vs. Δ^{199}Hg (r^2=0.75, p=0.005) (Figure 17) suggests that the Hg isotope compositions in DZ coals were possibly dictated by two end-members. The first one is thought to be organically-bound Hg with extremely negative δ^{202}Hg (<−2.5‰) and slightly positive Δ^{199}Hg (>0.1‰), while the other is inorganically-bound Hg with circum-zero δ^{202}Hg and Δ^{199}Hg. Controlled

experiments show that under equilibrium conditions thiol-bound Hg is enriched in the lighter Hg isotopes by ~0.6‰ (δ^{202}Hg) relative to dissolved Hg(II) species (Wiederhold et al., 2010). Therefore, it is possible that the lighter Hg isotopes in coal swamp water were preferentially removed by the decayed organic matters. Photo-reduction of *in-situ* organic-bound Hg(II) or incorporation of recycled atmospheric and fluvial Hg with positive Δ^{199}Hg into decayed organic matters might explain the supposed >0.1‰ Δ^{199}Hg of organically-bound Hg.

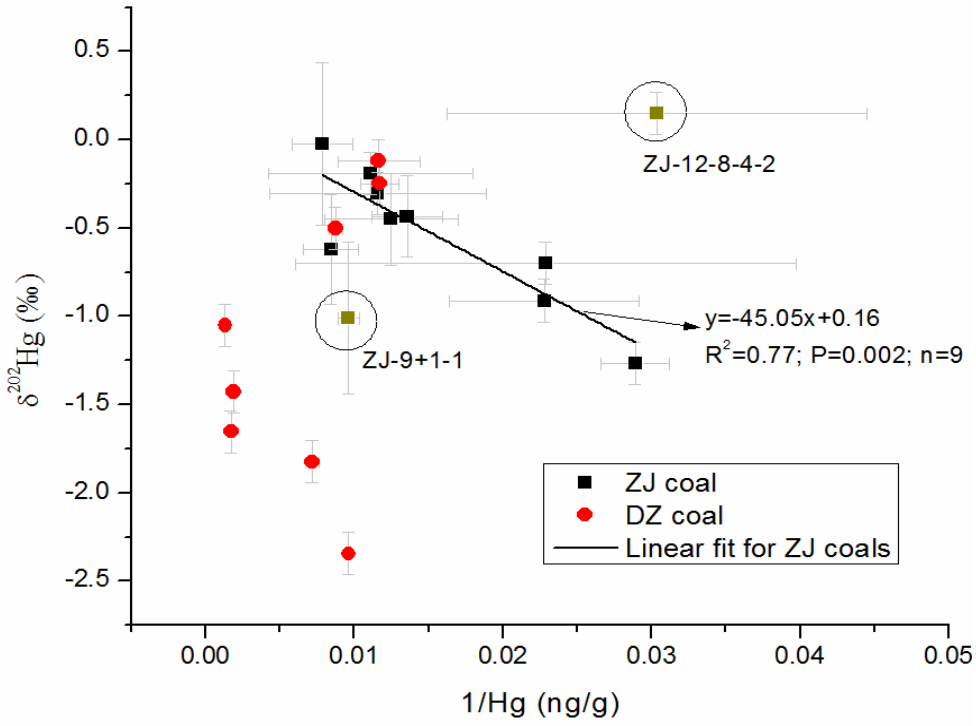

Figure 20 Plot of δ^{202}Hg vs. 1/Hg in Zhuji and Daizhuang coals. Coal samples ZJ-12-8-4-2 and ZJ-9+1-1 in circles are treated as the outliers. ZJ-12-8-4-2 has positive δ^{202}Hg and is possibly affected by magmatic intrusion (see Section 4.3 in text); ZJ+9+1-1 is an unworkable coal seam and has an extremely high ash yield (Table 5).

Float fractions for upper two coal benches (DZ-3-1-C9-F and DZ-3-1-C10-F) have the same Hg isotope compositions as raw coals (Table 7), indicating Hg input from extraneous sources probably occurred at early-stages of coal formation, and the late-stage diagenesis and metamorphic processes homogenized Hg isotope compositions in both coal benches. In contrast, another float fraction from the highest Hg containing bench DZ-3-1-C6 had 0.4‰ lower δ^{202}Hg than raw coal (Table 7). This implies that the mineral fraction (primary pyrite as indicated by XRD) has a higher δ^{202}Hg value than raw coal, which is similar to Illinois coals where epigenetic pyrite samples of circum-zero δ^{202}Hg

values are 0.9-1.3‰ higher than their corresponding organic matter rich coal fractions (Lefticariu et al., 2011).

6.5.3. Hg isotope compositions in natural cokes

Natural coke samples in ZJ have either distinctly higher (0.7 to 0.91±0.12‰, 2SD) or lower δ^{202}Hg (−4.00 to −3.47±0.12‰, 2SD) than coal samples (-1.62 to 0.44±0.12‰, 2SD) (Figure 17), which suggests that significant Hg isotope fractionation probably happened during the coal to coke transformation processes. The intensive magmatic intrusion occurred during the Late Cretaceous at ZJ and upgraded a large area of coal seams (primarily at lower No's. 3 and 4 coal seams) into natural coke (Yang et al., 2012). When the Permian coal seams were subjected to thermal perturbations from magmatic intrusion, a part, even all of the Hg in coal would be lost (Finkelman et al., 1998). The volatilized Hg was supposed to enrich lighter Hg isotopes and the complementary heavier isotopes were enriched in Hg-depleted coke. However, our coke samples are on average enriched ~2 times in Hg (140 ng/g) compared to coal, which implies that secondary Hg enrichment processes possibly occurred to cokes following Hg volatilization from intruded coal (Finkelman et al., 1998). The hydrothermal system derived from magmatic intrusions is a common factor to contribute to Hg enrichment in coal (Dai et al., 2012a; Diehl et al., 2004b). In coal seam No. 3 of borehole 8-5, the upward lithologies are coke (DZ-8-5-3U-J and DZ-8-5-3D-J, Table 7), gabbro dike and sandstone. Although pyrite phases were not identified in neither ZJ-8-5-3u-J nor ZJ-8-5-3D-J by XRD, postdating cross-cutting pyrite veins were observed in overlying sandstone, indicating a local hydrothermal system development. The extremely high Hg concentration in ZJ-8-5-3u-J (445 ng/g) possibly reflects a hydrothermal Hg delivery. Some cokes (e.g. ZJ-8-5-3D-J, ZJ-8+1-3U-J and ZJ-14-5-4-2D-J, Table 7) of lowest δ^{202}Hg values probably captured large proportions of Hg vapor volatilized from intruded coal. The well-developed porous structure of cokes could enhance their adsorption ability to Hg vapor after ambient temperatures decreased.

6.6. Implications

This study explored Hg isotope ratios to understand the possible mechanisms that control Hg occurrences in coal. The results have potential applications for geochemical and environmental tracing. The increasing δ^{202}Hg values from older to younger coal seams of ZJ suggests a progressive shift of the coal swamp source rocks from sedimentary to metamorphic rocks. The negative correlation of δ^{202}Hg vs. Δ^{199}Hg in DZ coals suggests that the Hg isotope variation in a single coal

seam were possibly controlled by the proportion of organic and inorganic-bound Hg. The prominent MIF values observed in certain coal seams may find application in the identification and stratigraphic inter-correlation of coal seams (traditionally using chemical characteristics and bio- or geo-markers), especially of splitting coal seams (e.g. No. 11-1 vs. 11-2), during coal exploration and exploitation (Dai et al., 2011; Kosanke, 1947; Ward, 2002). The significant Hg isotope fractionation between cokes and coal will be useful to distinguish Hg emissions from coal and coke combustion.

Acknowledgements

This work is supported by research grants ANR-09-JCJC-0035-01 from the French Agence Nationale de Recherche and ERC-2010-StG_20091028 from the European Research Council to JES. RS acknowledges his PhD scholarship from the Chinese Scholarship Council.

References

AICE, 2007. Anhui Institution of Coal Exploration: Zhuji coal exploration report.

Bechtel, A., Sachsenhofer, R.F., Gratzer, R., Lücke, A., Püttmann, W., 2002. Parameters determining the carbon isotopic composition of coal and fossil wood in the Early Miocene Oberdorf lignite seam (Styrian Basin, Austria). Organic Geochemistry 33, 1001-1024.

Bergquist, B.A., Blum, J.D., 2007. Mass-Dependent and -Independent Fractionation of Hg Isotopes by Photoreduction in Aquatic Systems. Science 318, 417-420.

Bergquist, B.A., Blum, J.D., 2009. The Odds and Evens of Mercury Isotopes: Applications of Mass-Dependent and Mass-Independent Isotope Fractionation. Elements 5, 353-357.

Biswas, A., Blum, J.D., Bergquist, B.A., Keeler, G.J., Xie, Z., 2008. Natural Mercury Isotope Variation in Coal Deposits and Organic Soils. Environmental Science & Technology 42, 8303-8309.

Blum, J., Bergquist, B., 2007. Reporting of variations in the natural isotopic composition of mercury. Analytic and Bioanalytic Chemistry 388, 353-359.

Chen, J., Hintelmann, H., Dimock, B., 2010. Chromatographic pre-concentration of Hg from dilute aqueous solutions for isotopic measurement by MC-ICP-MS. Journal of Analytical Atomic Spectrometry 25, 1402-1409.

Chen, J., Hintelmann, H., Feng, X., Dimock, B., 2012. Unusual fractionation of both odd and even mercury isotopes in precipitation from Peterborough, ON, Canada. Geochimica et Cosmochimica Acta 90, 33-46.

Dai, S., Ren, D., Chou, C.-L., Finkelman, R.B., Seredin, V.V., Zhou, Y., 2012a. Geochemistry of trace elements in Chinese coals: A review of abundances, genetic types, impacts on human health, and industrial utilization. International Journal of Coal Geology 94, 3-21.

Dai, S., Wang, X., Seredin, V.V., Hower, J.C., Ward, C.R., O'Keefe, J.M.K., Huang, W., Li, T., Li, X., Liu, H., Xue, W., Zhao, L., 2012b. Petrology, mineralogy, and geochemistry of the Ge-rich coal from the Wulantuga Ge ore deposit, Inner Mongolia, China: New data and genetic implications. International Journal of Coal Geology 90–91, 72-99.

Dai, S., Wang, X., Zhou, Y., Hower, J.C., Li, D., Chen, W., Zhu, X., Zou, J., 2011. Chemical and mineralogical compositions of silicic, mafic, and alkali tonsteins in the late Permian coals from the Songzao Coalfield, Chongqing, Southwest China. Chemical Geology 282, 29-44.

Diehl, S.F., Goldhaber, M.B., Hatch, J.R., 2004a. Modes of occurrence of mercury and other trace elements in coals from the warrior field, Black Warrior Basin, Northwestern Alabama. International Journal of Coal Geology 59, 193-208.

Diehl, S.F., Goldhaber, M.B., Hatch, J.R., 2004b. Modes of occurrence of mercury and other trace elements in coals from the warrior field, Black Warrior Basin, Northwestern Alabama. International Journal of Coal Geology 59, 193-208.

Estrade, N., Carignan, J., Sonke, J.E., Donard, O.F.X., 2009. Mercury isotope fractionation during liquid-vapor evaporation experiments. Geochimica et Cosmochimica Acta 73, 2693-2711.

Finkelman, R.B., Bostick, N.H., Dulong, F.T., Senftle, F.E., Thorpe, A.N., 1998. Influence of an igneous intrusion on the inorganic geochemistry of a bituminous coal from Pitkin County, Colorado. International Journal of Coal Geology 36, 223-241.

Gratz, L.E., Keeler, G.J., Blum, J.D., Sherman, L.S., 2010. Isotopic Composition and Fractionation of Mercury in Great Lakes Precipitation and Ambient Air. Environmental Science & Technology 44, 7764-7770.

Graydon, J.A., St. Louis, V.L., Hintelmann, H., Lindberg, S.E., Sandilands, K.A., Rudd, J.W.M., Kelly, C.A., Tate, M.T., Krabbenhoft, D.P., Lehnherr, I., 2009. Investigation of Uptake and Retention of Atmospheric Hg(II) by Boreal Forest Plants Using Stable Hg Isotopes. Environmental Science & Technology 43, 4960-4966.

Haitzer, M., Aiken, G.R., Ryan, J.N., 2002. Binding of Mercury(II) to Dissolved Organic Matter: The Role of the Mercury-to-DOM Concentration Ratio. Environmental Science & Technology 36, 3564-3570.

Haitzer, M., Aiken, G.R., Ryan, J.N., 2003. Binding of Mercury(II) to Aquatic Humic Substances: Influence of pH and Source of Humic Substances. Environmental Science & Technology 37, 2436-2441.

Han, D., Ren, D., Yanbin, W., Jin, K., Mao, H., Qin, Y., 1996. Coal Petrology of China. China University of Mining & Technology Press.

Han, D., Yang, Q., 1980. Coal Geology of China, Vol. 2. Coal Industry Publishing House, Beijing.

Han, S., Gill, G.A., Lehman, R.D., Choe, K.-Y., 2006. Complexation of mercury by dissolved organic matter in surface waters of Galveston Bay, Texas. Marine Chemistry 98, 156-166.

Han, S.F., 1990. Coal-forming conditions and coalfield prediction in Huaibei-Huainan region. Geological Publishing House, Beijing.

Hesterberg, D., Chou, J.W., Hutchison, K.J., Sayers, D.E., 2001. Bonding of Hg(II) to Reduced Organic Sulfur in Humic Acid As Affected by S/Hg Ratio. Environmental Science & Technology 35, 2741-2745.

Holdgate, G.R., McGowran, B., Fromhold, T., Wagstaff, B.E., Gallagher, S.J., Wallace, M.W., Sluiter, I.R.K., Whitelaw, M., 2009. Eocene–Miocene carbon-isotope and floral record from brown coal seams in the Gippsland Basin of southeast Australia. Global and Planetary Change 65, 89-103.

Hower, J.C., Campbell, J.L., Teesdale, W.J., Nejedly, Z., Robertson, J.D., 2008. Scanning proton microprobe analysis of mercury and other trace elements in Fe-sulfides from a Kentucky coal. International Journal of Coal Geology 75, 88-92.

Hower, J.C., Eble, C.F., Quick, J.C., 2005a. Mercury in Eastern Kentucky coals: Geologic aspects and possible reduction strategies. International Journal of Coal Geology 62, 223-236.

Hower, J.C., Mastalerz, M., Drobniak, A., Quick, J.C., Eble, C.F., Zimmerer, M.J., 2005b. Mercury content of the Springfield coal, Indiana and Kentucky. International Journal of Coal Geology 63, 205-227.

Ketris, M.P., Yudovich, Y.E., 2009. Estimations of Clarkes for Carbonaceous biolithes: World averages for trace element contents in black shales and coals. International Journal of Coal Geology 78, 135-148.

Kosanke, R.M., 1947. Plant Microfossils in Correlation of Coal Beds. The Journal of Geology 55, 280-284.

Kritee, K., Blum, J.D., Barkay, T., 2008. Mercury Stable Isotope Fractionation during Reduction of Hg(II) by Different Microbial Pathways. Environmental Science & Technology 42, 9171-9177.

Kritee, K., Blum, J.D., Johnson, M.W., Bergquist, B.A., Barkay, T., 2007. Mercury Stable Isotope Fractionation during Reduction of Hg(II) to Hg(0) by Mercury Resistant Microorganisms. Environmental Science & Technology 41, 1889-1895.

Lauretta, D.S., Klaue, B., Blum, J.D., Buseck, P.R., 2001. Mercury abundances and isotopic compositions in the Murchison (CM) and Allende (CV) carbonaceous chondrites. Geochimica et Cosmochimica Acta 65, 2807-2818.

Lefticariu, L., Blum, J.D., Gleason, J.D., 2011. Mercury Isotopic Evidence for Multiple Mercury Sources in Coal from the Illinois Basin. Environmental Science & Technology 45, 1724-1729.

Liu, G., Yang, P., Peng, Z., Chou, C.-L., 2004. Petrographic and geochemical contrasts and environmentally significant trace elements in marine-influenced coal seams, Yanzhou mining area, China. Journal of Asian Earth Sciences 23, 491-506.

Liu, G., Zheng, L., Gao, L., Zhang, H., Peng, Z., 2005. The characterization of coal quality from the Jining coalfield. Energy 30, 1903-1914.

Pacyna, E.G., Pacyna, J.M., Sundseth, K., Munthe, J., Kindbom, K., Wilson, S., Steenhuisen, F., Maxson, P., 2010. Global emission of mercury to the atmosphere from anthropogenic sources in 2005 and projections to 2020. Atmospheric Environment 44, 2487-2499.

Pirrone, N., Cinnirella, S., Feng, X., Finkelman, R.B., Friedli, H.R., Leaner, J., Mason, R., Mukherjee, A.B., Stracher, G.B., Streets, D.G., Telmer, K., 2010. Global mercury emissions to the atmosphere from anthropogenic and natural sources. Atmospheric Chemistry and Physics 10, 5951-5964.

Querol, X., Alastuey, A., Lopez-Soler, A., Plana, F., Zeng, R., Zhao, J., Zhuang, X., 1999. Geological controls on the quality of coals from the West Shandong mining district, Eastern China. International Journal of Coal Geology 42, 63-88.

Quick, J.Q., Brill, T.B., Tabet, D.T., 2003. Mercury in US coal: observations using the COALQUAL and ICR data. Environmental Geology 43, 247-259.

Ren, D., Zhao, F., Wang, Y., Yang, S., 1999. Distributions of minor and trace elements in Chinese coals. International Journal of Coal Geology 40, 109-118.

Sherman, L.S., Blum, J.D., Keeler, G.J., Demers, J.D., Dvonch, J.T., 2012. Investigation of Local Mercury Deposition from a Coal-Fired Power Plant Using Mercury Isotopes. Environmental Science & Technology

Sherman, L.S., Blum, J.D., Nordstrom, D.K., McCleskey, R.B., Barkay, T., Vetriani, C., 2009. Mercury isotopic composition of hydrothermal systems in the Yellowstone Plateau volcanic field and Guaymas Basin sea-floor rift. Earth and Planetary Science Letters 279, 86-96.

SICE, 2010. Shandong Institution of Coal Exploration: Daizhuang coal exploration report.

Skyllberg, U., Bloom, P.R., Qian, J., Lin, C.-M., Bleam, W.F., 2006. Complexation of Mercury(II) in Soil Organic Matter: EXAFS Evidence for Linear Two-Coordination with Reduced Sulfur Groups. Environmental Science & Technology 40, 4174-4180.

Smith, C.N., Kesler, S.E., Blum, J.D., Rytuba, J.J., 2008. Isotope geochemistry of mercury in source rocks, mineral deposits and spring deposits of the California Coast Ranges, USA. Earth and Planetary Science Letters 269, 399-407.

Smith, C.N., Kesler, S.E., Klaue, B., Blum, J.D., 2005. Mercury isotope fractionation in fossil hydrothermal systems. Geology 33, 825-828.

Sonke, J.E., 2011. A global model of mass independent mercury stable isotope fractionation. Geochimica et Cosmochimica Acta 75, 4577-4590.

Streets, D.G., Devane, M.K., Lu, Z., Bond, T.C., Sunderland, E.M., Jacob, D.J., 2011. All-Time Releases of Mercury to the Atmosphere from Human Activities. Environmental Science & Technology 45, 10485-10491.

Sun, R., Heimbürger, L.-E., Sonke, J.E., Liu, G., Amouroux, D., Berail, S., 2013a. Mercury stable isotope fractionation in six utility boilers of two large coal-fired power plants. Chemical Geology 336, 103-111.

Sun, R., Enrico, M., Heimbürger, L.-E., Scott, C., Sonke, J.E., 2013b. A double-stage tube furnace – acid trapping protocol for the pre-concentration of mercury from solid samples for isotopic analysis. Analytical and Bioanalytic Chemistry. DOI: 10.1007/s00216-013-7152-2.

Sun, R., Liu, G., Zheng, L., Chou, C.-L., 2010a. Characteristics of coal quality and their relationship with coal-forming environment: A case study from the Zhuji exploration area, Huainan coalfield, Anhui, China. Energy 35, 423-435.

Sun, R., Liu, G., Zheng, L., Chou, C.-L., 2010b. Geochemistry of trace elements in coals from the Zhuji Mine, Huainan Coalfield, Anhui, China. International Journal of Coal Geology 81, 81-96.

Toole-O'Neil, B., Tewalt, S.J., Finkelman, R.B., Akers, D.J., 1999. Mercury concentration in coal--unraveling the puzzle. Fuel 78, 47-54.

Ward, C.R., 2002. Analysis and significance of mineral matter in coal seams. International Journal of Coal Geology 50, 135-168.

Wiederhold, J.G., Cramer, C.J., Daniel, K., Infante, I., Bourdon, B., Kretzschmar, R., 2010. Equilibrium Mercury Isotope Fractionation between Dissolved Hg(II) Species and Thiol-Bound Hg. Environmental Science & Technology 44, 4191-4197.

Wu, F.D., Chen, Z.H., Zhang, S.L., Ge, L.G., 1995. Transgressions during Permo-Carboniferous Period in North China. Geoscience 9, 284-292.

Yang, M., Liu, G., Sun, R., Chou, C.-L., Zheng, L., 2012. Characterization of intrusive rocks and REE geochemistry of coals from the Zhuji Coal Mine, Huainan Coalfield, Anhui, China. International Journal of Coal Geology 94, 283-295.

Yin, R., Feng, X., Shi, W., 2010. Application of the stable-isotope system to the study of sources and fate of Hg in the environment: A review. Applied Geochemistry 25: 1467-1477.

Yudovich, Y.E., Ketris, M.P., 2005. Mercury in coal: a review: Part 1. Geochemistry. International Journal of Coal Geology 62, 107-134.

Zambardi, T., Sonke, J.E., Toutain, J.P., Sortino, F., Shinohara, H., 2009. Mercury emissions and stable isotopic compositions at Vulcano Island (Italy). Earth and Planetary Science Letters 277, 236-243.

Zheng, L., Liu, G., Qi, C., Zhang, Y., Wong, M., 2008. The use of sequential extraction to determine the distribution and modes of occurrence of mercury in Permian Huaibei coal, Anhui Province, China. International Journal of Coal Geology 73, 139-155.

Zheng, L.G., Liu, G.J., Chou, C.L., 2007a. The distribution, occurrence and environmental effect of mercury in Chinese coals. Science of Total Environment 384, 374-383.

Zheng, W., Foucher, D., Hintelmann, H., 2007b. Mercury isotope fractionation during volatilization of Hg(0) from solution into the gas phase. Journal of Analytical Atomic Spectrometry 22, 1097-1104.

Zheng, W., Hintelmann, H., 2009. Mercury isotope fractionation during photoreduction in natural water is controlled by its Hg/DOC ratio. Geochimica et Cosmochimica Acta 73, 6704-6715.

Zheng, W., Hintelmann, H., 2010. Nuclear Field Shift Effect in Isotope Fractionation of Mercury during Abiotic Reduction in the Absence of Light. The Journal of Physical Chemistry A 114, 4238-4245.

Chapter 7

Hg stable isotope compositions of selected world coals

Chapter 7. Hg stable isotope compositions of selected world coals (article in preparation for *Environmental Science and Technology*)

Résumé

Ce Chapitre résume une compilation isotopique du Hg dans des charbons, basé sur 108 nouveaux échantillons de charbon provenant des basins importants en Afrique, Chine, Europe, Inde, Indonésie, l'ancien Russie et les USA et ~50 charbons déjà publiés. Nous observons une variation isotopique de 4.7‰ en δ^{202}Hg (−3.9 a 0.8‰) et de 1‰ en Δ^{199}Hg (−0.6 a 0.4‰). La moitié des 28 comparaisons possibles entre les huit principales régions producteur du charbon du monde sont statistiquement différenciable selon leurs δ^{202}Hg, Δ^{199}Hg ou les deux ($p<0.05$). Nous y en déduisons l'application potentiel des signatures isotopiques du Hg en tant que traceurs des émissions du Hg des centrales au charbon. Dans un deuxième temps, il parait que la signature Δ^{199}Hg augmente avec la charbonification (du lignite au sous-bitumineux au bitumineux à l'anthracite) et avec l'âge de déposition (du Cénozoïque au Mésozoïque au Paléozoïque)

Hg stable isotope compositions of selected world coals

Ruoyu Sun [1*], Jeroen Sonke [1], Harvey Belkin[2], Guijian Liu [3], Debasish Shome [4], Ewa Cukrowska [5], Oleg Pokrovsky[1]

[1]Observatoire Midi-Pyrénées, Laboratoire Géosciences Environnement Toulouse, CNRS/IRD/Université de Toulouse, France

[2]U.S. Geological Survey, 956 National Center, Reston, VA 20192, USA

[3]CAS Key Laboratory of Crust-Mantle Materials and Environment, School of Earth and Space Sciences, University of Science and Technology of China, Hefei, Anhui 230026, China

[4] Dept. of Geology, Jadavpur University, India

[5]Molecular Sciences Institute, School of Chemistry, University of the Witwatersrand, P.Bag X3, WITS 2050, Johannesburg, South Africa

Abstract

Hg emissions from coal combustion contribute approximately half (~700-900 tons/year) of all anthropogenic Hg emissions to the atmosphere. With the implementation of the first global, legally-binding UNEP treaty aimed at reducing anthropogenic Hg emissions, the identification and traceability of coal Hg emissions from different countries or regions is critically important. Here, we present a coal Hg isotope library by reporting the isotope composition of 108 new coal samples from major coal-producing basins in Africa, China, Europe, India, Indonesia, former USSR and the USA, adding to the thus far ~50 published coal samples. A 4.7‰ range in δ^{202}Hg (−3.9 to 0.8‰) and a 1‰ range in Δ^{199}Hg (−0.6 to 0.4‰) are observed. 14 ($p<0.05$) to 17 ($p<0.1$) of the 28 pairwise comparisons between eight global regions are statistically distinguishable on the basis of δ^{202}Hg, Δ^{199}Hg or both. This highlights the potential application of Hg isotope signatures to coal Hg emission tracing. Significant correlations were observed between Hg isotope compositions (δ^{202}Hg or Δ^{199}Hg) and Hg concentration, coal rank or coal-forming ages, suggesting geochemical and source-related controls. Industrial processes (e.g. coal washing and combustion) may shift the isotope compositions of coal Hg.

*Corresponding author: Ruoyu Sun, E-mail: roysun1986@gmail.com

7.1. Introduction

Mercury (Hg) is a persistent toxic element. Once released from natural and anthropogenic sources, it can be transported globally by atmospheric circulation before being deposited. Following deposition, a portion of Hg will be transformed into neurotoxic methylmercury (MeHg). Methylmercury can be bioaccumulated and biomagnified stepwise along food chains and poses a great threat to the health of humans and wild life. Mercury is commonly present at trace levels of 10-1000 ng/g in coal (Dai et al., 2012; Ketris and Yudovich, 2009). However, the large volumes of coal used in industrial processes have made coal become the dominant Hg emission source. On a global scale, coal contributed more than a quarter of the cumulative anthropogenic Hg emissions (21500 tons) between 1850 and 2008 (Streets et al., 2011). Mercury emissions from stationary coal combustion facilities, primarily coal-fired utility boilers (CFUBs), have soared over the recent two decades, especially in developing countries (e.g. China, India South Africa), and have reached 700-900 tons/yr at present, representing approximately half of the anthropogenic Hg emissions into the atmosphere (Pacyna et al., 2006b; Pacyna et al., 2010; Pirrone et al., 2010; Streets et al., 2011). In addition, considerable amounts of Hg are removed from CFUB flue gases into fly ash, gypsum and waste water, and may potentially contaminate the local environment (Yang et al., 2012)

Quantitative assessment of the impact of coal Hg emission on local, regional and global ecosystems is of substantial interest to environmental scientists and decision-makers. Moreover, with the implementation of the first global, legally-binding treaty aiming at reducing anthropogenic Hg emissions, a distinction of coal Hg emissions from different countries or regions is critically important. Global Hg chemistry and transport models have been used to estimate the trans-boundary impact of Hg emissions (Seigneur et al., 2004; Selin et al., 2008). Measured Hg/CO ratios have been used as tracers for long-range Asian Hg emissions (Weiss-Penzias et al., 2007). However, a widely applicable chemical source tracing signature for coal Hg emissions has not been developed thus far. Over one decade of Hg stable isotope research has shown that the various Hg isotope signatures carry information on Hg sources and environmental transformations (Sonke and Blum, 2013). Incomplete Hg transformations in natural and man-made environments separate the seven stable Hg isotopes as a function of isotope mass, nuclear volume or nuclear magnetic moment (Bergquist and Blum, 2007; Estrade et al., 2009). Additional isotope fractionation mechanisms, including nuclear self-shielding, are suspected to exist (Mead and Johnson, 2010). Most natural samples, including the coals considered here, show Hg isotope variations that are controlled by mass dependent

fractionation (MDF, denoted by δ^{202}Hg) and mass independent fractionation (MIF, denoted by Δ^{199}Hg or Δ^{201}Hg) related to the magnetic isotope effect.

Published Hg isotope signatures in coals have revealed a 3‰ variation in δ^{202}Hg and a 1‰ variation in Δ^{199}Hg (Biswas et al., 2008; Lefticariu et al., 2011; Sun et al., 2013a). Two important observations have strengthened the potential application of Hg isotope signatures as CFUB Hg emission tracers. Firstly, different coal basins can be distinguished using the combined δ^{202}Hg and Δ^{199}Hg isotope signatures (Biswas et al., 2008; Lefticariu et al., 2011). Secondly, the Hg isotopic shift between Hg in feed coal and CFUB flue gas Hg emissions are small (<0.3‰) and predictable for δ^{202}Hg, and absent for Δ^{199}Hg (Sun et al., 2013a). We did point out in the latter study that the various gaseous elemental Hg (GEM), gaseous oxidized Hg (GOM) and particle bound Hg (PBM) species in flue gas may carry different δ^{202}Hg signatures. GEM is enriched in the heavier Hg isotopes, whereas GOM and PBM are in the lighter Hg isotopes. Hg isotope evidences show that precipitation (snow and rain water), soils and lichens were possibly contaminated by local and regional coal combustion Hg emissions (Biswas et al., 2008; Chen et al., 2012; Estrade et al., 2010, 2011; Sherman et al., 2012). In addition, the environmental compartments in the vicinity of coal-fired power plants showed contrasting Hg isotope signatures as compared to those far away from coal combustion emissions (Estrade et al., 2010, 2011; Sherman et al., 2011). However, our current tracing to coal Hg is still based on speculations and limited Hg isotope data of world selected coal specimens.

In this study, we develop a coal Hg isotope library by analyzing 108 new coal samples, adding to ~50 published coal samples (Biswas et al., 2008; Lefticariu et al., 2011; Sun et al., 2013a). The coal samples cover the main coal-producing basins in ten countries and coals formed from the Carboniferous to the Tertiary. We group the Hg isotope signatures (δ^{202}Hg and Δ^{199}Hg) in coals of different regions. The natural (hydrothermal fluids, magmatic intrusion events) and artificial processes (coal washing, pyrite rejection, combustion, combustion products removal) that potentially shift the Hg isotope signatures in original coals are discussed.

7.2. Samples and analysis

7.2.1. Samples collection and processing

Coal samples were chosen from the world main coal-forming basins in primary coal production/consumption regions including South Africa, China, the USA, India, Indonesia, Former USSR (Russia, Kazakhstan, Ukraine), Mongolia and some European counties (mainly Romania)

(Figure 10). Coal samples from China and the USA are from the University of Science and Technology in China, and were homogenized before delivery. Indonesian (large-granular coal), Mongolian (large-granular coal) and Romanian (pulverized coal) coal samples are from the USGS WoCQI project (Tewalt et al., 2010). Bulk Indian coal samples are from the Dept. of Geology collection, Jadavpur University, India. Pulverized coal samples from South African power plants are from the Witwatersrand University collection (Lusilao-Makiese et al., 2012), coals from former USSR are from the Moscow State University collection, and from other regions were supplied by C. Liousse (Laboratoire d'Aerologie, Toulouse, France). Bulk and large-granular coal samples were pulverized in a motorized agate grinder (Fritsch pulverizer 2) to <150 μm particles before analysis. The agate mortar was cleaned with high purity ethanol and then Milli-Q water, and dried by compressed air before processing each sample. In between samples, ~15 g Hg-clean quartz sand was processed in the same way as coal samples to monitor and minimize the possible cross-contamination.

7.2.2. Hg and Hg isotope determinations

Hg concentrations in solid samples were determined by a combustion atomic absorption technique (Milestone DMA-80). Hg extraction and purification for isotope analyses were performed following a double-stage tube furnace combustion and acid trapping protocol. Trapping solutions were analyzed by cold vapor atomic fluorescence spectrometry (CV-AFS, Brooks Rand Model III) following EPA protocols (EPA-1631E, 2002). Hg isotope ratios in trapping solutions of CRMs and samples (diluted to 20% (v/v) acid with a Hg concentration range of 1-2.5 ng/g) were determined by cold vapor multi-collector inductively coupled plasma mass spectrometry (Thermo-Finnigan Neptune) at the Midi-Pyrenees Observatory, Toulouse, France. The detailed protocols for Hg concentration, extraction and isotope analysis can be found in Sun et al. (2013b).

7.2.3. Blank, recovery and uncertainty

The cross-contamination of Hg during sample pulverization and homogeneity was <1% of processed samples (typically >200 ng Hg), as evaluated by clean quartz sand crushed in-between samples. Besides, Hg concentrations in acid blanks and procedural blanks prepared along with samples were consistently <0.03 ng/g, which is insignificant (<5%) as compared to trapping solutions of combusted certified reference materials (CRM, NIST SRM 2685b and 1632d) and samples. All analyzed CRMs and samples have Hg extraction recoveries between 80% and 120%, reflecting quantitative Hg transfer from solid samples to trapping solutions in the limits of DMA-80 and AFS

measurement uncertainties (±10%, 2RSD). The long-term external uncertainty of the method was determined by repeated analyses of the UM-Almaden standard at various Hg concentrations (1-2.5 ng/g in 20% of $2HNO_3$/1HCl, v/v,) during different analysis sessions over 2011 and 2012. The average value is −0.57±0.11‰ (2SD, n=53) for δ^{202}Hg and −0.02±0.06‰ (2SD, n=53) for Δ^{199}Hg (Table A1 in Appendix A). The measured δ^{202}Hg and Δ^{199}Hg for long-term combusted procedural NIST 1632d are −1.79±0.17‰ (2SD, n=10) and −0.04±0.05‰ (2SD, n=10), and for NIST 2685b are −2.75±0.18‰ (2SD, n=11) and 0.01±0.05‰ (2SD, n=10) (Table A1 in Appendix A). The largest values of the 2SD (e.g. δ^{202}Hg uncertainty = 0.18‰, Δ^{199}Hg uncertainty = 0.06‰ and Δ^{201}Hg uncertainty = 0.08‰) of the Hg isotope compositions for the procedural CRMs and UM-Almaden were taken as the analytical uncertainties of sample Hg isotope compositions. If uncertainties of replicate sample Hg isotope compositions were higher than these uncertainties, then the sample replicates uncertainties applied.

7.3. Results and discussions

Background information, Hg concentrations and Hg isotope compositions in the studied 115 samples (108 coal, 3 natural coke, 2 fly ash, 1 sapropel, 1 shungite) are summarized in Table A1 in Appendix A, along with coal samples reported elsewhere.

7.3.1. Mercury isotope compositions

A 4.7‰ variation in δ^{202}Hg values (−3.90 to 0.77±0.18‰, 2SD) is observed in the studied world coals, which significantly expands the previously reported δ^{202}Hg range of 3.4% (−2.98 to 0.45‰) (Figure B1 in Appendix B). The MIF variation, both Δ^{199}Hg (−0.55 to 0.33±0.06‰, 2SD) and Δ^{201}Hg (−0.48 to 0.25±0.08‰, 2SD) are similar to the previously reported 1% range (−0.63 to 0.34‰ for Δ^{199}Hg and −0.53 to 0.29‰ for Δ^{201}Hg). The Δ^{199}Hg and Δ^{201}Hg data set in our studied coals define a Δ^{199}Hg/Δ^{201}Hg slope of 1.10±0.03 (2SE, n=108, P<0.001) (Figure 21A). By incorporating previously reported coals, we obtain a Δ^{199}Hg/Δ^{201}Hg slope of 1.09±0.02 (2SE, n=155, P<0.001) (Figure 21B). The Δ^{199}Hg/Δ^{201}Hg slope of world coals is within those (1.0-1.3) produced during photo-reduction of Hg(II)-organic matter species in aqueous environments (Bergquist and Blum, 2007; Zheng and Hintelmann, 2009).

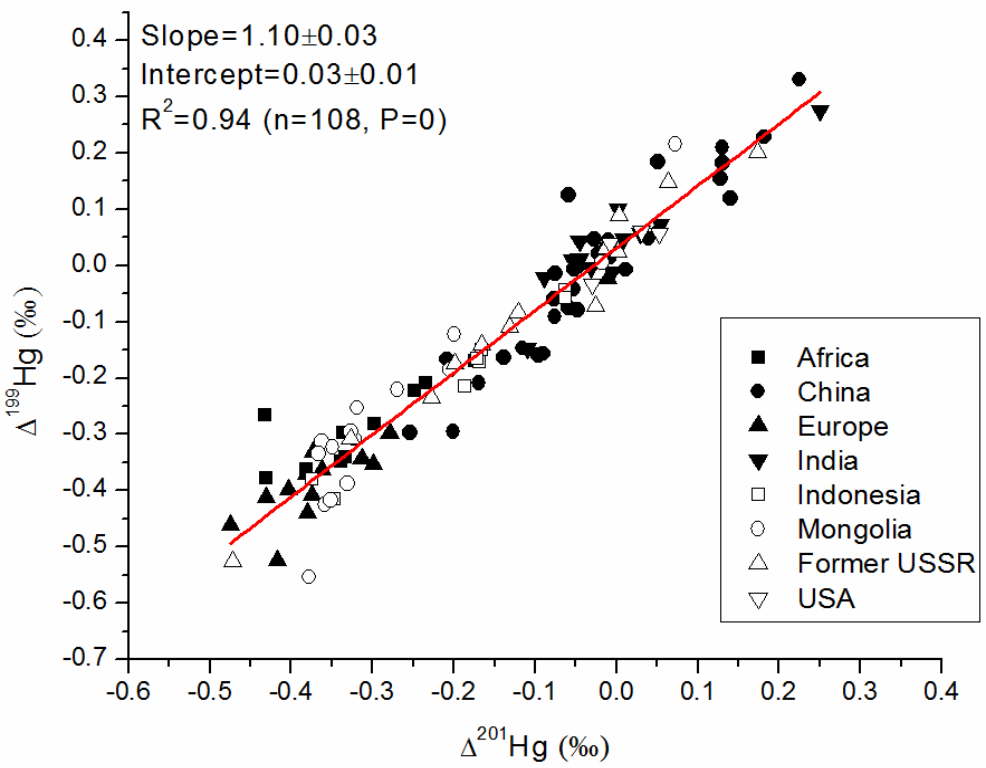

(A)

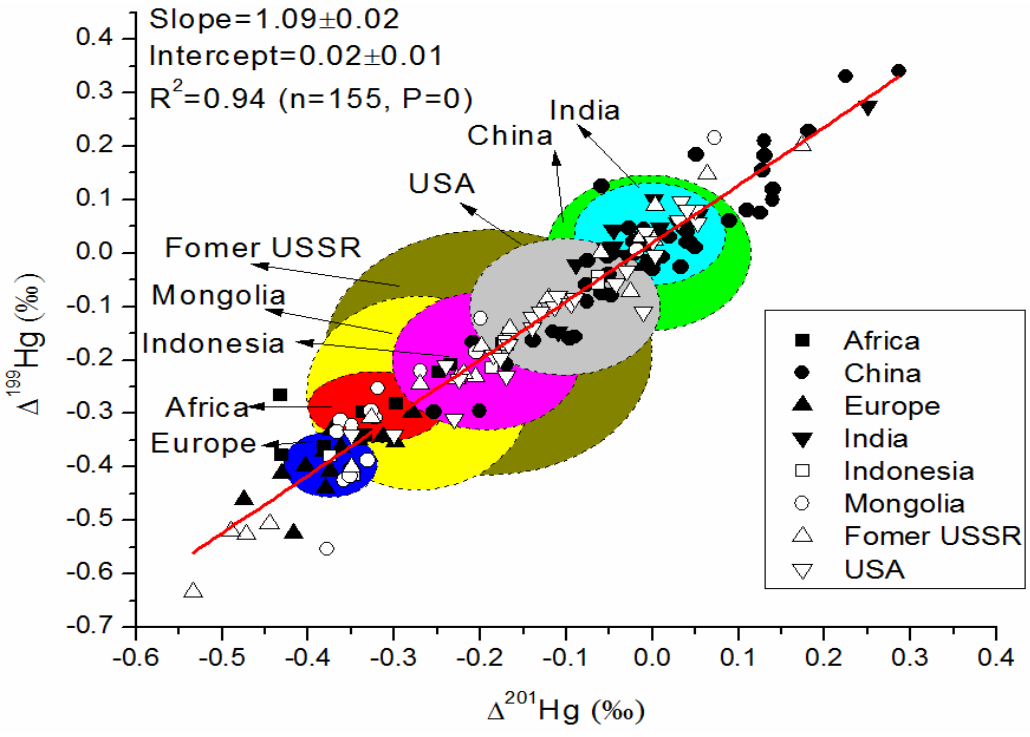

(B)

Figure 21 Δ^{201}Hg vs. Δ^{199}Hg in studied world coals (n=108) (A) and all world coals (n=155) (B). The centre, horizontal and vertical axis of ellipse denotes respectively means of Δ^{199}Hg and Δ^{201}Hg, 1SD on Δ^{199}Hg and 1SD on Δ^{201}Hg.

On average, δ^{202}Hg is highest for Indonesia (−0.55±0.53‰, 1SD, n=8), followed by Africa (mainly South Africa, −0.93±0.43‰, 1SD, n=10), Mongolia (−1.02±0.90‰, 1SD, n=15), China (−1.04±0.84‰, 1SD, n=49, including 16 previously reported samples by Biswas et al., 2008 and Sun et al., 2013a), Europe (mainly Romania, −1.17±0.68‰, 1SD, n=13), the USA (−1.45±0.64‰, 1SD, n=27, including 23 previous reported samples by Biswas et al., 2008) and Lefticariu et al., 2011), former USSR (Russia, Ukraine and Kazakhstan, −1.69±1.13‰, 1SD, n=21, including 8 previously reported samples by Biswas et al., 2008) and India (−1.87±0.54‰, n=12) (Figure 22A and Table 8). Most of Chinese and Indian coals show little to no MIF (Figure 22B and Table 8). The positive Δ^{199}Hg in selcted Indian and Chinese coals are countered by negative Δ^{199}Hg in other areas, which results in mean Δ^{199}Hg for both countries of 0.00±0.14‰ (1SD, n=49) and 0.04±0.09‰ (1SD, n=12) respectively. In contrast, most of the coals from USA and former USSR are characterized by negative Δ^{199}Hg, with mean values of −0.10±0.13‰ (1SD, n=27) and −0.19±0.23‰ (1SD, n=21), respectively. The Δ^{199}Hg in coals from Indonesia, Mongolia, Africa and Europe are exclusively negative, with mean values of −0.20 ±0.13‰ (1SD, n=8), −0.26±0.18‰ (1SD, n=15), −0.29±0.07 ‰ (1SD, n=10) and −0.36 ±0.11‰ (1SD, n=13), respectively.

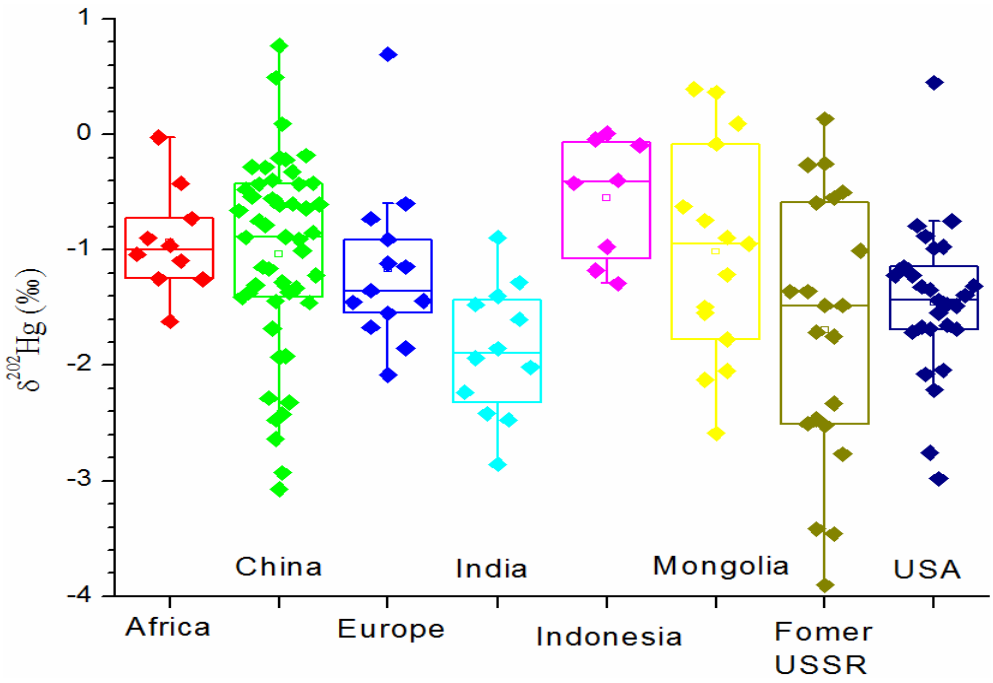

(A)

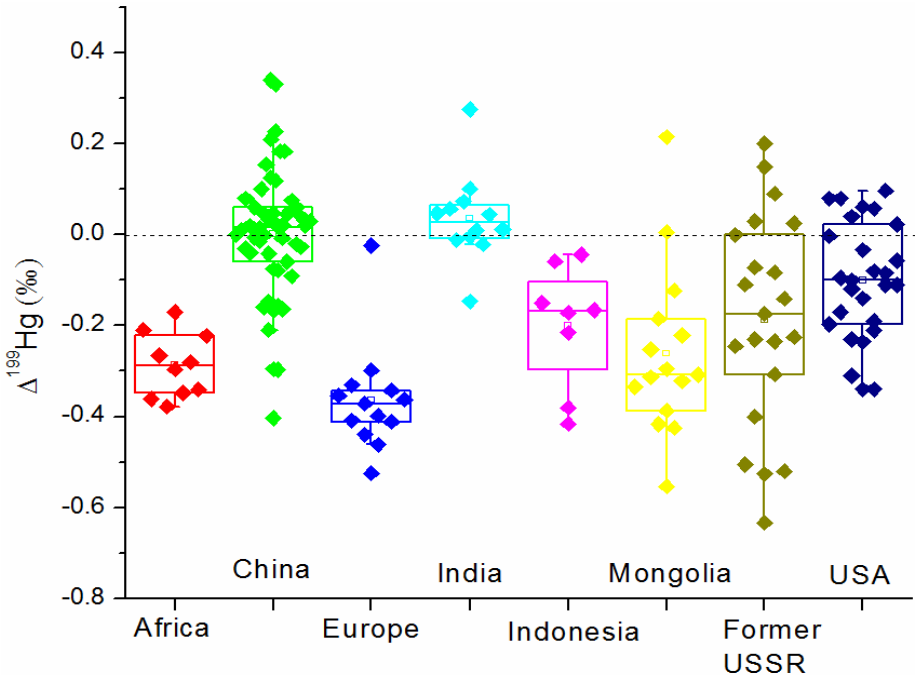

(B)

Figure 22 Box plots showing δ^{202}Hg (A) and Δ^{199}Hg (B) in all world coals (n=155). The horizontal lines at the bottom, middle and top of each boxplot are the lower quartile (below which 25% lowest values are found), median and upper quartile (above which 25% highest values are found), respectively. The box height (the difference between lower quartile and upper quartile) is defined as interquartile range (IQR). The data points either greater than the upper quartile+1.5 IQR or less than the lower quartile-1.5 IQR are considered to be extreme values. Square symbol denotes mean

Table 8 Summary of the means of δ^{202}Hg, Δ^{199}Hg and Δ^{201}Hg in world coals

	δ^{202}Hg	1SD	Δ^{199}Hg	1SD	Δ^{201}Hg	1SD
Africa (South Africa)	-0.93	0.43	-0.29	0.07	-0.32	0.08
China	-1.04	0.84	0.00	0.14	-0.01	0.12
Euro (Romania)	-1.17	0.68	-0.36	0.11	-0.35	0.11
India	-1.87	0.54	0.04	0.09	0.00	0.09
Indonesia	-0.55	0.49	-0.20	0.13	-0.19	0.11
Mongolia	-1.02	0.90	-0.26	0.18	-0.27	0.13
Former USSR	-1.69	1.13	-0.19	0.23	-0.19	0.19
USA	-1.45	0.64	-0.10	0.13	-0.10	0.11

The δ^{202}Hg and Δ^{199}Hg values for different regions are grouped in a δ^{202}Hg vs. Δ^{199}Hg plot (Figure 23). To test whether the means of δ^{202}Hg and Δ^{199}Hg values in studied regions are statistically different, we performed pairwise post-hoc multiple comparisons by One-Way ANOVA analysis

(*IBM SPSS Statistics 20*) (Table A2 in Appendix A). On the basis of δ^{202}Hg, Indonesian coals of highest mean value can be distinguished from those of USA (p=0.03), former USSR (p=0.03) and India (p<0.01). In addition, Indian coals of lowest mean δ^{202}Hg can be distinguished from those of China (p=0.01) and Africa (p=0.01). As compared to δ^{202}Hg, Δ^{199}Hg of coal is a more robust indicator to discriminate coals from different regions. Eleven pairwise comparisons between regions can be distinguished from each other using mean Δ^{199}Hg at significance levels α of 0.05 and 0.01 (Table A2 in Appendix A). For example, average Indian coals of circum-zero Δ^{199}Hg can be distinguished from those of the rest of regions except China; coals from USA can be distinguished from those of India, Europe and Africa. In total, 14 (p<0.05) or 17 (p<0.1) of the 28 pairwise comparisons between countries (regions) are statistically distinguishable on the basis of δ^{202}Hg, Δ^{199}Hg or both (Figure 24).

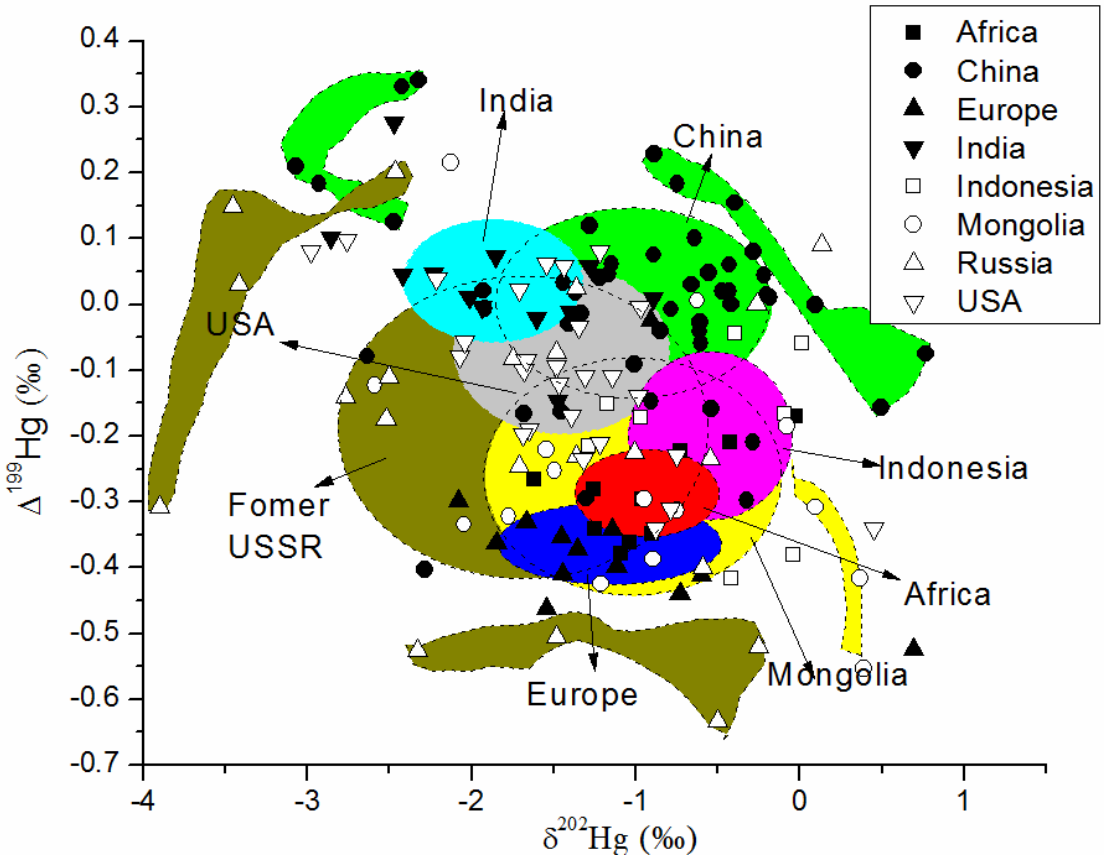

Figure 23 δ^{202}Hg vs. Δ^{199}Hg in all world coals (n=155). The centre, horizontal and vertical axis of ellipse denotes respectively means of δ^{202}Hg and Δ^{199}Hg, 1SD on δ^{202}Hg and 1SD on Δ^{199}Hg.

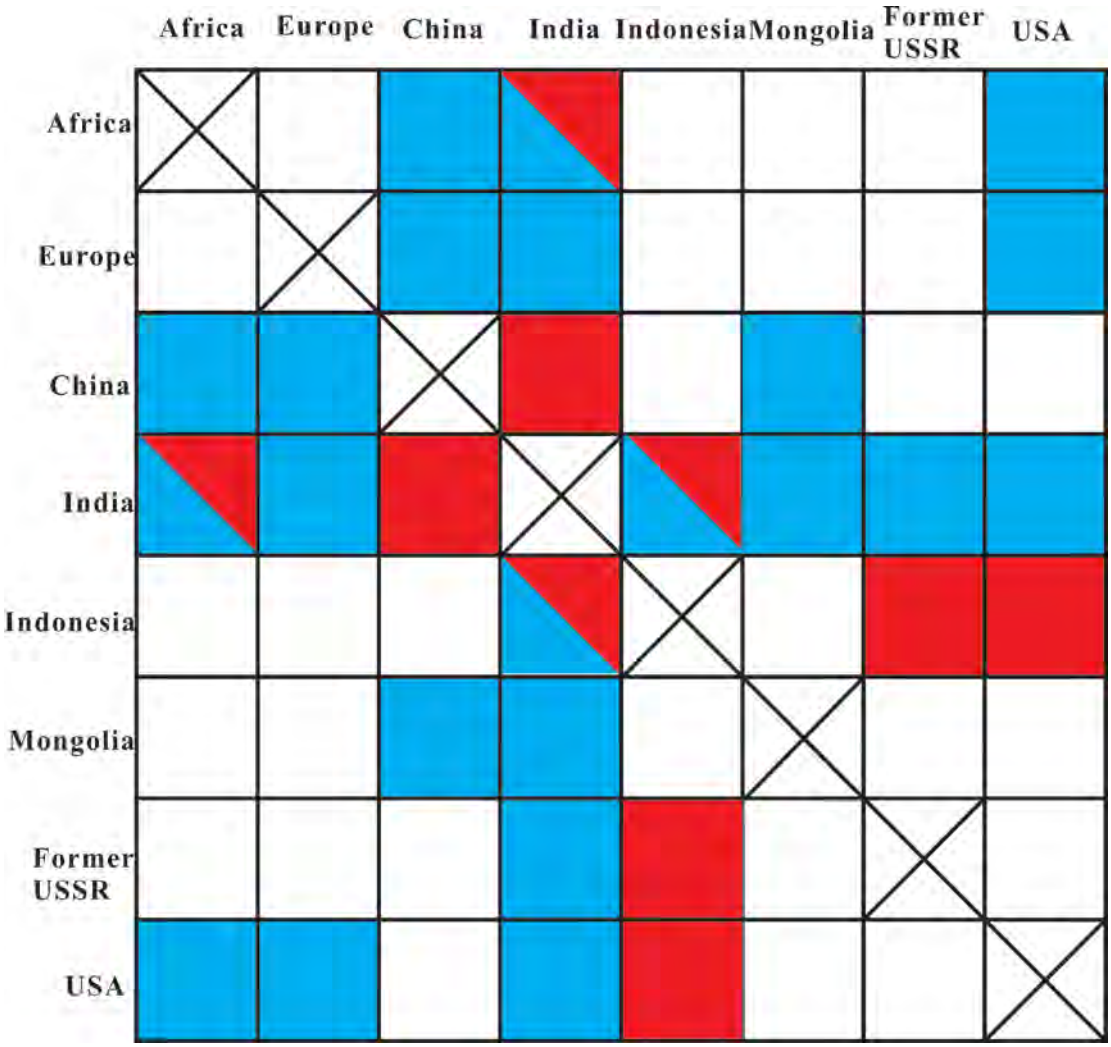

Figure 24 Matrix representation of statistical pairwise comparisons between regions (α=0.05 or 0.01, by *IBM SPSS Statistics 20)*. The compared regions can be distinguished by δ^{202}Hg (red square), Δ^{199}Hg (blue square) or both (1/2 blue +1/2 red square)

7.3.1.1. South African coal

Stationary coal combustion in power generation sectors and gold mining in Africa are the leading anthropogenic Hg contributors to atmosphere (Pacyna et al., 2010; Pirrone et al., 2010). Nearly all African coal production is from South Africa. South Africa produced ~255 Mt (million metric tons) of coal (mainly bituminous coal) in 2011 and is the world's 7th largest coal producer (~3.5% world share) (BP, 2012). More than 90% of the nation's electricity demand is provided by dozens of coal-fired power plants which commonly utilize low-rank bituminous coals (Cairncross et al., 1990; DME, 2010). Coal combustion releases 10-50 t/yr Hg to atmosphere and is considered to be the largest Hg pollution source in South Africa and an important contributor to the global atmospheric Hg inventory (Dabrowski et al., 2008; Leaner et al., 2009; Pacyna et al., 2006b; Pacyna et al., 2010).

In addition to domestic coal consumption, ~30% of South African coal (~70 Mt) is exported to European countries (>75% share, mainly Germany and Spain) and East Asian countries (mainly Japan), ranking South Africa as the world's 6th largest net exporter (AEO, 2011; DME, 2010).

Of the ten South African coal samples, six were taken from six power stations (Duvha, Kriel, Lethabo, Majuba, Camden, Tutuka) located in the Mpumalanga Province (Highveld Region) and their Hg concentrations and speciation have been reported elsewhere (Lusilao-Makiese et al., 2012). There is a ~1.6‰ variation in δ^{202}Hg (−1.62 to −0.03‰, n=10) and ~0.2‰ variation in Δ^{199}Hg (−0.38 to −0.17‰, n=10) (Figure 22). Statistically, African coals with mean δ^{202}Hg of −0.93 ±0.43‰ and Δ^{199}Hg of −0.29 ±0.07‰ (1SD, n=10) can be significantly distinguished from Chinese and USA coals by Δ^{199}Hg ($p<0.001$), and from Indian coals by both δ^{202}Hg ($P<0.001$) and Δ^{199}Hg ($p=0.01$) (Figure 24).

7.3.1.2. Chinese coal

China is the largest coal producing (~50% world share), consuming (~50% world share) and coal importing (~18% world share) country in the world (BP, 2012; IEA, 2012). China contributes nearly half (~400 t/yr) of all Hg emissions from stationary coal combustion worldwide (Pacyna et al., 2010). Consequently, Hg istope compositions of worldwide coal emissions in atmosphere are dominated by those of Chinese coals. More than 90% of Chinese coals were formed at Late Carboniferous and Early Permian (~38%, occurring mainly in northern China), Early and Middle Jurassic (~40%, occurring mainly in northwestern China), and Late Jurassic and Early Cretaceous (~12%, occurring mainly in northeastern China) (Dai et al., 2012). Previously published Hg isotope compositions of Chinese coals were exclusively sampled from Permian formations (Biswas et al., 2008; Sun et al., 2013a). In the present study, we include coals sampled from Mesozoic (Jurassic and Early Cretaceous, in Shanxi, Inner Mongolia, Xinjing and Liaoning Province), Cenozoic (Tertiary, sampling from Yunnan Province) and Paleozoic (Late Carboniferous and Permian) coals (Table A1 in Appendix A). Geographically, our samples cover 11 provinces and ~75% of Chinese coal producing basins (NBSC, 2012).

Figure B2 in Appendix B summarizes δ^{202}Hg and Δ^{199}Hg variability of Chinese coals in 12 provinces by incorporating coal samples previously reported (Biswas et al., 2008; Sun et al., 2013a). A ~3.8‰ variation in δ^{202}Hg (−3.07 to 0.77‰) and a ~0.7‰ variation in Δ^{199}Hg (−0.40 to 0.34‰) are observed. Statistically, Chinese coals can be significantly distinguished from Indian coals by δ^{202}Hg ($p=0.01$), and African ($p<0.001$), European ($p<0.001$) and Mongolian ($p<0.001$), the USA ($p=0.07$),

former USSR (p=0.06) and Indonesian (p=0.09) coals by Δ^{199}Hg (Table A2 in Appendix A and Figure 24). A few of the coal deposits in China are characterized by significantly positive and negative MIF. For example, coals from Inner Mongolia have positive Δ^{199}Hg of 0.20±0.02‰ (1SD, n=2), whereas coals from Henan and Shanxi Provinces are dominated by negative Δ^{199}Hg with values of −0.28±0.12‰ (1SD, n=2) and −0.10±0.19‰ (1SD, n=7), respectively.

Being able to distinguish coal Hg emissions from different provinces has important implication for local and regional Hg tracing in China. Figure 25 shows the variations of δ^{202}Hg and Δ^{199}Hg in different provinces. Based on the combined signatures of δ^{202}Hg and Δ^{199}Hg, we can distinguish coals from the main coal-producing provinces, i.e. Inner Mongolia (26% national share), Shanxi (23% share), Henan (5% share), Guizhou (4% share), Anhui (3% share).

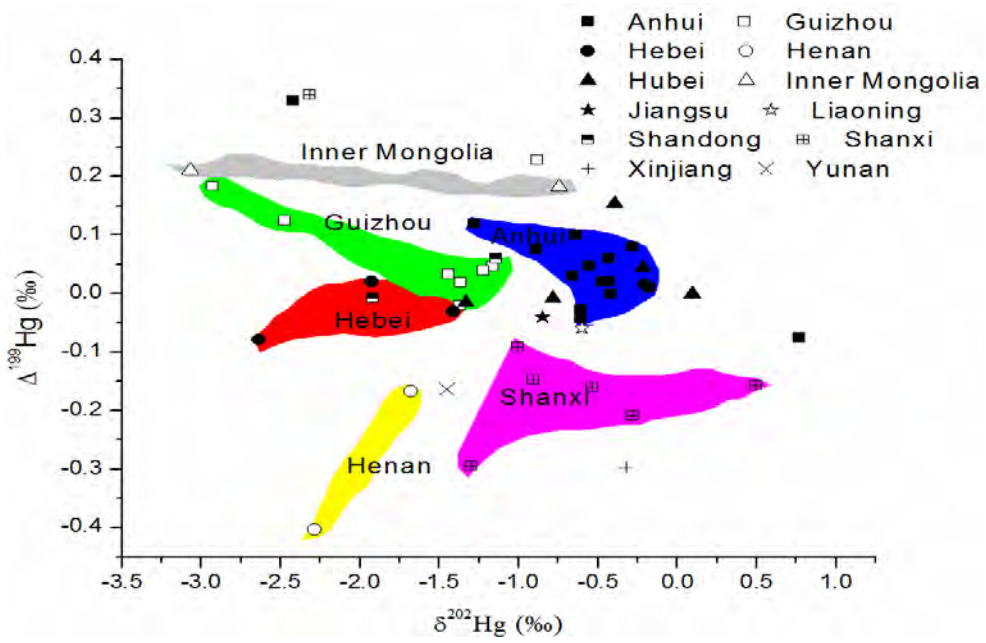

Figure 25 δ^{202}Hg vs. Δ^{199}Hg in all Chinese coals (n=49).

7.3.1.3. European (Romania) coal

Anthropogenic Hg emissions in Europe (excluding former USSR) have decreased significantly since the 1990s and stabilized at ~120 t/yr of which coal combustion in power plants and residential boilers is still the largest contributor (Pacyna et al., 2006a; Streets et al., 2011). The top anthropogenic Hg emitting countries are Poland, Yugoslavia and Romania in Eastern Europe, and Germany, Spain, France, Italy and the United Kingdom in Western Europe (Pacyna et al., 2006a). Our European coal samples were mainly from Romania. Only one coal sample was obtained from France and Germany. Coal deposits in Germany and Romania were mainly formed in the Cenozoic

and in ranks of subbituminous coal and lignite. Germany, which has an estimated coal reserve of ~40000 Mt (4.7% world share) is a moderate coal producing (1.1% world share) and consuming (~2.1% world share) country. Romania also has abundant coal deposits (~290 Mt) and 30-40% of its electricity relies on coal. France produces and consumes little coal as 80% of its electricity production is from nuclear plants. Most of consumed coal in Eastern Europe is imported from South Africa, South America, Australia, former USSR and the USA (Figure B3 in Appendix B). Coal samples from Romania were collected in 2001 under the USGS WoCQI project (Tewalt et al., 2010), and included 10 active mines (Valea de Brazi, Uricani, Barbateni, Lupeni, Paroseni, Vulcan, Aninoasa, Livezeni, Lonea, and Petrila) in the Jiu Valley. The geochemistry, mineralogy and organic petrography of these Oligocene bituminous coals can be found in Belkin et al., (2010).

There is a ~3.8‰ variation in δ^{202}Hg (−2.08 to 0.70‰) and ~0.5‰ variation in Δ^{199}Hg (−0.52 to 0.02‰) in European coals. By looking at box plots of European coals in Figure 22, one Romanian coal (R11) has very abnormally positive δ^{202}Hg (0.70±0.18‰, 2SD), and one French coal formed in Carboniferous has typical Δ^{199}Hg (−0.02±0.06‰, 2SD). Coals from Europe have the lowest Δ^{199}Hg values (mean=−0.36±0.11‰, 1SD, n=13) and can be statistically distinguished from China ($P<0.001$), India ($P<0.001$) and USA ($P<0.001$). However, European coals cannot be distinguished from other regions by δ^{202}Hg (mean=−1.17±0.68‰, 1SD, n=13).

7.3.1.4. Indian coal

India is the world's 4th coal producing (5.6% world share) and 3rd coal consuming country (7.9% world share). The discrepancy between coal production and consumption implies that India has to import a large amount of coal (~100 Mt/yr) from other coal exporters (e.g. Indonesia and Australia) to satisfy its domestic need (Figure B3 in Appendix B). Coal combustion in thermal power plants is also the most dominant anthropogenic Hg source to the atmosphere (Mukherjee et al., 2009; Pacyna et al., 2010).

Indian coals show a ~2‰ variation in δ^{202}Hg (−2.86 to −0.89‰) and ~0.4‰ variation in Δ^{199}Hg (−0.15 to 0.28‰). Indian coals were characterized by the lowest δ^{202}Hg (−1.87±0.54‰, n=12), and are distinguishable from coals of Indonesia ($p<0.001$), Africa ($p<0.001$) and China ($p=0.01$) with the highest mean δ^{202}Hg. In addition, MIF (−0.02 to 0.10‰ for Δ^{199}Hg) is not significant in Indian coals except for two samples from the Jharia coal basin (i.e. JB-3 and JR-3 with Δ^{199}Hg of 0.28‰ and −0.15%, respectively) (Figure 22B). On average, Δ^{199}Hg in Indian coals is the highest (0.04±0.09‰,

1SD, n=12). Except Chinese coals, Indian coals can be distinguished from all other coal producing regions by Δ^{199}Hg (Figure 24).

7.3.1.5. Indonesian coal

With ~0.6% world coal reserve, Indonesia has become the world's 5th largest coal producing country (5.1% world share) and the largest coal exporting country (~30% world share) (IEA, 2012). Approximate 70-90% of the mined coal (~250-300 Mt) in Indonesia is exported primarily to Asia-Pacific region (Japan, China and South Korea) (AEO, 2011; EIA, 2012; IEA, 2012) (Figure 5). Most of Indonesian coals were formed during the Cenozoic (Paleogene and Neogene) and are of low to moderate ranks (Belkin et al., 2009). The eight coal samples from Indonesia, sampled during the USGS WoCQI project, were taken from the main coal-producing areas (Sumatra, Kalimantan, Sulawesi and Papua) with ranks of sub-bituminous and high volatile bituminous coal. A detailed description of the geochemistry and petrology of these coal samples was reported elsewhere (Belkin et al., 2009).

In Indonesian coals, ~1.3‰ range in δ^{202}Hg (−1.29 to 0.01‰) and ~0.4‰ in Δ^{199}Hg (−0.42 to -0.04‰) are observed (Figure 22). The δ^{202}Hg in Indonesian coals is highest (−0.55±0.49‰, 1SD, n=8) as compared to other regions, and is distinguishable from Indian ($p<0.001$), the USA ($p=0.03$) and former USSR coals ($p=0.03$). On the basis of Δ^{199}Hg (mean=−0.20±0.14‰, 1SD, n=8), Indonesian coals can only be distinguished from Indian coal ($p=0.03$)

7.3.1.6. Mongolian coal

The International Energy Statistics 2008 of the EIA reported ~2500 Mt of total recoverable coals in Mongolia (EIA, 2012). Recent coal survey reports estimated that the potential coal reserve in Mongolia is >100 billion tons, accounting for ~10% of world coal reserves (M.L., 2013). Due to poor infrastructure, coal production was only 30 Mt in 2011 of which >60% was exported primarily to China. Coal production and export are expected to increase significantly in the near future because of electricity demands in China. Mongolian coals were deposited in freshwater environments with relatively low sulfur contents and were mainly hosted in Permian (low-rank bituminous coal) and Cretaceous fomations (lignite) (Erdenetsogt et al., 2009). The 15 analyzed Mongolian samples were selected from the 37 coals of the USGS WoCQI (Tewalt et al., 2010).

Mogolian coals show a ~3‰ variation in δ^{202}Hg (−2.59 to 0.39‰) and ~0.8‰ variation in Δ^{199}Hg (−0.55 to 0.22‰) (Figure 22). Due to the predominantly negative Δ^{199}Hg (−0.26±0.18‰, 1SD,

n=15), Mongolian coals can be statistically distinguished from Indian ($p<0.001$) and Chinese coals ($p<0.001$).

7.3.1.7. Former USSR coal (Russia, Kazakhstan, Ukraine)

The former USSR has large coal reserves within the Russia Federation, Kazakhstan and Ukraine accounting for 18%, 4% and 4% of world coal reserve, respectively (BP, 2012). Correspondingly, they are also the among the primary coal producing, consuming and exporting countries (BP, 2012; EIA, 2012; IEA, 2012). Similar to other developed nations, anthropogenic Hg emissions in the former USSR have declined considerably since the 1990s (Streets et al., 2011). At present, total anthropogenic Hg emission to atmosphere are estimated around 150 t/yr, to which coal combustion is the main contributor (Streets et al., 2011).

Our coal samples in the former USSR include the main coal basins in Russia (n=8), Kazakhstan (n=1) and Ukraine (n=4), which are supplemented by eight coal samples previously reported (Biswas et al., 2008). Former USSR are characterized by the largest variations in δ^{202}Hg (~4‰, −3.90‰ to 0.14‰) and Δ^{199}Hg (~0.8‰, from −0.63 to 0.20‰). Due to the relatively lower δ^{202}Hg (mean=−1.69 ±1.13, 1SD, n=21) and Δ^{199}Hg (mean=−0.19±0.23, n=21), former USSR coals are distinguishable from Indonesian coals by δ^{202}Hg ($p=0.03$) and Indian coals by Δ^{199}Hg ($p=0.02$).

7.3.1.8. USA coal

The USA are the third largest anthropogenic Hg emitting country (Pacyna et al., 2010). More than 80% of anthropogenic Hg emissions in North and Central America are from the USA (Pacyna et al., 2010; Pirrone et al., 2009). Like other main anthropogenic Hg emitting countries, coal combustion in the USA accounts for half of total Hg emission to the atmosphere (Streets et al., 2011). With the largest share of world coal reserves, the USA produces nearly 1000 Mt/yr coal, which is 14% of world coal production (BP, 2012). Most of the produced coal is self-consumed by power plants, and < 100 Mt of coal is exported (EIA, 2012) (Figure B3 in Appendix B). The main coal producing states include Wyoming and Montana in the Western USA, and West Virginia, Kentucky, Pennsylvania, Illinois and Virginia in the Eastern USA. As Hg isotope compositions of coal samples in 12 states of the USA have been reported (Biswas et al., 2008; Lefticariu et al., 2011), only four coal samples (three from Illinois and one from Pennsylvania) were analyzed in the present study.

The Hg isotope values of our samples are within those previously reported (Figure B2 in Appendix B). USA coals have a ~3.4‰ variation in δ^{202}Hg (−2.98 to 0.45‰) and ~0.4‰ variation in Δ^{199}Hg

(−0.34 to 0.10‰). By excluding the three extreme values, the USA coals only have ~1.5‰ variation in δ^{202}Hg (−2.21 to −0.75‰). Statistically, coals from the USA can be distinguished from Indonesian coals by δ^{202}Hg ($p=0.03$), and Indian ($p=0.03$) and European coals by Δ^{199}Hg ($p<0.001$).

7.3.2. Biogeochemical factors influencing Hg isotope compositions in coals

Hg isotope compositions in global coal deposits are a combined result of different Hg sources (e.g. coal-forming vegetation, source rocks, hydrothermal fluids, volcanic emissions) and biogeochemical processes (e.g. bacterial degradation, peatification, diagenesis, coalification) that occurred during and after coal deposition (Biswas et al., 2008; Lefticariu et al., 2011).

Assuming that Hg in coal is present in two distinct forms, organic and inorganic, with contrasting Hg isotope compositions, we can test a binary mixing model to identify their possible Hg isotope compositions. This is done by plotting a linear regression between δ^{202}Hg or Δ^{199}Hg and the reciprocal of Hg concentration (1/Hg). However, no relationships were found for δ^{202}Hg vs. 1/Hg and Δ^{199}Hg vs. 1/Hg in all the world coal samples ($n=120$). This is not a surprise as coals were collected from different coal producing regions with contrasting coal forming environments and coalification processes. For some specific countries (i.e. China, Romania, Mongolia and the USA), we observed significant relationships in δ^{202}Hg vs. 1/Hg or Δ^{199}Hg vs. 1/Hg (Figure 26). Lefticariu et al., (2011) interpreted the observed negative correlation of Δ^{199}Hg vs. 1/Hg in the Illinois coal basin, USA (Figure 26A) as the mixing of hydrothermally derived Hg with coal organic Hg. The hydrothermal Hg of circum-zero Δ^{199}Hg was admixed to the organic matrix of negative Δ^{199}Hg during multi-stage hydrothermal intrusion events. Low-temperature hydrothermal fluids are a well known factor to increase Hg concentration in coals (Dai et al., 2012; Diehl et al., 2012). The Chinese samples from Anhui, Guizhou and Inner Mongolia with high Hg concentrations in this study were sampled from coal deposits with hydrothermal influences (Dai et al., 2012; Yan et al., 2013). The comparable negative correlation of Δ^{199}Hg vs. 1/Hg in Chinese coals (Figure 26B) implies a similar hydrothermal mixing process. However, hydrothermal end-members in Chinese coals were higher in Δ^{199}Hg (ca. 0.15‰, $n=8$, by averaging Δ^{199}Hg of samples with Hg concentration >380 ng/g) as compared to the USA coals, but comparable to hydrothermal fluids (mean=0.13‰) from Yellowstone Plateau Volcanic field, USA (Sherman et al., 2009). Although a linear negative relationship of Δ^{199}Hg vs. 1/Hg is also observed in Romanian coals, the suggested end-members are very different from both Chinese and the USA coals and this correlation would be invalid if the sample (R11) with the lowest Hg concentration and Δ^{199}Hg is excluded (Figure 26C).

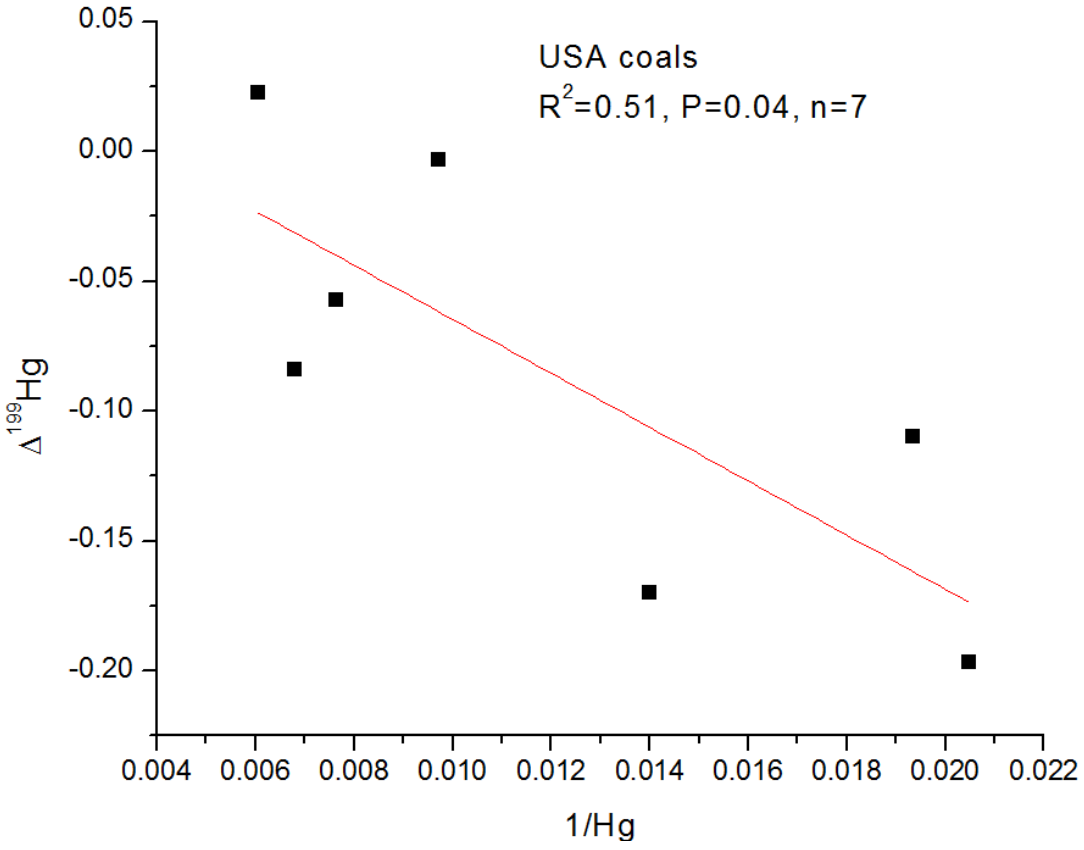
USA coals
R2=0.51, P=0.04, n=7
Δ199Hg
1/Hg
0.05
0.00
-0.05
-0.10
-0.15
-0.20
0.004
0.006
0.008
0.010
0.012
0.014
0.016
0.018
0.020
0.022

(A)

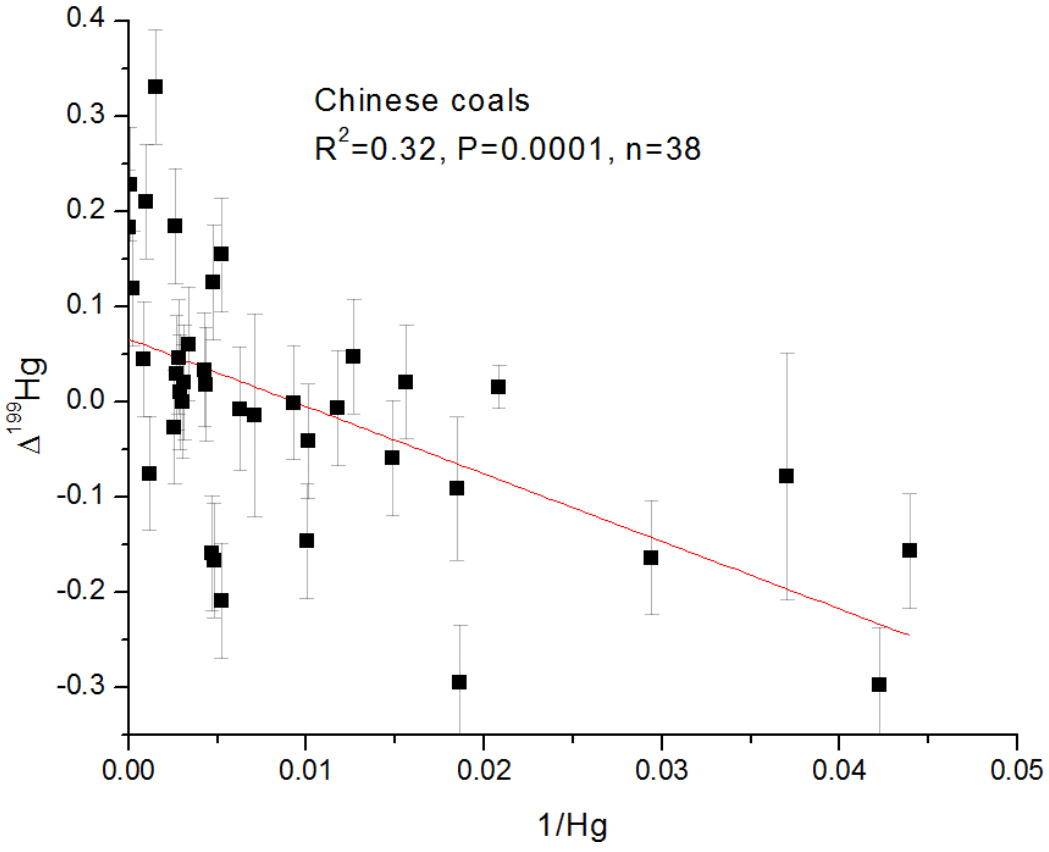
Chinese coals
R2=0.32, P=0.0001, n=38
Δ199Hg
1/Hg
0.4
0.3
0.2
0.1
0.0
-0.1
-0.2
-0.3
0.00
0.01
0.02
0.03
0.04
0.05

(B)

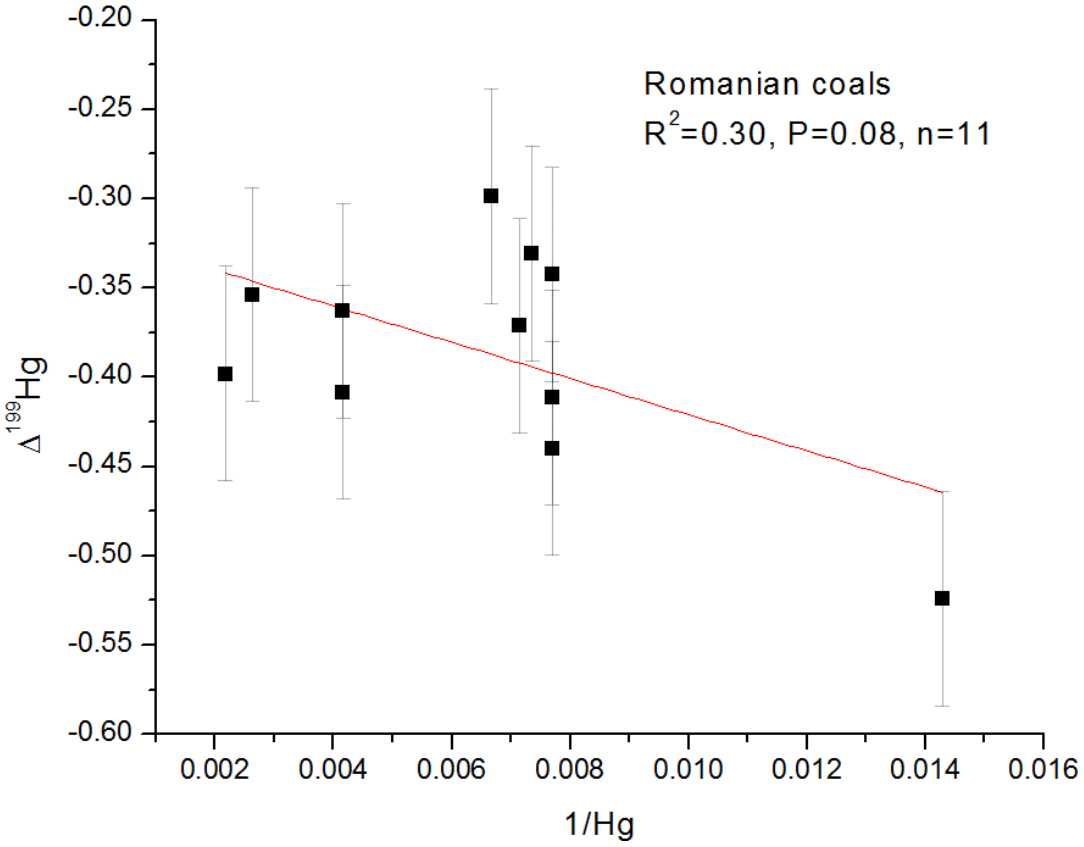
Romanian coals
R2=0.30, P=0.08, n=11
Δ199Hg
1/Hg
-0.20
-0.25
-0.30
-0.35
-0.40
-0.45
-0.50
-0.55
-0.60
0.002
0.004
0.006
0.008
0.010
0.012
0.014
0.016

(C)

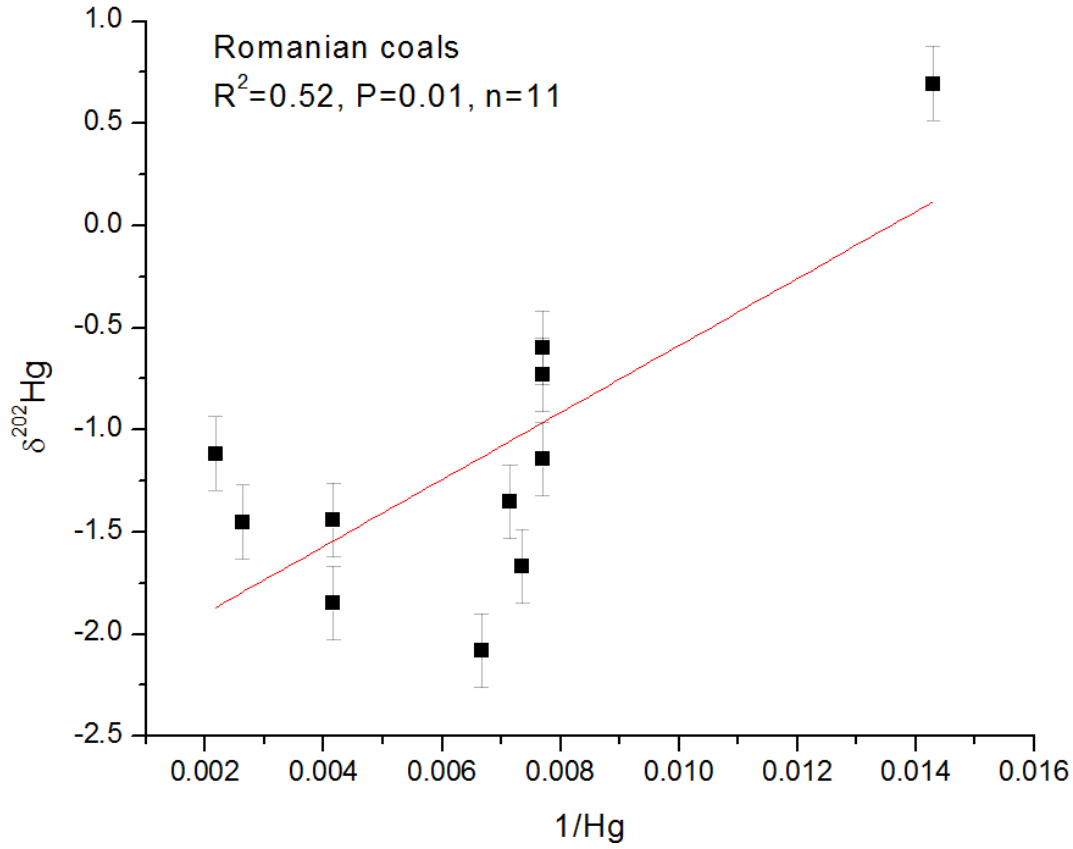
Romanian coals
R2=0.52, P=0.01, n=11
δ202Hg
1/Hg
1.0
0.5
0.0
-0.5
-1.0
-1.5
-2.0
-2.5
0.002
0.004
0.006
0.008
0.010
0.012
0.014
0.016

(D)

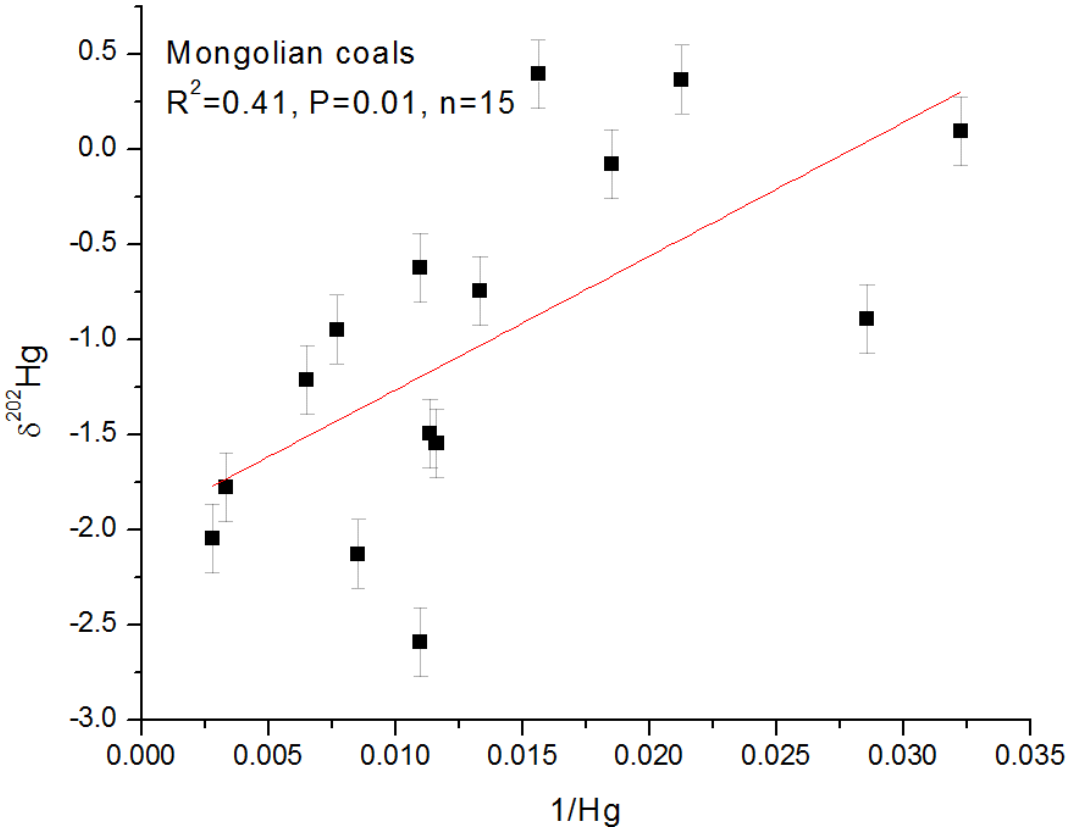

(E)

Figure 26 Linear relationship of δ^{202}Hg vs. 1/Hg or Δ^{199}Hg vs. 1/Hg in coals from the USA (A), China (B), Romania (C, D) and Mongolia (E). The coal samples in the USA are from the Illinois coal basin reported elsewhere (Lefticariu et al., 2011), and are averaged on a coal mine basis; the significant relationship of δ^{202}Hg vs. 1/Hg and Δ^{199}Hg vs. 1/Hg in Romanian coals would disappear when the lowest Hg sample (R11) is excluded.

In contrast to the negative correlation of Δ^{199}Hg vs. 1/Hg, δ^{202}Hg vs. 1/Hg shows a positive correlation as seen for Romanian and Mongolian coals (Figure 26D,E). This suggests that the variation of Δ^{199}Hg in coals is opposite to that of δ^{202}Hg. Significant negative correlation of δ^{202}Hg vs. Δ^{199}Hg is shown in Romanian coals (R^2=0.83) (Figure 27). Although the positive correlation of δ^{202}Hg vs. 1/Hg in Romanian and Mongolian coals can be explained by binary mixing of end-members, they likely reflect the evolution of δ^{202}Hg of coals with diagenesis and coalification. After the accumulation of sediments on peat deposits, the increased temperature and pressure due to sedimentary burial and magmatic intrusion may reduce the weakly-bound Hg(II) into Hg(0) vapor (Yudovich and Ketris, 2005). The volatilization of Hg(0) from coals could induce MDF of Hg isotopes and enrich the remaining Hg in coal in the heavier Hg isotopes. Therefore, our observations of increasing δ^{202}Hg with decreasing Hg concentrations in Romanian and Mongolian coals may

reflect diagenesis and coalification. Significant MIF of Hg isotopes is only invoked by photochemical reactions (Bergquist and Blum, 2007), we therefore do not expect MIF of ^{199}Hg and ^{201}Hg in coals during diagenesis and coalification.

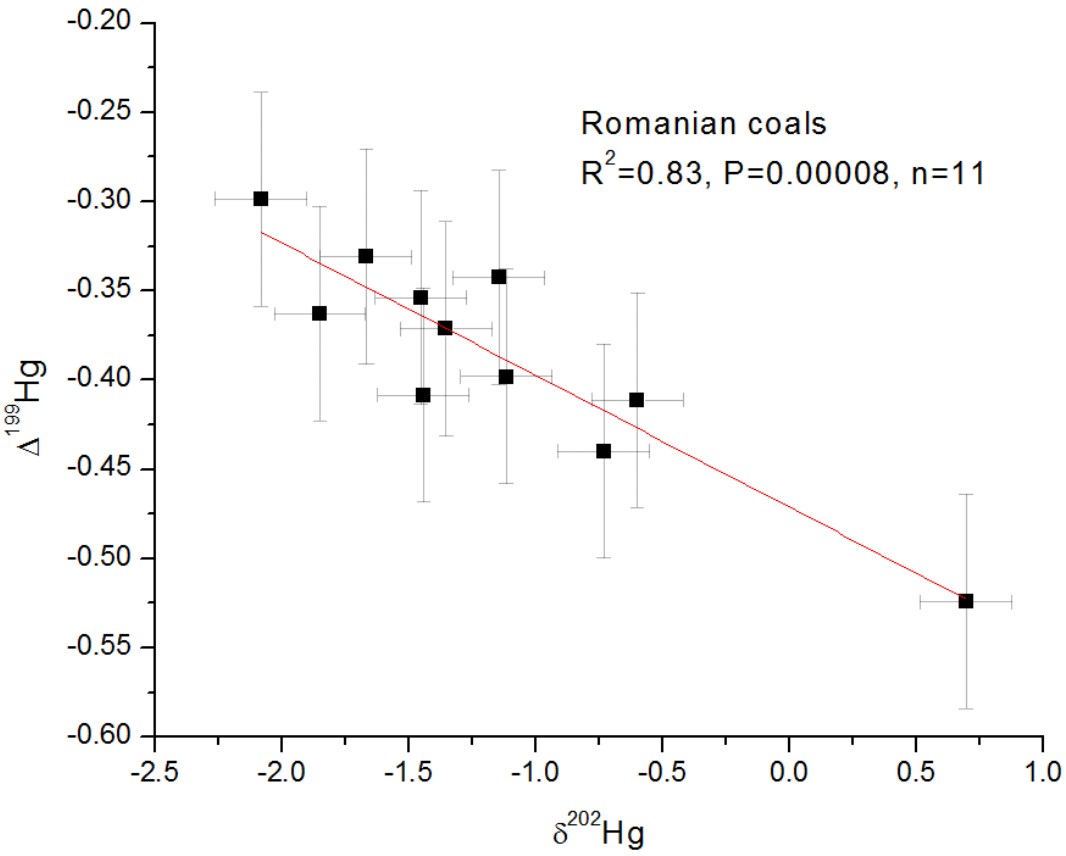

Figure 27 Linear relationship of δ^{202}Hg vs. Δ^{199}Hg in Romanian coals

With the increase of pressure and temperature, the buried peat evolved to lignite, then to subbituminous coal, to bituminous coal, to anthracite and finally to natural cokes. Therefore, the relationship of coal rank vs. δ^{202}Hg or Δ^{199}Hg can be used to explore the effect of coalification processes on Hg isotope fractionation in coals. No clear relationship is observed in coal rank vs. δ^{202}Hg in world coal samples (Figure 28A). However, an increase of Δ^{199}Hg with increasing coal ranks is visible Figure 28B. This may suggest that hydrothermal fluids are a major factor to upgrade coal ranks during coalification and the hydrothermally derived Hg of circum-zero to slightly positive Δ^{199}Hg was sequestered into high-rank coals. Coal rank is closely related to coal-forming periods. Coals formed in the Paleozoic were usually deeply buried and subjected to multi-stage tectonic activity, and thus are commonly anthracite or bituminous coal in rank. Cenozoic coals are less evolved and commonly in ranks of sub-bituminous coal and lignite. By plotting coal-forming periods vs. δ^{202}Hg or Δ^{199}Hg (Figure 29), we can observe similar trends as coal ranks vs. δ^{202}Hg or Δ^{199}Hg.

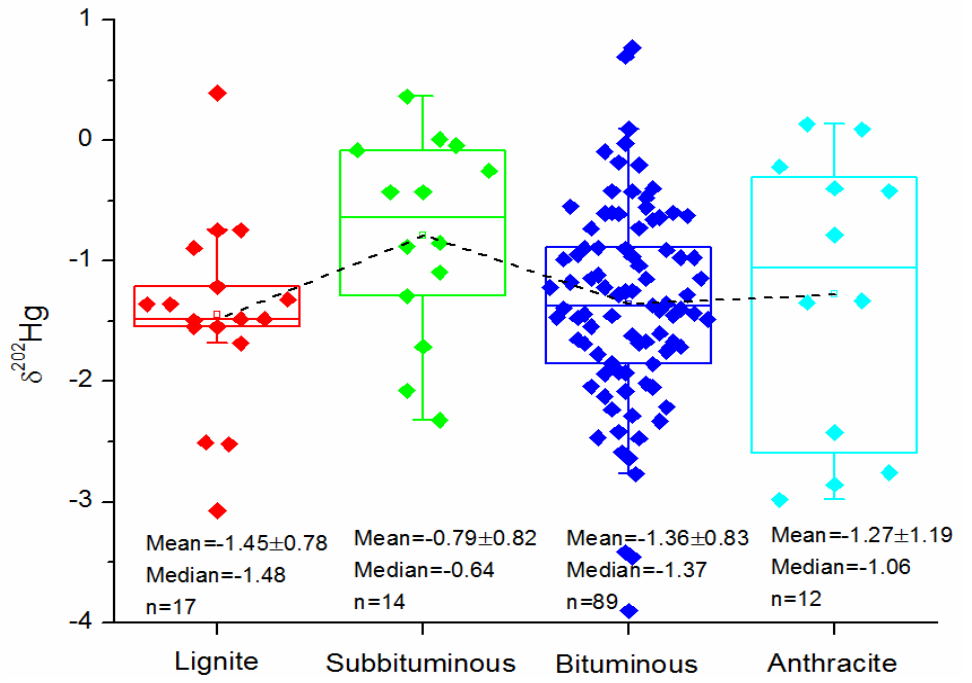

(A)

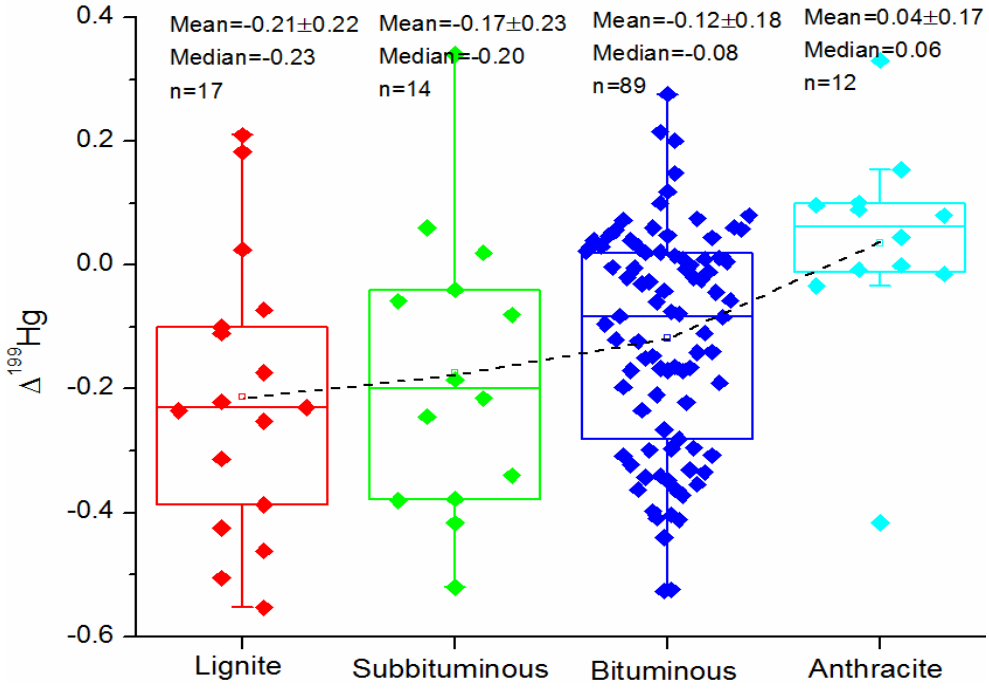

(B)

Figure 28 Box plots showing variations of δ^{202}Hg (‰, A) and Δ^{199}Hg (‰, B) in world coals of different ranks

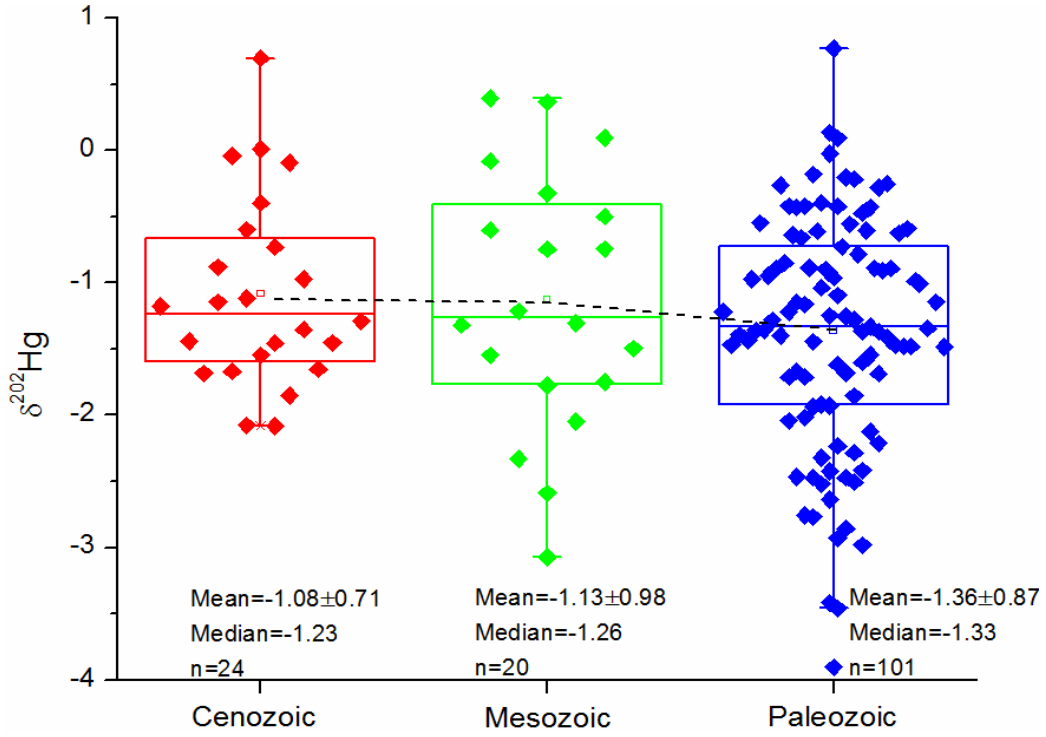

(A)

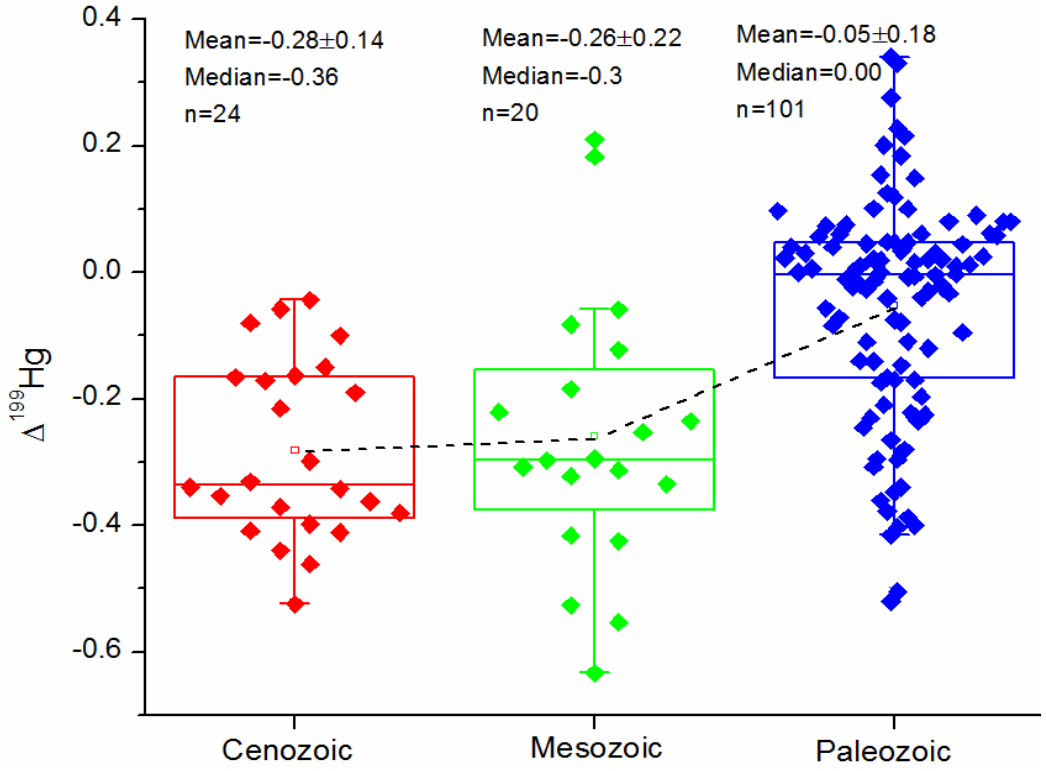

(B)

Figure 29 Box plots showing variations of δ^{202}Hg (‰, A) and Δ^{199}Hg (‰, B) in world coals of different coal-forming periods

7.3.3. Industrial processes influencing Hg isotope compositions of coal Hg emissions

Before application of Hg isotope signatures to trace Hg emission from coals, it should be noted that a number of industrial processes during coal preparation and utilization potentially fractionate Hg isotopes in coal, and thus generate coal related products (e.g. stack flue gas in coal-fired power plants) with Hg isotope compositions that are significantly different from raw coals. As most of the produced coals are combusted in CFUB of power plants for electricity generation, we will discuss below the Hg isotope fractionation caused by coal preparation and combustion

7.3.3.1 Coal preparation

Coal cleaning before combustion in CFUB is a low-cost, common practice for power plants to remove pyritic sulfur and ash along with their associated hazardous air pollutants including Hg (Akers, 1996). Due to the high affinity of Hg with pyrite, 10-70% of coal Hg can be removed, depending on different coal cleaning techniques and physicochemical characteristics of coal (Pavlish et al., 2003). Different Hg-binding components in coal were shown to carry different Hg isotope compositions (Lefticariu et al., 2011). These authors found that pyrite has circum-zero δ^{202}Hg and Δ^{199}Hg which is enriched by 0.9-1.3‰ and 0.04-0.15‰, respectively, relative to their corresponding organic Hg components in coal. This suggests that the removal of pyrite fractions during coal preparation would possibly decrease δ^{202}Hg and Δ^{199}Hg of coal. The degree to which δ^{202}Hg and Δ^{199}Hg in cleaned coal are fractionated from raw coal is determined by the Hg removal efficiency, and the differences of δ^{202}Hg and Δ^{199}Hg between raw coal and coal rejections (primarily pyrite). δ^{202}Hg and Δ^{199}Hg in clean coal can be estimated by Hg isotope mass balance for δ^{202}Hg and Δ^{199}Hg:

$$\delta^{202}\mathrm{Hg}_{\mathrm{RC}}\ (\Delta^{199}\mathrm{Hg}_{\mathrm{RC}})=\delta^{202}\mathrm{Hg}_{\mathrm{CC}}\ (\Delta^{199}\mathrm{Hg}_{\mathrm{CC}})\times\varphi_{\mathrm{CC}}+\delta^{202}\mathrm{Hg}_{\mathrm{PY}}\ (\Delta^{199}\mathrm{Hg}_{\mathrm{CR}})\times\varphi_{\mathrm{CR}}$$

$$\varphi_{\mathrm{CC}}+\varphi_{\mathrm{CR}}=1$$

where subscript RC, CC and CR stand for raw coal, clean coal and coal rejections, respectively. Given Hg removal fraction in coal rejections (φ_{CR}), δ^{202}Hg and Δ^{199}Hg in coal rejections (assuming to be zero, identical to those of pyrite), δ^{202}Hg and Δ^{199}Hg in clean coal can be expressed as:

$$\delta^{202}\mathrm{Hg}_{\mathrm{CC}}\ (\Delta^{199}\mathrm{Hg}_{\mathrm{CC}})=\frac{\delta^{202}\mathrm{Hg}_{\mathrm{RC}}\ (\Delta^{199}\mathrm{Hg}_{\mathrm{RC}})}{(1-\varphi_{\mathrm{CR}})}$$

7.3.3.2. Coal combustion in CFUBs

By measuring the Hg isotope compositions of feed coal, bottom ash, fly ash, and desulfurization by-product gypsum, Sun et al., (2013a) used a Hg isotope mass balance equation to infer that coal combustion flue gases emitted at the stack are enriched by at most 0.3‰ in δ^{202}Hg relative to feed coal. No obvious MIF of Hg isotopes was observed during coal combustion and downstream transport of combusted flue gases through air pollution control devices (APCD, i.e. electrostatic precipitators, ESP; Wet flue gas desulphurization systems, WFGD). Significant Hg isotope fractionation probably occurs during coal combustion in CFUBs, i.e.GEM transformation into GOM and PBM during downstream transport of flue gases. Depending on the types of combustion boilers, varying proportions of feed coal Hg can be retained in the boiler or bottom ash. Previous studies (Pavlish et al., 2003; Streets et al., 2009) concluded that Hg retention is negligible (1-2%) for pulverized boilers, which are the dominant boiler type. However, other boiler types such as stoker boilers and fluidized-bed boilers can have >7% Hg retention. A 7% retention would be too low to shift the Hg isotope compositions of the generated GEM from those of feed coal given the high temperatures (>500 °C) (Schauble, 2007).

Another important Hg isotope fractionation processes happens between the outlet of boiler and the inlet of APCDs where a fraction of GEM is oxidized into GOM and PBM. For CFUBs equipped with ESP and WFGD, the produced PBM and GOM will be sequentially removed with fly ash in the ESP and with gypsum in WFGD. Emitted flue gases are in such case primarily composed of GEM. Our observations on PBM (fly ash) and GOM (gypsum) show that they are significantly enriched in the lighter Hg isotopes relative to feed coals, suggesting the emitted GEM to be enriched in the heavier Hg isotopes by up to 0.3‰ (Sun et al., 2013a). Preliminary direct species-specific Hg isotope measurement on stack emission components let to an identical conclusion (Khawaja et al., 2010). However, the fractionation mechanisms, extent, and signs among GEM, GOM and PBM species in emitted flue gas should be further explored, as they are critical in near-field and far-field coal Hg emission tracing.

7.3.4. Coal import-export flow control on a regional/national coal Hg isotope emission inventory

In order to distinguish coal Hg emissions from different regions, it is necessary to develop a Hg isotope emission inventory of combusted coals on a regional/national basis. Specific countries that rely on coal import from other regions (Figure B3 in Appendix B) can be expected to have different Hg isotope compositions of coal emissions than those based on use of indigenous coals only. This depends on the ratio of exported and indigenous coal consumption and their differences in Hg

isotope compositions. For the regions that are indistinguishable based on δ^{202}Hg and Δ^{199}Hg (Figure 24), Hg isotope change in consumed coals due to coal import-export trades is thought to be small, whereas significant Hg isotope change can be seen among distinguishable regions when imported coal becomes comparable to or exceeds indigenous coal consumption. For example, the import of South African coals to Europe does not seem to significantly shift the Hg isotope compositions of European coals due to similar Hg isotope compositions. Although export of South African coals to India has increased recently, its share relative to the large coal production in India is very small and can't significantly change the Hg isotope compositions of Indian coal Hg emissions.

7.4. Implications

The coal Hg isotope library we created has been an important first step in tracing coal Hg emissions. The significant differences in δ^{202}Hg and Δ^{199}Hg between regions allow us to distinguish coal Hg emissions from different regions. Combing historical coal production statistics, coal import-export statistics, and Hg removal efficiencies by APCDs during coal combustion, we can reconstruct an all-time historical evolution of the Hg isotope compositions of atmospheric coal Hg emissions. Where we have enough information, such a Hg isotope emission inventory can be made on a regional/national basis. We can then start to understand and explain the Hg isotope information in natural archives such as peat, sediment and ice cores or soils and biomonitors. A preliminary Hg isotope evolution model of world coals from 1815-2010 is shown in Figure B4 of Appendix B. δ^{202}Hg in world coals progressively decreases from ~−1.2‰ at the dawn of the industrial revolution to ~−1.35‰ during the world war II, and then returned back to ~−1.2‰ in the new millennium. In contrast, Δ^{199}Hg and Δ^{201}Hg in world coal emissions progressively increased from ~−0.3 to ~−0.1 ‰. We expect that Δ^{199}Hg and Δ^{201}Hg of world coal Hg emissions have similar values and trends of world coals, as pre- and post-combustion processes do not shift Δ^{199}Hg and Δ^{201}Hg of coal Hg emissions relative to raw coals. However, δ^{202}Hg in world coal emissions is difficult to estimate without the information on Hg removal efficiencies of pre- and post-combustion processes. Pyrite Hg removal before coal combustion enriches combusted coals in the lighter Hg isotopes relative to raw coals, whereas Hg removal by APCDs enriches coal Hg emissions in the heavier Hg isotopes.

Acknowledgements

This work is supported by research grants ANR-09-JCJC-0035-01 from the French Agence Nationale de Recherche and ERC-2010-StG_20091028 from the European Research Council to JES. RS acknowledges his PhD scholarship from the Chinese Scholarship Council.

References

AEO, 2011. Annual Energy Outlook Report: Flows By Importing Regions and Exporting Countries.

Akers, D.J., 1996. Coal cleaning controls HAP emissions. Journal Name: Power Engineering (Barrington); Journal Volume: 100; Journal Issue: 6; Other Information: PBD: Jun 1996, Medium: X; Size: pp. 33-36.

Belkin, H.E., Tewalt, S.J., Hower, J.C., Stucker, J.D., O'Keefe, J.M.K., 2009. Geochemistry and petrology of selected coal samples from Sumatra, Kalimantan, Sulawesi, and Papua, Indonesia. International Journal of Coal Geology 77, 260-268.

Belkin, H.E., Tewalt, S.J., Hower, J.C., Stucker, J.D., O'Keefe, J.M.K., Tatu, C.A., Buia, G., 2010. Petrography and geochemistry of Oligocene bituminous coal from the Jiu Valley, Petroşani basin (southern Carpathian Mountains), Romania. International Journal of Coal Geology 82, 68-80.

Bergquist, B.A., Blum, J.D., 2007. Mass-Dependent and -Independent Fractionation of Hg Isotopes by Photoreduction in Aquatic Systems. Science 318, 417-420.

Biswas, A., Blum, J.D., Bergquist, B.A., Keeler, G.J., Xie, Z., 2008. Natural Mercury Isotope Variation in Coal Deposits and Organic Soils. Environmental Science & Technology 42, 8303-8309.

BP, 2012. BP (Petroleum British) Statistical Review of World Energy (2011).

Cairncross, B., Hart, R.J., Willis, J.P., 1990. Geochemistry and sedimentology of coal seams from the Permian Witbank Coalfield, South Africa; a means of identification. International Journal of Coal Geology 16, 309-325.

Chen, J., Hintelmann, H., Feng, X., Dimock, B., 2012. Unusual fractionation of both odd and even mercury isotopes in precipitation from Peterborough, ON, Canada. Geochimica et Cosmochimica Acta 90, 33-46.

Dabrowski, J.M., Ashton, P.J., Murray, K., Leaner, J.J., Mason, R.P., 2008. Anthropogenic mercury emissions in South Africa: Coal combustion in power plants. Atmospheric Environment 42, 6620-6626.

Dai, S., Ren, D., Chou, C.-L., Finkelman, R.B., Seredin, V.V., Zhou, Y., 2012. Geochemistry of trace elements in Chinese coals: A review of abundances, genetic types, impacts on human health, and industrial utilization. International Journal of Coal Geology 94, 3-21.

Diehl, S.F., Goldhaber, M.B., Koenig, A.E., Lowers, H.A., Ruppert, L.F., 2012. Distribution of arsenic, selenium, and other trace elements in high pyrite Appalachian coals: Evidence for multiple episodes of pyrite formation. International Journal of Coal Geology 94, 238-249.

DME, 2010. Digest of South African Energy Statistics 2009. Department of Minerals and Energy Pretoria

EIA, 2012. International Energy Statistics 2008: coal, in: Administration, U.S.E.I. (Ed.).

EPA-1631E, 2002. Mercury in Water by Oxidation, Purge and Trap, and Cold Vapor Atomic Fluorescence Spectrometry.

Erdenetsogt, B.-O., Lee, I., Bat-Erdene, D., Jargal, L., 2009. Mongolian coal-bearing basins: Geological settings, coal characteristics, distribution, and resources. International Journal of Coal Geology 80, 87-104.

Estrade, N., Carignan, J., Donard, O.F.X., 2010. Isotope Tracing of Atmospheric Mercury Sources in an Urban Area of Northeastern France. Environmental Science & Technology 44, 6062-6067.

Estrade, N., Carignan, J., Donard, O.F.X., 2011. Tracing and Quantifying Anthropogenic Mercury Sources in Soils of Northern France Using Isotopic Signatures. Environmental Science & Technology 45, 1235-1242.

Estrade, N., Carignan, J., Sonke, J.E., Donard, O.F.X., 2009. Mercury isotope fractionation during liquid-vapor evaporation experiments. Geochimica et Cosmochimica Acta 73, 2693-2711.

IEA, 2012. Key World Energy Statistics 2012.

Ketris, M.P., Yudovich, Y.E., 2009. Estimations of Clarkes for Carbonaceous biolithes: World averages for trace element contents in black shales and coals. International Journal of Coal Geology 78, 135-148.

Leaner, J., Dabrowski, J., Mason, R., Resane, T., Richardson, M., Ginster, M., Gericke, G., Petersen, C., Masekoameng, E., Ashton, P., Murray, K., 2009. Mercury emissions from point sources in South Africa, in: Mason, R., Pirrone, N. (Eds.), Mercury Fate and Transport in the Global Atmosphere. Springer US, pp. 113-130.

Lefticariu, L., Blum, J.D., Gleason, J.D., 2011. Mercury Isotopic Evidence for Multiple Mercury Sources in Coal from the Illinois Basin. Environmental Science & Technology 45, 1724-1729.

Lusilao-Makiese, J., Tessier, E., Amouroux, D., Tutu, H., Chimuka, L., Cukrowska, E.M., 2012. Speciation of mercury in South African coals. Toxicological & Environmental Chemistry 94, 1688-1706.

M.L., 2013. Mongolia 2013: Coal & Power generation Mining leader 22-27.

Mead, C., Johnson, T.M., 2010. Hg stable isotope analysis by the double-spike method. Analytical and Bioanalytic Chemistry 397, 1529-1538.

Mukherjee, A., Bhattacharya, P., Sarkar, A., Zevenhoven, R., 2009. Mercury emissions from industrial sources in India and its effects in the environment, in: Mason, R., Pirrone, N. (Eds.), Mercury Fate and Transport in the Global Atmosphere. Springer US, pp. 81-112.

NBSC, 2012. Statistical bulletin of national economic and social development in 2011, People's Republic of China Beijing.

Pacyna, E.G., Pacyna, J.M., Fudala, J., Strzelecka-Jastrzab, E., Hlawiczka, S., Panasiuk, D., 2006a. Mercury emissions to the atmosphere from anthropogenic sources in Europe in 2000 and their scenarios until 2020. Science of Total Environment 370, 147-156.

Pacyna, E.G., Pacyna, J.M., Steenhuisen, F., Wilson, S., 2006b. Global anthropogenic mercury emission inventory for 2000. Atmospheric Environment 40, 4048-4063.

Pacyna, E.G., Pacyna, J.M., Sundseth, K., Munthe, J., Kindbom, K., Wilson, S., Steenhuisen, F., Maxson, P., 2010. Global emission of mercury to the atmosphere from anthropogenic sources in 2005 and projections to 2020. Atmospheric Environment 44, 2487-2499.

Pavlish, J.H., Sondreal, E.A., Mann, M.D., Olson, E.S., Galbreath, K.C., Laudal, D.L., Benson, S.A., 2003. Status review of mercury control options for coal-fired power plants. Fuel Processing Technology 82, 89-165.

Pirrone, N., Cinnirella, S., Feng, X., Finkelman, R., Friedli, H., Leaner, J., Mason, R., Mukherjee, A., Stracher, G., Streets, D., Telmer, K., 2009. Global Mercury Emissions to the Atmosphere from Natural and Anthropogenic Sources, in: Mason, R., Pirrone, N. (Eds.), Mercury Fate and Transport in the Global Atmosphere. Springer US, pp. 1-47.

Pirrone, N., Cinnirella, S., Feng, X., Finkelman, R.B., Friedli, H.R., Leaner, J., Mason, R., Mukherjee, A.B., Stracher, G.B., Streets, D.G., Telmer, K., 2010. Global mercury emissions to the atmosphere from anthropogenic and natural sources. Atmospheric Chemistry and Physics 10, 5951-5964.

Schauble, E.A., 2007. Role of nuclear volume in driving equilibrium stable isotope fractionation of mercury, thallium, and other very heavy elements. Geochimica et Cosmochimica Acta 71, 2170-2189.

Seigneur, C., Vijayaraghavan, K., Lohman, K., Karamchandani, P., Scott, C., 2004. Global Source Attribution for Mercury Deposition in the United States. Environmental Science & Technology 38, 555-569.

Selin, N.E., Jacob, D.J., Yantosca, R.M., Strode, S., Jaeglé, L., Sunderland, E.M., 2008. Global 3-D land-ocean-atmosphere model for mercury: Present-day versus preindustrial cycles and anthropogenic enrichment factors for deposition. Global Biogeochemical Cycles 22, GB2011.

Sherman, L.S., Blum, J.D., Keeler, G.J., Demers, J.D., Dvonch, J.T., 2011. Investigation of Local Mercury Deposition from a Coal-Fired Power Plant Using Mercury Isotopes. Environmental Science & Technology 46, 382-390.

Sherman, L.S., Blum, J.D., Keeler, G.J., Demers, J.D., Dvonch, J.T., 2012. Investigation of Local Mercury Deposition from a Coal-Fired Power Plant Using Mercury Isotopes. Environmental Science & Technology

Sherman, L.S., Blum, J.D., Nordstrom, D.K., McCleskey, R.B., Barkay, T., Vetriani, C., 2009. Mercury isotopic composition of hydrothermal systems in the Yellowstone Plateau volcanic field and Guaymas Basin sea-floor rift. Earth and Planetary Science Letters 279, 86-96.

Sonke, J.E., Blum, J.D., 2013. Advances in mercury stable isotope biogeochemistry. Chem. Geol. 336, 1-4.

Streets, D.G., Devane, M.K., Lu, Z., Bond, T.C., Sunderland, E.M., Jacob, D.J., 2011. All-Time Releases of Mercury to the Atmosphere from Human Activities. Environmental Science & Technology 45, 10485-10491.

Streets, D.G., Hao, J., Wang, S., Wu, Y., 2009. Mercury emissions from coal combustion in China, in: Mason, R., Pirrone, N. (Eds.), Mercury Fate and Transport in the Global Atmosphere. Springer US, pp. 51-65.

Sun, R., Heimbürger, L.-E., Sonke, J.E., Liu, G., Amouroux, D., Berail, S., 2013a. Mercury stable isotope fractionation in six utility boilers of two large coal-fired power plants. Chemical Geology 336, 103-111.

Sun, R., Enrico, M., Heimbürger, L.-E., Scott, C., Sonke, J.E., 2013b. A double-stage tube furnace – acid trapping protocol for the pre-concentration of mercury from solid samples for isotopic analysis. Analytical and Bioanalytical Chemistry DOI: 10.1007/s00216-013-7152-2.

Tewalt, S.J., Belkin, H.E., SanFilipo, J.R., Merrill, M.D., Palmer, C.A., Warwick, P.D., Karlsen, A.W., Finkelman, R.B., Park, A.J., comp., 2010. Chemical analyses in the World Coal Quality Inventory, version 1, U.S. Geological Survey: p. 4.

Weiss-Penzias, P., Jaffe, D., Swartzendruber, P., Hafner, W., Chand, D., Prestbo, E., 2007. Quantifying Asian and biomass burning sources of mercury using the Hg/CO ratio in pollution plumes observed at the Mount Bachelor observatory. Atmospheric Environment 41, 4366-4379.

Yan, Z., Liu, G., Sun, R., Wu, D., Wu, B., Zhou, C., 2013. Mercury distribution in coals influenced by magmatic intrusions, and surface waters from the Huaibei Coal Mining District, Anhui, China. Applied Geochemistry 33, 298-305.

Yang, Y., Huang, Q., Wang, Q., 2012. Ignoring Emissions of Hg from Coal Ash and Desulfurized Gypsum Will Lead to Ineffective Mercury Control in Coal-Fired Power Plants in China. Environmental Science & Technology 46, 3058-3059.

Yudovich, Y.E., Ketris, M.P., 2005. Mercury in coal: a review: Part 1. Geochemistry. International Journal of Coal Geology 62, 107-134.

Zheng, W., Hintelmann, H., 2009. Mercury isotope fractionation during photoreduction in natural water is controlled by its Hg/DOC ratio. Geochimica et Cosmochimica Acta 73, 6704-6715.

Chapter 8

Mercury stable isotope fractionation in six utility boilers of two large coal-fired power plants

Chapter 8. Mercury stable isotope fractionation in six utility boilers of two large coal-fired power plants (published article in *Chemical Geology*)

Résumé

Ce Chapitre adresse la question si la combustion du charbon dans les centrales au charbon modifie oui ou non la composition isotopique de ses émissions du Hg. Nous avons mesuré la composition isotopique du Hg dans les charbons, les cendres résiduels et volants, et le gypse produit par la désulfurisation des gaz. Par rapport au charbon combusté, les cendres et gypse sont tous enrichis en isotopes légers du Hg. Par conséquence la signature isotopique des émissions du Hg par la cheminée, calculeé par bilan de masse, est légèrement enrichi en isotopes lourds (δ^{202}Hg <0.3‰), mais reste inchangé pour la signature Δ^{199}Hg.

Chemical Geology 336 (2013) 103–111

Contents lists available at SciVerse ScienceDirect

Chemical Geology

journal homepage: www.elsevier.com/locate/chemgeo

Mercury stable isotope fractionation in six utility boilers of two large coal-fired power plants

Ruoyu Sun [a,*], Lars-Eric Heimbürger [a], Jeroen E. Sonke [a,*], Guijian Liu [b], David Amouroux [c], Sylvain Berail [c]

[a] Observatoire Midi-Pyrénées, Laboratoire Géosciences Environnement Toulouse, CNRS/IRD/Université Paul Sabatier Toulouse 3, 14 avenue Edouard Bélin, 31400 Toulouse, France
[b] CAS Key Laboratory of Crust-Mantle Materials and Environment, School of Earth and Space Sciences, University of Science and Technology of China, Hefei, Anhui 230026, China
[c] LCABIE, IPREM, Université de Pau et des Pays de l'Adour/CNRS UMR 5254, Hélioparc, 2 Avenue du Président Pierre Angot, Pau 64053, France

ARTICLE INFO

Article history:
Accepted 29 October 2012
Available online 6 November 2012

Keywords:
Mercury
Isotopes
Coal
Coal combustion products
Power plant

ABSTRACT

Coal-fired utility boiler (CFUB) emissions of mercury (Hg) represent the largest anthropogenic Hg source to the atmosphere. Hg stable isotope signatures in coal have been shown to vary among coal deposits and coal basins. There is therefore a substantial interest in tracing CFUB Hg emissions at local, regional and global scales. However, CFUB operating conditions, Hg capture technologies and post-emission Hg transformations may potentially alter the original feed coal Hg isotope signatures. Here we investigate Hg isotopic fractionation between feed coal and coal combustion products in six utility boilers of two large power plants in Huainan City, Anhui Province, China. We observe identical trends in all six boilers: relative to feed coal with δ^{202}Hg ranging from −0.67 to −0.18‰, oxidized Hg species in bottom ash and fly ash are enriched in the lighter isotopes with δ^{202}Hg from −1.96 to −0.82‰. Flue gas desulphurization by-product gypsum shows δ^{202}Hg from −0.99 to −0.47‰. No mass independent fractionation was observed during the transport and transformation of Hg inside the boilers. An isotope mass balance suggests that gaseous stack Hg emissions are enriched by up to 0.3‰ in the heavier Hg isotopes relative to feed coal and that the enrichment depends on the Hg capture technology. The observation that oxidized Hg species are enriched in the lighter isotopes suggests that oxidized and reduced forms of Hg in stack emission carry different isotope signatures. This has implications for near-field and far-field Hg emission tracing.

1. Introduction

The physicochemical properties of mercury (Hg) such as its high volatility, active redox and organometallic chemistry make it a mobile, and under certain conditions, toxic element. Consequently, Hg actively participates in complex biogeochemical cycles among atmospheric, terrestrial and aquatic reservoirs (Mason et al., 1994; Fitzgerald et al., 2007). At present, Hg emissions to the atmosphere from anthropogenic sources exceed emissions from natural sources (Lindberg et al., 2007). Coal combustion Hg emissions from stationary facilities (~800 Mg/yr), such as coal-fired utility boilers (CFUB) and commercial boilers, are estimated to be the dominant contributors (Pirrone et al., 2010). Three operationally defined forms of Hg, i.e. gaseous elemental Hg (GEM), gaseous oxidized Hg (GOM) and particulate bound Hg (PBM), are emitted into the atmosphere through exhaust stacks in CFUBs. The total Hg emission and speciation depend on feed coal characteristics, combustion conditions and air pollution control device (APCD) deployment (Streets et al., 2009, 2011). GEM emissions are thought to be transported trans-continentally due to the long residence time (~1 year) of GEM in the atmosphere (Seigneur et al., 2003; Selin et al., 2007). GOM and PBM are readily deposited in the vicinity of power plants and are potentially methylated to toxic methylmercury in the aquatic environment. Assessing the impact of regional CFUB Hg emissions on the local and transnational boundary environments has been hampered due to the lack of an appropriate tracer.

Mercury stable isotope biogeochemistry has demonstrated the ability to unravel the complex Hg cycling among different reservoirs or ecosystems (Bergquist and Blum, 2009; Sherman et al., 2010; Point et al., 2011; Sonke, 2011). Both mass dependent fractionation (MDF, reported as δ^{202}Hg) (Kritee et al., 2007, 2008, 2009; Zheng et al., 2007; Foucher et al., 2008) and mass independent isotope fractionation (MIF, reported as Δ^{199}Hg) (Bergquist and Blum, 2007; Sherman et al., 2010; Zheng and Hintelmann, 2010a, 2010b; Point et al., 2011; Sonke, 2011) can induce significant variations in natural Hg isotope signatures. The range of variation in δ^{202}Hg and Δ^{199}Hg values approaches 10‰ for natural materials including soils, rocks, coal, peat, and biological tissues. By combining the sign and magnitude of MDF and MIF, Hg isotopic fingerprinting helps understand the processes that relate Hg sources to sinks.

High precision Hg isotope data have been reported in coals (Biswas et al., 2008; Lefticariu et al., 2011; Sherman et al., 2012). The available data suggest that coals from different geographic

* Corresponding authors.
E-mail addresses: roysun1986@gmail.com (R. Sun), sonke@get.obs-mip.fr (J.E. Sonke).

0009-2541/$ – see front matter © 2012 Elsevier B.V. All rights reserved.
http://dx.doi.org/10.1016/j.chemgeo.2012.10.055

locations (e.g. different countries and coal-bearing basins) and different coal-forming periods display significant variations in isotopic composition (up to 3‰ for δ^{202}Hg and 1‰ for Δ^{199}Hg), and can be isotopically distinguished from each other using the combination of δ^{202}Hg and Δ^{199}Hg signatures (Biswas et al., 2008; Lefticariu et al., 2011). Consequently, these studies highlight the potential of using Hg isotopes to discriminate atmospheric Hg emitted by CFUBs at different locations. Sherman et al. (2012) showed that δ^{202}Hg and Δ^{199}Hg signatures in wet precipitation downwind from a CFUB in Florida (USA) were substantially different from regional background Hg. However, they also found that precipitation Hg isotope signatures were different from the feed coal used, and suggested both Hg removal from flue gas by APCDs and in-cloud Hg transformations to be the potential causes.

In the high temperature combustion zone of a utility boiler, the Hg in the coal matrix will be transformed to GEM in flue gas. As the flue gas cools down through the heat exchanger, GEM is partly oxidized to GOM, and GOM is partly scavenged onto fly ash as PBM (Hower et al., 2010). In the low temperature regime of the APCDs these transformations slow down, and the various forms of Hg are partly removed from the flue gas (Fig. S1 of Supporting information). The transformation of GEM into GOM and PBM involves physical (condensation, evaporation, and diffusion) and chemical processes (oxidation, reduction, and adsorption). These processes likely fractionate Hg stable isotopes between the oxidized GOM and PBM forms and the residual GEM. Observations for Pb, Zn, Cd and Hg in an industrial incinerator, a refinery smelter and a CFUB indicated that significant isotopic fractionation occurred during high temperature evaporation and condensation processes (Sivry et al., 2008; Sonke et al., 2008; Stetson et al., 2009; Borrok et al., 2010; Gehrke et al., 2011). The bulk δ^{202}Hg and Δ^{199}Hg signatures of CFUB feed coal therefore possibly generate combustion residues and discharged flue gas with modified Hg isotope signatures.

In order to address the potential Hg isotope fractionation in CFUBs, we investigate the Hg isotopic variations in feed coals and combustion residues (i.e. fly ash, bottom ash and gypsum) from 6 CFUBs in two large scale power plants in Huainan City, Anhui Province, China. Our study focuses on: 1) the isotopic composition of Hg in feed coal and its redistribution among the combustion residues; 2) the fractionation mechanisms of Hg isotopes during coal combustion and flue gas transport through post-combustion APCDs; 3) the magnitude of Hg isotopic variation of stack emission (calculated by Hg isotopic mass balance) relative to the feed coal.

2. Experimental details

2.1. Sample collection and preparation

Solid samples consisting of feed coal (bulk and pulverized), fly ash, bottom ash and gypsum were collected from three boilers (H1-1, H1-2 and H1-3, all subcritical units) at Huainan power plant-1 (HPP-1) and three boilers (H2-1 and H2-2 of subcritical, and H2-3 of supercritical units) at Huainan power plant-2 (HPP-2), representing different combustion technologies and APCDs deployments (Fig. S1 and Table 1). The supercritical boiler is operated at higher steam temperature and pressure conditions resulting in 10% higher thermal efficiency than the subcritical boilers. All six utility boilers were equipped with electrostatic precipitators (ESP) for capturing particulate matter with a removal efficiency of >99%. Half of the utility boilers had wet flue gas desulphurization systems (WFGD) to sequester SO_2 in flue gas, and the SO_2 removal efficiency was always >90% (Table 1). No NO_x control devices were in place at the plants during the sampling period. Combustion temperatures are in the range of 1200–1500 °C in the combustion zone of the boiler and decrease downstream to about 100–200 °C at the ESPs, to 40–100 °C at the WFGD, and to >80 °C (re-heating) at the stack (Fig. S1).

Feed coals of HPP-1 and HPP-2 were mainly provided by coal mines from the Huainan Coalfield. The main coal suppliers for HPP-1 and for HPP-2 were the Xinji and Panji Coal Mines, respectively (>90%). The bulk feed coal was collected at the coal bunker and the pulverized feed coal was sampled from pneumatic conveying ducts connected to the CFUBs. Bottom ash evacuated below the boilers, fly ash removed by ESPs and gypsum produced by the WFGD reaction of limestone slurry with SO_2 were sampled during the active combustion process. Sample collection was conducted over a limited time period of 2 h for each boiler. Each time 3–4 subsamples were taken at 30 min intervals and pooled. In addition, bottom ash, fly ash and gypsum were obtained 15 min after sampling the pulverized coal in order to assure representativeness of all samples. About 1 kg of various composite samples were collected and stored in sealed polyethylene bags.

Samples (coal and bottom ash) were manually crushed in an agate mortar to obtain homogenized samples with a particle diameter of <0.075 mm. The agate mortar was cleaned with high purity ethanol and then with Milli-Q water, and dried at 75 °C before processing the next samples to avoid cross-contamination. Powdered samples

Table 1
The boiler parameters and sample ID (information) in HPP-1 and HPP-2 power plants.

HPP-1 (all subcritical units)			
Samples	Boiler 1 (H1-1, 300 MW)	Boiler 2 (H1-2, 300 MW)	Boiler 3 (H1-3, 600 MW)
Feed coal	H1-C (bulk coal for H1-1 and H1-2 boilers)		Not sampled
	H1-1-C (pulverized coal)	H1-2-C (pulverized coal)	H1-3-C (pulverized coal)
Bottom ash	H1-1-B	H1-2-B	H1-3-B
Fly ash	H1-1-F-1 (hopper 1)	H1-2-F[a]	H1-3-F[a]
	H1-1-F-2 (hopper 2)		
	H1-1-F-3 (hopper 3)		
	H1-1-F-4 (hopper 4)		
Gypsum	No WFGD	No WFGD	H1-3-G
HPP-2 (boilers 1 and 2 are of subcritical units, and 3 of supercritical unit)			
Samples	Boiler 1 (H2-1, 600 MW)	Boiler 2 (H2-2, 600 MW)	Boiler 3 (H2-2, 600 MW)
Feed coal	H2-C (bulk coal for all boilers)		
Bottom ash	H2-1-B	H2-2-B	H2-3-B
Fly ash	H2-1-F[b]	H2-2-F[b]	H2-3-F[b]
	H2-1-F-G[c]	H2-2-F-G[c]	H2-3-F-G[c]
Gypsum	No WFGD	H2-2-G	H2-3-G

[a] Composite fly ash from four ESP hoppers.
[b] Fly ash from hopper A.
[c] Fly ash from hopper B.

were stored in two amber glass bottles (each containing ~500 g) and then were sub-sampled for subsequent analysis.

2.2. Hg preconcentration

Hg concentrations in solid samples of coal, fly ash, bottom ash and gypsum were analyzed using a direct combustion mercury analyzer (DMA-80, Table S1 of Supporting information). For isotopic analyses, Hg in samples was extracted and preconcentrated by two techniques: acid digestion and combustion-trapping methods. In the first method, between 20 and 200 mg of powdered sample was digested by acid mixtures in 15 mL pre-cleaned Teflon beakers at 120 °C. In the second method, two off-line programmable tube furnaces were used to thermally release and trap the Hg in an oxidizing solution (see the Supporting information). Procedural blanks and standards were periodically processed with the samples.

2.3. Hg isotopic analysis

Isotopic compositions of the sample solutions were determined by cold vapor multi-collector inductively coupled plasma mass spectrometry (CV-MC-ICPMS) (see the Supporting information). Mass bias of MC-ICPMS was corrected by internal NIST 997 Tl standard using the exponential law and by NIST 3133 Hg standard-sample bracketing methods. The Hg isotopic composition is reported in delta notation (δ) in units of per mil (‰) referenced to the bracketed NIST 3133 Hg standard (Blum and Bergquist, 2007), which is expressed as:

$$\delta^{XXX}\mathrm{Hg}\ (‰) \quad \left(\left({}^{XXX}\mathrm{Hg}/{}^{198}\mathrm{Hg}\right)_{\mathrm{Sample}}/\left({}^{XXX}\mathrm{Hg}/{}^{198}\mathrm{Hg}\right)_{\mathrm{NIST\ 3133}}-1\right)\times 1000 \quad (1)$$

where *XXX* is Hg isotope mass between 199 and 204, $({}^{XXX}\mathrm{Hg}/{}^{198}\mathrm{Hg})_{\mathrm{sample}}$ is the measured isotope ratio of the sample, and $({}^{XXX}\mathrm{Hg}/{}^{198}\mathrm{Hg})_{\mathrm{NIST\ 3133}}$ is the average isotope ratio of the bracketing Hg standard solutions measured before and after each sample. MIF values are indicated by "capital delta (Δ)" notation (‰), which is the difference between the measured values of δ^{199}Hg, δ^{200}Hg, δ^{201}Hg and those predicted from δ^{202}Hg using the kinetic MDF law (Blum and Bergquist, 2007):

$$\Delta^{199}\mathrm{Hg} = \delta^{199}\mathrm{Hg} - 0.252\times\delta^{202}\mathrm{Hg} \quad (2)$$

$$\Delta^{200}\mathrm{Hg} = \delta^{200}\mathrm{Hg} - 0.502\times\delta^{202}\mathrm{Hg} \quad (3)$$

$$\Delta^{201}\mathrm{Hg} = \delta^{201}\mathrm{Hg} - 0.752\times\delta^{202}\mathrm{Hg}. \quad (4)$$

2.4. Recovery and uncertainty

The recoveries for most of the samples processed by the combustion-trapping method were in the range of 80–110%, with the exception of two bottom ash samples (>70%, Tables S1 and S2). However, only one third of the samples extracted by acid digestion satisfied >80% recoveries (not included in Table S1). As such, we cannot recommend digestion methods for coal and coal fly ash type of samples. For those samples with >80% extraction efficiency, we obtained an excellent agreement in isotopic compositions between the acid digestion and combustion-trapping methods. Hg concentrations of procedural blanks, determined by CV atomic fluorescence spectroscopy, were<0.03 μg/L (0.029 ± 0.01 μg/L, 1 SD, n=7) which is negligible (<5%) compared to the concentrations of trapped solutions and standards (0.7–1.5 μg/L for combustion-trapping samples and 1.7–6.9 μg/L for acid digestion samples).

Typical internal precision of Hg isotope ratio (e.g. $^{202}\mathrm{Hg}/^{198}\mathrm{Hg}$) measurement was below 0.03‰ (1 SE) for individual sample analysis. The long-term external uncertainty of the method was determined by repeated analyses of the UM-Almaden standard during different analysis sessions in 2011 and 2012. The average value for Nu plasma HR was −0.57 ± 0.14‰ (2 SD, n=111) for δ^{202}Hg and −0.03 ± 0.09‰ (2 SD, n=111) for Δ^{199}Hg, and for Neptune was −0.53 ± 0.14‰ (2 SD, n=33) for δ^{202}Hg and −0.02 ± 0.05‰ (2 SD, n=33) for Δ^{199}Hg, in agreement with published values (Blum and Bergquist, 2007; Estrade et al., 2010) (Table S2). The measured δ^{202}Hg and Δ^{199}Hg of fly ash standard BCR 176R were −1.02 ± 0.09‰ (2 SD, n=2) and −0.08 ± 0.07‰ (2 SD, n=2), consistent with data reported by Estrade et al. (2010). The measured δ^{202}Hg and Δ^{199}Hg values of coal standard NIST 1632d were similar to its predecessor NIST 1632c as analyzed by others (Lefticariu et al., 2011; Sherman et al., 2012) (Table S2). We also analyzed NIST 2685b to facilitate future intercomparisons (Table S2). The uncertainty of the isotopic compositions of the procedural standards NIST 1632d (e.g. δ^{202}Hg uncertainty = 0.14‰) was taken as the maximum analytic uncertainty of sample isotopic compositions. If uncertainty of the isotopic compositions associated with sample replicates was higher than this uncertainty, the uncertainty associated with sample replicates applied.

3. Results and discussion

3.1. Hg concentrations

Hg concentrations (320–389 ng/g) in the bituminous feed coals are homogeneous in both power plants and higher than those of average Chinese coals (163 ng/g) (Dai et al., 2012) and average world hard coals (100 ng/g) (Ketris and Yudovich, 2009). Bottom ashes (5–36 ng/g, except H1-2-B with 191 ng/g) are depleted in Hg relative to feed coal. Hg concentrations in fly ash collected at ESP hoppers are variable and range from 34 to 704 ng/g. A significant correlation (r^2 = 0.35, p<0.05, n=12) of Hg concentration and unburned carbon content (approximated by loss on ignition, LOI, Table S1) was observed for fly ash samples. Despite its low concentration in fly ash (0.3 to 2.6%, Table S1), unburned carbon has a 100-fold higher surface area than the silicate fraction in fly ash, and is thought to dominate Hg capture from flue gas. It is well documented that Hg capture by unburned carbon in fly ash increases with the increase of carbon content, the decrease of fly ash particle size and the decrease of flue gas temperature (Hower et al., 2010). In the CFUBs we studied, temperature slightly decreased from the inlet (160–200 °C) to the outlet of ESPs (100–120 °C) accompanied by a parallel decrease in particle size of fly ash (not quantified, but macroscopically visible across consecutive hoppers). There is however, neither clear relationship between Hg concentrations in fly ash and particle size or temperature (Fig. 1), nor between normalized Hg/LOI and particle size.

The operating conditions of the boilers possibly contribute to the large variation of Hg concentrations in fly ash. Fly ash Hg concentrations for the modern 600 MW subcritical boilers built in the year around 2000 (H1-3, H2-1 and H2-2) are in a range of 263–704 ng/g. This is significantly higher than the older 300 MW subcritical boilers built in the year 1982 (H1-1 and H1-2) with 197–285 ng/g Hg and the modern 2007 built 600 MW supercritical boiler (H2-3) with 34–127 ng/g Hg. The supercritical boiler of higher thermal efficiency is operated at a higher temperature. This typically results in a more complete combustion of feed coal reflected in the lower content of unburned carbon in fly ash (0.3–0.8%, Table S1).

WFGD is proven to have an excellent co-benefit of Hg abatement (mainly GOM) besides desulphurization of flue gas through production of gypsum (>90% purity with small amount of limestone, inorganic salts and fly ash in this study) in reactions of limestone slurry and SO_2 in flue gas (Álvarez-Ayuso et al., 2006; Wang et al., 2010). GOM species (e.g. $HgCl_2$ and HgO) are readily soluble in the slurry of limestone and then are incorporated into the gypsum (Yudovich and Ketris, 2005). Compared to feed coal, bottom ash and fly ash, Hg concentrations in gypsum are the highest (1500–4600 ng/g).

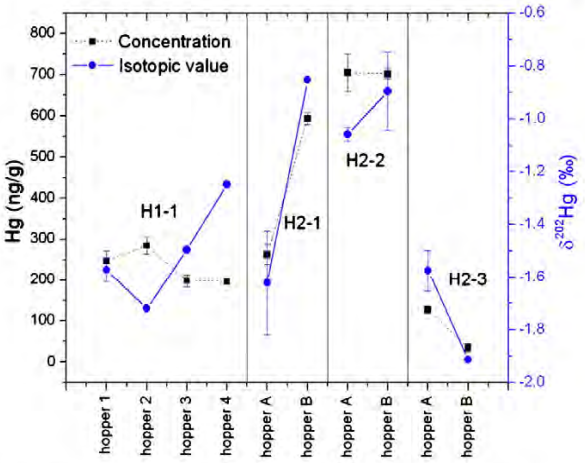

Fig. 1. The variation in Hg concentrations and δ^{202}Hg values for fly ash of different particle size and ambient temperature. The temperature and particle size decreased from hoppers 1 to 4 in boiler H1-1 and from hoppers A to B in boilers H2-1, H2-2 and H2-3. In three out of four ESPs, δ^{202}Hg increases in successive hoppers with lower temperature and smaller particle size (except supercritical boiler H2-3).

3.2. Hg mass balance

The calculation of a Hg mass balance in the CFUBs is necessary to estimate Hg emission factors, APCD Hg removal efficiencies and assist the interpretation of Hg isotopic variations (see the Supporting information). The estimated Hg emissions at the stack are 37 ± 3 g/h (2 SD), 37 ± 3 g/h (2 SD), 42 ± 7 g/h (2 SD), 78 ± 23 g/h (2 SD), 52 ± 20 g/h (2 SD), 72 ± 21 g/h (2 SD) for boilers H1-1, H1-2, H1-3, H2-1, H2-2 and H2-3, respectively (Table 2).

The mass fractions of Hg retained in bottom ash are <2%, and thus >98% of Hg originally present in the feed coal was released downstream of the boilers with flue gas (Table 2). The fractions of Hg in fly ash removed by ESPs vary from 5 to 42%, and the fly ash Hg fractions are larger for the modern subcritical boilers with higher 600 MW capacities (average values of 37 ± 9% vs. 21 ± 6% for 600 MW vs. 300 MW, 2 SD, $p<0.05$). The Hg fraction removed with fly ash for the single 600 MW supercritical boiler (H2-3) is the lowest (<5%). This is coherent with the low unburned carbon levels and low fly ash Hg concentration of the H2-3 supercritical boiler, as discussed in Section 3.1. The Hg fraction removed by WFGD for subcritical boilers (H1-3 and H2-2) is 9 and 14%. There is an apparent improvement of Hg removal by WFGD for the supercritical boiler (H2-3, 26%). Again, this is coherent with the low fly ash Hg concentration for the H2-3 supercritical boiler. We suggest that in H2-3 the impeded scavenging of GOM on fly ash due to the low unburned carbon fraction in fly ash results in a relatively larger GOM fraction that is subsequently scavenged by WFGD.

We did not perform Hg speciation measurements in flue gas in this study. Nevertheless approximations can be made based on the fact that coal Cl content and the GEM fraction at the ESP inlet have been shown to be broadly correlated (Senior and Johnson, 2005; Wang et al., 2010). Accordingly, the Huainan bituminous coal with an average Cl content of 180 μg/g (Sun et al., 2010a) may be expected to generate a GEM fraction at the ESP inlet of approximately 65 ± 20% for the subcritical boilers studied. The remaining 35 ± 20% consists of oxidized Hg species in the gas (GOM) and fly ash (PBM) phases. This is roughly consistent with the 19–51% removal of oxidized Hg species by ESP and WFGD (Table 2), yet does not permit an estimation of residual GOM after WFGD.

Overall, a major fraction of Hg in the feed coal, in a range of 75–80% for ESP only and 49–69% for ESP + WFGD, was emitted through the stack into the atmosphere (Table 2). These Hg emission fractions can be compared to the most recent Chinese CFUB Hg emission model (Zhang et al., 2012). The model shows P50 probability levels of emitted Hg fractions of 74% for ESP only and 35% for ESP + WFGD equipped CFUBs, suggesting that the Huainan CFUBs in this study have typical ESP performance and below average WFGD performance. The latter may be related to the low S contents of Huainan coal (Sun et al., 2010a,b) and the subsequent low gypsum production and associated Hg scavenging by WFGD.

3.3. Hg isotope signatures

Hg isotopic compositions (δ^{199}Hg to δ^{204}Hg and Δ^{199}Hg to Δ^{201}Hg) for all the samples are given in Table S1. The magnitude of MIF for most of the samples is insignificant compared to the uncertainty of the method (Fig. 2). This indicates that no significant MIF processes occurred during coal formation and the original absence of a MIF signature in the feed coal was conserved in the combustion residues. In the following, only δ^{202}Hg values are discussed to represent MDF. A large variation of δ^{202}Hg values, up to 2‰, is observed between feed coal and combustion residues (Fig. 2). An ANOVA analysis indicates that the δ^{202}Hg values of the feed coals, bottom ash and fly ash are isotopically distinguishable from each other ($p<0.02$).

Table 2
Summary of the stack Hg emission rate (g/h), % fractions of Hg in bottom ash, fly ash, gypsum and stack emissions, the measured δ^{202}Hg (‰) of feed coal, and the calculated δ^{202}Hg (‰) values of stack emissions. 2 SD uncertainties are calculated by propagating the 2 SD uncertainties of Hg concentrations and δ^{202}Hg values in feed coal and combustion residues.

Boiler		H1-1	H1-2	H1-3	H2-1	H2-2	H2-3	Average	2 SD
	Capacity	300 MW	300 MW	600 MW	600 MW	600 MW	600 MW		
	APCDs	ESP	ESP	ESP + WFGD	ESP	ESP + WFGD	ESP + WFGD		
Hg emission rate	Average	37	37	42	78	52	72	53	36
	2 SD	3	3	7	23	20	21		
f_{BA} (bottom ash)	Average	0.31	1.63	0.19	0.06	0.11	0.03	0.39	1.13
	2 SD	0.05	0.22	0.01	0.04	0.03	0.01		
f_{ESP} (fly ash)	Average	19	20	32	25	42	5	24	23
	2 SD	3	4	5	11	8	3		
f_{WFGD} (gypsum)	Average			14		8.9	26	16	15
	2 SD			6		1.7	5		
f_{SE} (stack emission)	Average	80	79	54	75	49	69	68	24
	2 SD	8	8	9	26	22	24		
$\delta^{202}Hg_{FC}$ (feed coal)	Average	−0.43			−0.61			−0.52	0.09
	2 SD	0.34			0.12				
$\delta^{202}Hg_{SE}$ (stack emission)	Average	−0.17	−0.15	−0.14	−0.39	−0.31	−0.39	−0.26	0.22
	2 SD	0.42	0.43	0.63	0.21	0.25	0.17		
$\delta^{202}Hg_{SE} - \delta^{202}Hg_{FC}$	Average	0.26	0.28	0.29	0.21	0.29	0.22	0.26	0.06
	2 SD	0.54	0.55	0.72	0.24	0.28	0.21		

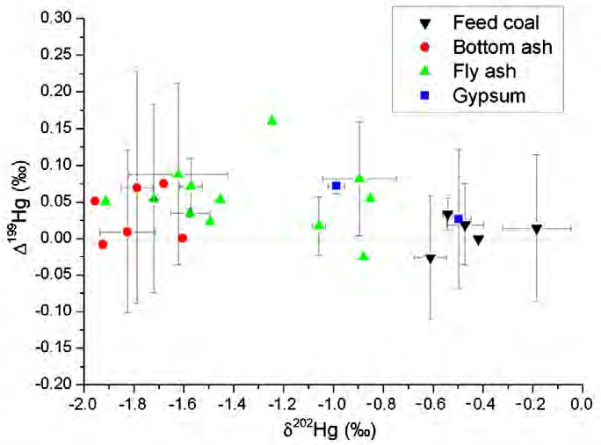

Fig. 2. MDF (δ^{202}Hg) vs. MIF (Δ^{199}Hg) diagram for all feed coals, bottom ash, fly ash, and gypsum samples. Combustion, transport, transformation and removal of Hg by ACPDs induce insignificant MIF.

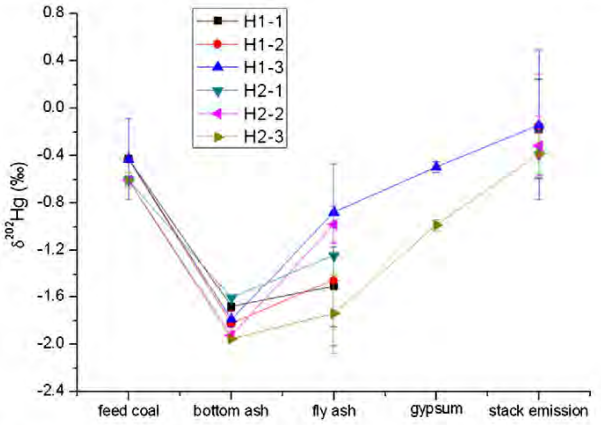

Fig. 3. The measured δ^{202}Hg values for feed coals and combustion residues, and calculated δ^{202}Hg values for stack emissions. The value of feed coal for HPP-1 is averaged from four feed coal samples (H1-C, H1-1-C, H1-2-C and H1-3-C) and the value for fly ash in each ESP is averaged from all the collected hoppers. Mass balance considerations imply that calculated stack emissions δ^{202}Hg are enriched by 0.26‰ in the heavier isotopes relative to feed coal.

3.3.1. Feed coal

The δ^{202}Hg values in feed coals range from -0.67 ± 0.14 to -0.18 ± 0.14‰ (2 SD), with an average value of -0.47 ± 0.17‰ (1 SD, n = 5), and overlap with those reported by Biswas et al. (2008) for the same coalfield (-0.89 to -0.28‰). Insignificant to small positive MIF (0.02 to 0.10‰ for Δ^{199}Hg and 0.04 to 0.15‰ for Δ^{201}Hg) for Huainan coals were also reported in that study, which is comparable to our observation (-0.09 ± 0.04 to 0.06 ± 0.04‰ for Δ^{199}Hg and -0.02 ± 0.09 to 0.06 ± 0.09‰ for Δ^{201}Hg, 2 SD). The δ^{202}Hg values of feed coals for HPP-1 and HPP-2 were not statistically different from those of the same areas also reported by Biswas et al. (2008) (-0.43 ± 0.17‰ vs. -0.43 ± 0.21‰ for Xinji coal mine; -0.61 ± 0.06‰ vs. -0.43 ± 0.09‰ for Panji coal mine, 1 SD). Minor but significant variation was observed between bulk feed coal (H1-C with δ^{202}Hg of -0.18 ± 0.14‰, 2 SD) and pulverized feed coals (H1-1-C with δ^{202}Hg of -0.47 ± 0.14‰, H1-2-C with δ^{202}Hg of -0.42 ± 0.14‰, 2 SD) at HPP-1. Sulfide minerals in coal, such as pyrite, are enriched in heavier Hg isotopes compared to the organic bound Hg fraction in coal (Lefticariu et al., 2011). It has therefore been suggested that sulfide removal during coal crushing at the pulverizer could cause the pulverized coal to be depleted in the heavier Hg isotopes (Sherman et al., 2012). However, due to the low sulfur content in Huainan feed coal, no physical or chemical sulfide removal was in place at both studied power plants at the time of sampling. Therefore, we attribute the observed variation of δ^{202}Hg values to limited heterogeneity of the feed coal.

3.3.2. Combustion residues

The main physicochemical processes acting during the combustion assembly can be divided into four stages: 1) thermal reduction of matrix Hg in feed coal and vaporization of generated GEM in the boiler at 1200–1500 °C; 2) partial oxidation of GEM below 600 °C into GOM and PBM compounds, of which PBM is quantitatively removed with fly ash in the ESPs; 3) partial dissolution of residual GOM compounds into the limestone slurry and subsequent incorporation into WFGD products (mainly gypsum) and 4) the emission of remaining gaseous GEM and GOM contained in flue gas into the atmosphere. As Hg in bottom ash represents a negligible mass fraction (<2%) relative to feed coal and Hg speciation in the high temperature section of the boilers is 100% GEM, we will assume here that the newly generated GEM in the boilers inherits the isotopic composition of the feed coal.

3.3.2.1. Bottom ash at the boilers. The most negative δ^{202}Hg values, ranging from -1.96 ± 0.14 to -1.61 ± 0.14‰ (2 SD), were found in the bottom ash (Figs. 2 and 3). The severe depletion of heavy isotopes in bottom ash relative to feed coal is incompatible with the results of non-ferrous metal refining at high temperatures (Sivry et al., 2008; Sonke et al., 2008; Stetson et al., 2009; Gehrke et al., 2011). During Hg ore (cinnabar) refining process, the resulted smelting residuals (calcine) were consistently enriched in the heavier isotopes, by >3‰ for δ^{202}Hg, relative to the feed ores (Stetson et al., 2009). Although no investigations have been conducted on the Hg fractionation during coal combustion in CFUBs, an analogous study on the moderately volatile element Zn showed that the bottom ash (0.31‰ for δ^{66}Zn) was also slightly enriched in heavier isotopes relative to the feed coal (0.24‰ for δ^{66}Zn) (Borrok et al., 2010). The prominent differences between Hg ore refining in a smelter and coal combustion in a boiler are the magnitude of Hg concentration in feed ore and coal and the operating temperatures. The relatively lower temperatures in smelters (600–700 °C) always leave substantial non-vaporized Hg in the calcines (often retaining preferentially the heavier Hg isotopes relative to the feed ore) (Rytuba, 2003; Stetson et al., 2009; Gehrke et al., 2011), whereas the higher temperatures in CFUBs (1200–1500 °C) volatilize all Hg contained in the feed coal (Yudovich and Ketris, 2005). The bottom ash samples were collected after the ash was quenched with water and air dried as part of the industrial process. We therefore suspect that the relatively high Hg levels in bottom ash are due to contamination.

Hg concentration in bottom ash sample H1-2-B (191 ng/g) is approximately one order of magnitude higher than other bottom ash samples (5–36 ng/g). Its isotopic composition (-1.83 ± 0.14‰ for δ^{202}Hg, 2 SD) however cannot be distinguished from other bottom ash samples (-1.96 ± 0.14 to -1.61 ± 0.14‰ for δ^{202}Hg, 2 SD). This suggests that the high Hg level in sample H1-2-B is not derived from feed coal Hg, which has higher δ^{202}Hg, but has been scavenged outside of the boiler environment. Upon collection, a large portion of unburned carbon was surrounded by mineral aggregates in bottom ash of H1-2-B. Loss on ignition of H1-2-B (18%) is significantly higher than other bottom ash samples (4–10%) (Table S1). Unburned carbon is known to enhance adsorption of Hg from flue gas and therefore potentially explains the high Hg level in bottom ash of H1-2-B (Carpi, 1997; Yudovich and Ketris, 2005).

3.3.2.2. Fly ash in ESPs. Fly ash shows a wide range in δ^{202}Hg from -1.91 ± 0.14 to -0.85 ± 0.14‰ (2 SD, Figs. 1 and 2). We observe that oxidized Hg species in fly ash PBM are enriched in the lighter Hg isotopes relative to feed coal derived GEM. This result is inconsistent with equilibrium MDF as the underlying isotope fractionation mechanism. Theoretical estimates of equilibrium Hg MDF during gas phase oxidation reactions indicate an enrichment of the heavier isotopes in the oxidized phases, i.e. $HgCl_2$, $HgBr_2$ (Schauble, 2007). The light isotope enrichment of PBM therefore supports the notion of kinetic MDF as the dominant isotope fractionation mechanism. Regardless of the exact oxidation and scavenging mechanisms, both homogeneous and heterogeneous Hg oxidation are susceptible to kinetic isotope fractionation due to the faster reaction rates of the lighter Hg isotopes. For example, faster diffusion of light Hg isotopes towards gaseous oxidants, or faster diffusion of product GOM towards unburned carbon surfaces of fly ash could result in negative δ^{202}Hg observed in fly ash. Without Hg isotope observations on the different gaseous Hg species we cannot identify which kind of transformation dictated the MDF.

The small positive MIF values observed in the three fly ash samples (H1-F-3, H1-F-4 and H2-1-F, Table S1) are comparable to those in coals reported by Biswas et al. (2008), which suggests that they were possibly inherited from the feed coals.

3.3.2.3. Gypsum in WFGD. Hg species incorporated into the gypsum are thought to be predominantly residual GOM forms that were not scavenged as PBM in the ESP section (Wang et al., 2009; Hower et al., 2010). The Hg that entered the WFGD section via limestone slurry (limestone and processing water) was <0.02 g/h, while the Hg that was scavenged by gypsum was 9–28 g/h and the Hg enriched in WFGD waste water was 0.03–0.45 g/h. The added Hg from limestone slurry was therefore negligible and the isotopic values associated with gypsum can be used to represent that of the WFGD Hg capture process. Gypsum samples from boilers H1-3 and H2-3 have higher δ^{202}Hg values than the respective fly ash samples from the same boilers (Fig. 3). There is no difference in δ^{202}Hg values between feed coal (-0.43 ± 0.34‰, 2 SD) and gypsum (-0.50 ± 0.14‰, 2 SD) for H1-3 boiler in HPP-1. Gypsum in the H2-3 boiler of HPP-2 (-0.99 ± 0.14‰, 2 SD) is slightly depleted in the heavier Hg isotopes compared to feed coal (-0.61 ± 0.14‰, 2 SD).

3.3.3. Stack emission

All collected combustion residues show a consistent enrichment in the lighter Hg isotopes relative to the feed coals (Fig. 3). Therefore, the residual gaseous Hg compounds emitted with flue gas (stack emission) should to a first approximation be enriched in the heavier Hg isotopes. A Hg isotopic mass balance equation can be formulated to estimate the magnitude of δ^{202}Hg in stack emissions ($\delta^{202}Hg_{SE}$):

$$f_{SE}\times\delta^{202}Hg_{SE}=f_{FC}\times\delta^{202}Hg_{FC}-f_{BA}\times\delta^{202}Hg_{BA}-f_{ESP}\times\delta^{202}Hg_{ESP}-f_{WFGD}\times\delta^{202}Hg_{WFGD} \quad (5)$$

where 'f' are the mass fractions of stack emissions (SE), feed coal (FC), bottom ash (BA), fly ash (ESP) and gypsum (WFGD), respectively (Table 2). Under ideal conditions, the sum of these fractions is 100%, equaling the Hg input from feed coal (f_{FC}):

$$f_{FC}=1=f_{SE}+f_{BA}+f_{ESP}+f_{WFGD}. \quad (6)$$

As discussed above, the Hg fraction in bottom ash is consistently <2% and possibly was contaminated by cooling water and ambient Hg. It will therefore be neglected in the isotopic mass balance. By combining Eq. (5) and Eq. (6), the δ^{202}Hg of stack emission can be expressed as:

$$\delta^{202}Hg_{SE}=\frac{\delta^{202}Hg_{FC}-f_{ESP}\times\delta^{202}Hg_{ESP}-f_{WFGD}\times\delta^{202}Hg_{WFGD}}{1-f_{ESP}-f_{WFGD}}. \quad (7)$$

For boilers that only have ESPs, the δ^{202}Hg of stack emission is:

$$\delta^{202}Hg_{SE}=\frac{\delta^{202}Hg_{FC}-f_{ESP}\times\delta^{202}Hg_{ESP}}{1-f_{ESP}}. \quad (8)$$

The resulting $\delta^{202}Hg_{SE}$ are summarized in Table 2 for all six boilers and range from -0.39 to -0.14‰ (Fig. 3). Considering the propagated uncertainties on $\delta^{202}Hg_{SE}$ (2 SD = 0.17–0.63‰), the isotope signatures of stack emissions are not significantly different from feed coal at the individual boilers. Nevertheless, averaging the relative differences between $\delta^{202}Hg_{SE}$ and $\delta^{202}Hg_{FC}$ over all six boilers suggests that bulk stack emissions of the Huainan CFUBs are on average enriched by 0.26 ± 0.06‰ (2 SD) (Table 2). In the next section, we will explore if we can predictively model Hg isotope fractionation in the CFUBs.

3.3.4. Flue gas Hg speciation and isotope fractionation

The MDF signatures, δ^{202}Hg (normalized to feed coal), of the oxidized forms of Hg in fly ash and gypsum are significantly correlated to the total amount of Hg removed by ESP and WFGD ($r^2=0.86$, Fig. 4). Considering the differences in boiler type, the correlation is quite remarkable, and can be empirically parameterized for the purpose of predicting Hg isotope fractionation in CFUBs:

$$\delta^{202}Hg_{ESP+WFGD}=\delta^{202}Hg_{FC}+2.37\times f_{ESP+WFGD}-1.35. \quad (9)$$

Based on mass balance, we can then also express $\delta^{202}Hg_{SE}$ at the stack as a function of Hg capture by APCDs:

$$\delta^{202}Hg_{SE}=\frac{\left(\delta^{202}Hg_{FC}-\left(\delta^{202}Hg_{FC}+2.37\times f_{ESP+WFGD}-1.35\right)\times f_{ESP+WFGD}\right)}{1-f_{ESP+WFGD}}=\delta^{202}Hg_{FC}+\frac{2.37\times f_{ESP+WFGD}{}^2-1.35\times f_{ESP+WFGD}}{f_{ESP+WFGD}-1}. \quad (10)$$

Note that Eqs. (9) and (10) are only valid over the Hg removal interval for which we have observations, i.e. $f_{ESP+WFGD}$ between 5 and 46%. The parameterization could represent, for example, the sequential

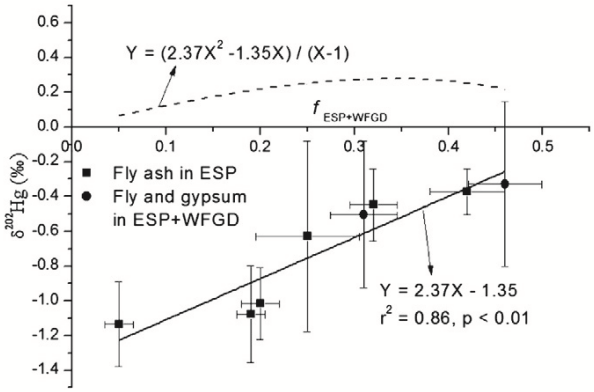

Fig. 4. δ^{202}Hg values of the oxidized Hg species (filled squares for fly ash; filled circles for weighted average of fly ash and gypsum) as a function of the amount of Hg removed by APCDs. The significant correlation ($r^2=0.86$) can be interpreted as the successive removal of light isotope enriched PBM in the ESPs and the less light isotope enriched GOM in the FGD sections. Empirical δ^{202}Hg curve of stack emission (i.e. $Y=(2.37X^2-1.35X)/(X-1)$, derived from Eq. (10), dash line) is also plotted. All the δ^{202}Hg values are normalized to the feed coal $\delta^{202}Hg_{FC}$.

removal of two oxidized Hg fractions that are progressively less enriched in the lighter Hg isotopes. This is confirmed for PBM removed with fly ash being more enriched in the lighter isotopes than GOM removed with gypsum at a later stage. In the following we will discuss whether a more mechanistic interpretation, based on the determination of ESP and WFGD isotope fractionation factors, is possible.

By looking at the CFUB as a flow through reaction cell, where elemental Hg is continuously oxidized and removed from the system in fly ash and gypsum, one can recognize the typical properties of an open Rayleigh-type isotope fractionation system. Several observations support this notion, such as the progressively less light isotope enriched fly ash and gypsum products as more Hg is removed from the flue gas (Fig. 4). In addition, three subcritical boilers show that as temperature and fly ash particle size decrease from ESP hoppers 1 to 4 or A to B, the δ^{202}Hg values of fly ash increase. Only the supercritical boiler H2-3 is an exception to this trend (Fig. 1). We have therefore tested the potential of a single Rayleigh fit to approximate a mass dependent fractionation factor between PBM and flue gas, α_{ESP}, for all six boilers. Fig. 5 shows the corresponding Rayleigh diagram for α_{ESP} (0.9992 ± 0.0002, 2 SE). It appears that the intra-boiler variations in δ^{202}Hg for different fly ash removal fractions exceed the limits of a single Rayleigh fit for α_{ESP}. This result suggests an anticipated but complex dependence of α_{ESP} on the flue gas composition, boiler physics, and boiler operating conditions. Due to a lack of fly ash mass flux data for individual hoppers we cannot explore in further detail the relationship between δ^{202}Hg of fly ash in consecutive hoppers (Fig. 1) and fractionation factors. Based on the unrealistic simple Rayleigh fit (Fig. 5), and despite of the open system nature of a CFUB, we do not have sufficient evidence for Rayleigh-type Hg isotope fractionation. While we could fit an individual α_{ESP}, and where applicable an α_{WFGD} for each boiler, the predictive power of such isotope fractionation factors would be unconstrained. In fact, looking closely at the evolution of fly ash δ^{202}Hg from one hopper to the next (Fig. 1) and along the intra-boiler fly ash δ^{202}Hg trend (Fig. 5) it is clear that fly ash δ^{202}Hg evolves too fast to be captured by a single process Rayleigh model.

One of the difficulties with a mechanistic interpretation for the Hg isotope observations is the fact that the physicochemical mechanisms of Hg speciation changes in CFUBs are a topic of debate. Homogeneous gas phase reactions have conventionally been used to explain GEM oxidation in flue gas (Sliger et al., 2000; Niksa et al., 2001). Recent reviews however suggest an important role for both heterogeneous chemistry, involving reactants in both the gas and solid phases, and a kinetic control on Hg transformations (Schofield, 2008; Hower et al., 2010). Our observation that fly ash and gypsum are enriched in the lighter Hg isotopes supports such non-equilibrium conditions. Homogeneous and heterogeneous non-equilibrium Hg oxidation pathways and associated scavenging onto fly ash can be depicted as follows:

Homogeneous : GEM→GOM→PBM

Heterogeneous : GEM→PBM→GOM.

Under non-equilibrium conditions, each of the transformations indicated by the arrows likely enriches the reaction product in the lighter Hg isotopes, leaving behind a reactant that becomes gradually enriched in the heavier Hg isotopes. Yet we know neither which of these four simplified reaction steps dominates our observations, nor how boiler and ESP design or temperature gradient influences isotope fractionation. To our knowledge, there is no information on whether the reactions continue at lower temperatures through the ESP and WFGD units. It appears however that only the homogeneous pathway can generate progressively lighter isotope enrichment of GOM and then PBM.

In summary, despite the observation of a clear trend between Hg removal by APCDs and δ^{202}Hg (Fig. 4), we do not have sufficient data to constrain a mechanistic Rayleigh model for Hg isotope fractionation in CFUBs. More observations are needed, in particular for CFUBs with >50% Hg removal by APCDs. Ideally, Hg isotope analysis on stack emissions should confirm the suggested overall enrichment in the heavier Hg isotopes and can help discern between Rayleigh-type isotope fractionation and the current ESP vs. WFGD source removal parameterization (Eqs. (9) and (10)). The difference between the two scenarios is important, because the Rayleigh model predicts a substantial increase in $\delta^{202}Hg_{SE}$ of more than 0.5‰ for >50% Hg removal (Fig. 5), while the empirical parameterization suggests a maximum increase in $\delta^{202}Hg_{SE}$ of only 0.3‰ at 30% Hg removal (Fig. 4).

3.4. Implications

For the purpose of coupling coal Hg isotope signatures to coal Hg emission inventories, Eq. (10) can be used to estimate $\delta^{202}Hg_{SE}$ of bulk stack Hg emissions. Published average ESP and ESP + WFGD Hg removal efficiencies for bituminous coal are 36% and 74% in the USA and 26% and 53% in China (USEPA, 2002; Zhang et al., 2012). CFUBs equipped with ESP only in the USA and China would therefore generate stack emissions that are approximately 0.3‰ enriched in δ^{202}Hg relative to feed coals (Fig. 4). Average CFUBs with both ESP and WFGD have Hg removal efficiencies that slightly exceed the predictive range of Eqs. (9) and (10). Most likely bulk stack emission $\delta^{202}Hg_{SE}$ would approach an insignificant shift relative to feed coal $\delta^{202}Hg_{FC}$. For comparison, a Rayleigh-type isotope fractionation model would have predicted $\delta^{202}Hg_{SE}$ up to +0.8‰ relative to feed coal (Fig. 5).

We did not make direct isotopic observations on the two main stack emission components, GEM and GOM. However, we can assume that the $\delta^{202}Hg_{WFGD}$ of GOM removed by WFGD is representative of the $\delta^{202}Hg_{GOM}$ that is emitted through the stack. This would suggest that $\delta^{202}Hg_{GOM}$ is enriched in the lighter isotopes by −0.36 to −0.60‰ relative to bulk stack $\delta^{202}Hg_{SE}$. This implies that $\delta^{202}Hg_{GEM}$ of GEM that makes up the other bulk stack Hg emission component may be enriched in the heavier Hg isotopes.

As mentioned in the introduction, a study by Sherman et al. (2012) on the Hg isotopic compositions of precipitations adjacent to a large CFUB in Crystal River, Florida (USA) showed substantial difference of δ^{202}Hg and Δ^{199}Hg between feed coal and precipitation Hg. On average, precipitation δ^{202}Hg was shifted by −1.8‰ and Δ^{199}Hg by +0.6‰ compared to feed coal. The authors suggested that, similar

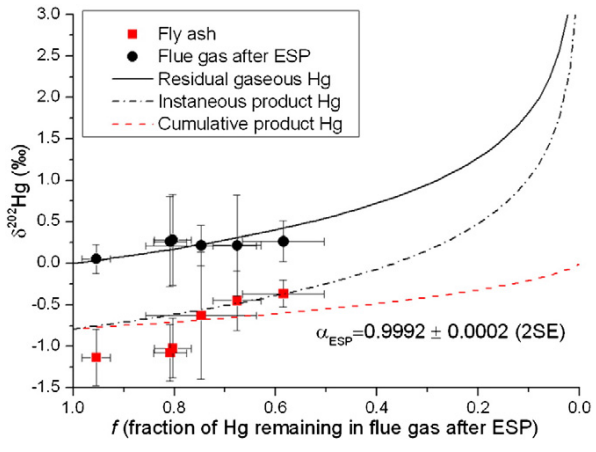

Fig. 5. Rayleigh model and fit for Hg MDF in the ESP section. The initial δ^{202}Hg values of feed coals are normalized to 0‰. The Hg MDF fractionation factor between flue gas and fly ash (α_{ESP}) is 0.9992 ± 0.0002 (2 SE) by fitting the δ^{202}Hg value of fly ash (normalized to feed coal, filled squares), using the Rayleigh equation for cumulative product Hg (dash line). The corresponding δ^{202}Hg values of flue gas after ESPs (filled circles) calculated by Hg isotopic mass balance are plotted against the predicted residual flue gas Hg (solid line).

to observations for oxidative Hg scavenging in a volcanic plume (Zambardi et al., 2009), equilibrium MDF during GEM oxidation inside the CFUB could enrich PBM removed by ESPs in the heavy Hg isotopes and enrich residual flue gas in the light Hg isotopes. Subsequent scavenging of light isotopes enriched CFUB Hg emissions by aqueous droplets might then explain the majority of the δ^{202}Hg shift observed between feed coal and precipitation Hg. Our findings indicate that the sign of fractionation inside CFUBs is opposite of this and renders total stack emissions slightly heavier in Hg isotopes than feed coal. As the Crystal River CFUB is equipped with ESPs only, we expect stack emissions to be shifted towards heavier δ^{202}Hg by about 0.3‰. However, our estimate for heavy isotopes enriched in bulk Hg stack emissions does not inform on the isotopic compositions of the individual GEM, GOM, and PBM fractions that may represent approximately 26, 68, and 6% (Sherman et al., 2012). For an average feed coal $\delta^{202}Hg_{FC}$ of −0.7‰, bulk stack emissions at the Crystal River CFUB could be ~ −0.4‰. Following the above outlined arguments, GOM at the stack could then have $\delta^{202}Hg_{GOM}$ as low as −0.8 to −1.0‰. In analogy to our observations on fly ash, the 6% fly ash emitted by the Crystal river stack could have $\delta^{202}Hg_{fly\text{-}ash}$ as low as −1.2 to −1.8‰. These potential $\delta^{202}Hg_{GOM}$ and $\delta^{202}Hg_{fly\text{-}ash}$ values are in the range of observed Hg δ^{202}Hg values in precipitation downwind of the Crystal River CFUB. Additional in-plume and in-cloud Hg isotope fractionation is still needed to explain Crystal River precipitation MIF observations.

Acknowledgment

This work is supported by research grants ANR-09-JCJC-0035-01 from the French Agence Nationale de Recherche and ERC-2010-StG_20091028 from the European Research Council to JES. Ruoyu Sun acknowledges his PhD scholarship from the Chinese Scholarship Council. Two anonymous reviewers and the Editor are thanked for their constructive comments that significantly improved the quality of this contribution.

Appendix A. Supplementary data

Supplementary data to this article can be found online at http://dx.doi.org/10.1016/j.chemgeo.2012.10.055.

References

Álvarez-Ayuso, E., Querol, X., Tomás, A., 2006. Environmental impact of a coal combustion-desulphurisation plant: abatement capacity of desulphurisation process and environmental characterisation of combustion by-products. Chemosphere 65 (11), 2009–2017.
Bergquist, B.A., Blum, J.D., 2007. Mass-dependent and -independent fractionation of Hg isotopes by photoreduction in aquatic systems. Science 318 (5849), 417–420.
Bergquist, B.A., Blum, J.D., 2009. The odds and evens of mercury isotopes: applications of mass-dependent and mass-independent isotope fractionation. Elements 5 (6), 353–357.
Biswas, A., Blum, J.D., Bergquist, B.A., Keeler, G.J., Xie, Z., 2008. Natural mercury isotope variation in coal deposits and organic soils. Environmental Science & Technology 42 (22), 8303–8309.
Blum, J., Bergquist, B., 2007. Reporting of variations in the natural isotopic composition of mercury. Analytical and Bioanalytical Chemistry 388 (2), 353–359.
Borrok, D.M., Gieré, R., Ren, M., Landa, E.R., 2010. Zinc isotopic composition of particulate matter generated during the combustion of coal and coal + tire-derived fuels. Environmental Science & Technology 44 (23), 9219–9224.
Carpi, A., 1997. Mercury from combustion sources: a review of the chemical species emitted and their transport in the atmosphere. Water, Air, and Soil Pollution 98 (3), 241–254.
Dai, S., et al., 2012. Geochemistry of trace elements in Chinese coals: a review of abundances, genetic types, impacts on human health, and industrial utilization. International Journal of Coal Geology 94, 3–21.
Estrade, N., Carignan, J., Sonke, J.E., Donard, O.F.X., 2010. Measuring Hg isotopes in bio-geo-environmental reference materials. Geostandards and Geoanalytical Research 34 (1), 79–93.
Fitzgerald, W.F., Lamborg, C.H., Hammerschmidt, C.R., 2007. Marine biogeochemical cycling of mercury. Chemical Reviews 107 (2), 641–662.
Foucher, D., Ogrinc, N., Hintelmann, H., 2008. Tracing mercury contamination from the Idrija Mining Region (Slovenia) to the Gulf of Trieste using Hg isotope ratio measurements. Environmental Science & Technology 43 (1), 33–39.
Gehrke, G.E., Blum, J.D., Marvin-DiPasquale, M., 2011. Sources of mercury to San Francisco Bay surface sediment as revealed by mercury stable isotopes. Geochimica et Cosmochimica Acta 75 (3), 691–705.
Hower, J.C., et al., 2010. Mercury capture by native fly ash carbons in coal-fired power plants. Progress in Energy and Combustion Science 36 (4), 510–529.
Ketris, M.P., Yudovich, Y.E., 2009. Estimations of Clarkes for Carbonaceous biolithes: world averages for trace element contents in black shales and coals. International Journal of Coal Geology 78 (2), 135–148.
Kritee, K., Blum, J.D., Johnson, M.W., Bergquist, B.A., Barkay, T., 2007. Mercury stable isotope fractionation during reduction of Hg(II) to Hg(0) by mercury resistant microorganisms. Environmental Science & Technology 41 (6), 1889–1895.
Kritee, K., Blum, J.D., Barkay, T., 2008. Mercury stable isotope fractionation during reduction of Hg(II) by different microbial pathways. Environmental Science & Technology 42 (24), 9171–9177.
Kritee, K., Barkay, T., Blum, J.D., 2009. Mass dependent stable isotope fractionation of mercury during mer mediated microbial degradation of monomethylmercury. Geochimica et Cosmochimica Acta 73 (5), 1285–1296.
Lefticariu, L., Blum, J.D., Gleason, J.D., 2011. Mercury isotopic evidence for multiple mercury sources in coal from the Illinois Basin. Environmental Science & Technology 45 (4), 1724–1729.
Lindberg, S., et al., 2007. A synthesis of progress and uncertainties in attributing the sources of mercury in deposition. AMBIO: A Journal of the Human Environment 36 (1), 19–33.
Mason, R.P., Fitzgerald, W.F., Morel, F.M.M., 1994. The biogeochemical cycling of elemental mercury: anthropogenic influences. Geochimica et Cosmochimica Acta 58 (15), 3191–3198.
Niksa, S., Helble, J.J., Fujiwara, N., 2001. Kinetic modeling of homogeneous mercury oxidation: the importance of NO and H_2O in predicting oxidation in coal-derived systems. Environmental Science & Technology 35 (18), 3701–3706.
Pirrone, N., et al., 2010. Global mercury emissions to the atmosphere from anthropogenic and natural sources. Atmospheric Chemistry and Physics 10 (13), 5951–5964.
Point, D., et al., 2011. Methylmercury photodegradation influenced by sea-ice cover in Arctic marine ecosystems. Nature Geoscience 4 (3), 188–194.
Rytuba, J., 2003. Mercury from mineral deposits and potential environmental impact. Environmental Geology 43 (3), 326–338.
Schauble, E.A., 2007. Role of nuclear volume in driving equilibrium stable isotope fractionation of mercury, thallium, and other very heavy elements. Geochimica et Cosmochimica Acta 71 (9), 2170–2189.
Schofield, K., 2008. Fuel-mercury combustion emissions: an important heterogeneous mechanism and an overall review of its implications. Environmental Science & Technology 42 (24), 9014–9030.
Seigneur, C., Vijayaraghavan, K., Lohman, K., Karamchandani, P., Scott, C., 2003. Global source attribution for mercury deposition in the United States. Environmental Science & Technology 38 (2), 555–569.
Selin, N.E., et al., 2007. Chemical cycling and deposition of atmospheric mercury: global constraints from observations. Journal of Geophysical Research 112 (D2), D02308.
Senior, C.L., Johnson, S.A., 2005. Impact of carbon-in-ash on mercury removal across particulate control devices in coal-fired power plants. Energy & Fuels 19 (3), 859–863.
Sherman, L.S., et al., 2010. Mass-independent fractionation of mercury isotopes in Arctic snow driven by sunlight. Nature Geoscience 3 (3), 173–177.
Sherman, L.S., Blum, J.D., Keeler, G.J., Demers, J.D., Dvonch, J.T., 2012. Investigation of local mercury deposition from a coal-fired power plant using mercury isotopes. Environmental Science & Technology 46 (1), 382–390.
Sivry, Y., et al., 2008. Zn isotopes as tracers of anthropogenic pollution from Zn-ore smelters. The Riou Mort–Lot River system. Chemical Geology 255 (3–4), 295–304.
Sliger, R.N., Kramlich, J.C., Marinov, N.M., 2000. Towards the development of a chemical kinetic model for the homogeneous oxidation of mercury by chlorine species. Fuel Processing Technology 65–66, 423–438.
Sonke, J.E., 2011. A global model of mass independent mercury stable isotope fractionation. Geochimica et Cosmochimica Acta 75 (16), 4577–4590.
Sonke, J.E., et al., 2008. Historical variations in the isotopic composition of atmospheric zinc deposition from a zinc smelter. Chemical Geology 252 (3–4), 145–157.
Stetson, S.J., Gray, J.E., Wanty, R.B., Macalady, D.L., 2009. Isotopic variability of mercury in ore, mine-waste calcine, and leachates of mine-waste calcine from areas mined for mercury. Environmental Science & Technology 43 (19), 7331–7336.
Streets, D.G., Zhang, Q., Wu, Y., 2009. Projections of global mercury emissions in 2050. Environmental Science & Technology 43 (8), 2983–2988.
Streets, D.G., et al., 2011. All-time releases of mercury to the atmosphere from human activities. Environmental Science & Technology 45 (24), 10485–10491.
Sun, R., Liu, G., Zheng, L., Chou, C.-L., 2010a. Geochemistry of trace elements in coals from the Zhuji Mine, Huainan Coalfield, Anhui, China. International Journal of Coal Geology 81 (2), 81–96.
Sun, R., Liu, G., Zheng, L., Chou, C.-L., 2010b. Characteristics of coal quality and their relationship with coal-forming environment: a case study from the Zhuji exploration area, Huainan coalfield, Anhui, China. Energy 35 (1), 423–435.
USEPA, 2002. Control of Mercury Emissions from Coal-fired Electric Utility Boilers. EPA-600/R-01-109. US Environmental Protection Agency, Washington, DC, USA.
Wang, Y., et al., 2009. Experimental study on mercury transformation and removal in coal-fired boiler flue gases. Fuel Processing Technology 90 (5), 643–651.
Wang, S.X., et al., 2010. Mercury emission and speciation of coal-fired power plants in China. Atmospheric Chemistry and Physics 10 (3), 1183–1192.
Yudovich, Y.E., Ketris, M.P., 2005. Mercury in coal: a review Part 2. Coal use and environmental problems. International Journal of Coal Geology 62 (3), 135–165.
Zambardi, T., Sonke, J.E., Toutain, J.P., Sortino, F., Shinohara, H., 2009. Mercury emissions and stable isotopic compositions at Vulcano Island (Italy). Earth and Planetary Science Letters 277 (1–2), 236–243.

Zhang, L., Wang, S., Meng, Y., Hao, J., 2012. Influence of mercury and chlorine content of coal on mercury emissions from coal-fired power plants in China. Environmental Science & Technology 46 (11), 6385–6392.
Zheng, W., Hintelmann, H., 2010a. Isotope fractionation of mercury during its photochemical reduction by low-molecular-weight organic compounds. The Journal of Physical Chemistry. A 114 (12), 4246–4253.
Zheng, W., Hintelmann, H., 2010b. Nuclear field shift effect in isotope fractionation of mercury during abiotic reduction in the absence of light. The Journal of Physical Chemistry. A 114 (12), 4238–4245.
Zheng, W., Foucher, D., Hintelmann, H., 2007. Mercury isotope fractionation during volatilization of Hg(0) from solution into the gas phase. Journal of Analytical Atomic Spectrometry 22 (9), 1097–1104.

Appendix A: supplementary data for Chapter 8

Experimental Details

Site Description

Huainan City is located in north Anhui Province, China. It is known as "Thermal Power Three Gorges", and is the energy base of Eastern China. The estimated total coal reserves of the Huainan coalfield are approximately 44,000 Mt, and have recently transformed Huainan City from a coal supplier to an electricity producer (Sun et al., 2010a). At present there are three main power plants (others are under construction) with a total capacity of nearly 10,000 MW and an electric power output of > 80 billion KWh/yr. The increasing coal production (~100 Mt, in the year 2010) in several dozens of coal mines and large coal consumption (~27 Mt, in the year 2010) in Huainan coal-fired power plants have generated environmental challenges such as air pollution control and the disposal of coal combustion residuals. Emission data showed that SO_2 and dust emission in Huainan city were 119 Mt and 33 Mt respectively in the year 2005, corresponding to an increase of 28% and 12% relative to the year 2000 (NAE&NAC, 2008). Moreover, the generated amount of coal waste (fly ash and bottom ash) and desulfurization by-products have been estimated at 11.6 Mt and 0.4 Mt respectively in the year 2010 (NAE&NAC, 2008).

Samples were obtained from a total of six utility boilers in the Huainan-1 (HPP-1) and Huainan-2 (HPP-2) power plants that had a similar installed capacity of 2400 MW (in the year 2007). All tested units (5 units were operated in subcritical condition and 1 unit in supercritical condition) were typical Chinese pulverized coal utility boilers and were mainly fired with medium to high volatile bituminous coal from the Huainan coalfield. The feed coal for both plants was characterized by low sulfur contents (on average < 0.5 wt.%), medium calorific value (on average of 19 – 23 MJ/Kg) and high ash yields (on average of 26 – 41 wt.%) (Sun et al., 2010b; Tang et

al., 2012).

Hg concentration in solid samples

The solid samples of coal, fly ash, bottom ash and gypsum were analyzed by a direct combustion mercury analyzer (Milestone DMA-80). The instrument was calibrated with 10 – 100 mg of standard reference materials (NIST 2685b bituminous coal; NIST 1944 NJ sediment; NIST 2976 mussel). By varying the mass of each sample (ranging from 5 to100 mg), the total amount of Hg analyzed was ensured fall within the range of the best-fitted calibration curve (0 – 20 ng, n = 13, r^2 = 0.999). Two empty boats and two standard samples NIST 2685b were run before and after about 10 samples. The periodically analyzed NIST 2685b had an average value of 153 ± 16 ng/g (1SD, n = 20) which showed an excellent agreement with the certified value of 146.2 ng/g. Hg concentrations for most replicated samples were within 10% (1RSD, 22 out of 24 samples), indicating sufficient stability of the instrument and homogeneity of the samples.

Hg preconcentration

In the first acid digestion (AD) method, between 20 and 200 mg of powdered sample was digested by acid mixtures in 15 mL pre-cleaned Teflon beakers. Two acid combinations, i.e. aqua regia (named as method AD-1, HNO_3:HCl = 1:3, v/v, 2 ml, double distilled) and reversed aqua regia plus concentrated ultrapure HF (named as method AD-2, HNO_3:HCl:HF = 3:1:1, v/v/v, 2.5 mL), were used to assist digestion on a conventional hot plate (120 °C, 24 h) (Table S1). After completing the digestion, deionized water (18.2 MΩ) was added to reach a typical Hg concentration of approximately 2 μg/L in 20% (v/v) acid solution. This solution was then passed through a plastic syringe interfaced filter (0.22 μm, Millipore, mixed ester of cellulose nitrate and cellulose acetate), and the filtered solution was collected in polypropylene

vials for determination of Hg concentrations followed by Hg isotopic analysis.

In the second combustion-trapping (CT) method, the off-line programmable two stage tube furnaces were used to thermally release and trap the Hg in oxidizing solution. The original method developed by Biswas et al. (2008) was modified in the present study: 1) only gold-trap filtrated oxygen (named as method CT-1) or air (named as method CT-2) was fed into the combustion furnace with a flow rate of 25 mL/min (Tables S1, S2); 2) the combustion furnace was heated from ambient temperature to 1000 °C at a linear ramp of 2.5 °C/min (CT-1) or from ambient temperature to 500 °C at a linear ramp of 2.5 °C/min and from 500 to 1000 °C at a linear ramp of 5 °C/min (CT-2), while the decomposition furnace was maintained at 1000 °C at all times (Tables S1, S2); 3) approximately 30 mL 40% (v/v) acid mixture of HNO_3 and HCl (2:1, v/v, 12 mL) was used as the oxidizing trapping solution for emitted Hg vapor. The sample was loaded in a 20 mm OD quartz-wool capped quartz tube that was then inserted into the center of the 25 mm OD quartz tube of the combustion furnace. The trapping solution of samples and procedural standards were adjusted to a final Hg concentration of 0.7 – 1.5 μg/L in 20% (v/v) acid solution.

Hg isotopic analysis

A Thermo-Finnigan Neptune (at the Midi-Pyrenees Observatory, Toulouse, France) a Nu plasma HR (at the IPREM-LCABIE institute, Pau, France) were used for the isotopic determination of samples. The use of two different MC-ICPMS was not a pre-defined objective in this study and was the result of instrument-time management. Hg concentrations in all the sample solutions were firstly determined by, either cold vapor atomic fluorescence spectrometry (CVAFS, Brooks Rand Model III) or CV-MC-ICPMS (by referring to the ^{202}Hg signal intensities of the samples relative to that of the NIST 3133 Hg standard solutions), to evaluate recoveries of the AD and CT

preconcentration methods. Only samples with recoveries above 80% were deemed acceptable to be analyzed for Hg isotopic composition. The NIST 3133 Hg standard and in-house UM-Almadén standard were matched to the concentration and matrix of the sample solutions within 10%. In between samples, the washout time was sufficient to ensure the blank levels were < 1% of the preceding sample or bracketed standard signal. The operation conditions and collection strategies of Faraday cups for MC-ICPMS are listed in Table S3.

Results and Discussion

Hg mass balance

The hourly average Hg mass flux of feed coal (m_{FC}, t/h), bottom ash (m_{BA}, t/h) and fly ash (m_{ESP}, t/h) can be calculated by Eqs. 1-3, respectively:

$$m_{FC} = M_{FC} \times C_{FC} \quad (1)$$

$$m_{BA} = M_{BA} \times C_{BA} \quad (2)$$

$$m_{ESP} = M_{ESP} \times C_{ESP} \quad (3)$$

Where M_{FC}, M_{BA}, M_{ESP} are the mass fluxes and C_{FC}, C_{BA}, C_{ESP} are the Hg concentrations of feed coal, bottom ash and fly ash, respectively. The calculation of the mass of Hg retained by WFGD (m_{WFGD}) should take into account the input (limestone, m_L, t/h; processing water, m_P, t/h) and output Hg flows (gypsum, m_G, t/h; waste water, m_W, t/h) in the WFGD installation, which can be expressed as:

$$m_{WFGD} = m_G + m_W - m_L - m_P = M_G \times C_G + M_W \times C_W - M_L \times C_L - M_P \times C_P \quad (4)$$

The mass of Hg emitted into atmosphere through stack emission (m_{SE}, t/h) can be estimated by calculating a Hg mass balance for input and output flows in the whole combustion assembly. In other words, the Hg in coal that enters into the combustion zone (m_{FC}, t/h) must equal the sum of Hg retained in bottom ash (m_{BA}, t/h), fly ash (m_{ESP}, t/h), WFGD (m_{WFGD}, t/h) and stack emission (m_{SE}, t/h):

$$m_{FC} = m_{BA} + m_{ESP} + m_{WFGD} + m_{SE} \quad (5)$$

By combing the Eqs.1 – 4, Eq. 5 can be resolved as:

$$M_{FC} \times C_{FC} = M_{BA} \times C_{BA} + M_{ESP} \times C_{ESP} + M_G \times C_G + M_W \times C_W - M_L \times C_L - M_P \times C_P + m_{SE} \quad (6)$$

The concentration of feed coal, bottom ash, fly ash and gypsum (C_{FC}, C_{BA}, C_{ESP} and C_G, respectively, ng/g) has been determined by DMA (Table S1); the consumption rate of coal (M_{FC}, t/h), limestone (M_L, t/h) and processing water (M_P, m^3/h), and the production rate of combustion residuals (M_{BA}, M_{ESP} and M_G for bottom ash, fly ash and gypsum, respectively, t/h) and waste water (M_W, m^3/h) were obtained from the operation records of each CFUB. The Hg concentration of processing water (0.1 μg/L for HPP-1 and 1.6 μg/L for HPP-2), limestone (2.5 ng/g for HPP-1 and 1 ng/g for HPP-2) and waste water (45 μg/L for HPP-1 and 3 μg/L for HPP-2) used in calculation are from published data on both plants (Tang et al., 2012). Based on these, the Hg mass fluxes in bottom ash (m_B, t/h), fly ash (m_B, t/h), WFGD (m_B, t/h) and stack Hg emission flux (m_{SE}, t/h) can be computed. Accordingly, the Hg mass fractions of bottom ash, fly ash, WFGD and stack emission (f_{BA}, f_{ESP}, f_{WFGD} and f_{SE}, respectively), relative to input coal Hg, are calculated.

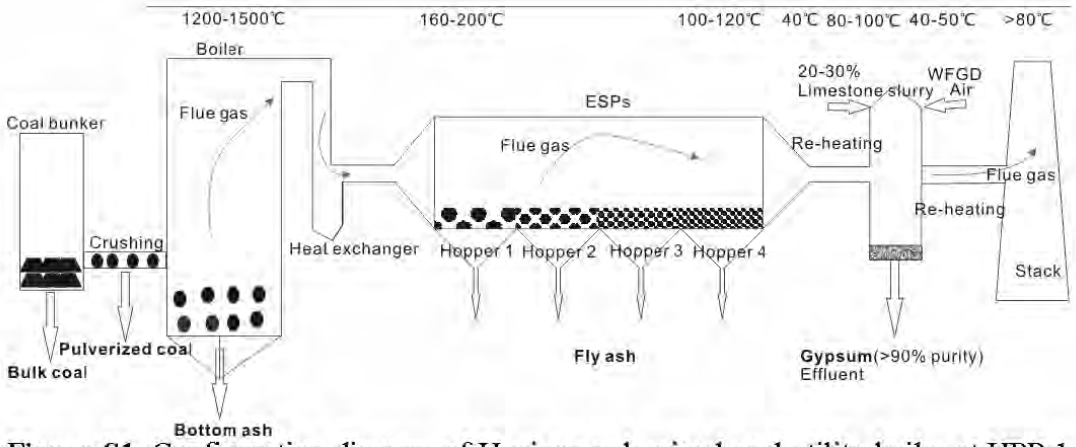

Figure S1. Configuration diagram of Huainan pulverized coal utility boiler at HPP-1 and HPP-2 showing the input and output materials, and temperature gradient. The samples investigated in this study are indicated in bold. Note the different deployment of ESPs for these two power plants: in HPP-1, there are four hoppers (hoppers 1 – 4) for each ESP, whereas in HPP-2, there are only two hoppers (hoppers A and B) for each ESP. Only boilers H1-3, H2-2 and H2-3 are equipped with WFGD.

. **Table S1. The Hg concentration (C_{Hg}, ng/g) and isotopic composition (‰) in the samples, and the recovery of the extracted samples.**

Sample ID	LOI	C_{Hg}	SD	n_1	n_2	Method	Recovery	$\delta^{202}Hg$	2SD	$\delta^{199}Hg$	2SD	$\delta^{200}Hg$	2SD	$\delta^{201}Hg$	2SD	$\delta^{204}Hg$	2SD	$\Delta^{199}Hg$	2SD	$\Delta^{200}Hg$	2SD	$\Delta^{201}Hg$	2SD
Feed coal																							
H1-C		346	21	3	2	CT-1	103%	-0.18	0.14	-0.03	0.14	-0.04	0.01	-0.09	0.02	-0.31	0.22	0.01	0.10	0.06	0.06	0.05	0.09
H1−1-C		320	26	2	1	CT-1	107%	-0.44		-0.13		-0.17		-0.30		-0.64		-0.02		0.04		0.03	
					1	AD-1	93%	-0.51		-0.07		-0.19		-0.32				0.06		0.07		0.06	
H1-2-C		327	14	6	1	CT-1	90%	-0.42		-0.11		-0.19		-0.33		-0.68		0.00		0.02		-0.02	
H1-3-C		369	5	3	1	CT-1	90%	-0.65		-0.14		-0.35		-0.45		-1.10		0.02		-0.02		0.03	
					2	AD-2	82%	-0.67	0	-0.12	0.03	-0.25	0.01	-0.49	0.01			0.04	0.03	0.08	0.01	0.01	0.01
H2-C		389	38	3	1	CT-1	85%	-0.6		-0.24		-0.44		-0.39		-0.67		-0.09		-0.14		0.06	
					1	AD-1	88%	-0.65		-0.15		-0.29		-0.44				0.01		0.04		0.05	
					1	AD-2	96%	-0.57		-0.15		-0.24		-0.44				0.00		0.05		-0.01	
Bottom ash																							
H1-1-B	9.5%	36	3	2	1	CT-2	100%	-1.68		-0.35		-0.77		-1.21		-2.53		0.08		0.07		0.05	
H1-2-B	18%	191	12	4	1	CT-1	101%	-1.77		-0.50		-0.91		-1.36		-2.76		-0.05		-0.02		-0.03	
					1	CT-2	109%	-1.88		-0.41		-0.94		-1.42		-2.78		0.06		0.00		0.00	
H1-3-B	6.3%	23	0	2	1	CT-1	76%	-1.82		-0.47		-0.89		-1.29		-2.71		-0.01		0.02		0.09	
					1	CT-2	70%	-1.76		-0.30		-0.99		-1.17		-2.47		0.15		-0.11		0.16	
H2-1-B	4.5%	9	3	2	1	CT-2	73%	-1.61		-0.41		-0.81		-1.15		-2.39		0.00		0.00		0.06	
H2-2-B	6.2%	16	1	2	1	CT-2	85%	-1.92		-0.50		-0.98		-1.37		-2.89		-0.01		-0.01		0.08	
H2-3-B	4.5%	5	1	4	1	CT-2	86%	-1.96		-0.45		-1.00		-1.39		-2.85		0.05		-0.02		0.09	
Fly ash																							
H1-1-F-1	1.5%	248	24	6	1	CT-1	92%	-1.59		-0.35		-0.72		-1.17		-2.39		0.05		0.08		0.03	
					1	AD-1	85%	-1.55		-0.30		-0.76		-1.08				0.09		0.02		0.08	
H1-1-F-2	1.6%	285	20	4	1	CT-1	93%	-1.72		-0.45		-0.83		-1.22		-2.43		-0.01		0.04		0.08	
					1	AD-1	74%	-1.72		-0.31		-0.82		-1.19				0.12		0.05		0.11	
H1-1-F-3	0.6%	198	15	3	1	CT-1	86%	-1.5		-0.36		-0.63		-0.86		-2.30		0.02		0.12		0.27	
H1-1-F-4	1.0%	197	8	3	1	CT-1	90%	-1.25		-0.16		-0.55		-0.83		-2.06		0.16		0.08		0.11	
H1-2-F	2.2%	238	21	5	1	AD-1	92%	-1.45		-0.31		-0.73		-1.00				0.05		0.00		0.09	
H1-3-F	1.3%	434	29	4	1	CT-1	104%	-0.88		-0.25		-0.41		-0.65		-1.41		-0.03		0.03		0.01	
H2-1-F	2.6%	263	25	9	1	CT-1	103%	-1.52		-0.36		-0.87		-1.11		-2.40		0.03		-0.10		0.04	

					1	AD-1	98%	-1.72		-0.28		-0.78		-1.21				0.15		0.09		0.08	
H2-1-F-G	1.9%	594	14	4	1	CT-2	108%	-0.85		-0.16		-0.34		-0.59		-1.33		0.05		0.09		0.05	
H2-2-F	2.4%	704	46	6	1	CT-1	100%	-1.05		-0.27		-0.54		-0.71		-1.71		0.00		-0.01		0.08	
					1	CT-1	106%	-1.07		-0.23		-0.47		-0.76		-1.62		0.04		0.06		0.04	
H2-2-F-G	1.9%	702	13	3	1	CT-1	101%	-0.97		-0.13		-0.48		-0.68		-1.48		0.12		0.01		0.05	
					1	CT-2	85%	-0.82		-0.17		-0.37		-0.62		-1.35		0.04		0.05		0.00	
H2-3-F	0.3%	127	9	2	1	CT-1	107%	-1.54		-0.35		-0.71		-1.16		-2.36		0.04		0.06		0.00	
					1	CT-1	96%	-1.61		-0.38		-0.80		-1.26		-2.30		0.03		0.01		-0.04	
H2 3 F G	0.8%	34	10	3	1	CT-1	101%	-1.91		-0.44		-0.90		-1.36		-2.85		0.05		0.07		0.08	
Gypsum																							
H1-3-G		1500	85	4	1	CT-1	93%	-0.47		-0.14		-0.24		-0.39		-0.85		-0.02		-0.01		-0.03	
						AD-2	100%	-0.52		-0.06		-0.22		-0.26				0.07		0.04		0.13	
H2-2-G		1550		1																			
H2-3-G		4590	33	2	2	AD-1	85%	-0.99	0.03	-0.18	0.01	-0.43	0.01	-0.65				0.07	0.01	0.06	0	0.09	0.03

LOI: loss of ignition, estimated by loss of weight of samples placed in a tube furnace at 800 °C for 2 h.

n1-sample replicates for Hg concentration determination

n2-replicate analyses of the samples for Hg isotopic ratio determination

12 **Table S2. The Hg isotopic composition (‰) of standard reference materials (including data of other studies) and the recovery of the**

13 **extracted samples.**

Standard	Method	n	Recovery	$\delta^{202}Hg$	2SD	$\delta^{199}Hg$	2SD	$\delta^{200}Hg$	2SD	$\delta^{201}Hg$	2SD	$\delta^{204}Hg$	2SD	$\Delta^{199}Hg$	2SD	$\Delta^{200}Hg$	2SD	$\Delta^{201}Hg$	2SD
UM-Almaden (Nu plasma)		**111**		**-0.57**	**0.14**	**-0.16**	**0.13**	**-0.28**	**0.10**	**-0.46**	**0.15**	**-0.87**	**0.26**	**-0.03**	**0.09**	**-0.02**	**0.12**	**0**	**0.07**
UM-Almaden (Neptune)		**33**		**-0.53**	**0.14**	**-0.15**	**0.06**	**-0.26**	**0.09**	**-0.44**	**0.13**			**-0.02**	**0.05**	**0.01**	**0.06**	**-0.04**	**0.07**
UM-Almaden[a]		**37**		**-0.58**	**0.07**	**-0.17**	**0.08**	**-0.28**	**0.07**	**-0.48**	**0.09**			**-0.02**	**0.07**	**0.01**	**0.05**	**-0.04**	**0.06**
UM-Almaden[b]		**10**		**-0.51**	**0.15**	**-0.14**	**0.09**	**-0.26**	**0.10**	**-0.41**	**0.11**			**-0.01**	**0.07**	**-0.01**	**0.06**	**-0.03**	**0.04**
NIST 2685b-1	CT-1	1	93%	-2.83		-0.71		-1.42		-2.13				0.00		0.00		0.00	
NIST 2685b-2	CT-1	1	100%	-2.66		-0.66		-1.29		-2.00				0.01		0.05		0.01	
NIST 2685b-3	CT-1	1	85%	-2.66		-0.73		-1.33		-1.95				-0.06		0.01		0.05	
NIST 2685b-4	CT-1	1	81%	-2.67		-0.66		-1.33		-2.02				0.01		0.02		0.00	
NIST 2685b-5	CT-2	1	95%	-2.75		-0.70		-1.36		-2.12				0.00		0.01		-0.05	
NIST 2685b (Average)			**91%**	**-2.71**	**0.13**	**-0.69**	**0.05**	**-1.35**	**0.09**	**-2.04**	**0.14**			**-0.01**	**0.05**	**0.02**	**0.03**	**0.00**	**0.07**
NIST 1632d-1	CT-2	1	86%	-1.77		-0.47		-0.86		-1.31				-0.03		0.03		0.03	
NIST 1632d-2	CT-1	1	87%	-1.76		-0.51		-0.85		-1.37				-0.07		0.04		-0.04	
NIST 1632d-3	CT-1	1	83%	-1.78		-0.51		-0.94		-1.29				-0.06		-0.04		0.05	
NIST 1632d-4	CT-1	1	95%	-1.89		-0.52		-0.92		-1.49				-0.04		0.03		-0.07	
NIST 1632d-5	CT-1	1	102%	-1.94		-0.50		-0.96		-1.50				-0.01		0.01		-0.04	
NIST 1632d (Average)			**91%**	**-1.83**	**0.14**	**-0.50**	**0.03**	**-0.91**	**0.09**	**-1.39**	**0.18**			**-0.04**	**0.04**	**0.01**	**0.06**	**-0.02**	**0.09**
NIST 1632c[a]				**-1.86**	**0.13**	**-0.49**	**0.04**	**-0.93**	**0.07**	**-1.44**	**0.10**			**-0.02**	**0.04**	**0.01**	**0.03**	**-0.04**	**0.03**
NIST 1632c[c]				**-1.86**	**0.11**									**-0.04**	**0.02**			**-0.03**	**0.04**
BCR176R-1	CT-1	1	86%	-1.06		-0.38		-0.58		-0.77		-1.75		-0.11		-0.05		0.03	
BCR176R-2	CT-1	2	100%	-0.97	0.06	-0.29	0.32	-0.50	0.05	-0.85	0.18	-1.54	0.19	-0.04	0.34	-0.01	0.08	-0.12	0.22
BCR 176R (Average)			**93%**	**-1.02**	**0.09**	**-0.34**	**0.09**	**-0.54**	**0.08**	**-0.81**	**0.09**	**-1.65**	**0.21**	**-0.08**	**0.07**	**-0.03**	**0.03**	**-0.04**	**0.15**
BCR 176R[b]				**-1.03**	**0.05**	**-0.32**	**0.03**	**-0.51**	**0.06**	**-0.83**	**0.04**			**-0.06**	**0.03**	**0.00**	**0.06**	**-0.06**	**0.03**

14 [a]data cited from Sherman et al. (2012); [b]data cited from Estrade et al. (2010); [c]data cited from Lefticariu et al. (2011). n-replicate analyses of the

15 standards

Table S3. The operation conditions of CV-MC-ICP-MS.

	Neptune	Nu plasma HR
Cold vapor generator	Perkin Elmer FIAS-400 using 3% (w/v) Sncl2 in 10% (v/v) bi-distilled HCl	Home made GLS using 3% (w/v) Sncl2 in 10% (v/v) HCl
Tl introduction	CETAC Aridus II desolvation unit, 20 μg/L NIST 997 in 2% HNO_3	DSN-100 desolvation unit, 15 μg/L NIST 997 in 2% HNO_3
RF power	1200 W	1300 W
Data acquisition	1 block, 84 cycles, 8 s integration time	1 block, 30 cycles, 10 s integration time
Wash-out time	12 min	10 min
Cups configuration	205 (H3), 203 (H2), 202 (H1), 201 (C), 200 (L1), 199 (L2), 198 (L3)	208 (H7), 206 (H5), 205 (H5), 204 (H4), 203 (H3), 202 (H2), 201 (H1), 200 (Ax), 199 (L1), 198 (L2), 196 (L3)

References

Biswas, A., Blum, J.D., Bergquist, B.A., Keeler, G.J., Xie, Z., 2008. Natural Mercury Isotope Variation in Coal Deposits and Organic Soils. Environmental Science & Technology, 42(22): 8303-8309.

Estrade, N., Carignan, J., Sonke, J.E., Donard, O.F.X., 2010. Measuring Hg Isotopes in Bio-Geo-Environmental Reference Materials. Geostandards and Geoanalytical Research, 34(1): 79-93.

Lefticariu, L., Blum, J.D., Gleason, J.D., 2011. Mercury Isotopic Evidence for Multiple Mercury Sources in Coal from the Illinois Basin. Environmental Science & Technology, 45(4): 1724-1729.

NAE&NAC, 2008. Energy Futures and Urban Air Pollution Challenges for China and the United States. National Academy of Engineering and National Research Council, Washington, DC.

Sherman, L.S., Blum, J.D., Keeler, G.J., Demers, J.D., Dvonch, J.T., 2012. Investigation of Local Mercury Deposition from a Coal-Fired Power Plant Using Mercury Isotopes. Environmental Science & Technology, 46(1): 382-390.

Sun, R., Liu, G., Zheng, L., Chou, C.-L., 2010a. Geochemistry of trace elements in coals from the Zhuji Mine, Huainan Coalfield, Anhui, China. International

Journal of Coal Geology, 81(2): 81-96.

Sun, R., Liu, G., Zheng, L., Chou, C.-L., 2010b. Characteristics of coal quality and their relationship with coal-forming environment: A case study from the Zhuji exploration area, Huainan coalfield, Anhui, China. Energy, 35(1): 423-435.

Tang, Q., Liu, G., Yan, Z., Sun, R., 2012. Distribution and fate of environmentally sensitive elements (arsenic, mercury, stibium and selenium) in coal-fired power plants at Huainan, Anhui, China. Fuel, 95(0): 334-339.

Chapter 9

Conclusions and perspectives

Chapter 9. Conclusions and perspectives

The goal of this PhD dissertation was to assess the use of Hg stable isotope signatures to trace the largest anthropogenic Hg emission source, coal fired power plants. We first developed an in-house customized Hg purification and preconcentration (combustion-trapping) method to subsequently analyze Hg isotope compositions by MC-ICPMS. Coals from worldwide coal basins and coal combustion residuals (i.e. bottom ash, fly ash and desulfurization gypsum) from coal-fired power plants were studied. A global coal Hg isotope library with wide spatial and temporal coverage was developed, and included more than 150 coal samples. *In-situ* sampling in coal-fired power plants allowed us to evaluate whether coal combustion shifts the Hg isotope compositions in emitted flue gases relative to original coals. Finally, a case study on the Hg isotope variation in a single coal mine and coal bench were done to assess the origin of Hg in coal. In this chapter we summarize our main findings, and indicate the perspectives that follow from our conclusions.

9.1. Conclusions

1. In Chapter 5, we detailed an in-house modified combustion-trapping protocol to extract, purify and pre-concentrate Hg for isotope analysis from various kinds of solid samples (coal, coal associated rocks, fly ash, bottom ash, peat and black shale) with Hg levels varying from <5 ng/g to 10 μg/g. Following controlled experiments on the optimum HNO_3/HCl acid ratio, carrier gas type and its flow rate, and temperature ramp, we recommend to use a 40% (v/v) $2HNO_3$/1HCl as acid trapping solution, 25 ml/min O_2 flow rate as carrier gas and a dynamic temperature program (15 °C/min for 25-150 °C and 600-900 °C; 2.5 °C/min for 150-600 °C) for the first combustion furnace. The second decomposition furnace is held at 1000 °C at all times. Our tested 340 samples over 20 months demonstrate that this method can achieve a median 89% extraction recovery of Hg for sample types as diverse as coals, peat or marine sedimentary rocks. No significant Hg isotope fractionation was observed for CRMs within the Hg recovery range of 81-102%. This protocol has the advantages of a short sample processing time (~3.5 hours), limited transfer of residual sample matrix into the Hg trapping solution and direct measurement by CV-MC-ICPMS after diluting the trapping solution to 20% (v/v) acid. However, special attention should be paid to iodine-rich samples that possibly suppress cold vapor generation of Hg for isotope determination.

2. In Chapter 6, we investigated the fractionation extent of Hg isotopes in coals deposited at the same geographical location at different coal-forming periods. The objective was to test the potential of using Hg isotope signatures to trace the sources and geochemical processes of Hg in coal deposits.

We found that natural processes caused a ~2‰ variation of δ^{202}Hg (−1.62 to 0.44±0.12‰, 2SD, n=18) and 0.35‰ of Δ^{199}Hg (−0.12 to 0.22±0.08‰, 2SD, n=18) among coal seams deposited at the same location over a period of ~20 Ma (Zhuji Coal Mine, Huainan Coalfield, Anhui Province). A similar range of variation was observed within a single coal seam (Daizhuang Coal Mine, Jining Coalfield, Shandong Province). Correlation between δ^{202}Hg and 1/Hg in Zhuji coals suggests a binary mixing of Hg end-members, suggesting that over 20 Ma of coal deposition the dominant Hg source shifted. However, no definitive conclusions are obtained for δ^{202}Hg vs. 1/Hg in Daizhuang coals. The distinctly higher (0.70 to 0.91±0.12‰, 2SD, n=2) and lower δ^{202}Hg (−4.00 to −3.47±0.12‰, 2SD, n=3) in natural cokes, a metamorphosed form of coal, suggests that significant Hg MDF occurred when coals were subjected to the perturbation of magmatic intrusion.

3. We developed a global coal Hg isotope library in Chapter 7. We measured Hg isotope compositions in 108 new coal samples from major coal-producing basins in Africa, China, Europe, India, Indonesia, Former USSR and the USA, adding to ~50 published coal samples. We observed a 4.7‰ range in δ^{202}Hg (−3.9 to 0.8‰) and a 1‰ range in Δ^{199}Hg (−0.6 to 0.4‰). Half of the 28 pairwise comparisons between eight coal-producing regions are statistically distinguishable on the basis of δ^{202}Hg, Δ^{199}Hg or both ($p<0.05$). This underlines the potential application of Hg isotope signatures to coal Hg emission tracing. In addition, we observe that with the increase of coal rank (from lignite to subbituminous to bituminous to anthracite) and with decreasing coal deposition ages (from Cenozoic to Mesozoic to Paleozoic), the Δ^{199}Hg signature increases stepwise, suggesting source-ralted controls on Hg isotope compositons in coals.

4. In Chapter 8 we investigate whether coal combustion processes in CFUB shift Hg isotope signatures from feed coal to stack Hg emissions. We measured the Hg isotope compositions in feed coals, bottom ash, fly ash and desulfurization by-product gypsum. Relative to feed coal with δ^{202}Hg ranging from −0.67 to −0.18‰, oxidized Hg species in bottom ash and fly ash are enriched in lighter isotopes with δ^{202}Hg from −1.96 to −0.82‰. Flue gas desulphurization by-product gypsum shows δ^{202}Hg from −0.99 to −0.47‰. The calculated isotopic shift of stack Hg emissions relative to feed coals is minor for δ^{202}Hg (<0.3‰) and negligible for Δ^{199}Hg.

9.2 Perspectives

Apart from the method development and exploration of the origin of Hg in coal, the most important outcome of this PhD research project is in the field of environmental tracing of coal Hg emissions. Our observations that numerous global coal producing regions can be distinguished based on their

coal Hg isotope signatures, and that those signatures are largely preserved into coal plant Hg emissions hold promise for quantitative tracing of coal Hg emissions. Here we address in detail the opportunities and caveats of 'what should be investigated next'.

9.2.1. Species-specific Hg isotope compositions of coal Hg emissions

Hg emissions from coal plant stacks consist of three operationally defined forms: gaseous elemental Hg, GEM; gaseous oxidized Hg, GOM, and particle bound Hg, PBM (i.e. residual fly ash). Due to varying atmospheric reactivity and life-time of Hg species, species-specific Hg isotopic information has important implications for near-field (PBM and GOM) and far-field (GEM) coal Hg emission tracing. In chapter 8, we speculated that the GEM, GOM and PBM in coal flue gas emission may carry contrasting Hg isotope signatures. Based on our analysis of fly ash and gypsum, we suggested that PBM and GOM are possibly enriched in the lighter Hg isotopes relative to feed coals, and consequently GEM must be enriched in the heavier Hg isotopes. However, we did not make direct species-specific Hg isotope measurements on stack emission components. The only pre-liminary species-specific Hg isotope measurement on flue gas of a CFUB indicates ~3.5‰ variation of MDF in δ^{202}Hg and negligible MIF (Khawaja et al., 2010). Relative to bulk Hg flue gas, these authors found indeed that GOM is enriched in the lighter Hg isotopes and GEM is enriched in heavier Hg isotopes. These observations are in agreement with our speculation. We suggest that more *in-situ* measurements on stack emissions are needed to better constrain the fractionation signs and extent in different Hg species of coal combustion flue gases.

9.2.2. Post-emission Hg isotope fractionation in coal flue gases

A field study by Sherman et al. (2012) showed that δ^{202}Hg and Δ^{199}Hg signatures in wet precipitation downwind from a CFUB in Florida (USA) were substantially different from those of regional background Hg and the combusted feed coals. On average, wet precipitation δ^{202}Hg was shifted by −1.8‰ and Δ^{199}Hg by +0.6‰ as compared to feed coal. Hg isotope fractionation within CFUB and in-cloud Hg transformations following flue gases emission were suggested to be the underlying reasons. In Chapter 8, we suggested that GOM and PBM in emitted flue gases have respectively the δ^{202}Hg of fly ash and gypsum, and thus explain part of the observed δ^{202}Hg in their wet precipitation samples. Due to the absence of photochemical Hg MIF during coal combustion and downstream transport of flue gases through APCDs, the inherited Δ^{199}Hg of flue gases from feed coals is significantly lower than observed Δ^{199}Hg in precipitation samples. Therefore, additional in-plume and in-cloud Hg isotope fractionation is still needed to explain the precipitation Hg MIF. One

possible pathway to imprint precipitation Hg(II) with significantly positive Δ^{199}Hg is photochemical reduction of aqueous Hg(II)-DOM (dissolved organic matter) complexes in cloud droplets. This plausible explanation requires further field and experimental study.

9.2.3. Geological controls on Hg isotope fractionation in coal deposits

In Chapter 6, we tested the potential of using Hg isotope compositions to trace Hg sources and geochemical processes involving Hg during and after coal deposition. We observed that thermal perturbations derived from magmatic intrusion events could significantly fractionate Hg isotopes between coal and natural coke. However, it is difficult to identify whether/which sources or geochemical processes generated the ~2‰ δ^{202}Hg variation in either a single seam or continuously deposited seams. In Chapter 7, we also observed some interesting relationships between δ^{202}Hg or Δ^{199}Hg vs. Hg concentrations, coal ranks and coal-forming ages in specific world regions. Due to complex Hg occurrences in coals and an unknown interplay between multiple factors including coal depositional environment, post-depositional Hg dynamics and coalification pathways, we are currently unable to meaningfully interpret our observations. Other elemental, isotope or mineralogical parameters could be used to help constrain the Hg isotope biogeochemistry of coal deposits.

9.2.4. Reconstructing the historical evolution of anthropogenic Hg isotope emission signatures

The coal Hg isotope library we created has been an important first step in tracing coal Hg emissions. With a few exceptions (German, UK and Australian coal) the library covers over 70% of past and future coal basins. Combining historical coal production statistics, coal import-export statistics, Hg removal efficiencies by APCDs during coal combustion, we can now start to reconstruct an all-time historical evolution of the Hg isotope compositions of atmospheric coal Hg emissions. Where we have enough information, such an isotope emission inventory can be made on a regional/national basis. We suggest that a similar ‘library’ type approach should be taken for other anthropogenic Hg emission sectors, such as non-ferrous metal smelting, cement production, chlor-alkali industries, and gold and silver mining. Once we know the historical geographical patterns of anthropogenic and natural Hg isotope emissions, we can then confront and better understand the Hg isotope information from natural archives such as peat, sediment and ice cores or soils and biomonitors.

Chapitre 9. Conclusions et perspectives

Le but principal de ces travaux de thèse a été l'exploration des signatures isotopiques du Hg en tant que traceur des émissions du Hg par les centrales au charbon. Nous avons d'abord développé une méthode d'extraction, de purification et de pré-concentration adapté au charbon, afin d'analyser sa composition isotopique par spectrométrie de masse. Ensuite nous avons exploré les variations isotopiques des charbons globaux et les produits de combustion (i.e. cendres résiduels et volants, gypse) des centrales au charbon. Une compilation isotopique du Hg dans des charbons, incluant plus de 150 charbons et une grande variation spatiotemporelle, a été établie. L'échantillonnage in-situ des centrales au charbon a permis d'étudier les éventuelles modifications des signatures isotopiques du Hg des émissions par rapport au charbon combusté. Enfin, une étude cas sur la variation isotopique de Hg de 20 millions d'années de dépôts de charbon au même endroit géographique a permis d'explorer l'isotopie du Hg comme traceur des sources et des processus du Hg dans le charbon. Dans ce Chapitre nous résumons nos observations et interprétations, et nous discutons les perspectives pour la suite.

9.1. Conclusions

1. Le Chapitre 5 résume le protocole d'extraction, purification and pré-concentration du Hg pour l'analyse isotopique. La méthode a été développée pour des échantillons solides divers tel que le charbon, des roches, cendres, tourbes et schistes noirs ayant des teneurs en Hg de <5 ng/g à 10 µg/g. Suivant des optimisations du mélange acide (HNO_3/HCl), flux et type de gaz vecteur, et rampe de température, nous recommandons l'utilisation de 40% (v/v) $2HNO_3$/1HCl dans le piège acide, 25 ml/min O_2 en gaz vecteur et un programme dynamique de rampe de température (15 °C/min for 25-150 °C and 600-900 °C; 2.5 °C/min for 150-600 °C) pour le 1^{ier} four de combustion. Le 2^{ieme} four, le pyrolyseur, est maintenu à 1000 °C durant toutes les extractions du Hg. Nous avons testé et effectué 340 extractions de Hg durant 20 mois, montrant une efficacité d'extraction de 89% (médiane) pour les différents types d'échantillons. L'extraction des matériaux de référence montre une absence de biais isotopique pour des rendements entre 81-102%. Ce protocole a l'avantage d'être rapide (3.5h), d'éviter le transfert de la matrice vers le piège acide, et permet une analyse directe des compositions isotopiques par spectrométrie de masse après dilution à 20% (v/v) acide. Cependant, nous avons remarqué des transferts de l'iode de la matrice du charbon vers le piège acide, posant des problèmes de réduction du Hg dans le générateur à vapeur froide du spectromètre de masse.

2. Le Chapitre 6 fait l'objet d'une étude de cas sur le fractionnement isotopique du Hg au sein d'une séquence de charbons déposé au même endroit géographique. Le but était d'explorer les signatures isotopiques du Hg comme traceurs des sources ou processus du Hg dans le charbon. Nous observons une variation ~2‰ en δ^{202}Hg (−1.62 to 0.44±0.12‰, 2SD, n=18) et de 0.35‰ en Δ^{199}Hg (−0.12 to 0.22±0.08‰, 2SD, n=18) au sein des couches de charbons déposées pendant 20 Ma (Mine de Zhuji, basin de Huainan, province d'Anhui, Chine). Une même variation est observée au sein d'une seule couche de charbon (mine de Daizhuang, basin de Jining, province de Shandong, Chine). Une corrélation entre le δ^{202}Hg et 1/Hg à Zhuji suggère une mélange binaire entre deux sources de Hg, témoignant d'un décalage dans la source dominante du Hg dans le bassin de Huainan. Dans la couche de charbon de Daizhuang aucune relation claire né parait entre δ^{202}Hg vs. 1/Hg. Enfin, des cokes naturels, une forme métamorphosée du charbon au contact avec des intrusions magmatiques, montre un fort fractionnement isotopique dépendent de la masse, avec δ^{202}Hg élevé (0.70 to 0.91±0.12‰, 2SD, n=2) ou plus bas (−4.00 to −3.47±0.12‰, 2SD, n=3).

3. Le Chapitre 6 résume la compilation isotopique du Hg dans des charbons, basé sur 108 nouveaux échantillons de charbon provenant des basins importants en Afrique, Chine, Europe, Inde, Indonésie, l'ancienne USSR et les USA et ~50 charbons déjà publiés. Nous observons une variation isotopique de 4.7‰ en δ^{202}Hg (−3.9 a 0.8‰) et de 1‰ en Δ^{199}Hg (−0.6 a 0.4‰). La moitié des 28 comparaisons possibles entre les huit principales régions productrices du charbon du monde sont statistiquement différenciable selon leurs δ^{202}Hg, Δ^{199}Hg ou les deux ($p<0.05$). Nous y en déduisons l'application potentielle des signatures isotopiques du Hg en tant que traceurs des émissions du Hg des centrales au charbon. Dans un deuxième temps, il parait que la signature Δ^{199}Hg augmente avec la charbonification (du lignite au sous-bitumineux au bitumineux à l'anthracite) et avec l'âge de dépôt (du Cénozoïque au Mésozoïque au Paléozoïque).

4. Le Chapitre 8 adresse question si la combustion du charbon dans les centrales au charbon modifie oui ou non la composition isotopique de ses émissions du Hg. Nous avons mesuré la composition isotopique du Hg dans les charbons, les cendres résiduels et volants, et le gypse produit par la désulfurisation des gaz. Par rapport au charbon combusté, les cendres et gypse sont tous enrichis en isotopes légers du Hg. Par conséquence la signature isotopique des émissions du Hg par la cheminée, calcule par bilan de masse, est légèrement enrichi en isotopes lourds (δ^{202}Hg <0.3‰), mais reste inchangé pour la signature Δ^{199}Hg.

9.2 Perspectives

Le résultat le plus important de ces travaux porte sur la possibilité de traçage des émissions du Hg des centrales au charbon vers l'atmosphère de notre planète. Nos observations que la plupart de charbons du monde se distinguent par leurs compositions isotopiques de Hg, et que ces signatures sont peu modifiées pendant la combustion, ouvrent le possibilité en traçage quantitative des émissions du Hg. Dans cette section nous parlons des opportunités et dangers de ces applications de traçage.

9.2.1. Les signatures isotopiques de formes spécifiques des émissions du Hg

Les émissions du Hg à la cheminée d'une centrale au charbon consiste de plusieurs formes chimiques, définies de façon opérationnelle : le Hg gazeux élémentaire (GEM), le Hg gazeux oxydé (GOM), et le Hg particulaire (PBM). Ces formes ont des réactivités et demi-vies différentes dans l'atmosphère, ce qui a des ramifications importantes pour le traçage des émissions du Hg a proximité (GOM, PBM) ou à longue distance (GEM) de la source. Dans le Chapitre 8 nous avons indiqués que les formes GEM, GOM et PBM dans les émissions des centrales au charbon peuvent avoir des signatures isotopiques contrastés. C'est-à-dire, nos analyses des cendres volants (PBM) et gypse (GOM) montrent que le PBM et GOM sont probablement enrichis en isotopes légers, et par conséquence le GEM est enrichi en isotopes lourds. Cependant nous n'avons pas effectué des analyses isotopiques à la sortie de la cheminée ou dans le panache d'une centrale au charbon. Une étude préliminaire aux USA sur la composition isotopique du GOM et GEM d'une centrale au charbon suggère qu'effectivement le GOM est enrichi en isotopes légers et le GEM en isotopes lourds (Khawaja et al., 2010). Ces observations sont donc en accord avec notre proposition. Nous proposons que plus de mesures isotopiques sur les émissions doivent être effectues afin de mieux cerner cet aspect important.

9.2.2. Post-emission Hg isotope fractionation in coal flue gases

Une étude par Sherman et al. (2012) a montré que les signatures δ^{202}Hg et Δ^{199}Hg dans les précipitations humide en aval d'une centrale au charbon en Florida (USA) étaient très différents des signatures des charbons combustés. En moyenne, les δ^{202}Hg et Δ^{199}Hg du Hg de la pluie ont été décalé de −1.8‰ en δ^{202}Hg et de +0.6‰ en Δ^{199}Hg par rapport au charbon combusté. Les auteurs ont suggéré que des fractionnements isotopiques du Hg durant la combustion et post-émission dans les nuages sont à l'origine de ces décalages (Sherman et al., 2012). Dans le Chapitre 8 nous avons

suggéré que les émissions du PBM et GOM, fractions dominantes vis-à-vis les dépôts du Hg à proximité de la centrale au charbon, sont enrichis en isotopes légers, permettant d'expliquer le décalage de −1.8‰ en δ^{202}Hg. Les mesures préliminaires de Khawaja et al. (2010) sur le GOM emit par une centrale au charbon confirme cette interprétation. Cependant le décalage de la signature Δ^{199}Hg de +0.6‰ entre le GOM/PBM émits et la pluie demande l'intervention d'un processus photochimique lequel ne peut pas avoir lieu dans la centrale au charbon même. Par conséquence une étape, post-émission, de photoreduction partielle du GOM doit intervenir afin d'expliquer ce décalage en MIF. L'endroit le plus probable de cette étape de photochimie est dans les gouttelettes de nuages. Vue la rapidité, en moins d'une heure, de la modification de la signature Δ^{199}Hg entre cheminée et pluie tombé, ce processus de photochimie atmosphérique peut sérieusement compliquer le traçage des émissions du Hg des centrales au charbon. Plus d'études sont souhaitables dans ce domaine.

9.2.3. L'origine des variations isotopiques du Hg d'un bassin de charbon.

Le Chapitre 6 documente en détail les variations isotopiques du Hg au sein d'un bassin de charbon, et au sein d'une seule couche de charbon. Nous avons remarqué que la perturbation thermique provenant des intrusions magmatiques fractionne significativement les isotopes du Hg entre charbon et coke. Cependant, il a été difficile d'identifier si l'origine des 2‰ de variation en δ^{202}Hg a travers du bassin mais également au sein de la couche de charbon unique est dû au changement de sources du Hg ou des transformations spécifiques du Hg. Dans la compilation des signatures isotopiques du charbon du Chapitre 7 nous avons noté des relations intéressants entre δ^{202}Hg ou Δ^{199}Hg et les teneurs en Hg, type de charbon, et âge de dépôt. Malheureusement à ce stade d'exploration nous ne sommes pas capable d'identifier les causes et effets de ces variations isotopiques, autre que les observations faits. Des études plus approfondies peuvent être souhaitable afin de mieux comprendre ces variations.

9.2.4. L'evolution historique des emissions isotopiques du Hg

La compilation isotopique du Hg dans des charbons constitue une 1^{iere} étape dans le traçage des émissions du Hg des centrales au charbon. Sauf quelques exceptions (charbon Allemands, Anglais et Australien), la compilation couvre 70% des bassins de charbon globaux. En considérant la production historique du charbon par pays, les statistiques sur les imports/exports du charbon, les mesures de captage du Hg dans les centrales au charbon, nous pouvons commencer à reconstruire l'évolution historique des signatures isotopiques du Hg des émissions liées au secteur du charbon. Si

nécessaire cette reconstruction peut être faite pour des régions ou nations. Nous proposons qu'une compilation similaire soit établie pour d'autres secteurs industrielles, tel que la métallurgie, le ciment, l'industrie chlore-alkali, et l'orpaillage. Une fois l'évolution isotopique de tous ces secteurs reconstruit, nous pouvons mieux comprendre les signatures isotopiques observes dans les archives naturels tel que les tourbières, les sédiments, la glace, ou les sols ou encore les biomoniteurs.

References

Khawaja, S.N., Odom, L., Landing, W., 2010. Isotopic Variations of Mercury Emitted by Coal Fired Power Plant Gases, AGU, San Francisco.

Sherman, L.S., Blum, J.D., Keeler, G.J., Demers, J.D., Dvonch, J.T., 2012. Investigation of Local Mercury Deposition from a Coal-Fired Power Plant Using Mercury Isotopes. Environmental Science & Technology

List of Figures

Figure 1 Classification and evolution of coal (Source: ACARP).....12

Figure 2 Trends in Hg emissions by (a) source types and (b) world regions (Source: Streets et al., 2011).....19

Figure 3 Global pre-industrial (a) and present-day biogeochemical cycle of mercury in GEOS-Chem. Inventories are in Mg, and rates are in Mg/yr (Source: Selin et al., 2008) 20

Figure 4 Three isotope plots of studied Chinese coals showing only MDF for the even isotope ^{200}Hg, and both MDF and MIF (Δ^{199}Hg and Δ^{201}Hg) for the odd isotopes ^{199}Hg and ^{201}Hg.....33

Figure 5 Summary of Δ^{199}Hg and Δ^{201}Hg data (n =722) for biological samples containing predominantly MMHg (dark grey circles), and for geochemical samples containing predominantly inorganic Hg(II) (open circles). Experimentally observed $\Delta^{199/201}$Hg slopes for aquatic Hg(II) (1.0-1.3) (Bergquist and Blum, 2007; Zheng and Hintelmann, 2009) and MMHg photodegradation (Bergquist and Blum, 2007), and the experimental slope for NVE fractionation (Zheng and Hintelmann, 2009). (Source: Sonke, 2011).....33

Figure 6 Fractionation factor (1000*ln $\beta^{202-198}$Hg) for Hg-bearing molecules relative to Hg(0) vapor. The solid line denotes MDF and dotted line denotes NVE (Source: Schauble, 2007).....35

Figure 7 Geographical map showing the locations of studied coal mines. DZ: Daizhuang Coal Mine; ZJ: Zhuji Coal Mine; J-C: Jining Coalfield; H-C: Huainan Coalfied 41

Figure 8 Generalized stratigraphic column and lithological characteristics of coal-bearing sequences in Zhuji Coal Mine of Huainan Coalfield (A) and Daizhuang Coal Mine of Jining Coalfield (B) showing sampled benches in No. 3-1 coal seam (C). C_2: Upper Carboniferous; P_1: Lower Permian; P_2: Upper Permian; Fm: Formation; TY: Taiyuan Formation; SX: Shanxi Formation; LS: Lower Shihezi Formation; US: Upper Shihezi Formation. Note that the coal seams are numbered in ascending order in Zhuji Coal Mine, and in descending order in Daizhuang Coal Mine along coal seams upward 42

Figure 9 Digital photographs of field drilling (A) and sampled coal and associated rocks (B) 44

Figure 10 The geographical locations of world coal samples 45

Figure 11 Location of Huainan City (A) showing Huainan-1 (B) and Huain-2 Power Plants (C).....47

Figure 12 Configuration diagram of Huainan pulverized coal utility boiler at HPP-1 and HPP-2 showing the input and output materials, and temperature gradient. Note the different deployment of ESPs for these two power plants: in HPP-1, there are four hoppers (TSP 1-4) for each ESP, whereas in HPP-2, there are only two hoppers (hoppers A and B) for each ESP. Only boilers H1-3, H2-2 and H2-3 are equipped with WFGD. Abbreviation: TSP-Total particulate matter; ESP: electrostatic precipitator; WFGD: wet flue-gas desulfurization 48

Figure 13 Overview of MC-ICPMS (Thermo-Finnigan Neptune at the Midi-Pyrenees Observatory, Toulouse, France) (A) and introduction system for Hg isotope measurement (B). 50

Figure 14 Plot of ln$^{202/198}$Hg vs. ln$^{205/203}$Tl of NIST 3133 Hg standard, secondary standard (UM-Almaden, BCR176R, NIST2685b) and samples (coal, coal combustion residuals) in a one-day analytical session on Nu plasma, Pau University, France. All the solutions were measured at ~1 ng/g. The dashed lines represent the $\delta^{202/198}$Hg values of samples and secondary standards relative to NIST 3133 Hg standard. 55

Figure 15 Overview of combustion-trapping system for Hg purification (for more detail, refer to Chapter 5).57

Figure 16 Inter-seam variation of $\delta^{13}C$, Hg concentration, $\delta^{202}Hg$ and $\Delta^{199}Hg$ values in the Zhuji Coal Mine (A) and intra-seam variation of Hg concentration, $\delta^{202}Hg$ and $\Delta^{199}Hg$ values in No. 3-1 coal seam of Daizhuang Coal Mine (B). The shaded areas for Hg concentrations of Zhuji coals depict the overall increasing trend; the vertical dashed line shows the zero value for $\Delta^{199}Hg$; for individual Zhuji coal seams with multiple samples, 1SD uncertainty of multiple samples is used if this value is larger than 2SD analytical uncertianty; the error bars in Hg concentrations of Daizhuang samples are covered by symbols. 82

Figure 17 $\delta^{202}Hg$ vs. $\Delta^{199}Hg$ diagram for coal and natural coke samples in the Zhuji Coal Mine, and for coal, coal floatfraction and rock samples in Daizhuang Coal Mine. The horizontal dashed line shows zero value for $\Delta^{199}Hg$.....84

Figure 18 Comparison of $\delta^{202}Hg$ and $\Delta^{199}Hg$ values between studied coals and coals form other areas. Russia-Kazakhstan coal data are from Biswas et al, (2008); the USA coal data are from Biswas et al. (2008), Lefticariu et al. (2011) and Sherman et al. (2012); Chinnese coal data are from Biswas et al. (2008) and Sun, et al. (2013b). The filled black circles in categories of China and "This study" indicate Huainan coals.....84

Figure 19 $\Delta^{199}Hg$ vs. $\Delta^{201}Hg$ values in coal and natural coke samples in Zhuji Coal Mine, and in coal, coal float fraction and rock samples in Daizhuang Coal Mine. Error bar represents measurement uncertainty of samples. The slope and intercept of samples regression line are calculated by the York regression method (York, 1968) that takes into account uncertainties in both $\Delta^{199}Hg$ and $\Delta^{201}Hg$. The vertical and horizontal dashed lines show the zero values for $\Delta^{199}Hg$ and $\Delta^{201}Hg$. 85

Figure 20 Plot of $\delta^{202}Hg$ vs. 1/Hg in Zhuji and Daizhuang coals. Coal samples ZJ-12-8-4-2 and ZJ-9+1-1 in circles are treated as the outliers. ZJ-12-8-4-2 has positive $\delta^{202}Hg$ and is possibly affected by magmatic intrusion (see Section 4.3 in text); ZJ+9+1-1 is an unworkable coal seam and has an extremely high ash yield (Table 5). 88

Figure 21 $\Delta^{201}Hg$ vs. $\Delta^{199}Hg$ in studied world coals (n=108) (A) and all world coals (n=155) (B). The centre, horizontal and vertical axis of ellipse denotes respectively means of $\Delta^{199}Hg$ and $\Delta^{201}Hg$, 1SD on $\Delta^{199}Hg$ and 1SD on $\Delta^{201}Hg$.....102

Figure 22 Box plots showing $\delta^{202}Hg$ (A) and $\Delta^{199}Hg$ (B) in all world coals (n=155). The horizontal lines at the bottom, middle and top of each boxplot are the lower quartile (below which 25% lowest values are found), median and upper quartile (above which 25% highest values are found), respectively. The box height (the difference between lower quartile and upper quartile) is defined as interquartile range (IQR). The data points either greater than the upper quartile+1.5 IQR or less than the lower quartile-1.5 IQR are considered to be extreme values. Square symbol denotes mean 104

Figure 23 $\delta^{202}Hg$ vs. $\Delta^{199}Hg$ in all world coals (n=155). The centre, horizontal and vertical axis of ellipse denotes respectively means of $\delta^{202}Hg$ and $\Delta^{199}Hg$, 1SD on $\delta^{202}Hg$ and 1SD on $\Delta^{199}Hg$. 105

Figure 24 Matrix representation of statistical pairwise comparisons between regions (α=0.05 or 0.01, by *IBM SPSS Statistics 20)*. The compared regions can be distinguished by $\delta^{202}Hg$ (red square), $\Delta^{199}Hg$ (blue square) or both (1/2 blue +1/2 red square) 106

Figure 25 $\delta^{202}Hg$ vs. $\Delta^{199}Hg$ in all Chinese coals (n=49). 108

Figure 26 Linear relationship of $\delta^{202}Hg$ vs. 1/Hg or $\Delta^{199}Hg$ vs. 1/Hg in coals from the USA (A), China (B), Romania (C, D) and Mongolia (E). The coal samples in the USA are from the Illinois coal basin reported

elsewhere (Lefticariu et al., 2011), and are averaged on a coal mine basis; the significant relationship of δ^{202}Hg vs. 1/Hg and Δ^{199}Hg vs. 1/Hg in Romanian coals would disappear when the lowest Hg sample (R11) is excluded.....115

Figure 27 Linear relationship of δ^{202}Hg vs. Δ^{199}Hg in Romanian coals 116

Figure 28 Box plots showing variations of δ^{202}Hg (‰, A) and Δ^{199}Hg (‰, B) in world coals of different ranks 117

Figure 29 Box plots showing variations of δ^{202}Hg (‰, A) and Δ^{199}Hg (‰, B) in world coals of different coal-forming periods 118

List of Tables

Table 1. Summary of world coal reserve, production, consumption, export and import in 2011 13

Table 2. Characteristics of stable Hg isotopes.....27

Table 3 'β' scaling factors for isotope ratios relative to $^{202}Hg/^{198}Hg$.....32

Table 4 Slopes of linear array of $lnR^{xxx/198}Hg_m$ vs. $lnR^{205/203}Tl_m$ assuming fractionation factors are identical for Hg and Tl.....54

Table 5 Ash yield, sulfur and iron content, Hg concentration and $\delta^{13}C$ values of coal and coke samples in the Zhuji Coal Mine, Huainan Coalfield.....76

Table 6 Hg isotope compositions of coal and coke samples in Zhuji Coal Mine, Huainan Coalfield.....78

Table 7 Hg concentrations and isotope compositions of coal and rock samples in Daizhuang Coal Mine, Jining Coalfield.....78

Table 8 Summary of the means of $\delta^{202}Hg$, $\Delta^{199}Hg$ and $\Delta^{201}Hg$ in world coals 104

Appendix A: supplementary data for Chapter 7

Table Al. Summary of Hg isotope compositons in world coals of this study and previously reported

Country	ID	Lithology	Source	Hg in ppb (as received basis)	δ^{199}Hg	2SD	δ^{200}Hg	2SD	δ^{201}Hg	2SD	δ^{202}Hg	2SD	Δ^{199}Hg	2SD	Δ^{200}Hg	2SD	Δ^{201}Hg	2SD
Benin	*Coal 1*	*charcoal*	*This study*	*3*	*-0.80*		*-1.54*		*-2.40*		*-3.19*		*0.01*		*0.08*		*0.01*	
South Africa	Coal 2 west B5	Coal	This study	127	-0.54	0.17	-0.45	0.11	-1.06	0.13	-0.96	0.06	-0.30	0.15	0.03	0.07	-0.34	0.08
South Africa	Coal 3	Coal	This study	114	-0.57	0.01	-0.45	0.20	-1.02	0.09	-0.90	0.11	-0.35	0.02	0.00	0.14	-0.34	0.01
South Africa	S-Africa	Coal	This study	621	-0.67	0.03	-0.86	0.03	-1.65	0.05	-1.62	0.03	-0.27	0.04	-0.05	0.01	-0.43	0.07
South Africa	SARM-20	Coal	This study	236	-0.65	0.08	-0.55	0.07	-1.25	0.00	-1.09	0.00	-0.38	0.08	0.00	0.07	-0.43	0.01
South Africa	Duvha	Coal	This study	226	-0.65	0.10	-0.63	0.16	-1.27	0.14	-1.25	0.13	-0.34	0.06	0.00	0.09	-0.33	0.04
South Africa	Kriel	Coal	This study	167	-0.60	0.08	-0.63	0.04	-1.24	0.09	-1.25	0.10	-0.28	0.05	0.00	0.01	-0.30	0.01
South Africa	Lethabo	Coal	This study	186	-0.32	0.03	-0.17	0.04	-0.55	0.02	-0.42	0.04	-0.21	0.02	0.05	0.01	-0.23	0.01
South Africa	Majuba	Coal	This study	275	-0.18	0.10	-0.02	0.11	-0.19	0.12	-0.03	0.15	-0.17	0.06	-0.01	0.04	-0.17	0.01
South Africa	Camden	Coal	This study	145	-0.41	0.03	-0.38	0.02	-0.80	0.06	-0.73	0.00	-0.22	0.03	-0.01	0.01	-0.25	0.06
South Africa	Tutuka	Coal	This study	262	-0.62	0.01	-0.54	0.04	-1.16	0.03	-1.04	0.02	-0.36	0.01	-0.02	0.03	-0.38	0.04
South Africa	*Tutuka fresh ash*	*Coal fly ash*	*This study*	*166*	*-0.65*	*0.17*	*-0.91*	*0.21*	*-1.56*	*0.26*	*-1.82*	*0.22*	*-0.19*	*0.12*	*0.00*	*0.10*	*-0.19*	*0.10*
South Africa	*Tutuka old ash*	*Coal fly ash*	*This study*	*123*	*-0.81*	*0.02*	*-0.85*	*0.12*	*-1.68*	*0.17*	*-1.68*	*0.04*	*-0.39*	*0.01*	*-0.01*	*0.10*	*-0.42*	*0.14*
Mean (n=10)					**-0.52**	**0.16**	**-0.47**	**0.23**	**-1.02**	**0.39**	**-0.93**	**0.43**	**-0.29**	**0.07**	**0.00**	**0.03**	**-0.32**	**0.08**
China	Anhui-1	Coal	This study	850	0.13		0.37		0.53		0.77		-0.08		-0.02		-0.06	
China	Anhui-2	Coal	This study	4102	-0.20		-0.59		-0.83		-1.28		0.12		0.06		0.14	
China	Anhui-3	Coal	This study	660	-0.29		-1.23		-1.59		-2.42		0.33		0.00		0.23	
China	Anhui-Huaian-4	Coal	This study	99	-0.20		-0.28		-0.51		-0.61		-0.04		0.03		-0.05	
China	Anhui-Huaian-5	Coal	This study	79	-0.09		-0.25		-0.38		-0.56		0.05		0.03		0.04	
China	Guiizhou-1	Coal	This study	234	-0.33		-0.71		-1.10		-1.44		0.03		0.02		-0.01	
China	Guizhou-2	Coal	This study	229	-0.33		-0.67		-1.05		-1.37		0.02		0.02		-0.02	

Country	ID	Lithology	Source	Hg in ppb (as received basis)	$\delta^{199}Hg$	2SD	$\delta^{200}Hg$	2SD	$\delta^{201}Hg$	2SD	$\delta^{202}Hg$	2SD	$\Delta^{199}Hg$	2SD	$\Delta^{200}Hg$	2SD	$\Delta^{201}Hg$	2SD
China	Guizhou-3	Coal	This study	355	-0.26		-0.60		-0.91		-1.16		0.05		-0.01		-0.03	
China	Guizhou-4	Coal	This study	210	-0.50	0.06	-1.34	0.04	-1.93	0.07	-2.47	0.11	0.13	0.03	-0.09	0.10	-0.06	0.02
China	Guizhou-5	Coal	This study	380	-0.56	0.03	-1.45	0.08	-2.16	0.17	-2.93	0.22	0.18	0.03	0.04	0.03	0.05	0.00
China	Guizhou-6	Coal	This study	12500	0.01		-0.39		-0.49		-0.89		0.23		0.06		0.18	
China	Hebei-1	Coal	This study	64	-0.47	0.02	-0.89	0.01	-1.47	0.05	-1.93	0.03	0.02	0.01	0.08	0.03	-0.02	0.02
China	Hebei-2	Coal	This study	27	-0.74	0.17	-1.29	0.26	-2.03	0.34	-2.64	0.16	-0.08	0.13	0.03	0.17	-0.05	0.22
China	Hebei-3	Coal	This study	48	-0.04	0.03	-0.09	0.04	-0.16	0.00	-0.20	0.03	0.02	0.02	0.01	0.02	-0.01	0.02
China	Henan-1	Coal	This study	208	-0.60	0.03	-0.90	0.08	-1.48	0.15	-1.68	0.15	-0.17	0.00	-0.05	0.01	-0.21	0.03
China	Hubei-1	Stone coal	This study	191	0.05	0.04	-0.13	0.04	-0.17	0.02	-0.40	0.01	0.15	0.03	0.07	0.03	0.13	0.03
China	Hubei-2	Stone coal	This study	108	0.02	0.01	0.09	0.02	0.02	0.06	0.09	0.02	0.00	0.01	0.05	0.01	-0.05	0.05
China	Hubei-3	Stone coal	This study	1146	-0.01	0.05	-0.06	0.08	-0.17	0.03	-0.22	0.02	0.04	0.05	0.05	0.07	-0.01	0.03
China	Hubei-4	Coal	This study	160	-0.21	0.09	-0.35	0.06	-0.58	0.16	-0.78	0.12	-0.01	0.07	0.04	0.00	0.01	0.07
China	Hubei-5	Coal	This study	141	-0.35	0.12	-0.65	0.08	-1.08	0.08	-1.33	0.06	-0.01	0.11	0.02	0.05	-0.08	0.04
China	IM-WL-33	Coal	This study	990	-0.56	0.10	-1.56	0.10	-2.19	0.24	-3.07	0.12	0.21	0.05	0.00	0.08	0.13	0.10
China	IM-WL-1	Coal	This study	90236	-0.01		-0.37		-0.43		-0.75		0.18		0.01		0.13	-0.05
China	Liaoning-1	Coal	This study	67	-0.21	0.04	-0.34	0.04	-0.53	0.07	-0.60	0.02	-0.06	0.05	-0.03	0.05	-0.08	0.06
China	Shandong-1	Coal	This study	85	-0.49		-0.92		-1.49		-1.92		-0.01		0.05		-0.05	
China	Shandong-2	Coal	This study	298	-0.23		-0.52		-0.81		-1.15		0.06		0.06		0.05	
China	Shanxi-1	Coal	This study	100	-0.38	0.01	-0.42	0.07	-0.80	0.02	-0.91	0.03	-0.15	0.00	0.04	0.06	-0.12	0.04
China	Shanxi-2	Coal	This study	54	-0.35	0.07	-0.47	0.03	-0.83	0.00	-1.01	0.03	-0.09	0.08	0.04	0.01	-0.08	0.02
China	Shanxi-3	Coal	This study	54	-0.62	0.01	-0.64	0.01	-1.18	0.02	-1.30	0.02	-0.30	0.02	0.01	0.02	-0.20	0.03
China	Shanxi-4	Coal	This study	23	-0.03	0.07	0.30	0.04	0.28	0.13	0.49	0.10	-0.16	0.05	0.06	0.01	-0.09	0.05
China	Shanxi-5	Coal	This study	213	-0.29	0.00	-0.23	0.05	-0.50	0.05	-0.54	0.04	-0.16	0.01	0.04	0.03	-0.10	0.02
China	Shanxi-6	Coal	This study	192	-0.28	0.02	-0.10	0.01	-0.38	0.00	-0.29	0.02	-0.21	0.01	0.05	0.02	-0.17	0.01

Country	ID	Lithology	Source	Hg in ppb (as received basis)	$\delta^{199}Hg$	2SD	$\delta^{200}Hg$	2SD	$\delta^{201}Hg$	2SD	$\delta^{202}Hg$	2SD	$\Delta^{199}Hg$	2SD	$\Delta^{200}Hg$	2SD	$\Delta^{201}Hg$	2SD
China	Xinjiang-1	Coal	This study	24	-0.40		-0.17		-0.51		-0.32		-0.30		0.00		-0.25	
China	Yunnan-1	Coal	This study	34	-0.54		-0.71		-1.24		-1.46		-0.16		0.02		-0.14	
China	SH-1 (triplicate)	Coal	Biswas et al., 2008								-2.32	0.40	0.34	0.06			0.29	0.05
China	AN-1	Coal	Biswas et al., 2008								-0.64	0.06	0.10	0.01			0.14	0.06
China	AN-2 (duplicate)	Coal	Biswas et al., 2008								-0.89	0.35	0.08	0.01			0.13	0.04
China	An-3	Coal	Biswas et al., 2008								-0.43	0.21	0.02	0.05			0.04	0.05
China	An-4	Coal	Biswas et al., 2008								-0.43	0.09	0.06	0.02			0.09	0.02
China	An-5	Coal	Biswas et al., 2008								-0.28	0.07	0.08	0.04			0.11	0.04
China	HE-1 (triplicate)	Coal	Biswas et al., 2008								-2.28	0.61	-0.40	0.03			-0.35	0.01
China	JI-1	Coal	Biswas et al., 2008								-0.85	0.15	-0.04	0.03			-0.05	0.06
China	GU-1	Coal	Biswas et al., 2008								-1.37	0.01	-0.02	0.02			0.00	0.04
China	GU-2	Coal	Biswas et al., 2008								-1.22	0.22	0.04	0.06			0.04	0.08
China	HB-1	Coal	Biswas et al., 2008								-1.41	0.14	-0.03	0.06			0.00	0.06
China	H1-C	Coal	Sun et al., 2013	346	-0.03	0.14	-0.04	0.01	-0.09	0.02	-0.18	0.14	0.01	0.10	0.06	0.06	0.05	0.09
China	H1−1-C	Coal	Sun et al., 2013	320	-0.10	0.04	-0.18	0.01	-0.31	0.01	-0.48	0.05	0.02	0.06	0.06	0.02	0.05	0.02
China	H1-2-C	Coal	Sun et al., 2013	327	-0.11		-0.19		-0.33		-0.42		0.00		0.02		-0.02	
China	H1-3-C	Coal	Sun et al., 2013	369	-0.13	0.01	-0.30	0.07	-0.47	0.03	-0.66	0.01	0.03	0.01	0.03	0.07	0.02	0.01
China	H2-C	Coal	Sun et al., 2013	389	-0.18	0.05	-0.32	0.10	-0.42	0.03	-0.61	0.04	-0.03	0.06	-0.02	0.11	0.03	0.04
Mean (n=49, including 16 previously reported samples)					**-0.26**	**0.21**	**-0.49**	**0.45**	**-0.78**	**0.65**	**-1.04**	**0.84**	**0.00**	**0.14**	**0.02**	**0.03**	**-0.01**	**0.12**
France	*Cokes Carmeaux*	*Natrue Coke*	*This study*	*5*	*-0.67*	*0.14*	*-1.53*	*0.28*	*-2.25*	*0.25*	*-3.06*	*0.25*	*0.10*	*0.07*	*0.00*	*0.16*	*0.05*	*0.06*
France	Decazeville	Coal	This study	29	-0.25	0.07	-0.47	0.14	-0.70	0.11	-0.91	0.11	-0.02	0.05	-0.01	0.09	-0.01	0.03
Germany	Lignite allemande	Coal	This study	70	-0.85	0.05	-0.81	0.01	-1.64	0.05	-1.55	0.08	-0.46	0.03	-0.03	0.03	-0.48	0.01

Country	ID	Lithology	Source	Hg in ppb (as received basis)	$\delta^{199}Hg$	2SD	$\delta^{200}Hg$	2SD	$\delta^{201}Hg$	2SD	$\delta^{202}Hg$	2SD	$\Delta^{199}Hg$	2SD	$\Delta^{200}Hg$	2SD	$\Delta^{201}Hg$	2SD
Romania	Romania-1 Valea de Brazi	coal	This study	150	-0.84		-1.05		-1.86		-2.08		-0.30		0.01		-0.28	
Romania	Romania-2 Uricani	coal	This study	130	-0.62		-0.38		-0.93		-0.73		-0.44		-0.02		-0.38	
Romania	Romania-3 Barbateni	coal	This study	460	-0.68		-0.63		-1.25		-1.12		-0.40		-0.07		-0.40	
Romania	Romania-4 Barbateni	coal	This study	140	-0.72		-0.71		-1.40		-1.35		-0.37		-0.03		-0.38	
Romania	Romania-5 Lupeni	coal	This study	130	-0.63		-0.59		-1.18		-1.15		-0.34		-0.02		-0.31	
Romania	Romania-6 Paroseni	coal	This study	136	-0.75		-0.85		-1.62		-1.67		-0.33		-0.01		-0.37	
Romania	Romania-7 Vulcan	coal	This study	240	-0.83		-0.97		-1.75		-1.85		-0.36		-0.04		-0.36	
Romania	Romania-8 Aninoasa	coal	This study	380	-0.72		-0.72		-1.40		-1.45		-0.35		0.01		-0.30	
Romania	Romania-9 Livezeni	coal	This study	130	-0.57		-0.35		-0.87		-0.60		-0.41		-0.05		-0.43	
Romania	Romania-10 Lonea	coal	This study	240	-0.78		-0.78		-1.46		-1.44		-0.41		-0.05		-0.37	
Romania	Romania-11 Petrila	coal	This study	70	-0.35		0.40		0.11		0.70		-0.52		0.05		-0.42	
Mean (n=13)					**-0.66**	**0.18**	**-0.61**	**0.35**	**-1.23**	**0.51**	**-1.17**	**0.68**	**-0.36**	**0.11**	**-0.02**	**0.03**	**-0.35**	**0.11**
Inida	JB-1	Coal	This study	127	-0.21	0.06	-0.34	0.06	-0.72	0.02	-0.89	0.05	0.01	0.08	0.11	0.04	-0.05	0.06
Inida	JB-2	Coal	This study	34	-0.39	0.02	-0.91	0.10	-1.34	0.14	-1.85	0.02	0.07	0.01	0.02	0.09	0.05	0.15
Inida	JB-3	Coal	This study	52	-0.35	0.03	-1.22	0.07	-1.63	0.03	-2.47	0.09	0.28	0.06	0.03	0.10	0.25	0.10
Inida	JB-4	Coal	This study	48	-0.50	0.05	-0.96	0.09	-1.49	0.08	-1.94	0.12	0.00	0.03	0.01	0.02	-0.03	0.01
Inida	JR-1	Coal	This study	29	-0.56	0.10	-1.20	0.03	-1.85	0.01	-2.42	0.02	0.04	0.12	0.01	0.04	-0.05	0.02
Inida	JR-2	Coal	This study	40	-0.36	0.08	-0.71	0.02	-1.05	0.08	-1.40	0.00	-0.01	0.08	-0.01	0.02	0.00	0.09
Inida	JR-3	Coal	This study	75	-0.51	0.00	-0.70	0.05	-1.22	0.05	-1.47	0.02	-0.15	0.01	0.05	0.04	-0.11	0.06
Inida	JR-4	Coal	This study	38	-0.27	0.01	-0.60	0.00	-0.94	0.14	-1.28	0.12	0.06	0.02	0.05	0.06	0.03	0.05
Inida	RB-1	Coal	This study	4	-0.62	0.19	-1.36	0.00	-2.13	0.00	-2.86	0.01	0.10	0.18	0.09	0.01	0.00	0.00
Inida	RB-2	Coal	This study	39	-0.43	0.02	-0.85	0.06	-1.29	0.04	-1.60	0.00	-0.02	0.02	-0.04	0.05	-0.09	0.03
Inida	RB-3	Coal	This study	289	-0.50	0.03	-0.98	0.02	-1.56	0.12	-2.02	0.05	0.01	0.02	0.03	0.00	-0.05	0.08
Inida	WM-1	Coal	This study	38	-0.51	0.04	-1.08	0.06	-1.67	0.05	-2.23	0.01	0.05	0.03	0.04	0.05	0.01	0.04

Country	ID	Lithology	Source	Hg in ppb (as received basis)	$\delta^{199}Hg$	2SD	$\delta^{200}Hg$	2SD	$\delta^{201}Hg$	2SD	$\delta^{202}Hg$	2SD	$\Delta^{199}Hg$	2SD	$\Delta^{200}Hg$	2SD	$\Delta^{201}Hg$	2SD
Mean (n=12)					**-0.43**	**0.12**	**-0.91**	**0.28**	**-1.41**	**0.38**	**-1.87**	**0.54**	**0.04**	**0.09**	**0.03**	**0.04**	**0.00**	**0.09**
Indonesia	CQ01	coal	This study	9	-0.13	0.00	-0.13	0.03	-0.37	0.01	-0.40	0.09	-0.04	0.00	0.09	0.03	-0.06	0.07
Indonesia	CQ02	coal	This study	43	-0.39	0.05	-0.06	0.07	-0.41	0.10	-0.04	0.09	-0.38	0.04	-0.05	0.03	-0.37	0.04
Indonesia	CQ03	coal	This study	106	-0.41	0.04	-0.48	0.01	-0.89	0.01	-0.97	0.04	-0.17	0.03	0.02	0.00	-0.17	0.01
Indonesia	CQ04	coal	This study	70	-0.54	0.02	-0.60	0.10	-1.15	0.14	-1.29	0.09	-0.22	0.01	0.05	0.05	-0.19	0.07
Indonesia	CQ05	coal	This study	51	-0.45	0.06	-0.57	0.09	-1.05	0.18	-1.18	0.10	-0.15	0.04	0.02	0.04	-0.17	0.11
Indonesia	CQ06	coal	This study	260	-0.19	0.01	-0.04	0.06	-0.24	0.00	-0.09	0.11	-0.17	0.04	0.00	0.02	-0.17	0.08
Indonesia	CQ07	coal	This study	193	-0.52	0.05	-0.27	0.05	-0.66	0.10	-0.42	0.05	-0.42	0.04	-0.06	0.01	-0.35	0.06
Indonesia	CQ08	coal	This study	78	-0.06	0.04	0.02	0.05	-0.06	0.05	0.01	0.00	-0.06	0.04	0.02	0.04	-0.06	0.04
Mean (n=8)					**-0.34**	**0.17**	**-0.27**	**0.24**	**-0.60**	**0.37**	**-0.55**	**0.49**	**-0.20**	**0.13**	**0.01**	**0.05**	**-0.19**	**0.11**
Mongolia	Hov-I-1-11/02	coal	This study	35	-0.60		-0.47		-0.99		-0.89		-0.39		-0.02		-0.33	
Mongolia	Chdg-2-B-10/02	coal	This study	153	-0.73		-0.63		-1.28		-1.21		-0.42		-0.02		-0.36	
Mongolia	Nal-5-B-1-7/02	coal	This study	47	-0.32		0.25		-0.07		0.37		-0.42		0.07		-0.35	
Mongolia	Sivo-II-1-8/02	coal	This study	64	-0.44		0.21		-0.08		0.39		-0.55		0.02		-0.38	
Mongolia	Adnh-710-1-10/02	coal	This study	75	-0.51		-0.42		-0.92		-0.75		-0.31		-0.04		-0.36	
Mongolia	Byne-28-1-8/02	coal	This study	300	-0.77		-0.88		-1.68		-1.77		-0.32		0.02		-0.35	
Mongolia	Byne-39-1-8/02	coal	This study	357	-0.86		-1.01		-1.91		-2.05		-0.33		0.03		-0.37	
Mongolia	Mogn-1-A-10/02	coal	This study	91	-0.78		-1.23		-2.15		-2.59		-0.12		0.07		-0.20	
Mongolia	Saio-6A-1-8/02	coal	This study	31	-0.28		0.06		-0.25		0.10		-0.31		0.00		-0.32	
Mongolia	Shar-Vln-1-9/02	coal	This study	54	-0.21		-0.03		-0.26		-0.08		-0.18		0.02		-0.20	
Mongolia	Nar-63-1-9/02	coal	This study	130	-0.54		-0.51		-1.04		-0.95		-0.30		-0.03		-0.33	
Mongolia	Tav-4-1-6/02	coal	This study	117	-0.33	0.04	-1.06	0.06	-1.54	0.01	-2.13	0.04	0.22	0.03	0.02	0.04	0.07	0.01
Mongolia	Tav-8-1-6/02	coal	This study	91	-0.15		-0.27		-0.49		-0.62		0.01		0.04		-0.02	
Mongolia	Talb-I-1-2/03	coal	This study	88	-0.64		-0.80		-1.46		-1.50		-0.25		-0.04		-0.32	

Country	ID	Lithology	Source	Hg in ppb (as received basis)	$\delta^{199}Hg$	2SD	$\delta^{200}Hg$	2SD	$\delta^{201}Hg$	2SD	$\delta^{202}Hg$	2SD	$\Delta^{199}Hg$	2SD	$\Delta^{200}Hg$	2SD	$\Delta^{201}Hg$	2SD
Mongolia	Talb-I-2-2/03	coal	This study	86	-0.62		-0.81		-1.44		-1.55		-0.22		-0.04		-0.27	
Mean (n=15)					**-0.52**	**0.21**	**-0.51**	**0.45**	**-1.04**	**0.66**	**-1.02**	**0.90**	**-0.26**	**0.18**	**0.01**	**0.03**	**-0.27**	**0.13**
	R8 (catalyst)	*Sapropel*	*This study*	*101*	*-0.39*		*-0.67*		*-1.14*		*-1.36*		*-0.05*		*0.01*		*-0.11*	
Ukraine	*R11-natural coke*	*Natural Cokes*	*This study*	*507*	*-0.32*	*0.03*	*-0.62*	*0.03*	*-0.94*	*0.06*	*-1.20*	*0.04*	*-0.02*	*0.02*	*-0.01*	*0.05*	*-0.04*	*0.03*
Russia	*R16-1-Shungite*	*Shungite*	*This study*	*101*	*-0.37*	*0.02*	*-0.67*	*0.01*	*-1.09*	*0.03*	*-1.36*	*0.03*	*-0.02*	*0.01*	*0.02*	*0.00*	*-0.07*	*0.01*
Ukraine	R1-1	Coal	This study	161	-0.81	0.12	-1.18	0.14	-2.09	0.08	-2.52	0.10	-0.17	0.10	0.08	0.09	-0.20	0.01
Ukraine	R1-2	Coal	This study	161	-0.74	0.16	-1.28	0.09	-2.01	0.14	-2.50	0.13	-0.11	0.13	-0.02	0.03	-0.13	0.05
Russia	R3-1	Coal	This study	60	-0.84	0.15	-1.37	0.13	-2.25	0.13	-2.77	0.19	-0.14	0.11	0.02	0.03	-0.17	0.01
Russia	R4	Coal	This study	262	-1.11	0.06	-1.19	0.10	-2.22	0.02	-2.33	0.03	-0.53	0.05	-0.02	0.08	-0.47	0.00
Russia	R5	Coal	This study	27	-0.52	0.08	-0.86	0.01	-1.44	0.10	-1.75	0.01	-0.08	0.08	0.02	0.01	-0.12	0.10
Russia	R6	Coal	This study	260	0.12	0.03	0.10	0.02	0.11	0.09	0.14	0.09	0.09	0.06	0.03	0.02	0.00	0.02
Russia	R7	Coal	This study	36	-0.37	0.10	-0.28	0.01	-0.64	0.05	-0.55	0.00	-0.23	0.10	0.00	0.01	-0.23	0.05
Russia	R9	Coal	This study	1000	-0.45	0.11	-0.65	0.17	-1.14	0.05	-1.48	0.13	-0.07	0.07	0.09	0.10	-0.03	0.05
Ukraine	R10	Coal	This study	35	-0.72	0.06	-1.75	0.02	-2.54	0.01	-3.46	0.01	0.15	0.06	-0.01	0.02	0.06	0.02
Russia	R12	Coal	This study	38	-0.83	0.05	-1.73	0.07	-2.58	0.13	-3.42	0.04	0.03	0.05	-0.01	0.09	-0.01	0.10
Ukraine	R13	Coal	This study	234	-0.32	0.02	-0.60	0.03	-1.02	0.09	-1.36	0.10	0.02	0.00	0.08	0.03	0.00	0.02
Kazakhstan	R14	Coal	This study	20	-1.29	0.01	-1.94	0.07	-3.26	0.06	-3.90	0.03	-0.31	0.02	0.02	0.06	-0.33	0.04
Russia	R15	Coal	This study	144	-0.42	0.04	-1.21	0.03	-1.68	0.01	-2.47	0.01	0.20	0.04	0.03	0.03	0.17	0.01
Kazakhstan	PO-1 (duplicate)	Coal	Biswas et al., 2008								-1.48	0.01	-0.51	0.02			-0.45	0.02
Kazakhstan	PO-2	Coal	Biswas et al., 2008								-0.25	0.17	-0.52	0.06			-0.49	0.06
Kazakhstan	PO-3	Coal	Biswas et al., 2008								-0.59	0.18	-0.40	0.69			-0.35	0.61
Russia	RO-1 (triplicate)	Coal	Biswas et al., 2008								-0.26	0.07	0.00	0.04			-0.06	0.04
Russia	KK-1 (triplicate)	Coal	Biswas et al., 2008								-0.50	0.46	-0.63	0.03			-0.53	0.03
Russia	MIX (duplicate)	Coal	Biswas et al., 2008								-1.36	0.25	-0.23	0.05			-0.21	0.01

Country	ID	Lithology	Source	Hg in ppb (as received basis)	$\delta^{199}Hg$	2SD	$\delta^{200}Hg$	2SD	$\delta^{201}Hg$	2SD	$\delta^{202}Hg$	2SD	$\Delta^{199}Hg$	2SD	$\Delta^{200}Hg$	2SD	$\Delta^{201}Hg$	2SD
Russia	CH-1 (duplicate)	Coal	Biswas et al., 2008								-1.01	0.02	-0.23	0.01			-0.22	0.00
Russia	KR-1 (duplicate)	Coal	Biswas et al., 2008								-1.71	0.14	-0.25	0.05			-0.27	0.08
Mean (n=21, including 8 previously reported samples)					**-0.64**	**0.35**	**-1.07**	**0.57**	**-1.75**	**0.87**	**-1.69**	**1.13**	**-0.19**	**0.23**	**0.02**	**0.04**	**-0.19**	**0.19**
USA	LMHS-1	Coal	This study	9	-0.33	0.00	-0.74	0.00	-1.13	0.05	-1.54	0.12	0.06	0.03	0.04	0.06	0.03	0.04
USA	LLH-1	Coal	This study	7	-0.52	0.02	-1.07	0.01	-1.67	0.04	-2.21	0.08	0.04	0.00	0.04	0.03	-0.01	0.10
USA	LMA-1	Coal	This study	11	-0.30		-0.72		-1.03		-1.44		0.06		0.00		0.05	
USA	BV	Coal	This study	918	-0.43	0.05	-0.77	0.07	-1.20	0.08	-1.34	0.07	-0.03	0.03	0.02	0.04	-0.03	0.13
USA	AL-1 (triplicate)	Coal	Biswas et al., 2008								-0.99	0.04	-0.14	0.02			-0.14	0.02
USA	PN-1 (triplicate)	Coal	Biswas et al., 2008								-1.47	0.17	-0.12	0.04			-0.14	0.03
USA	TX-1 (triplicate)	Coal	Biswas et al., 2008								-1.68	0.09	-0.10	0.05			-0.11	0.04
USA	AR-1	Coal	Biswas et al., 2008								-2.98	0.13	0.08	0.10			0.05	0.04
USA	CO-1 (duplicate)	Coal	Biswas et al., 2008								-1.65	0.04	-0.19	0.03			-0.19	0.01
USA	CO-2 (triplicate)	Coal	Biswas et al., 2008								-2.76	0.04	0.10	0.01			0.03	0.03
USA	WA-1	Coal	Biswas et al., 2008								-0.88	0.15	-0.34	0.04			-0.35	0.07
USA	UT-1 (quadruplicate)	Coal	Biswas et al., 2008								-2.08	0.15	-0.08	0.01			-0.11	0.01
USA	AK-1 (duplicate)	Coal	Biswas et al., 2008								-1.32	0.07	-0.24	0.01			-0.23	0.01
USA	AR-2 (duplicate)	Coal	Biswas et al., 2008								-1.49	0.16	-0.10	0.01			-0.10	0.01
USA	OK-1 (triplicate)	Coal	Biswas et al., 2008								-1.22	0.06	0.08	0.07			0.04	0.02
USA	Wildcat Hills, herrin (n=3)	Coal	Lefticariu et al., 2011	72							-1.39		-0.17				-0.17	
USA	Lively Grove, herrin (n=1)	Coal	Lefticariu et al., 2011	52							-1.15	0.02	-0.11	0.01			-0.13	0.01
USA	Galitia Herrin coal (n=6)	Coal	Lefticariu et al., 2011	147							-1.67		-0.08				-0.09	

Country	ID	Lithology	Source	Hg in ppb (as received basis)	δ^{199}Hg	2SD	δ^{200}Hg	2SD	δ^{201}Hg	2SD	δ^{202}Hg	2SD	Δ^{199}Hg	2SD	Δ^{200}Hg	2SD	Δ^{201}Hg	2SD
USA	Crown III, herrin coal (n=3)	Coal	Lefticariu et al., 2011	49							-1.69		-0.20				-0.18	
USA	Willow Lake, Springfield (n=2)	Coal	Lefticariu et al., 2011	165							-1.71		0.02				0.00	
USA	Viper, Springfield (n=3)	Coal	Lefticariu et al., 2011	103							-0.97		0.00				0.00	
USA	Crown Paum, Murphysboro, Mt Rorah (n=7)	Coal	Lefticariu et al., 2011	131							-2.04		-0.06				-0.04	
USA	Upper Kittanning seam; Barbour, WV	Coal	Sherman et al., 2012		-0.44	0.03	-0.65	0.06	-0.99	0.09	-1.31	0.10	-0.11	0.01	0.01	0.01	-0.01	0.02
USA	Elkhorn #3 seam; Floyd, KY	Coal	Sherman et al., 2012		-0.51	0.00	-0.42	0.02	-0.82	0.02	-0.79	0.02	-0.31	0.00	-0.03	0.03	-0.23	0.03
USA	Pond Creek seam; Pike, KY	Coal	Sherman et al., 2012		-0.23		0.16		0.03		0.45		-0.34		-0.06		-0.30	
USA	Stockton-Lewiston seam; Kanawha, WV	Coal	Sherman et al., 2012		-0.42	0.02	-0.38	0.02	-0.74	0.02	-0.75	0.02	-0.23	0.01	-0.01	0.01	-0.17	0.01
USA	Blend 4 seams; Raleigh, WV	Coal	Sherman et al., 2012		-0.52	0.07	-0.61	0.02	-1.15	0.00	-1.22	0.00	-0.21	0.08	0.01	0.03	-0.24	0.01
USA	*SF-V2m pyrite*	*pyrite*	*Lefticariu et al., 2011*	*7601*							*-0.05*	*0.02*	*0.04*	*0.02*			*0.01*	*0.04*
USA	*H6-WH1t pyrite (duplicate)*	*pyrite*	*Lefticariu et al., 2011*	*3255*							*-0.14*	*0.00*	*-0.03*	*0.03*			*-0.03*	*0.01*
Mean (n=27 including 23 previously reported samples)					**-0.41**	**0.10**	**-0.58**	**0.32**	**-0.97**	**0.43**	**-1.45**	**0.64**	**-0.10**	**0.13**	**0.00**	**0.03**	**-0.10**	**0.11**
USA	NIST SRM 1632c (n=6)	Coal	Lefticariu et al., 2011	93							-1.86	0.11	-0.04	0.02			-0.03	0.04
USA	NIST SRM 1632c (n=7)	Coal	Sherman et al., 2012	93	-0.49	0.04	-0.93	0.07	-1.44	0.10	-1.86	0.13	-0.02	0.04	0.01	0.03	-0.04	0.03
USA	NIST SRM 1632d (n=10 except 204Hg for which n=2)		This study	93	-0.49	0.06	-0.89	0.09	-1.37	0.18	-1.79	0.17	-0.04	0.05	0.01	0.06	-0.03	0.08
USA	NIST SRM 2685b (n=11 except 204Hg for which n=3)		This study	146	-0.69	0.07	-1.38	0.10	-2.08	0.17	-2.75	0.18	0.01	0.05	0.00	0.02	-0.02	0.08

Country	ID	Lithology	Source	Hg in ppb (as received basis)	$\delta^{199}Hg$	2SD	$\delta^{200}Hg$	2SD	$\delta^{201}Hg$	2SD	$\delta^{202}Hg$	2SD	$\Delta^{199}Hg$	2SD	$\Delta^{200}Hg$	2SD	$\Delta^{201}Hg$	2SD
USA	USGS CLB-1 (n=2)		This study	200	-0.38	0.01	-0.64	0.08	-1.05	0.02	-1.29	0.06	-0.04	0.01	0.01	0.06	-0.07	0.01
USA	UM-Almaden (n=53)		This study		-0.16	0.08	-0.27	0.10	-0.47	0.15	-0.57	0.11	-0.02	0.06	0.01	0.05	-0.05	0.07

Table A2. Multiple pairewise comparisions of δ^{202}Hg Δ^{199}Hg between world coals (Post Hoc Test, Tamhane's T2, equal variations not assumed)

Dependent Variable	Countries (I)	Countries (J)	Mean Difference (I-J)	Std. Error	Sig.	95% Confidence Interval		Dependent Variable	Countries (I)	Countries (J)	Mean Difference (I-J)	Std. Error	Sig.	95% Confidence Interval	
						Lower Bound	Upper Bound							Lower Bound	Upper Bound
δ^{202}Hg	USA	Former USSR	0.24	0.28	1.00	-0.73	1.20	Δ^{199}Hg	USA	Former USSR	0.09	0.06	0.99	-0.11	0.28
		Mongolia	-0.44	0.27	0.97	-1.40	0.52			Mongolia	0.16	0.05	0.19	-0.03	0.35
		Indonesia	-0.91*	0.22	0.03	-1.77	-0.05			Indonesia	0.10	0.05	0.93	-0.12	0.32
		India	0.41	0.21	0.80	-0.31	1.14			India	-0.14*	0.04	0.03	-0.27	-0.01
		Europe	-0.29	0.23	1.00	-1.11	0.54			Europe	0.26**	0.04	0.00	0.12	0.41
		China	-0.42	0.17	0.42	-0.99	0.15			China	-0.10	0.03	0.07	-0.21	0.00
		Africa	-0.53	0.19	0.27	-1.20	0.14			Africa	0.19**	0.03	0.00	0.07	0.30
	Former USSR	USA	-0.24	0.28	1.00	-1.20	0.73		Former USSR	USA	-0.09	0.06	0.99	-0.28	0.11
		Mongolia	-0.68	0.35	0.83	-1.86	0.50			Mongolia	0.07	0.07	1.00	-0.16	0.31
		Indonesia	-1.14*	0.31	0.03	-2.23	-0.06			Indonesia	0.01	0.07	1.00	-0.23	0.26
		India	0.18	0.30	1.00	-0.85	1.20			India	-0.22**	0.06	0.02	-0.42	-0.02
		Europe	-0.52	0.32	0.96	-1.61	0.56			Europe	0.18	0.06	0.16	-0.03	0.38
		China	-0.66	0.28	0.52	-1.61	0.30			China	-0.19	0.06	0.06	-0.38	0.00
		Africa	-0.76	0.29	0.32	-1.76	0.23			Africa	0.10	0.06	0.91	-0.09	0.29
	Mongolia	USA	0.44	0.27	0.97	-0.52	1.40		Mongolia	USA	-0.16	0.05	0.19	-0.35	0.03
		Former USSR	0.68	0.35	0.83	-0.50	1.86			Former USSR	-0.07	0.07	1.00	-0.31	0.16
		Indonesia	-0.47	0.30	0.98	-1.55	0.62			Indonesia	-0.06	0.07	1.00	-0.31	0.19
		India	0.85	0.29	0.19	-0.17	1.88			India	-0.30**	0.06	0.00	-0.50	-0.10
		Europe	0.15	0.31	1.00	-0.92	1.23			Europe	0.10	0.06	0.93	-0.10	0.31
		China	0.02	0.27	1.00	-0.94	0.98			China	-0.26**	0.05	0.00	-0.45	-0.07
		Africa	-0.09	0.28	1.00	-1.08	0.91			Africa	0.03	0.05	1.00	-0.17	0.22
	Indonesia	USA	0.91*	0.22	0.03334	0.05	1.77		Indonesia	USA	-0.10	0.05	0.93	-0.32	0.12
		Former USSR	1.14*	0.31	0.0320	0.06	2.23			Former USSR	-0.01	0.07	1.00	-0.26	0.23
		Mongolia	0.47	0.30	0.98	-0.62	1.55			Mongolia	0.06	0.07	1.00	-0.19	0.31
		India	1.32**	0.25	0.0019	0.40	2.25			India	-0.23*	0.06	0.03	-0.46	-0.01
		Europe	0.62	0.27	0.61	-0.36	1.61			Europe	0.16	0.06	0.33	-0.06	0.39
		China	0.49	0.22	0.73	-0.37	1.34			China	-0.20	0.05	0.09	-0.42	0.02
		Africa	0.38	0.23	0.98	-0.52	1.28			Africa	0.09	0.05	0.98	-0.13	0.31
	India	USA	-0.41	0.21	0.80	-1.14	0.31		India	USA	0.14*	0.04	0.03	0.01	0.27
		Former USSR	-0.18	0.30	1.00	-1.20	0.85			Former USSR	0.22**	0.06	0.02	0.02	0.42
		Mongolia	-0.85	0.29	0.19	-1.88	0.17			Mongolia	0.30**	0.06	0.00	0.10	0.50
		Indonesia	-1.32**	0.25	0.00	-2.25	-0.40			Indonesia	0.24*	0.06	0.03	0.01	0.46
		Europe	-0.70	0.25	0.28	-1.60	0.20			Europe	0.40**	0.04	0.00	0.25	0.55
		China	-0.83*	0.20	0.011	-1.55	-0.12			China	0.03	0.04	1.00	-0.09	0.16
		Africa	-0.94**	0.22	0.009	-1.72	-0.16			Africa	0.32**	0.04	0.00	0.19	0.45

Dependent Variable	Countries (I)	Countries (J)	Mean Difference (I-J)	Std. Error	Sig.	95% Confidence Interval		Dependent Variable	Countries (I)	Countries (J)	Mean Difference (I-J)	Std. Error	Sig.	95% Confidence Interval	
						Lower Bound	Upper Bound							Lower Bound	Upper Bound
	Europe	USA	0.29	0.23	1.00	-0.54	1.11		Europe	USA	-0.26**	0.04	0.00	-0.41	-0.12
		Former USSR	0.52	0.32	0.96	-0.56	1.61			Former USSR	-0.18	0.06	0.16	-0.38	0.03
		Mongolia	-0.15	0.31	1.00	-1.23	0.92			Mongolia	-0.10	0.06	0.93	-0.31	0.10
		Indonesia	-0.62	0.27	0.61	-1.61	0.36			Indonesia	-0.16	0.06	0.33	-0.39	0.06
		India	0.70	0.25	0.28	-0.20	1.60			India	-0.40**	0.04	0.00	-0.55	-0.25
		China	-0.13	0.23	1.00	-0.95	0.68			China	-0.37**	0.04	0.00	-0.50	-0.23
		Africa	-0.24	0.24	1.00	-1.11	0.62			Africa	-0.08	0.04	0.86	-0.22	0.07
	China	USA	0.42	0.17	0.42	-0.15	0.99		China	USA	0.10	0.03	0.07	0.00	0.21
		Former USSR	0.66	0.28	0.52	-0.30	1.61			Former USSR	0.19	0.06	0.06	0.00	0.38
		Mongolia	-0.02	0.27	1.00	-0.98	0.94			Mongolia	0.26**	0.05	0.00	0.07	0.45
		Indonesia	-0.49	0.22	0.73	-1.34	0.37			Indonesia	0.20	0.05	0.09	-0.02	0.42
		India	0.83**	0.20	0.01	0.12	1.55			India	-0.03	0.04	1.00	-0.16	0.09
		Europe	0.13	0.23	1.00	-0.68	0.95			Europe	0.37**	0.04	0.00	0.23	0.50
		Africa	-0.11	0.19	1.00	-0.76	0.55			Africa	0.29**	0.03	0.00	0.18	0.39
	Africa	USA	0.53	0.19	0.27	-0.14	1.20		Africa	USA	-.187**	0.03	0.00	-0.30	-0.07
		Former USSR	0.76	0.29	0.32	-0.23	1.76			Former USSR	-0.10	0.06	0.91	-0.29	0.09
		Mongolia	0.09	0.28	1.00	-0.91	1.08			Mongolia	-0.03	0.05	1.00	-0.22	0.17
		Indonesia	-0.38	0.23	0.98	-1.28	0.52			Indonesia	-0.09	0.05	0.98	-0.31	0.13
		India	0.94**	0.22	0.01	0.16	1.72			India	-0.32**	0.04	0.00	-0.45	-0.19
		Europe	0.24	0.24	1.00	-0.62	1.11			Europe	0.08	0.04	0.86	-0.07	0.22
		China	0.11	0.19	1.00	-0.55	0.76			China	-0.29**	0.03	0.00	-0.39	-0.18

* mean difference is significant at the 0.05 level.; ** mean difference is significant at the 0.01 level

Appendix B: supplementary data for Chapter 7

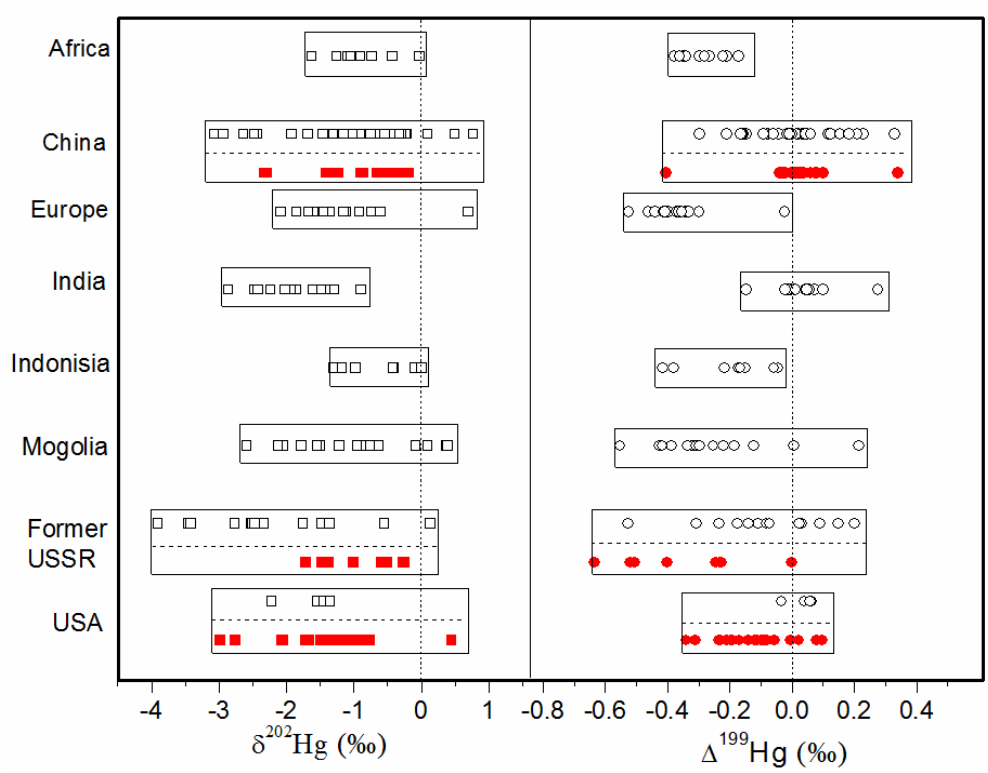

Figure B1. Comparison of $\delta^{202}Hg$ and $\Delta^{199}Hg$ in studied coal samples (n=108, black unfilled square and circle) with those (n=47, red filled square and circle) previously reported (Biswas et al., 2008; Lefticariu et al., 2011; Sun et al., 2013)

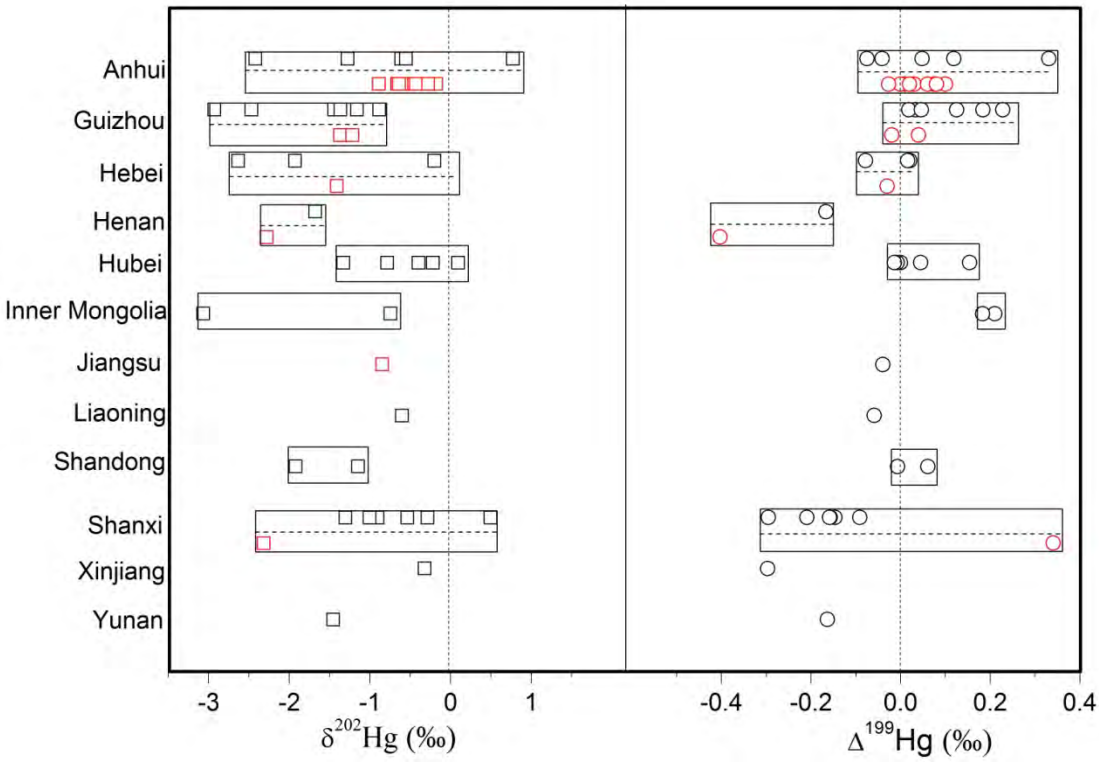

Figure B2. Comparison of δ^{202}Hg and Δ^{199}Hg in studied coal samples from China (n=33, black square and circle) with those (n=16, red square and circle) previously reported (Biswas et al., 2008; Sun et al., 2013)

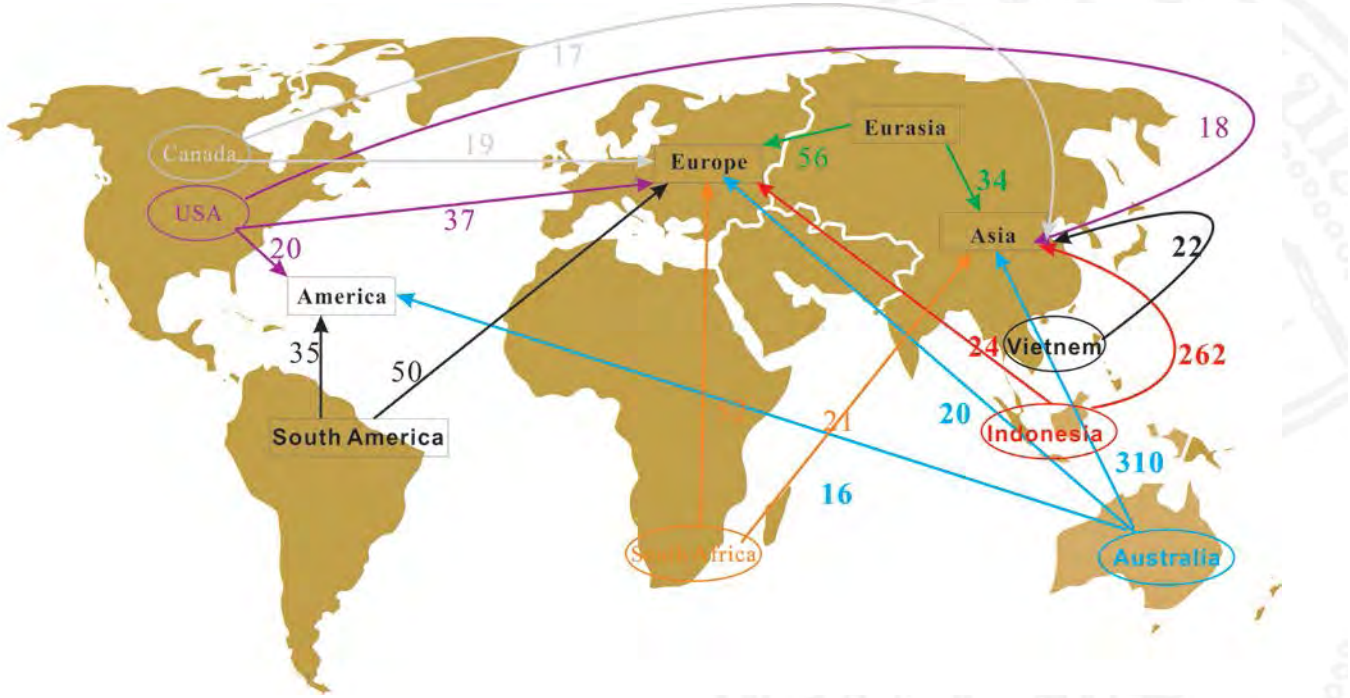

Figure B3. World coal import-export flow (short Million tons/yr)

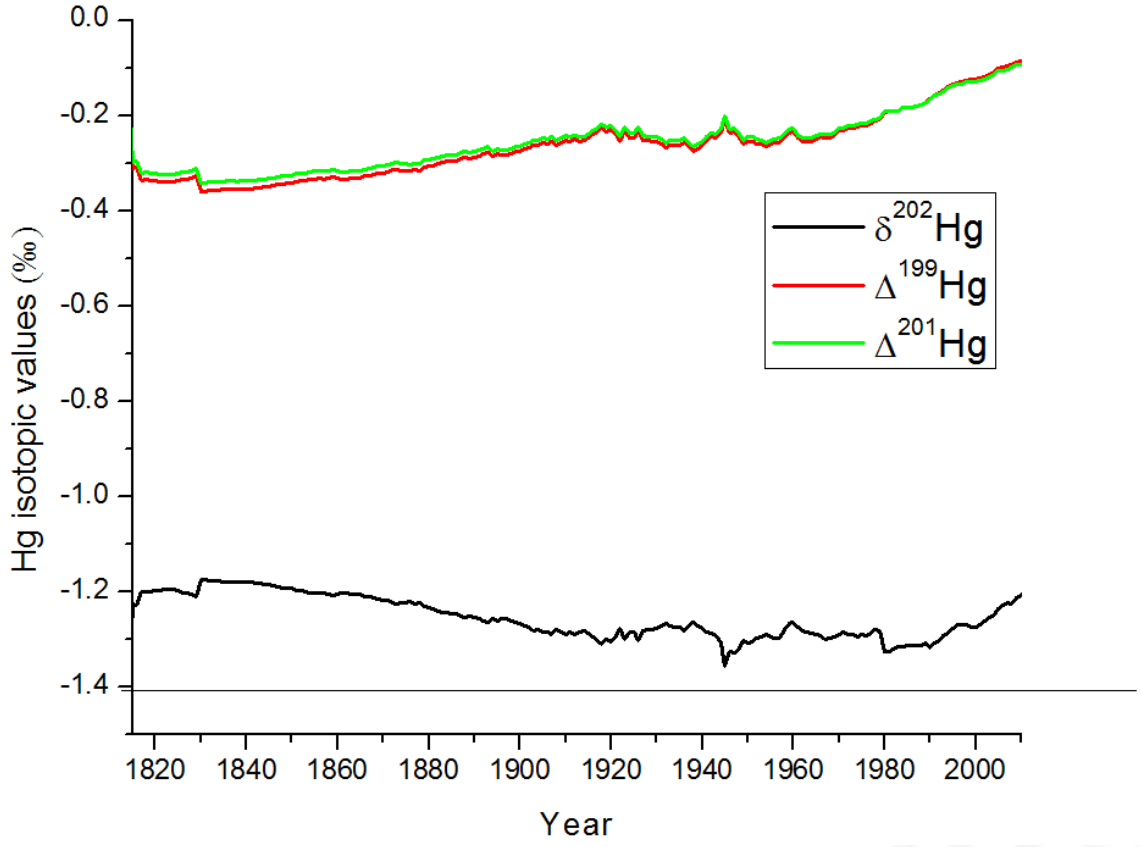

Figure B4. A preliminary Hg isotope evolution model of world coals from 1815-2010

Résumé

Le mercure (Hg) est un élément toxique et récalcitrant dans notre environnement. Depuis la révolution industrielle, les activités humains ont augmenté la quantité du Hg qui cycle à la surface de la Terre d'un facteur trois. Les émissions du Hg des centrales au charbon représentent à elles-seules la moitié de tous les émissions anthropiques du Hg. Désormais, le traçage quantitatif de ces émissions des différentes régions du globe n'est pas simple. L'objectif de cette thèse a été d'explorer les signatures isotopiques du Hg comme traceur potentiel des émissions du Hg des centrales au charbon. Dans un premier temps un protocole d'extraction, purification et de pré-concentration du Hg par voie de combustion et re-piégeage acide a été développé. Une fois purifie, le Hg a été analyse par spectrométrie de masse à haute précision (~0.1‰, 2σ). En résumé, nous observons que les charbons provenant du globe entier sont isotopiquement discernable à un niveau de p de <0.05 ou <0.1. Les processus de combustion et de captage du Hg dans les centrales au charbon ne modifient que minimalement les signatures isotopiques du Hg. Nous considérons ces deux résultats suffisamment prometteur à fin de recommander des études plus élaborées au sujet du traçage des émissions du Hg des centrales au charbon dans l'environnement. Il sera important d'étudier les signatures isotopiques des formes gazeuses et particulaires du Hg dans les panaches des centrales au charbon, afin de vérifier leur variation et évolution. La difficulté de tracer les sources du Hg réside dans la modification de ses signatures isotopiques par les transformations biogéochimiques omniprésentes dans l'atmosphère.

Abstract

Mercury (Hg) is a toxic, persistent and globally distributed pollutant. Since the industrial revolution, human activities have augmented the global Hg cycle at the Earth's surface by a factor of three. Hg emissions from coal-fired power plants represent at present the largest single anthropogenic source. However, quantitative tracing of the fate of coal Hg emissions from different countries or regions is a challenging issue. The objective of this PhD dissertation was to use Hg stable isotope signatures to address this problem. Firstly, we developed a combustion-trapping protocol to extract, purify and pre-concentrate Hg from solid samples with low Hg levels such as coal and coal combustion products. Purified coal Hg was then measured for its isotope compositions by high-precision (~0.1‰, 2σ) multi-collector inductively coupled plasma mass spectrometry. In summary we find that coals from different global coal basins are often isotopically distinguishable at the p=0.05 or 0.10 level, and that combustion and capture processes in coal-fired power plants do not substantially change feed coal Hg isotope signatures. We consider these combined results to be sufficiently promising to recommend detailed atmospheric Hg isotope tracer studies of coal plant Hg emissions. However, we anticipate that the different gaseous and particulate forms of Hg in coal flue gas emissions may carry more contrasting Hg isotope signatures than we estimated for bulk emissions. Therefore, caution should be taken in near-field and far-field coal Hg emission tracing, and additional studies on the Hg isotope signatures of coal plant Hg emissions are necessary.